T.C.
ISTANBUL GEDIK UNIVERSITY
INSTITUTE OF GRADUATE STUDIES

DESIGN AND ANALYSIS OF DOUBLE COMPOSITE TRUSS GIRDER FOR THE LONG SPAN BRIDGES USING PERFOBOND LEISTE

MASTER'S THESIS

Jaafar Jasim SALEEM

Civil Engineering Department

Master in Civil Engineering Turkish Program

FEBRUARY 2025
ISTANBUL

T.C.
ISTANBUL GEDIK UNIVERSITY
INSTITUTE OF GRADUATE STUDIES

DESIGN AND ANALYSIS OF DOUBLE COMPOSITE TRUSS GIRDER FOR THE LONG SPAN BRIDGES USING PERFOBOND LEISTE

MASTER'S THESIS

Jaafar Jasim SALEEM
(211282009)

Civil Engineering Department

Master in Civil Engineering Turkish Program

Thesis Advisor: Doç. Dr. Redvan GHASEMLOUNIA

Thesis Sec. Advisor: Prof. Dr. Haitham Hassan MUTEB

Istanbul 2025

T.C.
İSTANBUL GEDİK ÜNİVERSİTESİ
Lisansüstü Eğitim Enstitüsü Müdürlüğü

Jüri Tez Onay Formu

07/02/2025

LİSANSÜSTÜ EĞİTİM ENSTİTÜSÜ MÜDÜRLÜĞÜ

Bu çalışma 07/02/2025 tarihinde aşağıdaki jüri tarafından İnşaat Mühandisliği Anabilim Dalı, İnşaat Mühendisliği (Tezli Yüksek Lisans) Programı Yüksek Lisans Tezi olarak kabul edilmiştir.

TEZ JÜRİSİ

Doç. Dr. Redvan GHASEMLOUNIA
Danışman
İstanbul Gedik Üniversitesi

Dr. Öğr. Üyesi Hasan Bozkurt NAZİLLİ
Üye (İmza)
İstanbul Gedik Üniversitesi

Dr. Öğr. Üyesi Mert TOLON
Üye (İmza)
İstanbul Maltepe Üniversitesi

DECLARATION

I am Jaafar Jasim SALEEM, thus declare that the thesis titled “Design and Analysis of Double Composite Truss Girder for the Long Span Bridges Using Perfobond Leiste" is an original piece of work that I have done in order to be awarded the master's degree in Civil Engineering. I further certify that this thesis, or any section of it, has not been published and provided for any other graduation or study paper in any other university or institution. This applies to any and all parts of the thesis. (07/02/2025)

Jaafar Jasim SALEEM

DEDICATION

Thanks to the Minister of Construction and Housing, Mr. Minister Benken Rikani, and the Director General of Roads and Bridges Directorate, Mr. Hussein Jassim AL-Mousawi, who allowed us to complete the study and were prominent supporters of me and my colleagues in the field of science and research.

I would like to extend my best regards to the Dean of Istanbul Gedik University and the head of the Department of Civil Engineering and wish them success.

A special tribute goes to the supervisors of this thesis, Doç. Dr. Redvan Ghasemlouna and Prof. Dr. Haitham Hassan Muteb, for their tremendous and sufficient support.

My lovely family and friends, thank you for your continuous support throughout the research period without interruption and for waiting with great warmth and passion to complete this work.

To the person who has supported me throughout these periods, whose presence, the more difficulties were the incentive to start again, the supporter, with the deep soul and faith when difficulties are crowding out in all life small details, thank you for your positive influence in the most difficult moments.

ACKNOWLEDGMENT

First, great thanks to the great lord for enabling me to complete this valuable work, where I thank my god for this success and pray to him to light my way in other successful works.

Cordial thanks and deepest gratitude to my thesis supervisors Assoc. Dr. Redvan Ghasemlouna and Prof. Dr. Haitham Hassan Muteb for the continued valuable guidance and encouragement throughout the preparation of this study and for helping me to achieve and complete this research by broad scientific discussions.

And don't forget to mention my family; I am deeply thankful to you, especially to my parents for helping me all the time with their deeds and words throughout my studies.

Special thanks to my colleagues and my friends who always somehow be there with their support.

Finally, I want to thank all the workers and the technicians who contributed to the manufacture of samples, who were extremely accurate and professional.

February 2025 Jaafar Jasim SALEEM

TABLE OF CONTENTS

ABBREVIATIONS

A	: Cross-sectional area of the effective composite section
Ast	: Cross-sectional area of the structural steel section
Ab	: Cross-sectional area of bottom transverse reinforcement
Abh	: Cross-sectional area of bottom transverse reinforcement in a haunch
Ac	: Cross-sectional area of concrete
Act	: Cross-sectional area of the tensile zone of the concrete
Afc	: Cross-sectional area of the compression flange
Ap	: Cross-sectional area of profiled steel sheeting
Ape	: Effective cross-sectional area of profiled steel sheetin
As	: Cross-sectional area of reinforcement
Asf	: Cross-sectional area of transverse reinforcement
At	: Cross-sectional area of top transverse reinforcement
Av	: Shear area of a structural steel section.
A1	: Loaded area under the gusset plate
Ea	: Modulus of elasticity of structural steel
Ec,eff	: Effective modulus of elasticity for concrete
Ecm	: Secant modulus of elasticity of concrete
Es	: Design value of modulus of elasticity of reinforcing steel
(EI)eff	: Effective flexural stiffness for calculation of relative slenderness
(EI)eff,II	: Effective flexural stiffness for use in second-order analysis
(EI)2	: Cracked flexural stiffness per unit width of the concrete or composite slab
Ga	: Shear modulus of structural steel
Gc	: Shear modulus of concrete
I	: Second moment of area of the effective composite section
Ia	: Second moment of area of the structural steel section
Iat	: St. Venant torsion constant of the structural steel section
Ic	: Second moment of area of the un-cracked concrete section
Ict	: St. Venant torsion constant of the un-cracked concrete encasement

Is : Second moment of area of the steel reinforcement

I1 : Second moment of area of the effective equivalent steel section assuming that the concrete in tension is un-cracked

I2 : Second moment of area of the effective equivalent steel section neglecting concrete in tension but including reinforcement

Ksc : Stiffness related to the shear connection

L : Length; span; effective span

Le : Equivalent span

Li : Span

Lo : Length of overhang

Lp : Distance from center of a concentrated load to the nearest support

Ls : Shear span

Lx : Distance from a cross-section to the nearest support

M : Bending moment

Ma : Contribution of the structural steel section to the design plastic resistance moment of the composite section

Ma,Ed : Design bending moment applied to the structural steel section

Mb,Rd : Design value of the buckling resistance moment of a composite beam

Mc,Ed : The part of the design bending moment applied to the composite section

Mcr : Elastic critical moment for lateral-torsional buckling of a composite beam

Med : Design bending moment

MEd,i : Design bending moment applied to a composite joint

MEd, max, f : Maximum bending moment or internal force due to fatigue loading

MEd, min, f : Minimum bending moment due to fatigue loading

Mel,Rd : Design value of the elastic resistance moment of the composite section

Mmax, Rd : Maximum design value of the resistance moment in the presence of a compressive normal force

Mpa : Design value of the plastic resistance moment of the effective cross-section

Mperm : Most adverse bending moment for the characteristic combination

Mpl,a,Rd : Design value of the plastic resistance moment of the structural steel section

Mpl,N,Rd : Design value of the plastic resistance moment of the composite section

Mpl, Rd : Design value of the plastic resistance moment of the composite section with full shear connection

Mpl, y, Rd : Design value of the plastic resistance moment of the y-y axis of the composite section with full shear connection

Mpl, z, Rd : Design value of the plastic resistance moment of the y-y axis of the composite section with full shear connection

Mpr : Reduced plastic resistance moment of the profiled steel sheeting

MRd : Design value of the resistance moment of a composite section or joint

MRk : Characteristic value of the resistance moment of a composite section or joint

My,Ed : Design bending moment applied to the composite section about the y-y axis

Mz,Ed : Design bending moment applied to the composite section about the z-z axis

N : Compressive normal force; number of stress range cycles; number of shear connectors

Na : Design value of the normal force in the structural steel section of a composite beam

Nc : Design value of the compressive normal force in the concrete flange

Nc,f : Design value of the compressive normal force in the concrete flange with full shear

Nc, el : Compressive normal force in the concrete flange corresponding to Mel, Rd

Ncr,eff : Elastic critical load of a composite column corresponding to an effective flexural Stiffness

Ncr : Elastic critical normal force

Nc1 : Design value of normal force calculated for load introduction

NEd : Design value of the compressive normal force.

NG,Ed : Design value of the part of the compressive normal force that

is permanent

Np : Design value of the plastic resistance of the profiled steel sheeting

Npl, a : Design value of the plastic resistance of the structural steel section

Npl, Rd : Design value of the plastic resistance of the composite section to compressive normal force

Npl, Rk : Characteristic value of the plastic resistance of the composite section to compressive normal force

Npm, Rd : Design value of the resistance of concrete to compressive normal force

NR : Number of stress-range cycles

Ns : Design value of the plastic resistance of the steel reinforcement to normal force

Nsd : Design value of the plastic resistance of the reinforcing steel to tensile normal force

PRd : Design value of the shear resistance of a single connector

SCTG : Single composite truss girder

DCTG : Double composite truss girder

PPR : perfobond plate ribs

LIST OF TABLES

Page No:

LIST OF FIGURES

Page No:

DESIGN AND ANALYSIS OF DOUBLE COMPOSITE TRUSS GIRDER FOR THE LONG SPAN BRIDGES USING PERFOBOND LEISTE

ABSTRACT

This research aims to investigate behavior and collect analysis data on the response of a double composite truss girder (DCTG) under increasing static load compared to a single composite truss girder (SCTG) in the same circumstances

The study reveals the benefits of a composite structure by the ability to obtain a lightweight girder that is used at the superstructure bridge, especially for long continuous spans with the idea of converting the concrete web to steel truss.

The double composite feature will increase the ability of the girder to be high resentence hogging moment at the negative regions at the mid-support of continuous bridges and reduce the deflection ratio; furthermore, the decrease in girder weight will affect positively on the other bridge part design including piers and foundations due to increasing the dimension and steel reinforcement that will lead to lower bridge construction cost and structure durability.

The first part, which is the main subject of the experimental work involved fabrication and tested of eight composite truss girder specimens with constant dimensions 2620mm x 350mm x 400mm of steel truss girder divided into two categories depending on the composite installation type.

The first category (SCTG) involves implementing a single composite line between the top concrete and the steel truss frame, while the double composite (DCTG) consists of two composite lines between the top and bottom concrete girder and a steel truss frame.

The test procedure was made by installing the specimen on the steel support, two at edge and one at middle distance, with applied two-point load by two hydraulic jacks with maximum capacity 3000 KN of each one, the loading was at several stages till the modes of failure occurs.

The second part of this research was performed a validation study by numerical analysis method using Abaqus software program to simulating eight models, the dimension and materials parameters such as concrete strength, steel plate, reinforcement bars, also the test situation including applied load and support conditions was the same circumstances of the experimental test, the results get compared, analyzed and listed in detail at chapter six.

The experimental test results were clarified by several improvements, such as increasing the girder strength capacity in the double composite girder by 13% compared to the single composite girder.

Meanwhile, it’s worth mentioning that the stress and strain value of the top concrete surface that causes hogging moment cracks decreased by 42.7% compared to (SCTG) specimens.

In terms of perfobond leiste shear connector, it can be stated that these results have clarified the role of the bottom shear connector (double composite), which

revolves around the topic of influencing the stresses placed on the top shear connector resulting by the shear flow in the interface between the concrete and steel flange, when the results show decreeing in slip ratio by 18.7% at the top interface, al bond situation at all specimens considered as full interaction state.

In general, the most advantage featured of adding double composite was enhancement the ability of girder to decrease the deflection ratio by 31% at the sagging moments regions when the positive moment reach the maximum values due to the continuity of the girder.

Keywords: *Perfobond lieste shear connector, Double composite girder, Experiment study, Abaqus simulation, Hogging moment, Warren truss, Push out test, Static load, failure mode*

PERFOBOND KULLANARAK UZUN AÇIKLIKLI KÖPRÜLER İÇİN ÇİFT KOMPOZİT MAKAS KİRİŞİNİN TASARIMI VE ANALİZİ

ÖZET

Bu araştırma, aynı koşullarda tek bir kompozit kafes kirişe (SCTG) kıyasla artan statik yük altında bir çift kompozit kafes kirişin (DCTG) tepkisine ilişkin davranışı araştırmayı ve analiz verilerini toplamayı amaçlamaktadır.

Çalışma, özellikle beton ağın çelik kirişe dönüştürülmesi fikriyle uzun kesintisiz açıklıklar için üst yapı köprüsünde kullanılan hafif bir kiriş elde edebilmesiyle kompozit bir yapının faydalarını ortaya koymaktadır.

Sürekli köprülerin orta desteğindeki kirişin negatif bölgelerinde yüksek kırgınlık hogging momenti ve sapma oranı, çift kompozit özelliği sayesinde azaltılabilir. Ayrıca, kirişin ağırlığının azalması, iskeleler ve temeller gibi köprü parçalarının tasarımında daha düşük maliyetlere ve yapı dayanıklılığına yol açacaktır.

Deneysel çalışmanın ana konusu olan ilk bölüm, kompozit montaj tipine bağlı olarak iki kategoriye ayrılan 2620 mm x 350 mm x 400 mm çelik kafes kiriş örneğinin imalatını ve testini içeriyordu.

Çift kompozit (DCTG), üst ve alt beton kirişlerin bir çelik kafes çerçeve arasında iki kompozit hattan oluşur, birinci kategori (SCTG), üst ve alt beton kirişlerin bir çelik kafes çerçeve arasında tek bir kompozit hattan oluşur.

Test süreci, numunenin her biri en fazla 3000 KN kapasiteli iki hidrolik kriko ile iki noktalı yük uygulanarak birkaç aşamada yapıldı, numuneler orta mesafede ve ikisi kenarda olmak üzere iki çelik destek üzerine monte edildi, modları oluşana kadar.

Bu araştırmanın ikinci bölümünde, Abaqus yazılım programı kullanılarak sayısal analiz yöntemi kullanılarak sekiz modeli simüle edildi. Beton dayanımı, çelik levha ve donatı çubukları gibi boyut ve malzeme parametreleri ve uygulanan yük ve destek koşullarını içeren test durumu deneysel testin koşullarıyla aynıydı.

Deneysel test sonuçları, tek kompozit kirişe kıyasla çift kompozit kirişe kıyasla kiriş dayanım kapasitesinin %13 artması gibi çeşitli iyileştirmelerle netleştirildi.

Bununla birlikte, tıkanma momenti çatlaklarına neden olan üst beton yüzeyinin gerilme ve gerinim değerinin (SCTG) numunelere göre %42,7 düştüğünü belirtmek önemlidir.

Perfobond leiste kesme bağlayıcı ile ilgili olarak, bu bulgular ve sonuçlar, üst arabirimdeki kayma oranının %18,7 olduğunu ve beton ve çelik flanş arasındaki ara kesme akımı tarafından ortaya çıkan üst kesme bağlayıcı yerleştirilen gerilmeleri etkileyen bir konu etrafında dönen (çift kompozit), alt kesme bağlayıcı görevinin açık olduğunu göstermektedir.

Çift kompozit eklemenin en büyük avantajı, kirişin sürekliliği nedeniyle pozitif momentin en yüksek seviyelere ulaştığı sarkma momentleri bölgelerinde kirişin sapma oranını % 31 azaltma yeteneğiydi.

Anahtar Kelimeler: *Perfobond listeli kesme konnektörü, Çift kompozit kiriş, Deney çalışması, Abaqus simülasyonu, Tıkanma momenti, Warren makas, Itme testi, Statik yük, Arıza modu*

1. INTRODUCTION

1.1 General

Because of their great durability and quick construction time, steel-concrete composite girders are frequently utilized in structural constructions.

The benefits of amalgamating two building materials in girders were to get a higher span length to depth ratio, decreased deflections, and higher stiffness ratio than steel or concrete spirited beam structures.

It’s required to obtain the strength properties any material can be chosen for civil engineering projects to achieve the best behavior for the structure, such as buildings and bridges.

When a composite element is defined as the union of two or more elements accompanied together in a specific way to take advantage of each element's properties simultaneously, such as resisting various stresses applied to the composite member, the process of bonding steel to the concrete components works as one item.

Composite combination has its advantage where the steel can speed constructions project workplan.

Moreover, increasing the structure stiffness and load allowable capacity because steel and concrete have different characteristics [8].

Concrete structural members are generally very low strength in tension force regions and are tending to creep and shrink over time.

To reduce these risks of weakness in tensile strength, substantial required work has been included in designing the steel reinforcing bars that can substitute the weakness of concrete.

1.2 Composite Action

Composite structures possess a distinctive attribute when the steel beam may be regarded as having a consistent flexural strength over all sections of the beam,

consequently, during the design phase, it is essential to ensure that the flexural strength surpasses the maximum applied bending force.

A reinforced concrete beam shows a similar behavior of the steel beam except for locations in close contact to the ends of the reinforcing bars, in the opposite of steel beams or reinforced concrete beams the composite beam strength not consistent throughout its length.

Consequently, it is imperative to evaluate the strength of a composite beam at all points with the applied strain that is acting on the beam, and it's required that the shear connector is suitable in terms of strength and stiffness to achieve optimal bonding between these two elements to be connected, Figure 1.1 illustrated the composite girder.

The quality and behavior of these two composite elements depend on the quality of the shear connector regarding geometry and the process of shear force flow transfer [15].

In such a typical structure when there are a deponed between the two elements (steel and concrete) when the load applied over the concrete slab the steel girder will be subjected under two forces, while the tensile force located at bottom of the beam compressive force located at top of the beam, when the applied load exceed the maximum allowable bearing capacity lead to some failure as local buckling.

The second situation if the bonding between the two elements is integrated as full bonding, the compressive force will be transmitted from the upper part of the steel girder to the reinforcement concrete deck slab so the steel beam will resist the tensile force only.

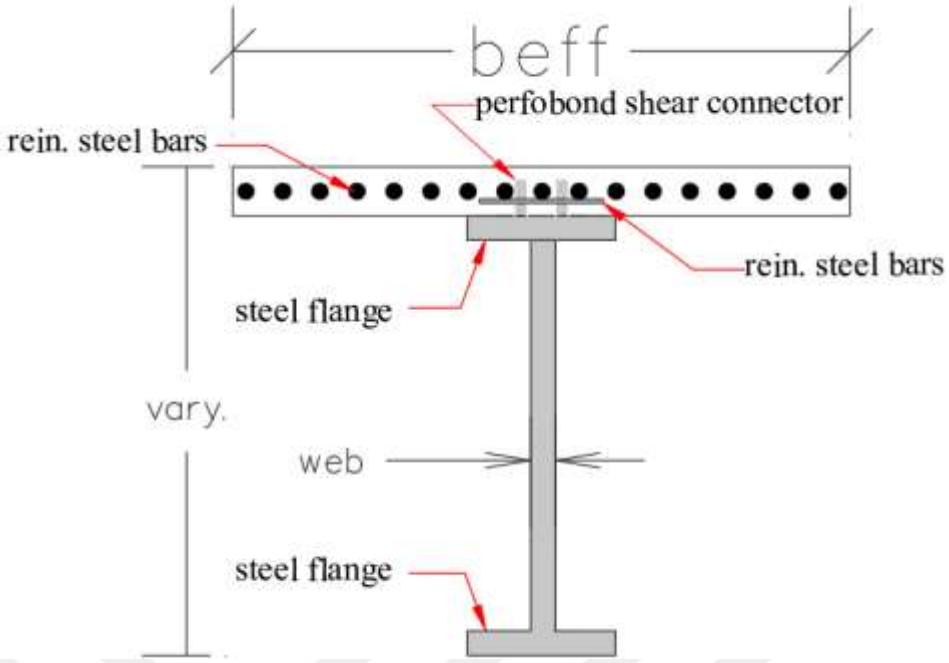

Figure 1.1: Steel and Concrete Composite Girder Element

From this principle it can be said that the composite member increases the resistance of the beam to the flexure force more than if steel girder acts as one element.

When flexural strength and stiffness resistance increases, then longer spans and smaller beam depths can be obtained, it's possible to obtain a faster with more convenient and economical construction [10].

As a composite steel-concrete girder there are several load-deformation characteristics as listed below:

- Initial stiffness: shear connectors consist of very high stiffness because of the concrete items' linking with steel.
- Nonlinear behavior: studies show that the relationship of slippage with loads is nonlinear, and this is revealed when the loads gradually increase with time.
- Ultimate strength: after the shear connector reaches the state of ultimate strength capacity a significant slip occurs.
- Post-ultimate behavior: in this stage the shear connector reaching the softening point, it is exposed to fracture failures including surrounding concrete cracks or yielding of steel parts status [14,19].

There are some factors that influence the deformation characteristics of shear

connector and the effect of the bonding formation such as the size and shape.

Also, the material properties which are represented by strength and ductility of the steel and the compressive resistance of concrete.

If compressive strength properties were high that’s led to enhance the composite member bearing capacity, also the embedded ratio of shear connector depth in the concrete section leading to increasing the efficiency of load transfer [14].

1.3 Shear Connectors

1.3.1 Mechanical behavior of shear connectors

The main aim of the implementation of shear connectors is to obtain optimal the interaction of concrete's structure and the steel compounds or any other two compounds, which required very high stress resistance to prevent any failure due to creep or separation of each element.

Since each element depends on the resistance of the other part in the fully interconnected cases.

The mechanism of the load transfer is divided into firstly direct shear where the transfer of loads through the connector itself and secondly bearing situation when the surrounding concrete exerts strain on the connection area to transmitting shear forces through bearing pressure method.

Thirdly, interlocking when concrete passing through the holes of steel plate, these situations present in several types of shear contactor and reveal the greatest assistance on the load transfer [18].

1.3.2 Types of shear connectors

Several types of shear connectors aim to connect two elements integrally thereby increasing the resistance of moment force due to the enhancement of the moment of inertia of the composite section.

Shear connector design concepts which are developed through several research can be classified into four categories such as the first mechanical joint, secondly, friction bonding techniques, including high-tensile bolts.

Thirdly, adhesion methods for protruded rolling steel, such as checkered steel plates and rugged-surface H-shaped steel; and adhesive materials, such as epoxy resin, each encompass several implementation methods [8].

Where the mechanical joints are considered the most common method among the rest of the methods, when even from few contacts areas it can get a high connection ratio between the two composite elements.

An example of mechanical joint methods such as steel welding stud, block dowels, perforated plate dowels and angle degree of connector where these methods are classified according to the material stiffness ratio under the loading to the rigid shear connector that be able to resist horizontal shear force.

Moreover, it's not only required to create a high shear resistant for shear connectors to get the optimum composite situation, where one of the expected failures is the weakness of the surrounding concrete of the shear connector. Therefore, it is required in designs to make the resistance of composite materials in equivalent status to prevent any slip, uplift, or concrete slab cracks failures. Some of these shear connector types are shown at Figure 1.2.

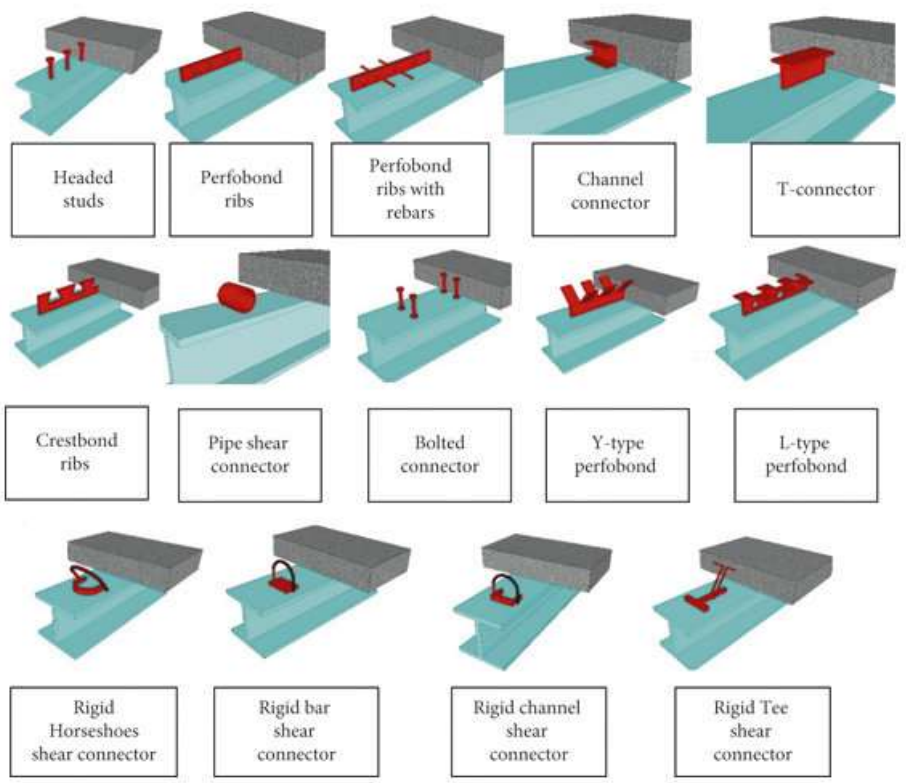

Figure 1.2: Types of Shear Connectors Systems in Composite Structure

The chosen methods of any of these shear connectors depend on the nature of the structure and type of transferring of shear force flow and also according to the direction and forces values, where the perfobond methods are considered the most common type due to the load transfer mechanism with perfect shear resistance including high load-bearing capacity with large bonding area, it's suitable for situations requiring high shear resistance, especially in bridge structures.

1.3.3 Perfobond leiste shear connector

This type of shear connector refers to either perfobond strip or perfobond plate rib, where this type is considered one of the advanced methods in the transfer of shear force, and this is one of the reasons why it's more used in bridges with long spans.

The dependence in terms of design is made on dowel action and mechanical interlock, which are the reason for the increased bearing capacity and strength of the composite member [15].

In a typical design of perfobond leiste shear connector it is consistence of a steel plate containing several holes, where several steel bars are passed through these holes to increase the structural bonding between the steel and concrete elements which are casting surrounding shear connector, Figure 1.3.

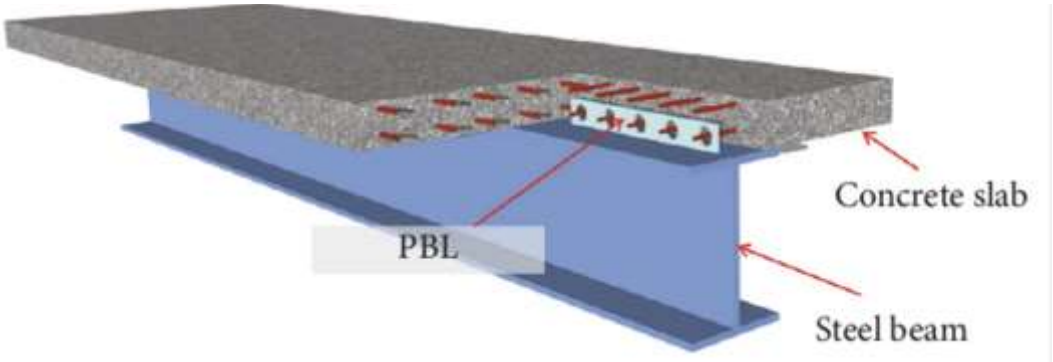

Figure 1.3: Perfobond Leiste Shear Connector with Rebars

Welding is the most chosen method to bond the connector with the steel beam and it can be bonded with bolts with high strength capacity.

The quality of the steel plate and the quantity and shape of the holes determine the load transfer mechanism of these connectors.

The interlock connection creates a mechanical interlock that resists shear force when concrete flows through the hole and hardens, forming a very strong bond between the concrete and steel plate, this process is known as dowel action.

In addition, presence of reinforcement bars passing through holes steel plate ribs, increasing the resistance of shear force including distributes loads through reinforced concrete increasing the bearing surface [1].

The main applications that use perfobond leiste shear connector are in the composite girder of the bridge superstructure.

1.3.4 Tests methods of shear connector

The design concept and analysis of any composite truss girders mostly rely on the composite action through the steel and concrete parts; so, the basic criteria in composite girders are related with bearing capacity and connection behavior of the shear transfer.

In the composite truss girder, the subject of slippage may occur in one way or another and the aim becomes how to reduce the excessive slip occurrence.

However, to prevent any issues that not just occur in the shear connector but also the failure of concrete it's necessary to examine the entire composite specimen [21].

Several methods of testing, such as push-out tests, full-scale girder tests, and by using numerical simulations to evaluate the execution of composite joints or members under various types of loading conditions.

The common experimental and numerical studies methods are used in this type of research to find specific data of composite member and failure mode [13].

1.3.4.1 Push-out test

This method is considered one of the most widely used methods in giving the results of the properties of the share connector.

Through this method, concentrated loads are applied vertically to the steel plate, which is fully bonded with reinforced concrete until the failure occurs, as shown in Figure 1.4.

This method can determine the slip ratio characteristics, shear strength capacity and stiffness of the connectors type that used.

1.3.4.2 Full-scale beam tests

This type of test depend on implementation a composite member in specific scale that act as real-world properties with certain loads applied on the girder to make the beam subjected to various compressive and tensile stresses on the entire parts of the composite member; however, this method considered as more expensive and complex compared to the other methods and it's provides comprehensive data of the shear connectors under bending and shear forces.

In beam tests where two points of loads are applied symmetrically on the beam as shown in Figure 1.5, the girder test for shear connectors when the shear flow continues to escalate with the augmentation of the load until failure occurs.

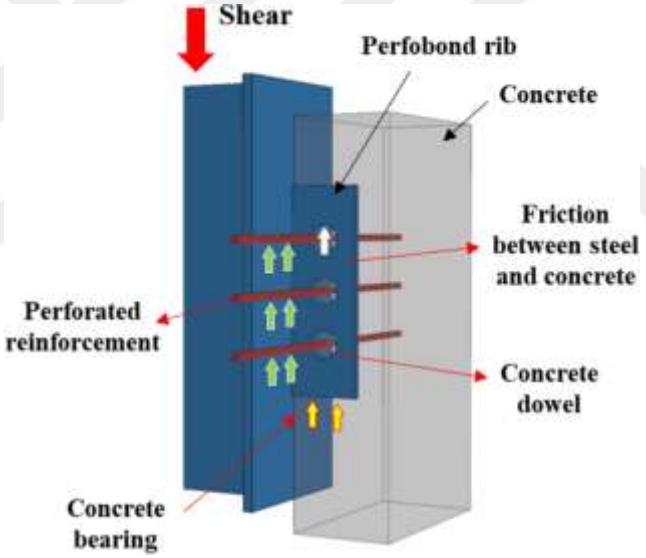

Figure 1.4: Push-Out Test of Perfobond Leiste Shear Connector

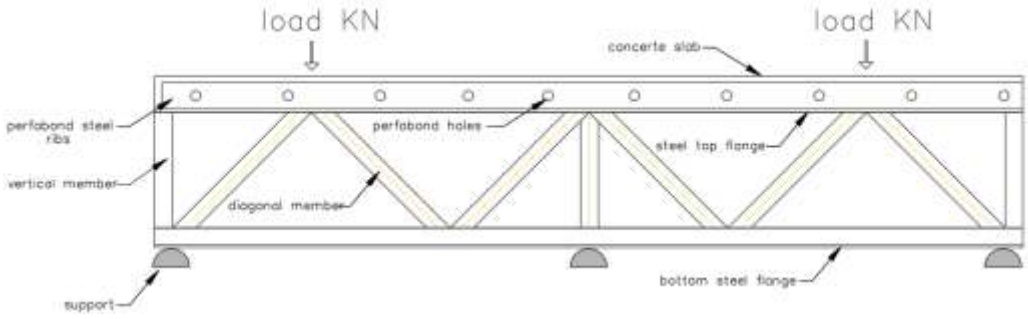

Figure 1.5: Girder Test of Shear Connectors Under Two Points of Load

1.3.4.3 Numerical simulations and finite element analysis (FEA)

Advanced computer programs are used for detailed simulations of shear connector behaviors in different loading conditions, in which it is possible to model the design of the shear connector and all the composite parameters, including the applied loads, to predict performance without extensive physical testing.

1.4 Double Composite Truss Continues Girder

Composite works are widely used worldwide in many structural forms with different span lengths, especially for long spans, such as the highway long bridges, railway bridges over river or valley, footbridges, etc.

Composite steel girder gives more efficiency and certified results, especially for bridges with long spans around 60-120 meters, and over 120 meters for the very long span bridge meets the seismic requirement factor in their designs [14].

The main advantages of continuous girder are the high load resistance with greater stiffness than the steel or girder concrete as a simply supported system and less deflection.

Most of the designs of the composite steel girder in the simply supported bridge meet the requirement of positive bending moment and the ultimate loading capacity, where the resistance of the forces will be by the compressive strength of the concrete elements and tensile strength resistance of the steel truss frame. In continuous superstructure bridge at the support piers zones the positions of the forces are reversed, Figure 1.6 illustrated where the tensile forces are at the top refers to negative bending moment and the compression force is at the bottom refers to positive bending moment and for composite beams may not be fully satisfied in this situation due to high negative value at the top concrete surface [22].

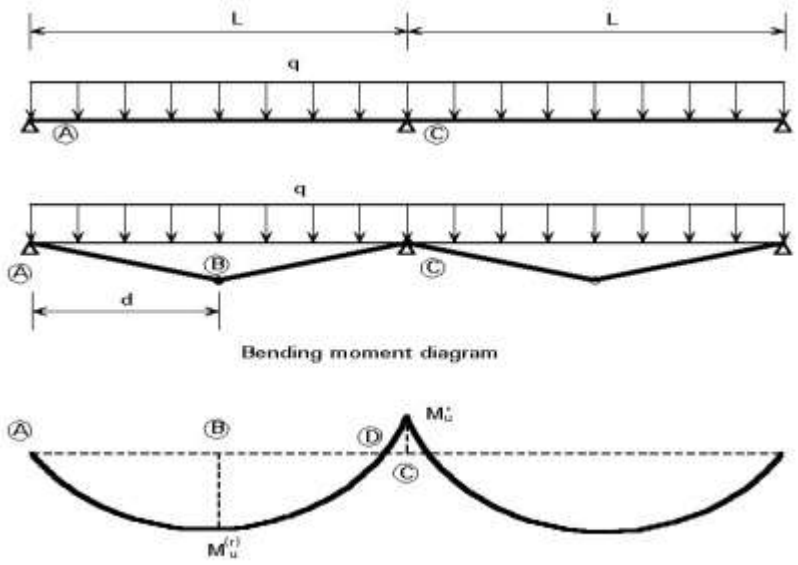

Figure 1.6: Hogging Moment Distribution at the support Regions of Continuous Girder

In the situation of concrete bridge deck slab being under a tensile force that led to several types of cracks, which it called cracks of the negative moment zones; however, this type of failure will cause the appearance of fissures in the asphalt surface, which subsequently increases the descent of rainwater into the concrete and then into the shear connector system.

This issue reduced the permanence of the interconnection between steel and concrete which in turn leads to other modes of composite girder failures [16].

Double composite truss continuous girder, Figure 1.7 which at this research study consisted of several features as listed below:

1. The composite girder with top and bottom steel flange.

2. The steel frame is formed as a steel truss type to reduce the dead load.

3. The perfobond leiste shear connector steel plate connected to the top and bottom of the girder flange with welding or by bolts connection with high shear flow resistance.

4. The steel ribs plate consists of holes with a specific diameter, a steel bar passes through these holes, the rein bars will bond with a reinforced concrete that is poured surround the perfobond steel plate in the top and bottom flange.

5. Top and bottom concrete elements with a certain width and thickness.

These double composite parameters listed above are conducted to resist failure modes of concrete cracks created by the negative bending moment zone (hogging moment), where this girder will be designed to resist the case of force inversion.

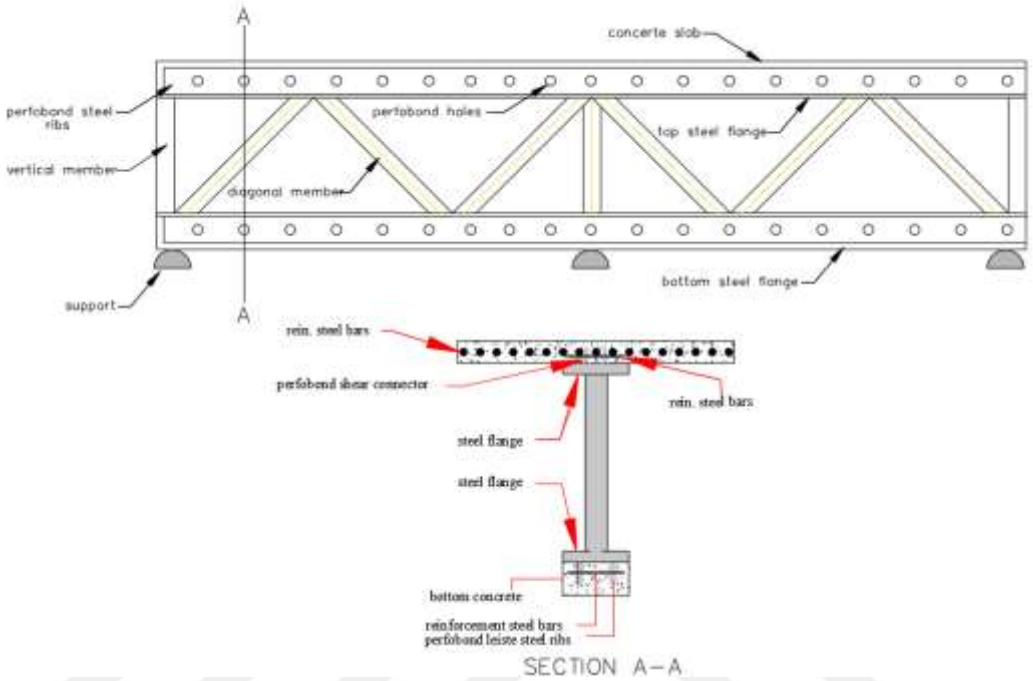

Figure 1.7: Typical Double Composite Truss Continuous Girder. (a) Girder Side View, (b) Composite Girder Cross- Section

1.5 Thesis Objective

This research's fundamental objective is to create a special model of a continues composite girder and make the experimental loading tests to analyze the model response and get the information data about the relationship of the slip ratio in the interface of connection, uplift resisting under different external force stages, resisting capacity and anti-crack characteristics of the concrete slab bridge in negative moment zones at the supported piers of mid span.

Beams are assumed to be double composite trusses girder that continues over mid-support to create the phenomena of the hogging bending moment and the positive sagging moment at the same time.

The Abaqus CAE software program results will be validated with the experimental study to analysis the omposite steel-concrete truss girder with the consideration of:

1. Determine the dimensions properties of the perfobond lesite by doing push out test for three individual samples, the results will make a vision of the shear connectors response and contribute with the final perfobond lesite design in the main composite girder samples.

2. The effectiveness of the variables of shear connector length, thickness, and plate holes on the load-relative slip ratio and the interface uplifts.

3. A composite bond, which refers to the ductility of shear connectors, will explain their ability to undergo significant plastic deformation before failure.

It indicates how much the shear connector can deform without losing its ability to transfer shear forces between the steel elements and the concrete deck in a composite structure.

A high ductile shear connector can resist higher shear flow, enhancing the composite beam's overall performance and safety under a specific applied load.

4. The effectiveness of the double composite girder on the hogging moment value and cracks resistance compared with the single composite girder at the mid supports.

5. The effectiveness of the double composite on the deflection ratio at the sagging regions, which are affected by the positive moments.

6. Analysis of all continuous girder samples according to modes of failures and strength capacity.

1.6 Thesis Layout

The methodology of the research topic strategies will be divided into seven chapters as illustrated below:

For chapter one, a brief introduction presented the type of shear connector that has been used in the composite member and its action behavior, the type of double composite girder and the causative problem for its specific design.

Chapter two, literature review of the previous research with the main same problem and its results.

Chapter three, a detailed study of double composite truss continues girder bridge specification will provide mechanics of work, general characteristics and case study example of long span double composite truss bridge illustrates the method of bonding and dimensions of all sections.

Chapter four illustrates the experimental applications on eight samples of single and double composite truss girders using perfobond leiste shear connectors that depend in the design methodology on the push-out of three samples and its fabrication steps at details.

Chapter five, deals with the Abaqus CAE software program to simulate the single and double composite continues truss girder with same experiential study dimensions and specifications to make validation study and compression the results according to the values of the stress-strain curve, load- deflection and modes of failures of eight specimens designed and acting as the same behavior of the entire actual long span composite bridge of the case study.

Chapter six, the results of the samples simulated by Abaqus program and the experiment study test results will be illustrated in detail in this chapter.

Chapter seven, detailed discussions of all the results and conclusions with relative recommendations, and suggestions for future studies are present.

2. LITERATURE REVIEW

2.1 Introduction

This chapter will review and describe prior studies concerning the behavior and strength of steel girders and composite steel-concrete girders subjected to hogging bending moments in continuous long-span bridges.

There are a few exist of literatures that concerning the composite member related to the double composite truss girder, to ensure the safety and integrity of the structure.

The main aim is to highlight key findings, methodologies, and gaps between past related research including analytical methods, numerical simulations and experimental investigations.

2.2 Review of Composite Girder

Weiwei lin (2011), Experimental study has been conducted investigation about the composite girder's performance according to hogging moment using different types of shear connectors such as shear studs and PBL in situation of applied loaded to the maximum state.

The results of this research suggest that the implementation of PBL improves the stiffness of the composite girder under both serviceability and ultimate limit states more effectively than stud connectors, based on the experimental load-displacement relationship; however, the stud exhibits superior mechanical properties at initial cracking .

The initial crack-load has been determined due to the most higher negative bending moment of composite girder, and it's gotten higher than the test results, even if in low load stage the composite beams suffer from cracks under negative bending moment, moreover, the calculated ultimate loads were closer to the experimental results.

The position of the neutral axis for the composite girder may have been affected, it seems to be moved between a range of elastic neutral axis and the plastics neutral axis.

The main decision has been made to disregard the effective of reinforcements strain hardening, however the situation of crack closure it was noticed in all laboratory-tested samples, the crack size has been the same as it's get found the crack spacing on the RC slab, these test results had been obtained from using six composite girders with three numerical models to simulating the exact kind of composite girders [22].

2.3 Review of Continuous Composite Girder under Hogging Bending Moment

Fahad Alsharari (2022), Examine the gradual deterioration of stud shear connections by numerical analyses regarding the residual static performance and remaining fatigue lifespan of post-tensioned steel-concrete composite beams. The results demonstrate the impact of stud failure on the shear stress at the beam ends where the stud fracture transpired.

The research shows that the interfacial slip contributed to reducing composite beam performance, where it shows when more studs get fractured lead to loss of the composite action and that increase the maximum compressive and tensile strains at the mid-spans, the remaining bending strength of the non-strengthened sample declined steadily when the studs were removed. Nevertheless, the rate of decrease for the reinforced sample significantly accelerated following the removal of five rows.

Upon the removal of 15% of the rows, the fortified sample exhibited a more advantageous response in terms of stress range, tensile and compressive stresses, and residual capacity; nevertheless, both the fortified and non-fortified samples had similar reactions to stud failure [28].

Chengquan W (2022), A novel steel-concrete composite link slab (SCC-LS) is introduced, a full-scale FE simulation to find the mechanical performance of the SCC-LS and get analyzed with theoretical calculations.

By means of the longitudinal force applied to the steel plate across the longitudinal connecting reinforcement and disperse it to the concrete with avoided

active engagement of the surface concrete in tension zone, the findings indicate to prevent the cracks from developing.

It was observed that when increasing of the steel plate thickness then the tensile strength on the concrete surface is significantly reduced [29].

Chengfeng Xue (2022), This study examined the shear behavior of composite connections by push-out experiments involving various shear connectors, supported by theoretical and numerical studies. The results indicate a distinction in the failure mechanisms among the different types of shear connectors. An increase in the quantity of welded studs and perforated holes boosts shear behavior.

Numerical experiments indicate that shear resistance improves with larger diameters of penetrating rebar and welded studs, as well as with increased concrete strength, generally, the region of compressive damage in concrete diminishes.

Overall, the new composite shear connectors turn out that they have the ability of higher performance than conventional connectors, and for the large-span composite bridges the discontinuous configuration of composite shear connections is suggested to reduce the welding deformation [30].

2.4 Review of Truss Composite Girder

Chisung Lim (2021), A type of truss composite girders was used in this research to verify the shear performance of composite girders, by the results of the crack indicators with failure modes all the behavioral characteristics of the composite girder get obtained with two specimens that named (P) and (W).

The horizontal shear fractures seen along the top chord controlled the shear behavior of the member for the (W) specimen using Pratt truss type.

The diagonal truss member failed to contribute efficiently to the shear resistance mechanism because the screw rod was exposed to shear failure especially at the EST node and that get happened before the diagonal web member arrived its yield strength, it’s noticed that the horizontal shield failure it's the most main failure situation when designing a composite girder, Figure 2.1 [31].

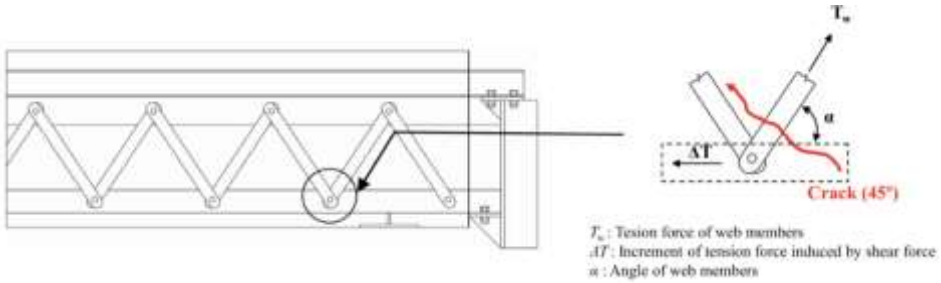

Figure 2.1: Freebody Diagram and the Crack Angle

Source: [31].

Yiyan Chen (2018), this study report presents a novel bridge construction, with the introduction of a composite box girder bridge including CSWs and trusses.

The main example that has been taken and the results show that the transition to the use of the corrugated steel webs and bottom trusses, it's made the self-weight of the structure can minimize and the main objective that can be reached it's to obtain a new structure would saving cost on money of the construction with a simple way of maintaining.

With experimental research results on a scale model shows this type of truss structure under flexural load, have strong ductility and integrity; when the flexural deformations may be separated into an elastic stage, elastic-plastic stage, final phase as a plastic stage , where the main failure can be accord in the bottom of the concrete slap show some transfers clocks because of shifting of natural axis of the cross section of the top concrete slap [32].

2.5 Review of Composite Girder under External Force

Jianqing Bu (2023), The result of static load test and theoretical analysis with two overhanging beams using MURSP connectors and ordinary studs shows how many different in deflections crack and slip especially in the negative moment region. This research presents modified and upgraded uplift limitations and slip permitted MURSP connectors.

The tensile stress off the concrete in the composite beam with MURSP can be unleashed, therefore, increasing the crack load capacity, moreover this type of connector shows more improvement behaviors and negative moment region and doesn't show any slip fader until the earlier load stage, the main disadvantage could be noticed in the weakness of bond between steel beam and the concrete slab.

The flexural stiffness of the composite beam with MURSP connectors get reduction with 3.08% if it's compared with ordinary stud connector.

The finite element analysis of two beam specimens with stud and MURSP connectors Shows a different result in synthesis and deformations in the negative bending moment region under the same load [33].

Kai Peng (2022), This research determines the shear capacity of PBL shear connectors in the composite member by experimental and numerical simulation.

Nevertheless, the results indicate that the PBL shear connection may be enhanced in terms of bearing capacity, ductility, and shear stiffness in SFRCC compared to NC samples, where the ultimate shear bearing capacity can be obtained for one hole in the PBL steel plate shear connector depending on the paradigm meter through the hole on the numbers of holes on strength of concrete.

Show on the specimen with single hole we can find the failure in the reinforcement bar however and the other specimen when we get strong the sheer capacity of bar by doing a multi hole so the fader can be obtained and illustration by cracking the concrete, multi factors will effect of the sheer capacity of PBL shear connectors such as SFRCC strength, steel plate opening diameter size and thickness.

For calculating the ultimate shear capacities of the PBL shear connector in SFRCC was proposed as below:

$$P_U = 6.76nA_{pr}f_y + 3.16nA_{cd} \cdot f_c \cdot \left(1 + 0.17V_f \frac{L_f}{\neg_f}\right) + 3.72A_{eb} \cdot f_c \qquad (2.1)$$

Overall, a push out test was needed with a numerical simulation to be made compared study with the experimental work [34].

Zhou Fan (2022), the main objective in this paper is to find the mechanical properties in the negative bending moment region of a new proposed girder steel-ECC composite girder that implementation with corrugated webs.

The experiment and numerical analysis result gave indications that the steel girder doesn't have a slip failure during the loading process, moreover, all specimens had the same failure mode and that illustration with the cracks on concrete slab with buckling in the bottom flange of steel girder.

This research compared the result of this type of girder with flat webs, and the result that obtained from that the stress was clear of each component of composite girders with corrugated webs.

And by using ECC instead of NC as the bridge deck slab can improve the crack performance and range control, moreover, The ECC type has enhanced the flexural load carrying capacity and rigidity by 6.04% and 10.54%, respectively.

Numerical simulation has been used to investigate the influence of ECC slab, so when the ECC material strength and slab thickness size increases it can be observed instantly rising flexural bearing capacity of the composite girders [35].

Yongjian Liu (2015), This is the main related research to our thesis which includes a new type of composite tubular truss bridge and more detail about the specification of design, where bridge superstructure is double composite section, it's continued of rectangular tubular chords with filled-concrete and prestressed concrete slab.

The main objective is to reach the goal of improving local strength and fatigue performance which leads to improving the performance of girders under hogging moments region and prevent the crack from occurring.

Though the hollow tubular truss gets results as the joint with PBR design punching shear is around 22% more than the joint without PBR, so that result lead us that the PBR has a special parameter of an enhancement the concrete performance [36].

Aiming Song (2022), the primary objective of this study is to determine the regular crack spacing in the negative moment zones of the continuous composite girder.

Many parameters are playing a main role in indicated the crack width such as, concrete cover, diameters of longitudinal tensile bars, tensile reinforcement ratio, spacing of stud connectors.

The novel model has been obtained from previous research that had been taking 38 specimen tests to find the influence factor of average crack spacing.

However, the experimental test has been done in this research to obtain the crack width under fatigue load situation, the result compared with the theoretical result.

The main result could be from the modified formula of crack spacing, when it showed that transfers reinforcement made a huge influence, compared with the empirical formulas for crack width under fatigue loading.

The analysis results show more consent with the measurement width of experimental test.

Three formulae suggested as average crack spacing prediction for the negative moment zones of continuous composite girders are shown below [37].

$$\mathrm{I_{cr}} = 2\left(c_s + \frac{ls}{10}\right) + K_1 K_2 \frac{d_{eq}}{p_{te}} \tag{2.2}$$

$$\mathrm{I_{cr}} = 1.1\left(2.7c_s + 0.11\frac{d_{eq}}{p_{te}}\right) \tag{2.3}$$

$$\mathrm{I_{cr}} = 1.1\left(1.9c_s + 0.08\frac{d_{eq}}{p_{te}}\right) \tag{2.4}$$

Where: lcr is normal average crack distance, k1 is a coefficient of bonding performance for longitudinal tensile, k2 component stress distribution's effect coefficient, cs is the thickness of concrete cover for reinforcement, while ls and la are the longitudinal bars and transverse bars spacing ratio, respectively, deq comparable diameters of longitudinal tensile specimens, dHeq is equivalent diameters of transverse bars, ρeq is tensile reinforcement ratio, ρHeq is transverse reinforcement ratio, Rp is combined force ratio, p the spacing of connections.

Hope Gill and Johnson (1976), This research deals with examination of the rotation capacity for hogging and sagging regions in continuous composite beams, by assessing the ultimate flexural strength for each section including the application of simple plastic theory to get information about behavior of the tested continuous beam under some circumstances of rotational and high shear.

The results show it's going to be determined the ultimate strength with the plastic design theory, at serviceability loads stage it can’t be determined the behavior of continuous being by current limits on yielding and cracking [38].

Vinicius Moura de Oliveira (2022), This research takes account to analysis that composite cellular beams with hogging moment loading, to get that data according to elastic and inelastic behavior.

ABAQUS software program has been used to analyze with finite element model, the result shows that the composite steel concrete member and hogging moment region exposed to and many failure such as lateral distortional buckling (LDB) and web post buckling (WPB), while the formation of plastic mechanism on the web-post, the LDB can't be identify as the lateral displacement with a rotational of the lower flange of the steel elements moreover the WPB can be define as the failure of the shear stresses it's shown as a double curvature at web post as (S) shape [39].

Hamoda and K.M.A. Hossain (2017), Static hogging moment applied on a composite girder consisting of steel I-shape type and concrete slab until the failure mode, this research take four specimen girders, named as (CG-1, CG-2, CG-3, CG-4).

Furthermore, for the fourth girder (CG-4), the utilization of SFRC end slabs linked by embedded steel bars extending into a 200 mm wide ultra-high performance fiber reinforced concrete (UHPFRC) closing strip at the peak moment zone has been proposed.

The research results show that it is a significant failure for all the specimens according to the local buckling influenced by the compression flange of the steel beam.

Also, a compressive cracking of the concrete slab, are your situation has been noticed at the maximum moment location in the steel reinforcement and the steel beam. Many decisions have been taken to enhance the behavior which include use ECC or SFRC for the deck slab, this option sure a higher elastic stiffness about 12% and 23% [41].

The below equation used as based on a normal concrete composite girder not considering any other addition, Figure 2.2 to Figure 2.4 [41].

The yield moment (My) was calculated based on Eq.

$$M_y = \frac{I_{GG} f_y}{Y_{topsteel}} \tag{2.5}$$

Where: fy is steel yield, ICG is elastic moment, Y ts is the distance from the top bars

The ultimate moment (Mu) was calculated based on Eq.

$$M_u = \sum(PY_{pl}) \quad (2.6)$$

Where: P is forces of the tensile or compressive, Ypl = distance between forces to the plastic neutral axis.

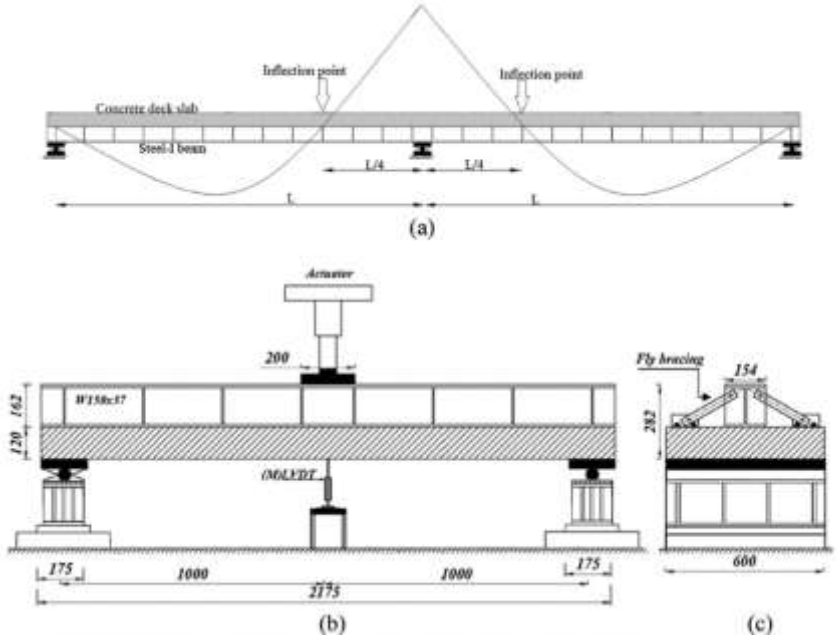

Figure 2.2: Dimensions of the Girders: (a) Regions of the Negative Moment, (b) Specimen 's Side View, (c) Girder Section (d) Test Installation Method [41].

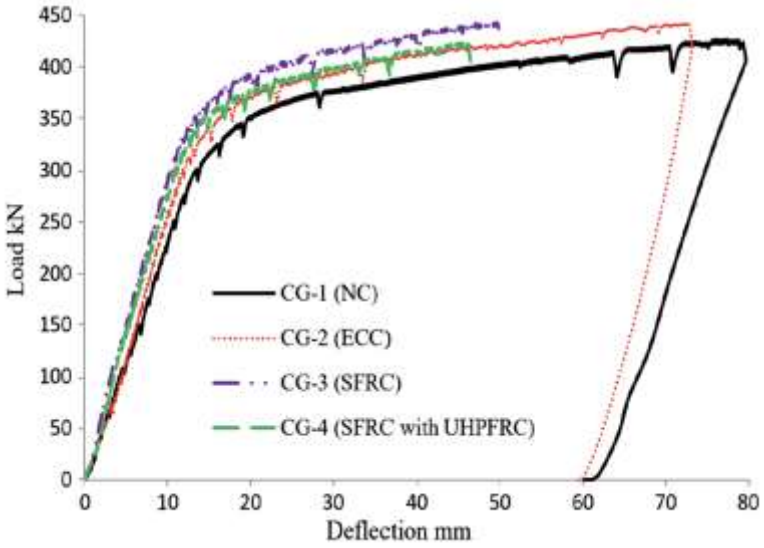

Figure 2.3: Load-Deflection Relationships [41].

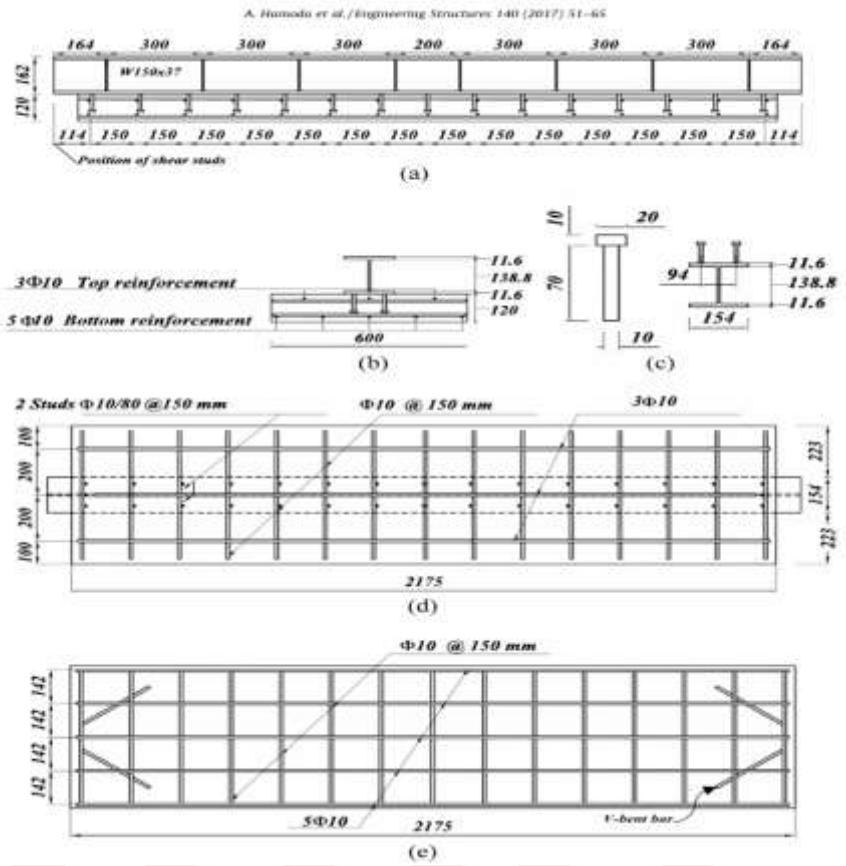

Figure 2.4: Details of the Continuous Composite Girders, (a) Girder Longitudinal Section, (b) Front View Cross Section, (c) Shear Connector (d) & (e) Reinforcement Bars Distribution [**41**]**.**

Guanxu Long and Ruigen Zho (2022), Present a new type of UHBC-RC composite steel concrete analyzed with experimental work and finite elements analysis program.

The result shows the addition of UHPC–RC composite deck can increase the properties of concrete to resisting the cracks in the hogging moment zoon and we got a more crack resistant value when increasing UHPC layer thickness [42].

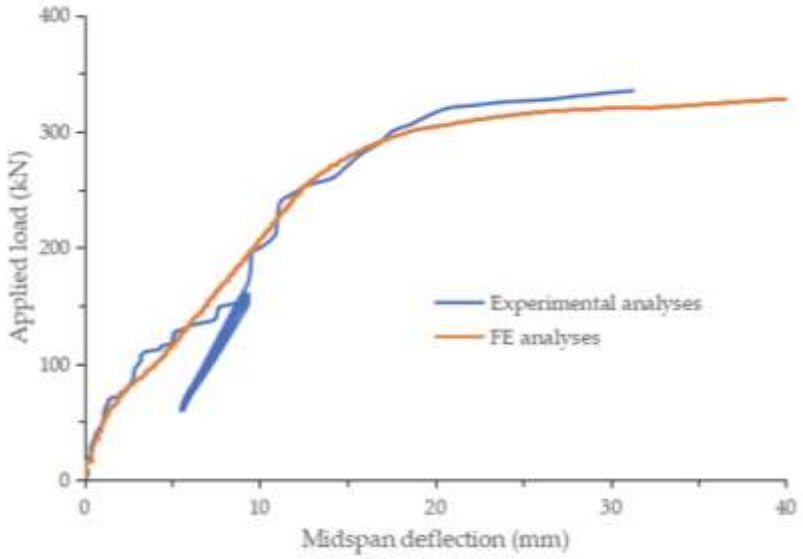

Figure 2.5: Deflection Ratio of the UHPC Layer Ratio [42]

Jae Kang and Jong Park (2014), This research focuses on increase the strength of concrete that used in the perfobond rib connector, depending on the push out test to get the results of the sheer strength of the sheer connector. However, many literatures review has been showed a crack failure mode in the concrete of the shear connector element when reinforcement bars and the perfobond rib hole get increasing.

Using compressive strengths of 80-180 MPa, the ultra-high-performance concrete type is the one that this research is aiming to adopt.

The experiment result revealed the concrete dowel action in the holes of the perfobond rib didn't make any difference for the shear strength at 180 MPa specimens, on other hand the opposite happened where increasing get noticed.

Among the prediction models which indicated the increase trend of the shear strength for the experimental results, the formula proposed in this study provided the most accurate predictions, Figure 2.6 to Figure 2.8 [26].

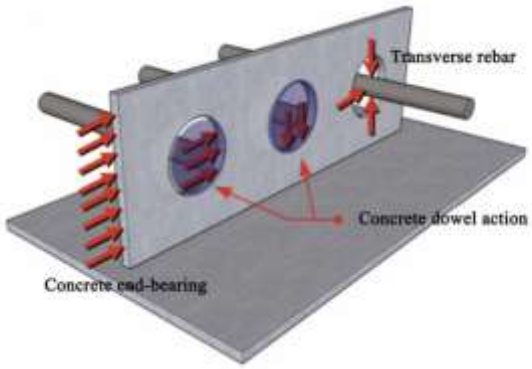

Figure 2.6: The Process by Which Perforated Ribs Withstand Shear Stress [26].

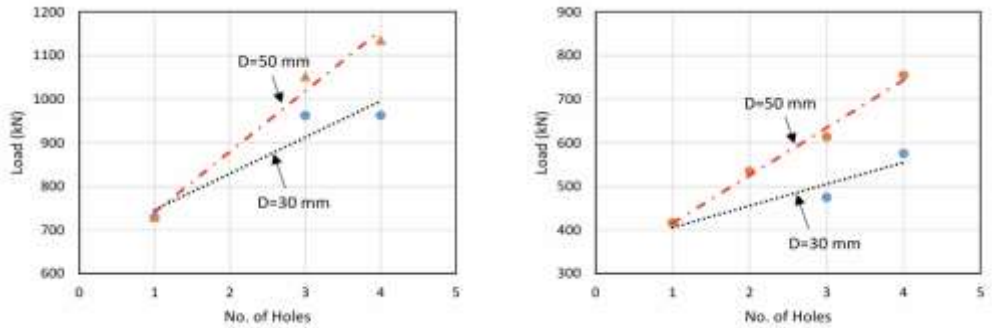

Figure 2.7: The Relationship between the Number of Holes and Shear Strength for the 180 MPa and 80 MPa [26]

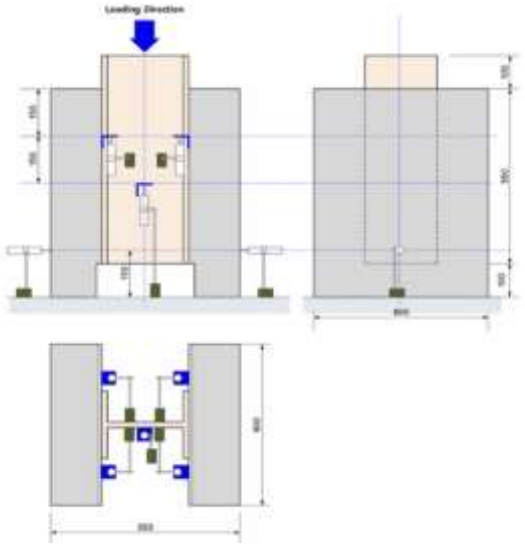

Figure 2.8: Layout of Displacement Sensors [26]

2.5 Previous Work Conclusion

From the illustrated literature review that has been conducted in this chapter, where it can notice that most of the previous experimental and modeling simulation works deal with several types of composite beam and mechanism behavior of the specimen under various types of loads to find the optimum solution as anti-crack methods in the region of hogging moment specially in the continuous composite beam.

The previous works conduct the ability of perfobond leiste to resist a high level of loads especially at the push test which is contribution of support the listed advantage of this shear connector type which are used in this research.

Even many equations that listed to predict the shear connector strength and it gives accreted results when it's compared to the experimental and finite elements simulations by software programs.

However, it's noticed that a rare, published works deals with the double composite girder to solve the hogging moment failure mood situation especially for truss type, and this is one of the fundamental reasons for choosing the current research study title and Based on all the results of previous research.

3. DOUBLE COMPOSITE TRUSS GIRDER FOR LONG SPAN BRIDGES USING PERFOBOND LEISTE

3.1 Introduction

In this chapter, the main objective for designing an analysis of the double continues composite girder will be illustration considering the main resource and specification, including the failure mode under the static load situation and specially for hogging moment and sagging moment force and how it effects on the composite steel- concrete girder element.

In a statically indeterminate construction like a continuous span, the portions at intermediate supports must withstand a relatively significant positive bending force.

Appropriate for construction foundations, a continuous span bridge has a somewhat high span capacity, where the three structure system showing at the Figure 3.1 (C) cantilever bridge type with a larger span capacity than that of a (A) simply supported bridge type, but the continuous bridge Figure 3.1 (B) has the most span capacity than the other system.

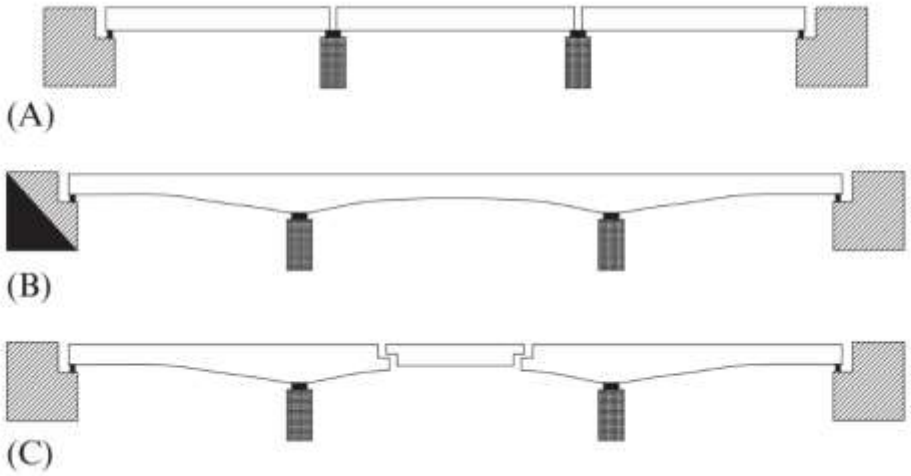

Figure 3.1: Bridge Support System

3.2 Continues Composite Girder for Long Span Bridge

Complex design is the main disadvantage of the continuous span, the actions on the any span will affect om the adjacent spans, and the most noted behavior is hat stiffness and bending resistance of the composite beam will be vary along the entire beam even if it's geometrically uniform due to cracking ratio of concrete and effective width of slab above the steel elements and essentially the variation in longitudinal reinforcement of the deck *slab* [10].

Additionally, it's very hard to predict the actual stresses and deflection in the continuous beam and the significant tension stress occurs only in hogging regions in the middle supports, the amount of these stresses influenced by the methods of construction.

The reaction to a specific series of activities is contingent upon whether it occurs before to or after to another series of events that induces cracking in a distinct section of the beam, and because of that the design will be depend on the ultimate strength method for predicting the all beam response and it can be checked by the experimental test or on the elastic theory calculations [10].

3.3 Hoggin Bending Moment

In a composite girder, the tensile force will be appearance at the top point of the concrete slab above the steel member, and as from the concrete weak against the negative moment then crack will occur.

The estimation of crack position and amount will be difficult, all the composite beam behavior and involves of first cracking outlined in the stress–strain diagram shown in Figure 3.2 [24].

In the first the concrete will be uncracked, and then at a load reaches (Nct) the concrete crack (line O–A), second at loads exceeds (Nct) to the (1.3Nct) further cracking occurs and force is transferred to the reinforcement bars (line A–B).

$$N_{ct} = A_c f_{ct} \tag{3.1}$$

Where: fct =is the tensile strength of concrete, Ac is the concrete section area.

From (1.3Nct) and (2.0Nct) the load will be transported by the tension stiffened section (line B–C), having an effective stiffness bigger than the reinforcement only and less than the concrete section (factor of k included):

$$(EA)_{\text{eff}} = kE_{\text{s}}A_{\text{s}} \tag{3.2}$$

$$k = \frac{n\rho + (1-\rho)}{n\rho + 0.6(1-\rho)} \tag{3.3}$$

Where: n is the modular ratio of the steel modulus elasticity over concrete modulus elasticity, r is the reinforcement ratio (r = As/Ac).

At load more than (2Nct) is assumed to be carried by the steel only until its ultimate load (Ns) (line C–D–E) in this stage the tensile forces in the slab will be more than (2Nct) the situation of fully cracked concrete section [24].

$$N_S = 0.87A_s f_{ys} \tag{3.4}$$

$$A_{s2} = 1.0A_c/100 \tag{3.5}$$

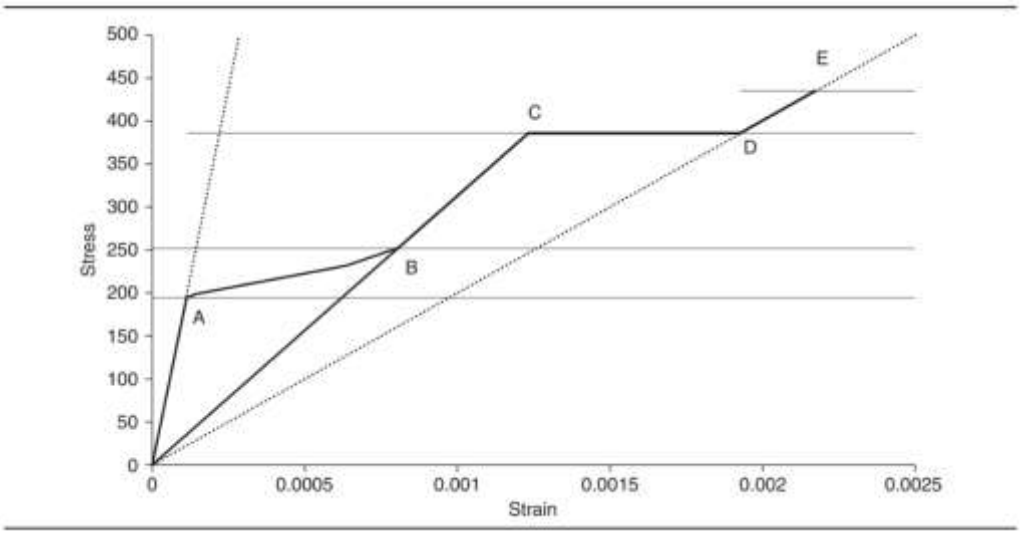

Figure 3.2: Stress- Strain Diagram Cracked and Tension of Slab Under Tensile Force [24]

Effective cross-sections of beams are relevant, the effective width of the upper concrete flange is ununiform along the beam length, it's bigger in the mid-span than the internal support, so the main definition of the width is when the longitudinal reinforcement bars in deck slab contribute to the hogging moment resistance, the position of the plastic neutral axis (N.A) at must situation lies below the slab so the

web enclosing is the only section that made a contribution from concrete parts at the compression region.

EN 1994-1-1 code, the effective width for the hogging bending moment region length can be illustrated as effective span (Le), it's equivalent to one-quarter of each span and from this concept the support piers of the bridge between spans of length (L1) and (L2) as shows at a, Equation 3.6.

$$b_{eff} = \frac{\left[\frac{(L1+L2)}{4}\right]}{4} + b_0 = \frac{l1+l2}{16} + b_0 \quad (3.6)$$

3.4 Plastic Moment of Resistance Capacity

A composite girder section of an in positive bending is shown in the details at Figure 3.3, the steel bottom flange in cross-section in compression.

To categorize the steel web according to the distance after determining the (xa) which is the distance from the plastic neutral axis to the (G) the centroid of steel section,

The design tensile force in this reinforcement will be:

$$N_s = A_s f_{sk} / \gamma_S = A_s f_{yd} \quad (3.7)$$

Where: fsk is characteristic yield strength of steel, As is the area of longitudinal rein bars and beff is the deck slab width.

While the steel segment alone would provide bending resistance in the absence of tensile reinforcement:

$$M_{pl,a,Rd} = W_a f_{yd} = N_a z_a \quad (3.8)$$

Where: Wa is the plastic section, fyd = the yield strength capacity, Na is stress of depth of half(ha).

Stress distribution in the depth (xa) of steel web, where (xa) is given by:

$$x_a t_w \, (2 f_{yd}) = N_s \quad (3.9)$$

From this situation the moment of resistance (M_{Rd}) equal to:

$$M_{\mathrm{Rd}} = M_{\mathrm{pl,a,Rd}} + N_{\mathrm{s}} z \tag{3.10}$$

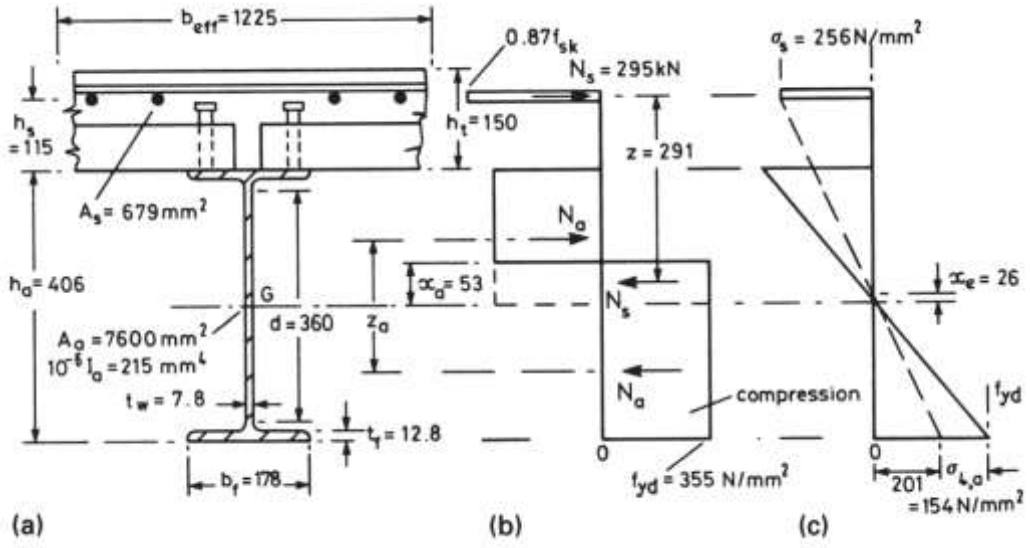

Figure 3.3: Stress Distribution for the Composite Section at Hogging Moment

3.5 Elastic Moment of Resistance

At this point the inelastic behavior of the steel before the plastic moment of resistance will cause hogging bending moments (Ma,Ed) in the steel elements alone and (Mc,Ed) for the composite member, so negating all the effects of creep, shrinkage, and temperature.

The distance (xe) above that of the steel section for the elastic neutral axis of the composite section Figure 3.3(c) can be determined by taking first moments of area about the axis.

$$x_{\mathrm{e}}(A_{\mathrm{a}} + A_{\mathrm{s}}) = A_{\mathrm{s}}(h_{\mathrm{a}}/2 + h_{\mathrm{s}}) \tag{3.11}$$

The composite section's second moment of area is:

$$I = I_{\mathrm{a}} + A_{\mathrm{a}} x_{\mathrm{e}}^2 + A_{\mathrm{s}}(h_{\mathrm{a}}/2 + h_{\mathrm{s}} - x_{\mathrm{e}})^2 \tag{3.12}$$

3.6 Vertical Shear and Moment-Shear Interaction

In general, the vertical shear force gets opposed by the web part of the steel beam or in our study by the truss members, the shear area (Av) for such a section is given in EN 1993-1-1 [15]**:**

$$A_v = A_a - 2b_f t_f + (t_w + 2r)t_f \tag{3.13}$$

Von Mises yield criterion, the shear resistance is determined from count that the yield strength in shear is fyd/$\sqrt{3}$ and whole area (Av) can be equal to this stress:

$$V_{pl,a,Rd} = A_v(f_{yd}/\sqrt{3}) \tag{3.14}$$

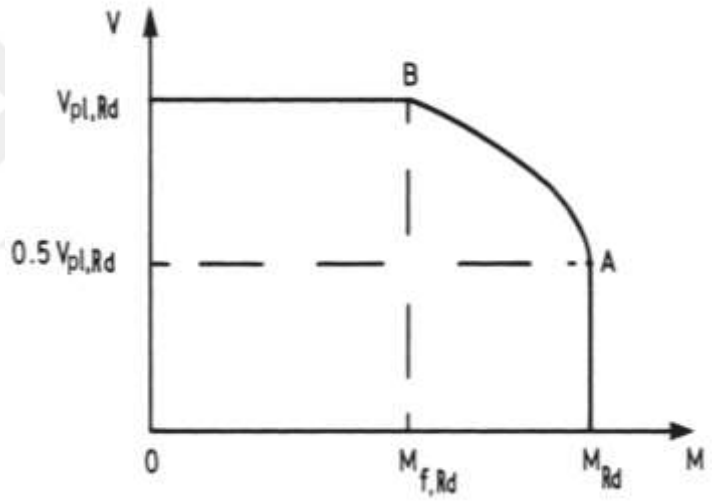

Figure 3.4: Section Resistance for Bending and Shear Forces

3.7 Longitudinal Shear Force

Longitudinal shear force generated at the continuous beams and cantilever's structure system, the span with uniformly loading along its length, the critical cross-sections will be at the supports at maximum hogging moment, and at the section of maximum sagging bending moment (positive moment)

Where a full shear connection is assumed in areas of hogging moment and may be spread equally between a support and the critical section at mid-span and for that the number of shear connectors necessary for a normal critical span length.

$$n = (N_c + N_t)/P_{Rd} \tag{3.15}$$

Where: Nt is tensile force for negative moment resistance, Nc is compressive force at mid-span, PRd is shear connectors resistance due to the shear flow.

3.7.1 Mechanisms of longitudinal shear transfer

Depending on whether the element is initially fractured or uncracked, the technique of longitudinal shear flow is applied from the shear connections inside a composite girder to the reinforced concrete component.

3.7.1.1 Initially uncracked reinforced concrete

Regarding the shear force transmission mechanism of an originally uncracked reinforced concrete, Figure 3.5 describes on the reinforced concrete slab, the sample (F), which indicates the longitudinal shear forces applied by the shear connections to the surrounding reinforced concrete.

As extremely obvious in area A, the element generates diagonal tensile stresses with loading applied via distortion, when this rotation enlarges the width of the elements (B-B); consequently, the tensile stresses will be conveyed to the transverse reinforcement.

Thus, the shear connector strength of an initially uncracked reinforced concrete element relies on both the strength of the transverse reinforcement and the strength of the concrete [10].

3.7.1.2 Initially cracked reinforced concrete

Mechanical aspects for shear connectors are transferred through a crack in a reinforced concrete element is illustrated in Figure 3.6, the transverse moments that will be generated on the deck slab of composite structure made these longitudinal cracks which is pointed on the shear force position and all the shear perfobond ribs get damaged along these specific crack line [10].

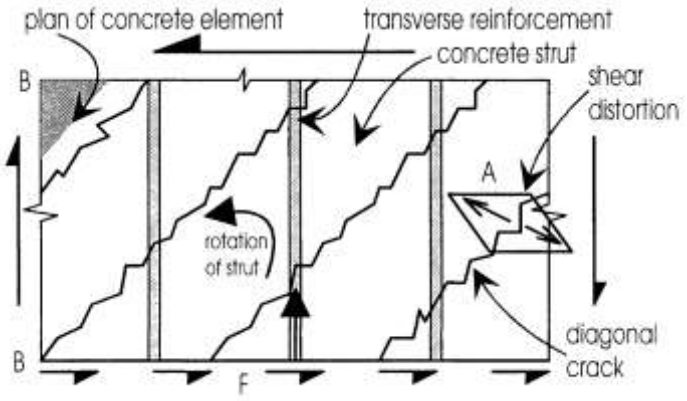

Figure 3.5: Initially Uncracked Concrete

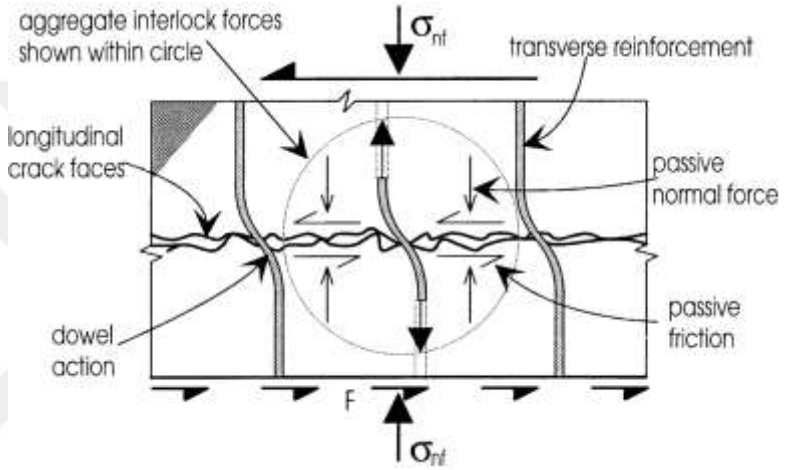

Figure 3.6: Initially Cracked Concrete

3.8 Calculate of hogging moment capacity for the composite girder

The hogging moment capacity (Mhog) of the composite girder can be reduced by the reduction factor (κ) at the full interaction situation shear connection, consider the stress distribution shown in Figure 3.7(a).

So the curvature in the steel section (κ) given by:

$$\kappa = \frac{M_{bs}}{E_s I_s} \tag{3.16}$$

Where: Is refers to steel section due to second moment of area value.

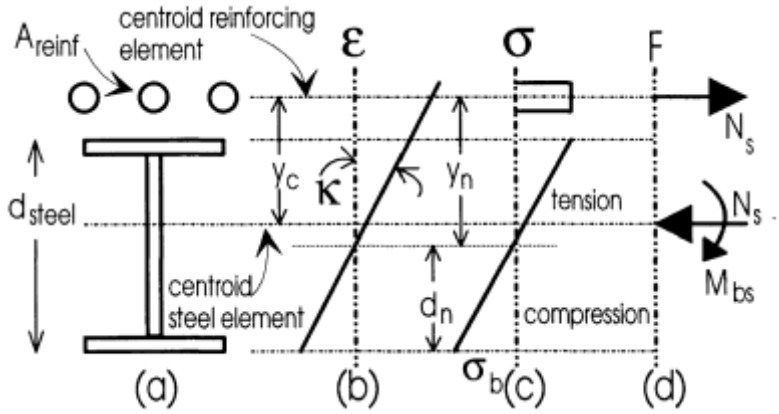

Figure 3.7: Steel Stresses At Non – Compact Girder

The hogging capacity (Mhog) for composite girder if the reinforcement is at yield stage:

$$M_{hog} = M_{bs} + y_c \, A_{reinf} \, f_{yr} \tag{3.17}$$

Where: yc is the distance from steel section to the centroid of the reinforcing bars. The hogging capacity (Mhog) for if the reinforcement below yield stage:

$$M_{hog} = M_{bs} + \frac{y_n \, M_{bs} \, A_{reinf} \, y_c}{I_s} \tag{3.18}$$

3.9 Local buckling

It's a kind of failure type that happens at flanges and web at compression status where the steel parts in a composite structure beam may buckle locally for the sagging and hogging bending regions [19].

As shown in Figure 3.8, first at the positive bending regions the neutral axis position will be below the steel web, so the top flange is subjected to compressive stresses and the local bucking may occurs, the presence of the concrete slab connected with the top flange by shear connectors will reduce this case of failure, in other meaning this failure could belong to many situations of the full plastic moment [19].

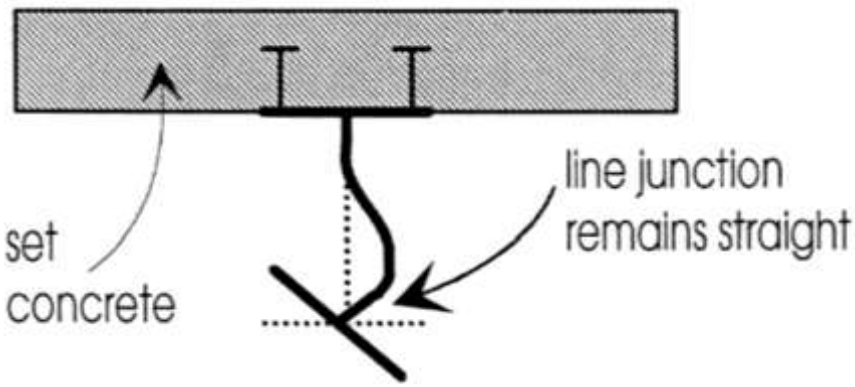

Figure 3.8: Local Buckling Deformation

Second in the hogging moment regions, local buckling can occur as shown in Figure 3.8 which is in situation that the web had distortion and rotation to the bottom steel flange, and the quantify method of local buckling will depend on web cross section which including the depth to thickness parameters, and the position of the neutral axis at the composite section, it's worth noting that to study the effect of the double composite on reducing the local buckling ratio.

3.10 Degree of Interaction of Composite Girders

As a case of a composite girder with oiled interface of steel and concrete this lead ensure that is no interface shear forces to restrict the interface slip of these two components by assuming there are no separation so that the curvatures are the same response, with this case the Fcon = Fsteel = 0 and the composite component of the flexural resistance Fcon (hc +hs) equal to zero.

This situation of process with two flexural members of the same curvature degree so any applied moment on this section will be internally resist by the concrete element flexure Mcon and the steel element flexure Msteel each part as one element, for instance, the strain curve for this arrangement illustrates in Figure 3.9(a).

If there is no resistance to the shear flow at the interface surface this mean to as no-interaction situation, if the slip for the interface surface has totally prohibited as in Figure 3.9(b) this case can reach when the two elements are perfectly connected together at the interface, the 8C = es and the slip strain equal to zero this situation considered as full interaction, for the case three as referred to Partial-interaction, as shown in Figure3.9(c) [19].

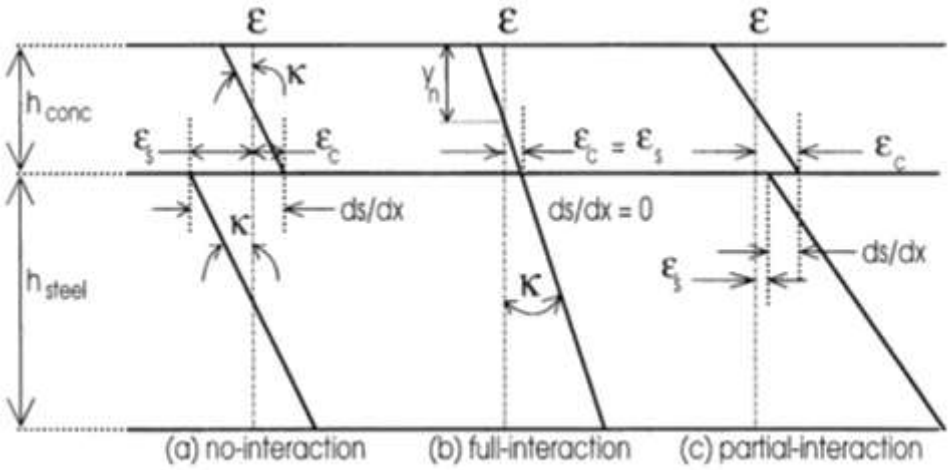

Figure 3.9: Degree of Interaction

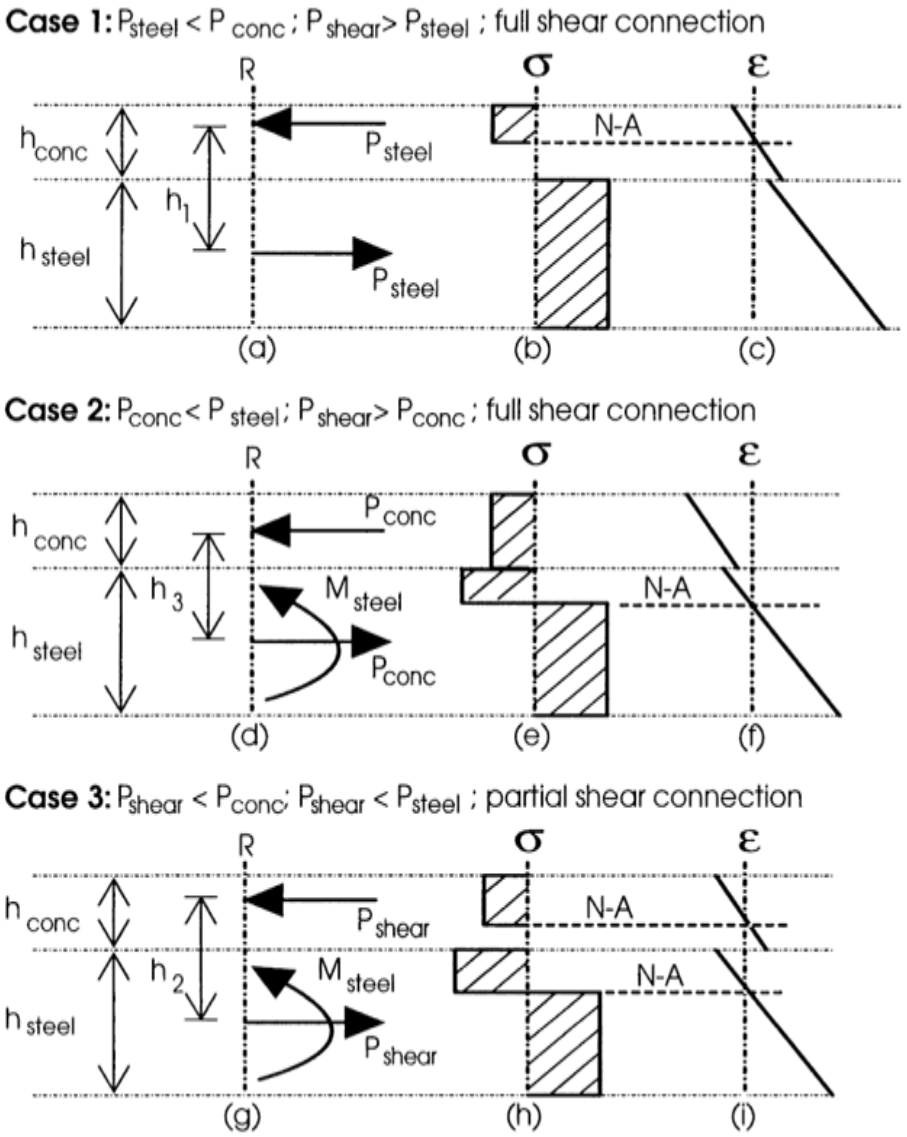

Figure 3.10: Degree of Shear Connection

Where the stiffness of the shear connectors and the strength force they provide determine the degree of shear connection in a composite beam, for example, the degree of connections get effected by the number of the connectors and it's bond system, the failure mode will be reduced in way of get high sufficient ductility of components which it's related to the relative slip of movement due to the external force [25].

More information about the interconnection between the degree of shear connection and the degree of interaction are illustrated in Figure 3.10, the case one to be talked about is the neutral axis at the full shear connection stage it will be below the concrete slab as showing in Figure 3.10(b) this means all the steel and concrete below the neutral axis of the composite section Subjected to tensile strain forces as illustrate in Figure 3.10(c), and about case two, when the neutral axis position at steel element with full shear connection the slip strain amount effected with the strain change of the same sign at compression stage, as show in Figure 3.10(i).

In general, the connection system of two materials in the composite girder at partial shear connection will make relative slip strain bigger than it was at full shear connections.

3.11 Stresses and Deflections Response in Continuous Girders

The bending stresses amount must be controlled to reduce the load-cracking of concrete slab by using elastic global analysis methods, deflections at continuous beams in most situations are much less than in simply supported spans and it's checked for ultimate limit states according to rigid-plastic global analysis.

For continuous beams, the deflection value is increased due to using partial shear connection and can be determined by using this equation:

$$\delta = \delta_c[1 + k(1 - \eta)(\delta_a/\delta_c - 1)] \tag{3.19}$$

Where: δ is the total deflection, k = 0.5 for scaffolding structure and k is 0.3 for unsupported structure, δa is the deflection value for the steel girder, δc was the deflection ratio for the concrete element and at full interaction the ($\eta = 1$) and $\eta = 0$ when it's required low result.

Only in areas with a positive bending moment, known as a sagging moment, is the partial shear connection used, in other hand, the effect of the external forces such as the shrinkage of concrete on the deflections for continuous beams in this way the prediction calculation will very complex due to the bending moments that creating by the movement which is directly proportional to shrinkage as well as in the last sagging curvature and the continuity of the beam it will have an effective effect on reduced the deflection.

The weather effect can be noticed on the deflect of the composite girder when the concrete slab is colder than the steel member due to these two materials having different modules of elasticity and this fracture is very important in beams for long spans bridges.

3.12 Truss Girder Elements

The truss structure elements response as the same reactions steel or concrete beam against the external force, for instance, the truss members connect two forces tension or compression as making triangular patterns, all external forces create internal forces that are connected to each other with connections.

Therefore, bending and torsion moments are typically expressly excluded due to all joints in resisting the axial forces and restricted against rotational motion and this feathering made the truss constructions quite effective, by depending on the strengths of construction the different in force distribution at the section in truss and beam illustrated in Figure 3.11.

The steel or concrete beam, it’s note that the element is exposed to the maximum compression at the top and the maximum tension at the bottom more even the decreeing in stress towards the natural axial are linear path, while the truss member had top and bottom cords are resist the bending moment and the diagonal and vertical members resist the shear forces and Interfere with increasing capacity truss span and high in a truss bridge that has a fixed depth, the top chords are typically parallel.

However, in a truss bridge that has varying depths, particularly in continuous trusses, the top chords may be constructed as inclined members, this system of a

variant of triangles in truss member make it more rigid than the normal beams due to the ability to spread the applied load along the truss length.

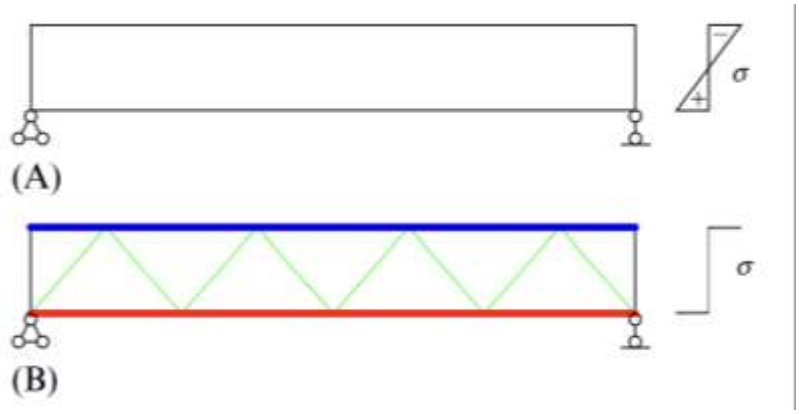

Figure 3.11: Truss and Beam Stresses Distribution. (a) Typical Girder, (b) Truss Girder

3.13 Joints and Connections Methods

The main bond intersection of truss members, where the Joints are the most valuable components and in the truss bridge design criteria, in general, there are two distinct kinds of joints, the first are pinned connections and second gusset plate connections used in the truss bridges construction industry.

For the pinned connection, it's needed to connect two or more members together by big metal pin for the past construction bridge and for the modern truss bridges the connect system of members is made by using metal gusset plates, the use of any method has a significant impact on the way the bridge structure response and the method of analysis and design however, the structures are statically indeterminate and the stress analysis is complex [9].

3.13.1 Welded joints

The full capacity of the beam is required or the truss cords in-line path construction then the welded joints are suitable, as well as the property of structure resistance to external environment influences, if there is any change in plate thickness of each side of connection joint then plate should be tapered at a minimum of 1: 4 to fit the limitation of the fatigue strength.

3.13.2 Bolted joints

For bridges constriction field, the steel bolts of high-strength friction grip (HSFG) are used for the main structural girder sections due to the featured of low initial slip to increase the rigid joint with good fatigue properties with good shear force resistance especially at the lapped joints or joints with cover plates.

The joint strength value that using HSFG bolts are determined by measured the first failure modes included in the intended joints, for instance, first the bolt holes as a tension failure (PT) or failure in steel plate bearing (PB) or failure of the bolts itself in shear force (PV).

3.14 Design the Span Number of the Truss Girder

The span number depends on the superstructure and substructures of bridge properties, for truss bridges design concept the reduction of span number leads to reduces the piers supports walls and longer span length, where less peris indicates a decrease in the expense of substructures in general because the peris had piles and walls and all the secondary considerations materials.

As well as the elastomeric bearing or steel pot bearing, and the focus of construction will be on the cost of superstructures which require a special design case for the long span.

Generally, at truss bridges constitutions the cost of one pier equals the cost of one superstructure span so the long span will be very economical methods.

3.15 Height of the Truss Girder

The height of the truss girder is primary decided from the span length, as taking an appropriate depth to span ratio ($\frac{H}{L}$) taking into consideration the railway or roadway clearances from the surface of the below road to the below elevation of the truss girder bridge.

Depth of the truss shall be in general:

$$\left(\frac{H}{L}=\frac{1}{6}\sim\frac{1}{8}\right) \tag{3.20}$$

For continuous trusses, a lower depth-to-span ratio is required, but a larger ratio is appropriate for spans of varying lengths [9].

Typical span to depth ratios for trusses is outlined in Table 3.1, As shown in railway structures have lower ratios due to the excessive of live loads.

The angle of the diagonals should generally be kept constant to avoid a disorganized graphic presentation and the diagonals member at 45^o to 68^o of the horizontal are generally the most efficient structurally, shallower angles tend to have less strength [9].

Table 3.1: Span – Depth Ratio In The Truss Span Bridge

Truss form	Typical span/depth ratio
Simply supported highway truss bridge	10–18
Continuous highway truss bridge	12–20
Simply supported railway truss bridge	7–15
Continuous railway truss bridge	10–18

3.16 Member Cross Section Type in Truss Girder

The truss bridge span length is the main feature that affected the type of member, furthermore the type of the internal force in that member carrying (tension or compression).

While the categories of rolled beam and channel or tubular sections are used in situations of small span length and moderate loads.

For most bridge trusses, a fabricated section (bults up steel sections) will be used, all the formations process will be made depending on the position the member, so for the chords in compressions situation.

The buckling out of the plane effective length going to be bigger than buckling in-plane length that’s led to used I-section member to be increasing the transverse radius of gyration, for the vertical member the I-section suitable for lower tensile flange that allowed it to handle the local bending applied from transverse beams.

For the (Open I, U or C-sections) theses known as very simple in fabrication stage especially the essay way to connect the splice–plate connections, for the huge truss bridge sections the box sections are used, Figure 3.12.

For the methodology of using a concrete-filled section member in its different ways of constructions to creating a steel–concrete composite section, which increase the capacity of the specific steel section as alone [24]

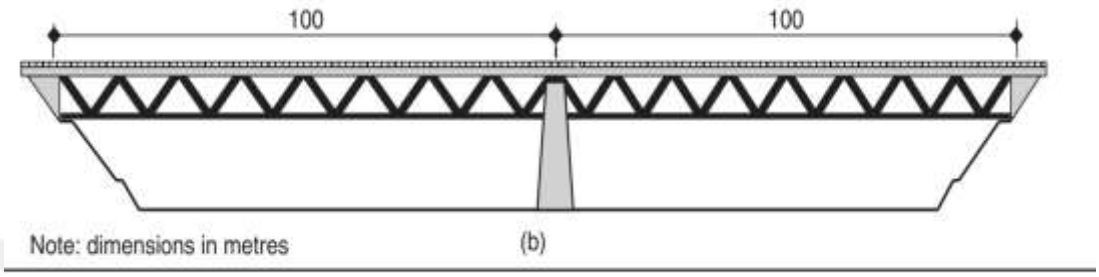

Figure 3.12: Typical Continuous Truss Bridge

3.17 Steel Sections under Axial Load

The limiting axial compression load being determined from equation below where the local buckling is reduced according to a limit of steel section geometry, Table 3.2.

In a steel-concrete composite, the steel is a key component in terms of both structural dimensions and the stress capacity that applied on the steel due to its yield strength.

$$N_{TD} = f_y A_{ae} / y_{am} \tag{3.21}$$

$$N_{TD} = f_y A_{ae} \tag{3.22}$$

Where: N_{TD} is the tensile force, Aae is an effective area of steel.

Figure 3.13 shows the limiting compressive stress curves, and the slenderness parameter used to compute the parameter (x) for steel sections subjected to compressive loads, where the maximum stress is restricted to the yield grade.

$$N_{\mathrm{CD}} = \chi f_{\mathrm{y}} A_{\mathrm{ae}} / \gamma_{\mathrm{am}} \tag{3.23}$$

$$N_{\mathrm{CD}} = 0.9 \chi f_{\mathrm{y}} A_{\mathrm{ae}} \tag{3.24}$$

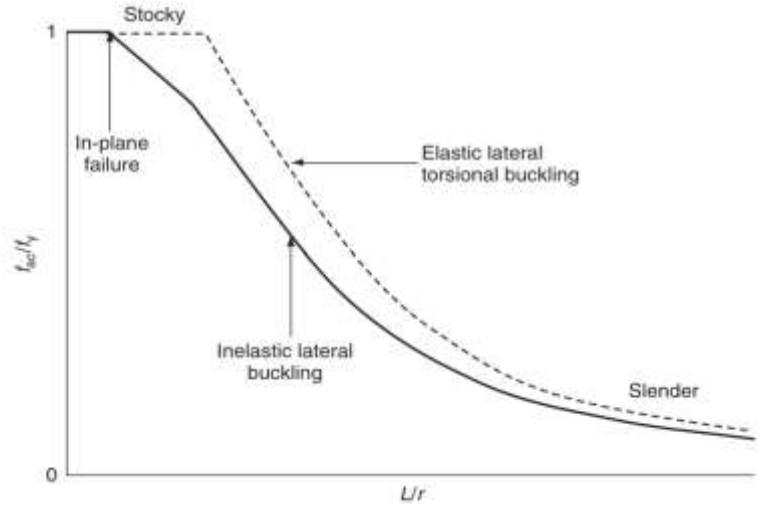

Figure 3.13: Limiting Compressive Stress for Buckling Failure

Table 3.2: Geometric Limits for the Local Bulking Resistance of Steel Plates (BSI.2004)

Element	Limit
Class 2 steel flange in compression	$8t_f$
Class 2 steel flange composite with concrete in compression	$18t_f$
Class 3 steel flange in compression	$11t_f$
Steel flange in tension	$16t_f$
Class 2 steel web in bending	$67t_w$
Class 3 steel web in bending	$100t_w$
Class 3 steel web in bending/tension	$220t_w$
Class 2 steel web in compression	$30t_w$
Class 3 steel web in compression	$34t_w$
Plate stiffener	$9t_s$
Class 2 steel circular section	$D_o = 46t_o$
Class 3 steel circular section	$D_o = 60t_o$
Class 2 connector spacing	$18t_f$ longitudinal, $7t_f$ edge distance
Class 3 connector spacing	Six times slab thickness or 600 mm
Composite circular section (without connectors)	$D_o = 73t_o$

The efficiency of section according to buckle failure modes the slenderness parameter (ƛ), which is a function of the member's effective length (Leff), cross-sectional characteristics, and, most importantly, the radius of gyration, may be used to forecast the critical buckling force of section resistance, which in turn depends on the applied force or bending moment [24].

$$\lambda = (N_E/N_{cr})^{1/2} \tag{3.25}$$

$$\lambda = L_{eff}/ik_1 \tag{3.26}$$

Where: NE is design load, Ncr is critical buckling, where k1= p(E/fy) ½ the reductions in stresses required.

Approximate effective lengths for truss members are given in Table 3.3, and in general the buckling of a truss member in situations out of plane is more dangerous than in plane, typically if the length of a section member surpasses around 3.5 times its minimum dimension, then buckling failure influences the compression capacity to a certain [24].

Table 3.3: Effective Length for Composite Structure

Element	Effective length	
Steel girders, prior to casting slab	$1.0L_B$	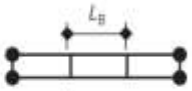
Compression chord of truss Truss diagonal	$0.85L_c$ $0.7L_D$	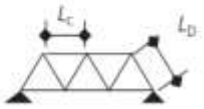
Column fixed to foundation but free at top	$2.0L_c$	
Column fixed to foundation but pinned at top	$1.5L_c$	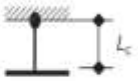
Column fixed to foundation and integral with deck	$1.0L_c$	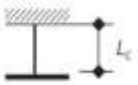

3.18 Global Analysis of Continuous Beams

This approach determines values for the ultimate limit state and serviceability of the bending moment and vertical shear in continuous beams (design values).

The plastic hinge analysis or rigid-plastic analysis is only applicable to the most extreme cases, permitting the use of potentially lighter or shallower structural components.

3.18.1 Redistribution of moments in continuous beams

In general, the redistribution method is modifying elastic global analysis, and this method shows the composite beam plastic behavior even if the load didn't reach the ultimate stage and especially for the cracking of concrete at serviceability limit states.

It’s founded to modify the bending-moment distribution for a particular loading in way keeping the equalizer between the loads and bending moments.

3.18.1.1 Moment-curvature response at hogging bending

The concrete element of a typical T-beam is fully or partially in tension under hogging in situation of good ratio acting of the composite beam and translate the shear load from the concrete slab reinforcement and steel part, the composite girder will be influence of the hogging bending moment as strain-hardening, and ductility value is limited by local buckling or secondary modes of failures.

Generally, the position of neutral axis at steel element leads to the cross-section including steel element and reinforcement bars, at this stage the concrete elements considered reaching the cracked situation as shown in Figure 3.14.

When the distance of elastic neutral axis from the top surface (dn):

$$d_n = \frac{d_r A_{reinf} + \left(h_{conc} + h_{steel}/2\right) A_{steel}}{A_{reinf} + A_{steel}} \tag{3.27}$$

Where: Asteel is area of the reinforcement steel, Areinf is area of the longitudinal reinforcement with distance (dr) from the top, Isteel is second moment of area of the steel element about its centroid, hconc is the depths of the concrete, hsteel is depths steel elements.

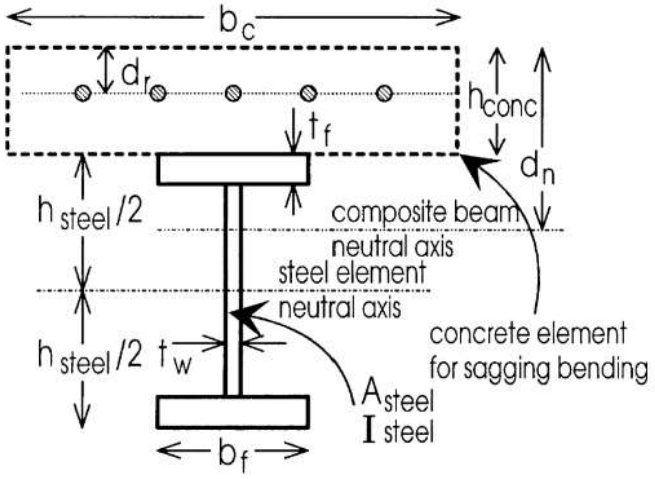

Figure 3.14: Hogging Bending for Typical Section

The relationship between the moment and curvature degree of straight curve illustrates in the Figure 3.15, including the elastic portion of stiffness (E_sI), when the p.n axis located in the top steel flange.

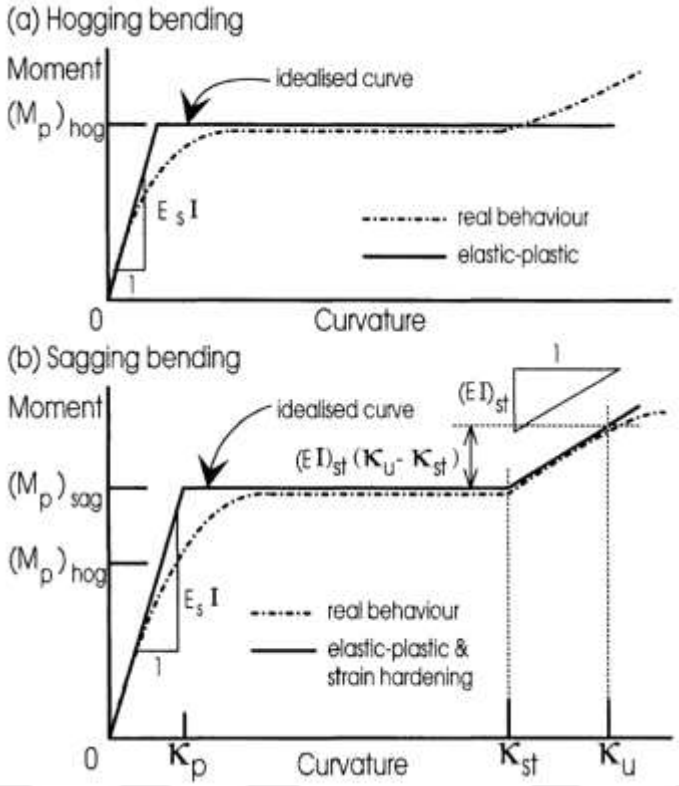

Figure 3.15: Moment-Curvature Response of the Composite Girder

Strain and hardening limitations of the steel section and for a local buckling requirements allow the moments amount reaching the 40% more than the plastic moment (Mp)hog.

On other hand, negative regions in continuous beams are subject to a huge shear force that affects the girder section capacity.

3.18.1.2 Moment-curvature response at sagging bending

At the full shear connection interaction for the composite girder, the strength capacity of cross-section resistance against the sagging bending comes from the top concrete element with the compression strength.

The relationship is linear between the depth of steel element with ductility and sustainability for high curvatures degree, however, as the compressive strains get increasing at the top concrete slab then the concrete exposed to situations of crushes leading to stress strength are reducing, as shown in Figure 3.16 and 3.17 the stress-

strain curve at the maximum curvature before the failures can be sustained by the geometric properties of the concrete element.

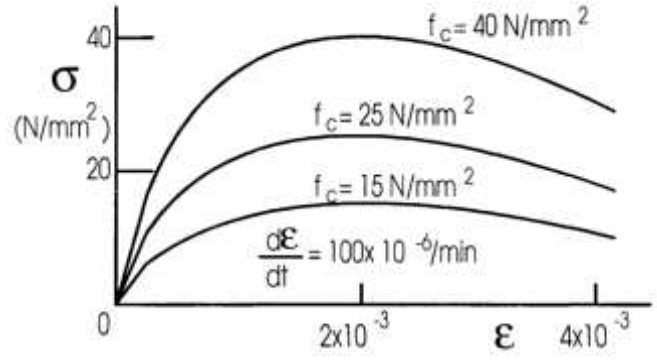

Figure 3.16: Typical Stress- Strain Curve of Concrete

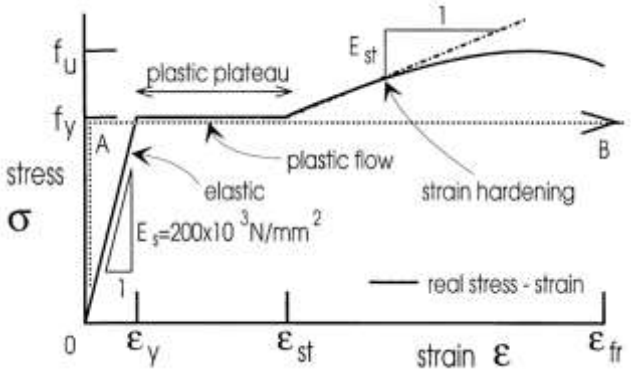

Figure 3.17: Typical Stress- Strain Curve of Steel

3.18.1.3 Ductility parameter

The ductility decreases with position of the plastic neutral axis begins from the top surface (compression part of the girder).

If the neutral axis is small the steel girder reaches the yield stage before concrete crushing (ductile girder), on other side if the plastic neutral axis was high then the concrete damaged in the first place and before the tensile steel yields then it's called (brittle girder).

To define composite girder at bending to be ductile due to the strain hardening of the bottom steel flange show up before concrete crushing.

3.19 Effective Size of Reinforced Concrete Elements

Effective geometric dimensions of the composite girder are used for the analysis procedures to give a space for the variation of concrete slab stress or changes in cross-section along the girder length and for sure for the local buckling of the steel elements and the shear lag.

3.19.1 Effective width

The effective width must account for the nonuniform stress distribution caused by shear lag.

By assume that the concrete element is shorter, represented by the rectangular stress block area (weff σc) illustrated in Figure 3.18(a), which equates to the area beneath the nonlinear stress block (σ_l) across the width (w).

This is analogous to the longitudinal stress (σ_l) in the concrete slab relative to the width (w), divided by the maximum stress value (σc):

$$w_{eff} = \frac{\int_{b_\ell}^{b_r} \sigma_\ell \, dx}{\sigma_C} \tag{3.28}$$

Where: bL and br refer to half of the transverse spans of the slab, as shown in Figure 3.20.

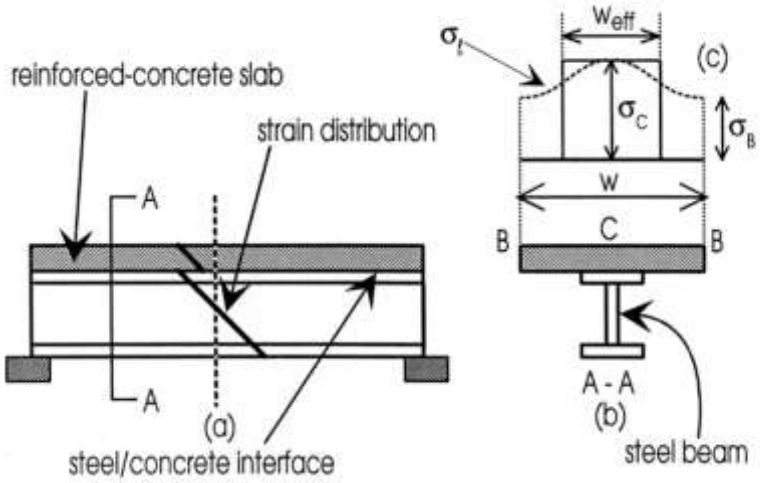

Figure 3.18: Strain Distribution over the Effective Width

For instance, at section A-A in Figure 3.18(a), the strain distribution in the concrete part is presumed to exist according to full width (w) of the concrete element in Figure 3.18(b).

So the stresses at the corner (B) show in Figure 3.18(c) are less of the stress located at center above the steel section at (C).

It can be obvious due to the variation stress curve; the figure 3.18(c) illustrates the curve path from (σ_b) at the corner to a maximum of (σ_c) above the steel element at the center.

The situation of shear lag occurs in steel beams with wide flanges, it's given the information data of required thicknesses of concrete slab (hconc) in contrast to the spacing (s) of the steel girder of bridge span (Tadj) in Figure 3.19.

The implications of shear lag must be integrated into the design, therefore it's essential to adjust the concrete element to account for the nonlinear effects of shear lag.

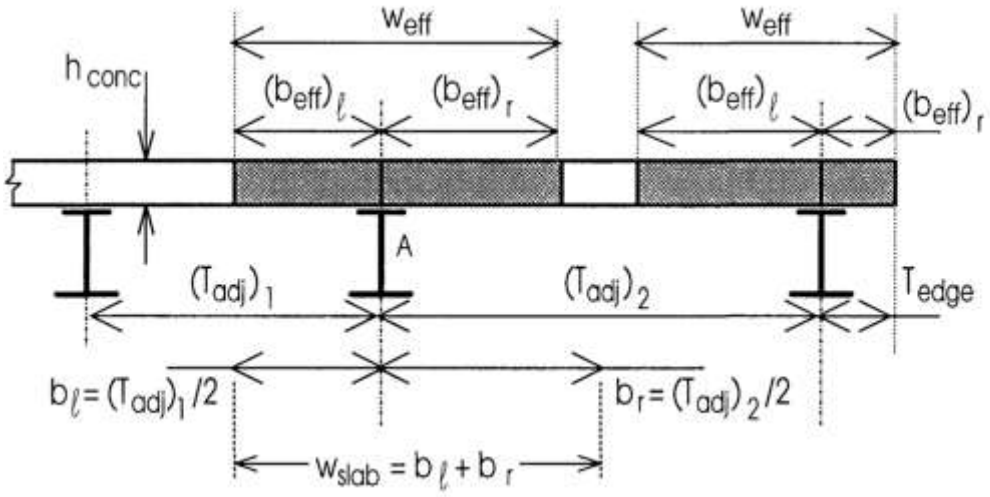

Figure 3.19: Slab Concrete Effective Width

3.19.2 Sizing of the concrete slab effective width

The determination of effective width is influenced by several complicated elements, with national standards providing various guides to address this intricate issue.

The guidelines for composite beams in bridges primarily rely on the spacing between two mid composite beams (Tadj) as illustrated in Figure 3.19, the distance

to the free edge (Tedge), the distance between points of contraflexure (Lc) depicted in Figure 3.20, and the length (L) between pier supports in continuous beams.

Defining the effective width as given in the following equations:

$$w_{eff} = (b_{eff})_{\ell} + (b_{eff})_{r} \tag{3.29}$$

Where: (beff)L is the effective breadth of deck slab, (beff)r is effective breadth on the right.

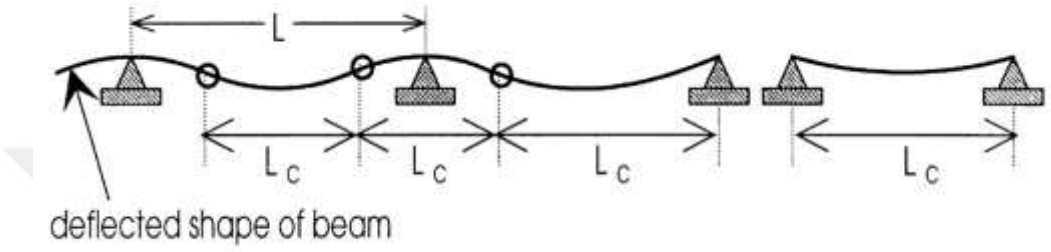

Figure 3.20: Effective Span Length

3.20 Perfobond Leiste Shear Connector

Ribs connectors are mainly used in composite slab implementation, the rib plate impanation along the full length of the girder or any structure and shear can traverse the contact between steel and concrete in full shear connection as uni-linear strain profile, on the other hand, it's transferred as interface interlock where interface slip occurs at initial low loads.

The perfobond leiste has two essential aims, firstly it gives the steel at the deck to act as a steel girder, in situations lead to support the eliminate concrete, and secondly to provide a bond between the hardened concrete and the steel decking.

The capacity to function as permanent shuttering and integrated shuttering is determined by the configuration of the ribs, rib shear connectors are used in the construction of composite girder as illustrated in Figure 3.21.

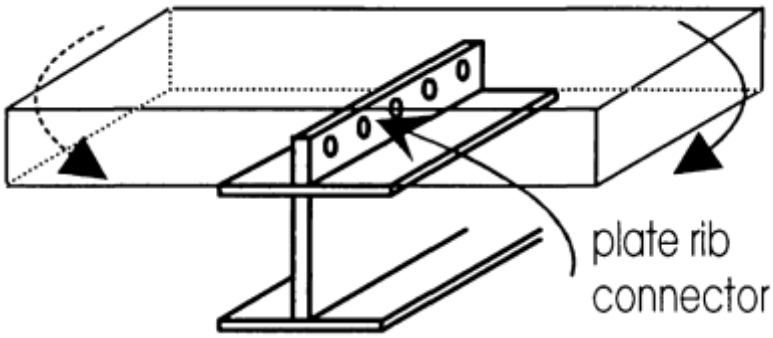

Figure 3.21: Perfobond Leiste Shear Connector Steel Plate

3.21 Shear Connectors Design

3.21.1 Design at elastic stage

Shear connections that are stiff or nonductile often employ this technique, at this stage the ultimate load can determine if any shear connector reached the shear resistance capacity, while the design of shear connector and its spacing will by influence by the shear forces distribution.

Elastic theory is employed to determine the longitudinal shear flow per unit length at the contact between the composite girder elements, as seen in Figure 3.22 below.

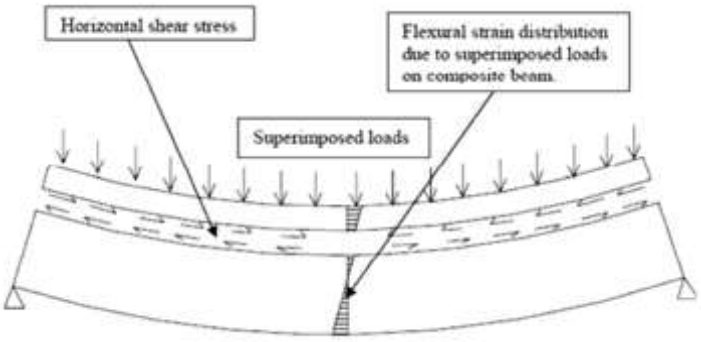

Figure 3.22: Longitudinal Shear Flow between the Steel and Concrete at Elastic Stage

3.21.2 Design at plastic stage

In this stage presumably representing the final condition, the shear connections are assigned an identical shear force value.

The maximum bending moment distribution and zero moment locations visually separate the composite girder into many areas when using this approach, as shown in Figure 3.23.

In every region, the steel shear connectors are equally distributed, but it's different from region to another one, in this method, the reinforcement in compression situation is neglected as shown in Figures 3.24.

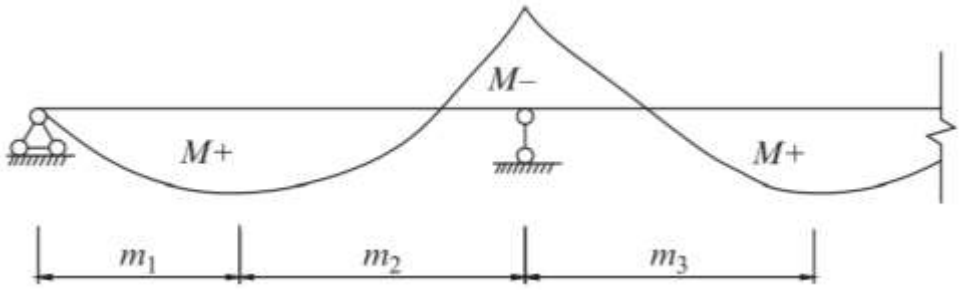

Figure 3.23: Shear Connector Spacing Zones in Continuous Girder at Plastic Stage

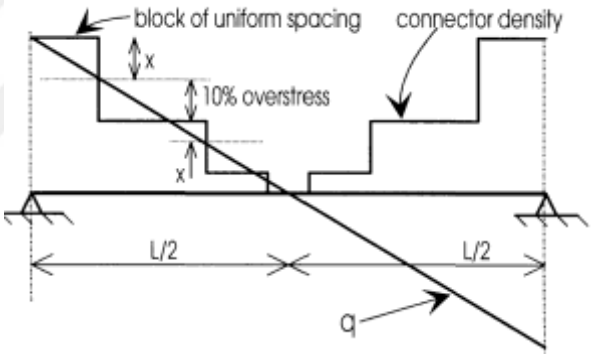

Figure 3.24: Shear Connector Density and Distribution Due to the Shear Flow (q)

3.23 Section Classification

The bending strength capability of a section is contingent upon its reaction to external bending forces; hence, a cross section with thick flanges and web enhances resistance to the development of a plastic hinge.

Conversely, narrow cross sections including thin flanges and webs will experience local buckling before to reaching the yield stress, as seen in Figure 3.25, which identifies four kinds of section in clause 3.5.2 of BS 5950.

3.23.1 Class 1 plastic

The plastic hinge of the cross sections at this category can reach the significant rotation capacity for the plastic design and all members of structural must be adequate to this type.

3.23.2 Class 2 compact

Although it is possible to produce cross sections with full plastic moment capacity, local buckling could prevent a plastic hinge with sufficient rotational capacity from being formed, which would hinder plastic design.

3.23.3 Class 3 semi-compact

At this category the local buckling prevents the full plastic moment capacity to be reachable, also, the cross sections can enhance their elastic moment capacity.

3.23.4 Class 4 slender

In the early stages, local buckling prevents the cross section from reaching its full elastic moment capacity, which happens when thin parts undergo compression force because of moment or axial stress.

Controlling the ratio of width to thickness for sections given in Table11 in BS 5950, part of it showing as Table 3.4, Any section that exceeds the limits will be calculated as class 4 (slender section).

Table 3.4: Limit of width – Thickness Ratio

Type of element (all rolled sections)	*Class of section*		
	(1) Plastic	*(2) Compact*	*(3) Semi-comp*
Outstand element of compression flange	$\frac{b}{T} \leq 9\varepsilon$	$\frac{b}{T} \leq 10\varepsilon$	$\frac{b}{T} \leq 15\varepsilon$
Web with neutral axis at mid-depth	$\frac{d}{t} \leq 80\varepsilon$	$\frac{d}{t} \leq 100\varepsilon$	$\frac{d}{t} \leq 120\varepsilon$
Web where the whole cross-section is subject to axial compression only	n/a	n/a	$\frac{d}{t} \leq 40\varepsilon$

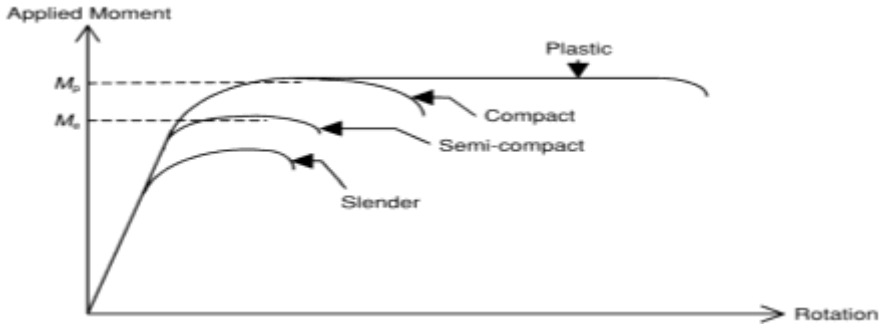

Figure 3.25: Rotation of Multiple Types of Portions in the Moment

3.24 Theoretical Analysis of Composite Truss Bridge Superstructure

3.24.1 Design criteria

3.24.1.1 Bridge geometry

The case study will illustrate a long span bridge with 300m (50m for each span), the bridge will be implemented along a wide valley in the ring road project around the city, the high of the bridge surface level to the bed level of the valley approximately around 20m, the main design will focus on the superstructure of the bridge.

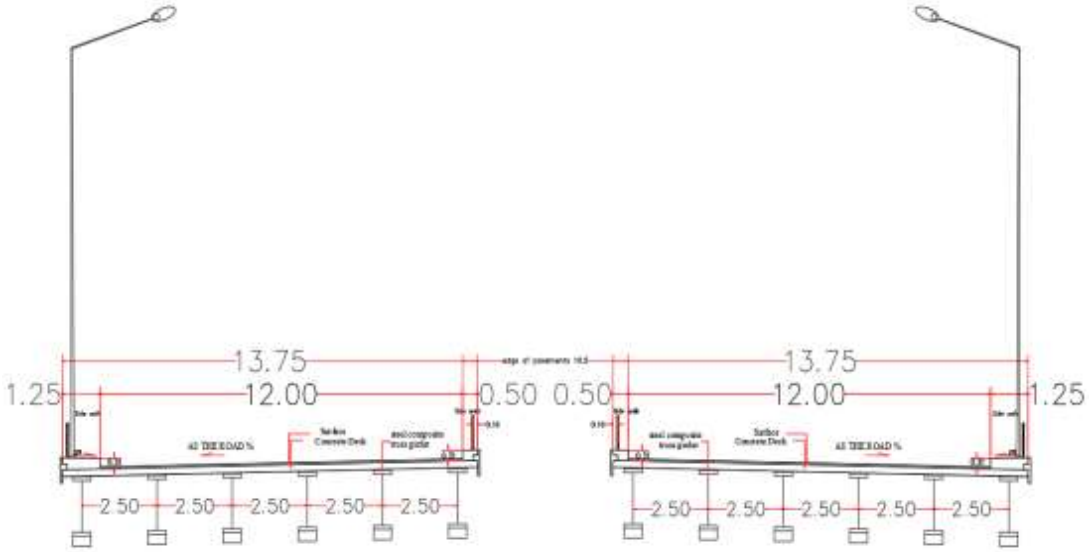

Figure 3.26: Composite Truss Bridge Section

The superstructure consists of a 12m wide carriageway with 1.25m sidewalk, and the type of girder will be a double composite truss steel girder with perfobond Leiste shear connector in both top and bottom flange.

The girder web truss will be warren type, where the chords carry the bending in tension or compression and the diagonals carry the show also in tension and compression and the vertical members carry only panel loads, the connection between the truss and web will be by welding methods as shown in above Figure 3.26 and Figure 3.27.

The analysis will be for each two continuous spans for 100m continuous span, and all the details analysis calculations illustrated in (Appendix A.1).

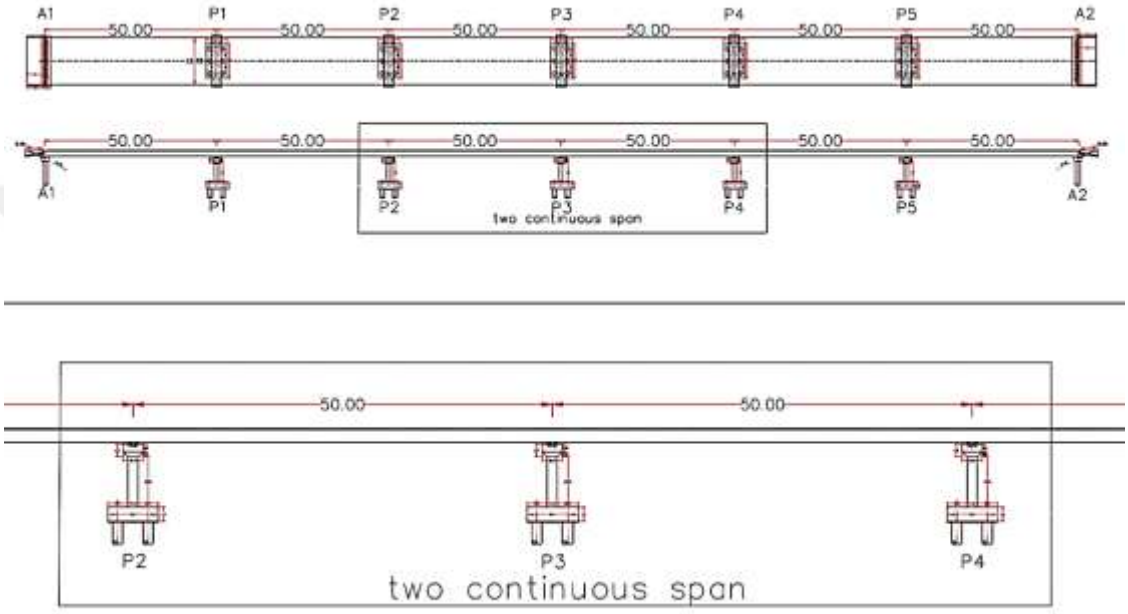

Figure 3.27: Bridge Side View and two Continuous Spans

3.24.1.2 Specification of materials

- Steel Reinforcement bars ASTM A615 yield strength fy = 650 MPa
- Steel truss members ST35 fy = 235 MPa (EN 10025)
- Compressive Strength of Concrete: 60 MPa (Girders, Deck Slab, Approach Slab).
- Compressive Strength of Concrete: 35 MPa (for Curb Stone, Shoulder, New jersey Barrier).

3.24.2 Loading analysis

3.24.2.1 Dead load

The following unit weights of construction materials illustrated at Table 3.5, shall be used in computing dead load applied to different parts of the bridge structure.

Table 3.5: Bridge Materials Density

Material	Density
Structural steel or cast steel	78.5 kN/m3
Cast iron	72.5 kN/m3
Plain concrete	23.0 kN/m3
Reinforced concrete	24.0 kN/m3
Asphaltic concrete	22.5 kN/m3

All structures willbe designed to carry an additional dead load (curb to curb) of 0.75kN/m2.

3.24.2.2 Live load

The live load category is well divided into civilian and military load, each of these categories consist of several types of standard loading simulations, at last the biggest value of them will be taken as live load for the design as below:

3.24.2.2.1 Civilian live load according to AASHTO LRFD

Truck design Live Load (HL-93) total weight 325Kn will be used as standard measured to calculate the total live load applied on the superstructure of the bridge spans as shown in Figure 3.28.

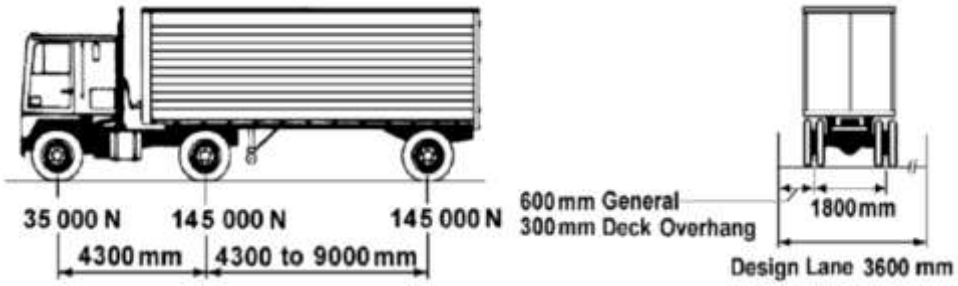

Figure 3.28: Truck design Live Load (HL-93)

Due to the Bending Moment (B.M.)

Simulation of two points of load in the mid spans' length as in Figure 3.29 to create the maximum hogging moment at the concrete deck slab and the maximum sagging moment at the middle of the two spans.

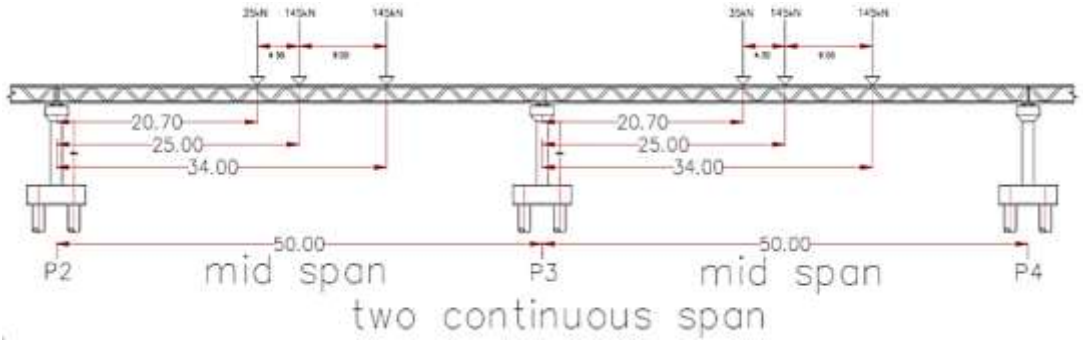

Figure 3.29: Truck Design Live Load at Mid Span

Due to Shear Force (VL.L.)

The first point of truck load will be at 1.5 from support (p3) of the span (1 & 2) to creating the maximum shear flow at the mid pier support (p3) as shown in detail by Figure 3.30.

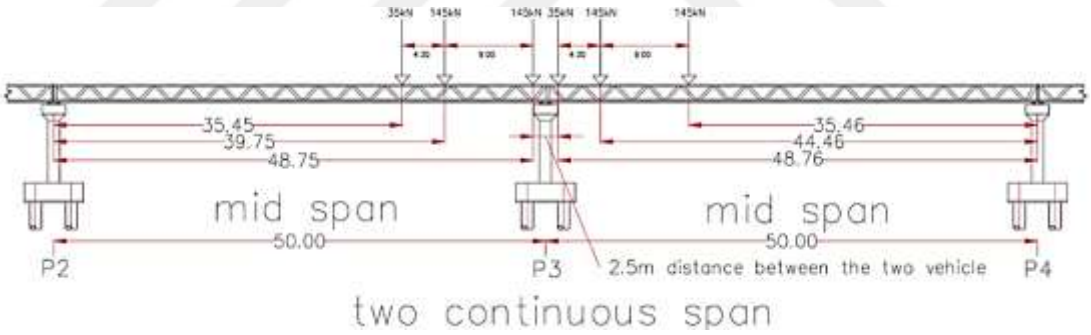

Figure 3.30: Truck Design Live Load at Support Pier (p3)

3.24.2.2.2 Military load

The military load classification is divided into two types, the first tracked vehicles class 100 and second the wheeled vehicles class 100 as illustrated in Table 3.6.

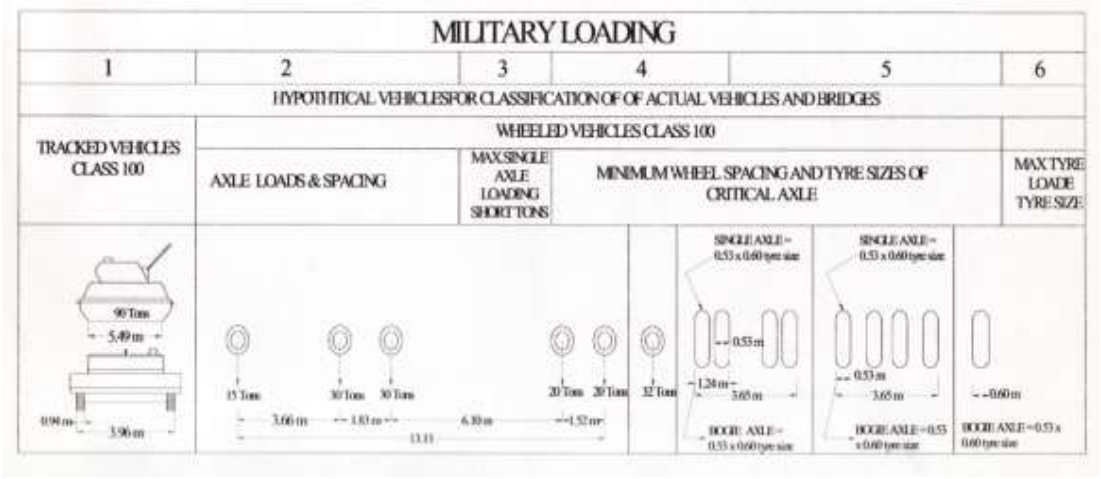

Figure 3.31: Military Loading Classification

Tracked vehicles class 100 total weight 900KN will be used as standard measured to calculate the total live load applied on the superstructure of the bridge spans as shown in Table 3.8.

Due to the Bending Moment (B.M.)

In this stage the load of the two tanks will be located on the mid spans as shown in Figure 3.32.

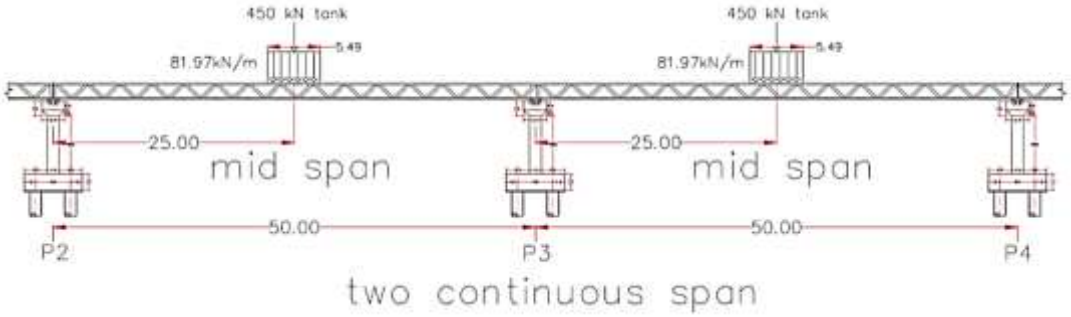

Figure 3.32: Tank Load Distribution at Mid Spans

Shear Force (VL.L.) Calculations

At this stage the load of the tanks will be located nearest the mid support of the (p3) getting the maximum shear force applied on the support (p3) as shown in Figure 3.33.

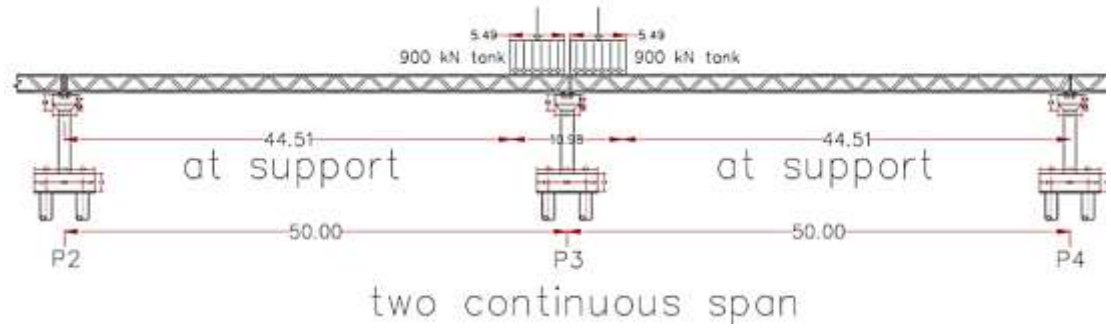

Figure 3.33: Tank Load Distribution at Supports

Military wheeled tracked vehicles class 100 live load as in Table 3.8 of the (ISHL specifications), that the Military wheeled has 5 axles with specific load for each axle with certain distance.

Bending Moment (B.M.) Calculations

At this stage the wheel tracked will located at the mid span to getting the maximum hogging moment (negative moment) and the sagging moment (positive moment) as shown in Figure 3.34.

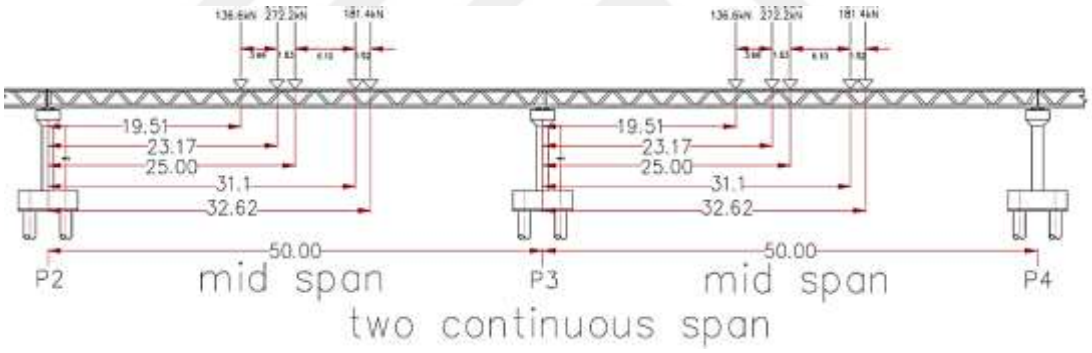

Figure 3.34: Military Wheeled Vehicles Load Distribution at Mid Span

Shear Force (VL.L.) Calculations

It can be noticed that is the critical case for shear forces where the two vehicles near to the support (P3), with 2m distance between the wheeled vehicles as shown in Figure 3.35.

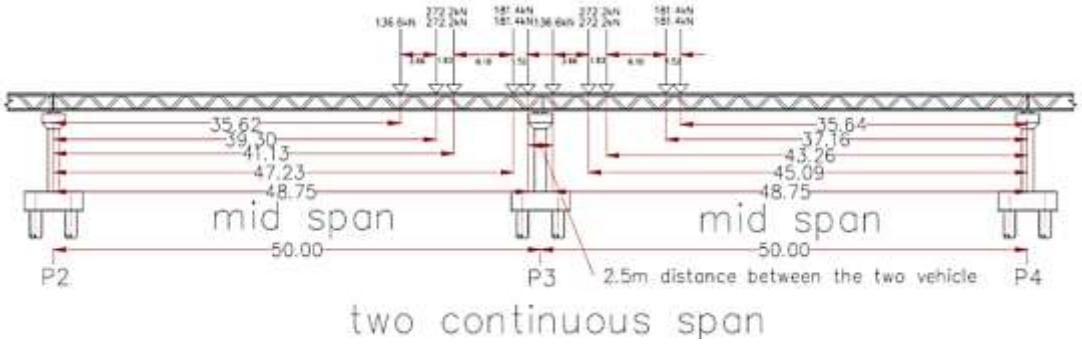

Figure 3.35: Military Wheeled Vehicles Load Distribution at Supports

3.24.3 Details bending moment and shear force results

The listed results collected simulated all the dead and live loading cases by robot structure analysis program, as shown in table 3.7 to table 3.9 gives the analysis data of the maximum hogging and sagging moment and shear force flow, the AASHTO LRFD and British specification (BS) 5400 are used at the calculations approach, which is illustrate in figure 3.35.

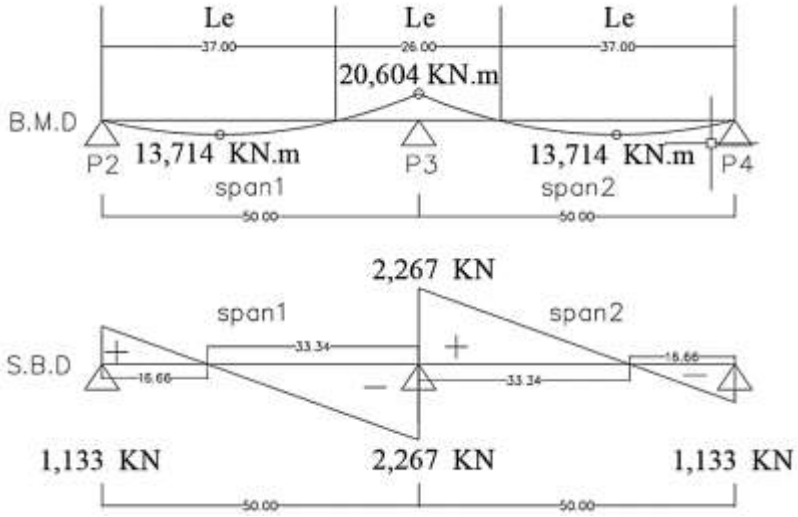

Figure 3.36: Maximum Bending Moment and Shear Diagram Per Continuous Girder

Table 3.6: Details of Dead Loading Results

Dead load of self-weight		
Bending moment (B.M)	HOG	5778.13 KN.m per girder
	SAG	3250 KN.m per girder
Shear force (V.L)		577.81 KN per girder

Table 3.7: AASHTO Live Load Results

AASHTO live load			
Truck load	B.M	HOG	5,063,976 kN.m per girder
		SAG	3,583.614 kN.m per girder
	V.L		264.061 kN per girder
Tandem load	B.M	HOG	3,425,556 kN.m per girder
		SAG	2,788 kN.m per girder
	V.L		182.851 kN per girder
Design lane load	B.M	HOG	2,420.906 kN.m per girder
		SAG	1,361 kN.m per girder
	V.L		242.403 kN per girder
Pedestrian load (PL)	B.M	HOG	1,639.344 kN.m per girder
		SAG	922.131 kN.m per girder
	V.L		163.268 kN per girder
Maximum bending moment (Hogging) = truck load + design lane load + PL			9,124,226 KN.m
Maximum bending moment (sagging) = truck load + design lane load + PL			3,585,897 KN.m

Table 3.8: BS 5400 and Iraqi Standards Specifications for Loading Results

BS 5400 and Iraqi standards specifications for loading			
UDL load	B.M	HOG	7812 KN.m per girder
		SAG	4394.44 KN.m per girder
	V.L		781 KN
KEL load	B.M	HOG	313.83 KN.m per girder
		SAG	261.52 KN.m per girder
	V.L		23 KN
Track military load	B.M	HOG	6,700 kN.m per girder
		SAG	5,094 kN.m per girder
	V.L		713,347 kN.m per girder
Wheeled military load	B.M	HOG	4,945.499 kN.m per girder
		SAG	5,808 kN.m per girder
	V.L		885.599 kN.m per girder
Maximum (B.M) Hog = track load + UDL and KEL load			14,825.83 kN.m
Maximum (B.M) sag = wheeled load + UDL and KEL load			10,463.96 kN.m

Maximum hogging moment = 14,825.83 + 5778.13 = 20,603.96 ► 20,604 KN.m

Maximum sagging moment = 10,463.96 + 3250 = 13,713.96 ► 13,714 KN.m

Maximum shear force at support p3 = 577.81 + 781+ 23 + 885.599 = 2,267 KN.m

4. EXPERIMENTAL PROGRAM

4.1 Introduction

The primary objective of this experiment is to investigate the behavior of composite girders made of truss steel with two double perfobond ribs shear connectors in the top and bottom cords installation on three support (two at the end edge and one in the middle) under two point of static to create sagging and hogging moment region and take the result of the performance, one type of design concrete mix will be proposed for the specimens which is a normal weight concrete (NWC), many features will be adopted for this test to evaluate this structural behavior such as the elastic and plastic cracks in the positive and negative moment (hogging and sagging region), the deflection ratio along the girder length, modes of failure, the load-slip curve for the top shear connector, load- bearing capacity and the girders ultimate strength.

Additionally, this chapter illustrates all the test steps and procedures for the specimens, conducting many tests on steel and concrete materials to obtain analysis data about the mechanical, chemical, and physical characteristics.

Also, the push-out test is used for three specimens of the shear connector to find the load-slip relationship curve.

This data provides the strength capacity for different dimensions of the perfobond leiste shear connectors.

4.2 Description and Classification of the Work Specimens

This research consisted of two categories of tested specimens, Overall, eight composite steel truss girders were cast and four specimens examined for each category where the length of all specimens was 2620 mm, and the depth of the steel section vertical and diagonal members of 350 mm, the top and bottom concrete was in different thickness in every specimen as illustrated later.

The required concrete compressive strength will be in the range 35 MPa for the eight main truss girders and 40 MPa for the three push-out tests to get the required performed leiste shear strength. All the steel sections are from grade Mild Steel (ASTM A36).

All the composite girders initials materials such as concrete mix, steel and reinforcement bars, however, all the mechanical and chemical properties well get tested at the Iraqi National Center for structural laboratories and Structural Consultant Laboratory at the Technological University.

The main objective and variables of the experimental work are:

1. The influence of variations perfobond leiste parameters on bond strength.
2. The effective of the ribs plate holes and penetrate steel reinforcement bars diameter on the slip ratio.
3. The impact of variations in concrete and steel flange thickness.
4. The effectiveness of interaction degree and perfobond leiste spacing on cracks resistance at hogging moment region and the deflection ratio
5. The effectiveness of the single and double composite on the negative moment values with influence on elastic hogging moment of resistance.

4.2.1 Specimens of first category

This group consists of four specimens as single composite truss girder (SCTG) with different dimension and thickness for the concrete and perfobond leiste ribs shear connector, using range of thickness for the steel flange and vertical and diagonal truss member with 45° angle and the vertical member located in the middle and edge, tested with two points of static load till the failure modes occur**,** Table 4.1, Table 4.2, Figure 4.1 to Figure 4.3, illustrate the specimens' details and sections dimension.

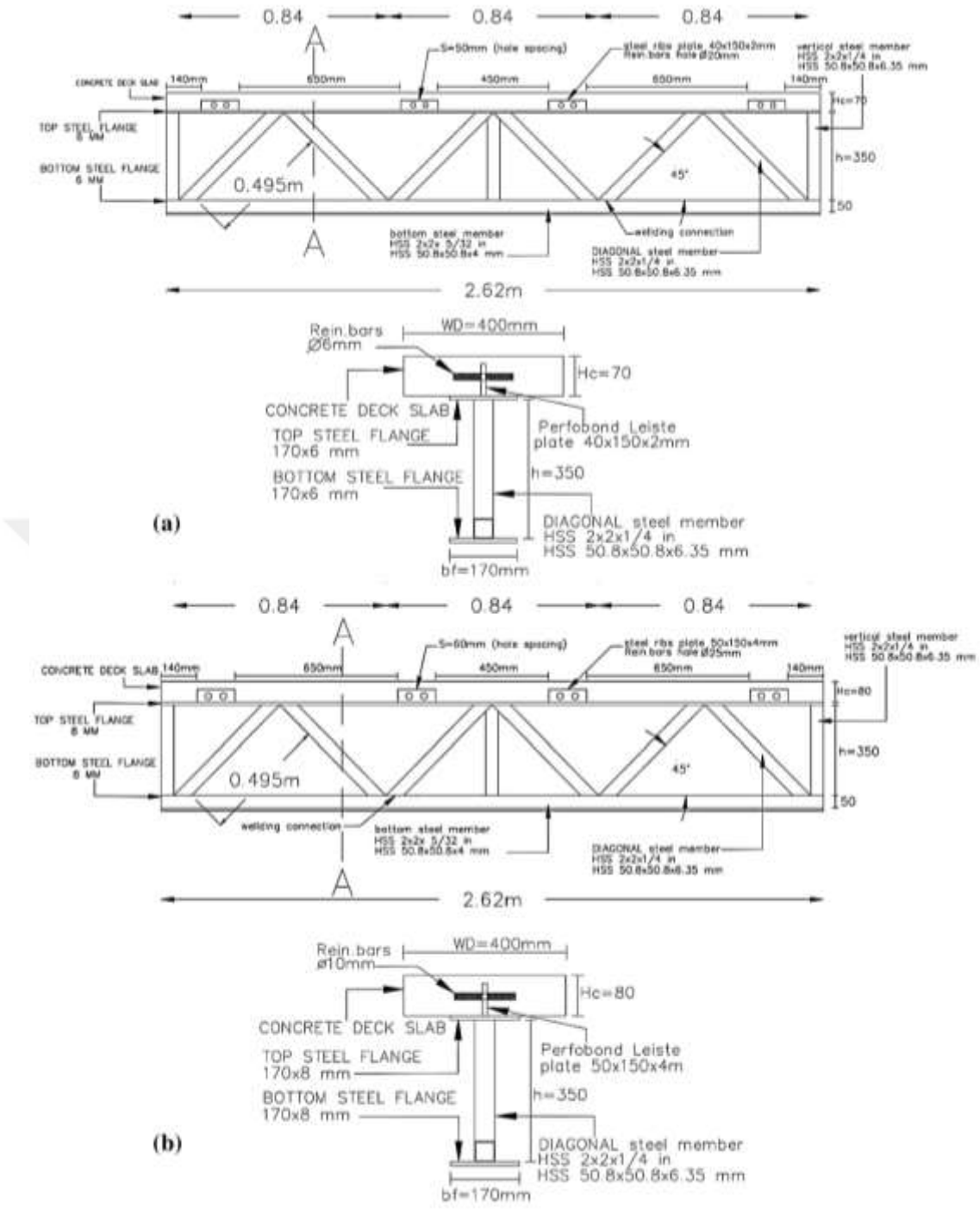

Figure 4.1: First Category Composite Truss Girder (SCTG) Models. (a) Layout of Specimen One (SCTG-1), (b) Layout of Specimen Two (SCTG-2).

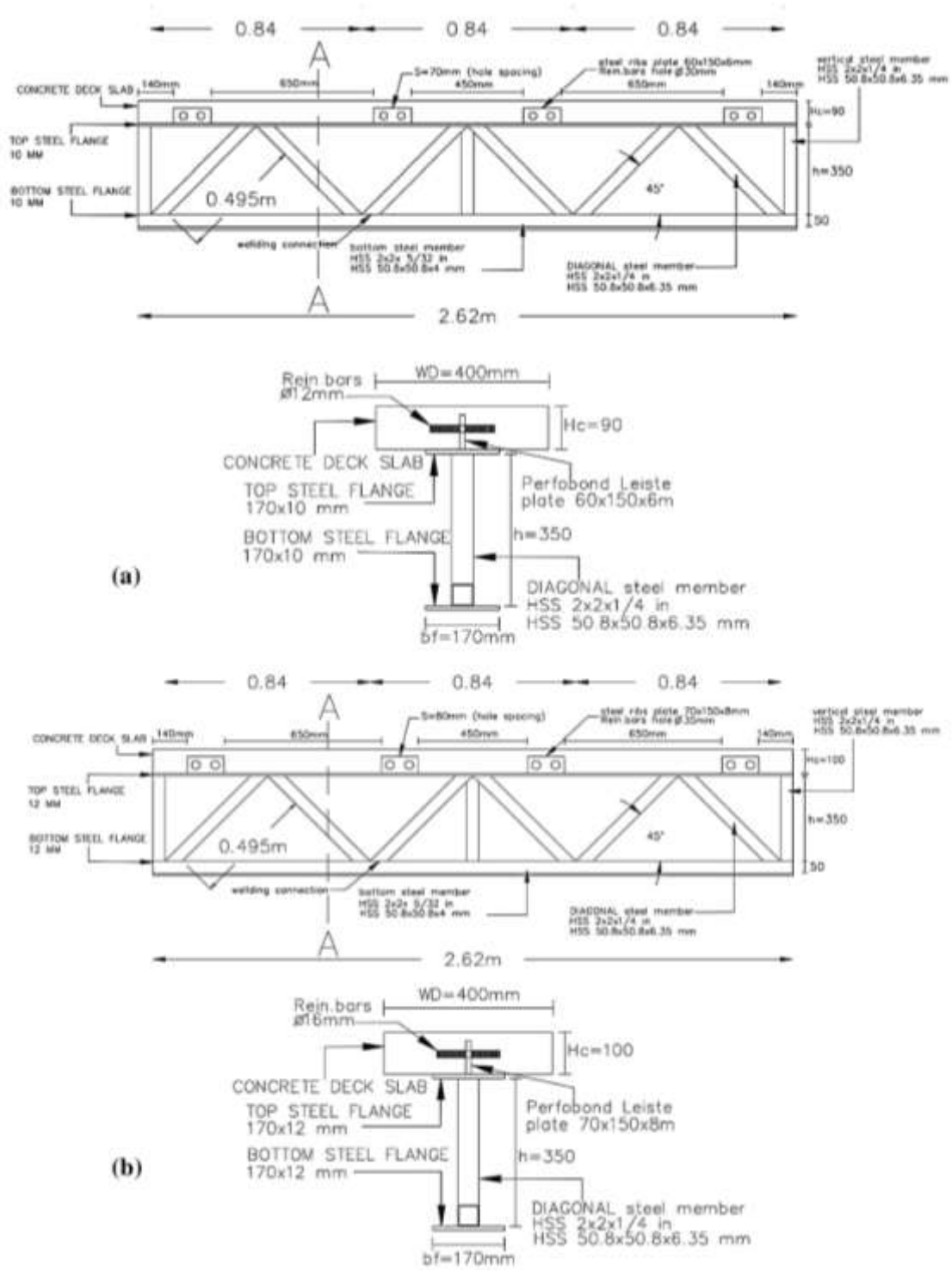

Figure 4.2: First Category Composite Truss Girder (SCTG) Models. (a) Layout of Specimen Two (SCTG-3), (b) Layout of Specimen Three (SCTG-4)

Table 4.1: Details of First Category Single Composite Girder Specimen's Dimension

Specimens Model	Length Of model (mm)	T- flange Thickness (mm)	B-flange Thickness (mm)	Deck slab Thickness (mm)	Diagonal Length (mm)	Concrete Strength (MPa)	Truss girder Depth (mm)
SCTG-1	2620	6	6	70	495	35	350
SCTG-2	2620	8	8	80	495	35	350
SCTG-3	2620	10	10	90	495	35	350
SCTG-4	2620	12	12	100	495	35	350

Table 4.2: Details of Shear Connector For the First Category Specimens

Specimens Model	Ribs Plate Spacing (mm)	Ribs Plate Hight (mm)	Ribs Thickness (mm)	Plate Hole Diameter (mm)	Connect Type (mm)	Ribs Plate hole Spacing (mm)	Rein. Steel bar diameter (mm)	Steel Strength (MPa)
SCTG-1	vary	40	2	20	D.W 3	50	¬ 6	235
SCTG-2	vary	50	4	25	D.W 3	60	¬ 10	235
SCTG-3	vary	60	6	30	D.W 3	70	¬ 12	235
SCTG-4	vary	70	8	35	D.W 3	80	¬ 16	235

Note: D.W3: double welding with 4 mm thickness.

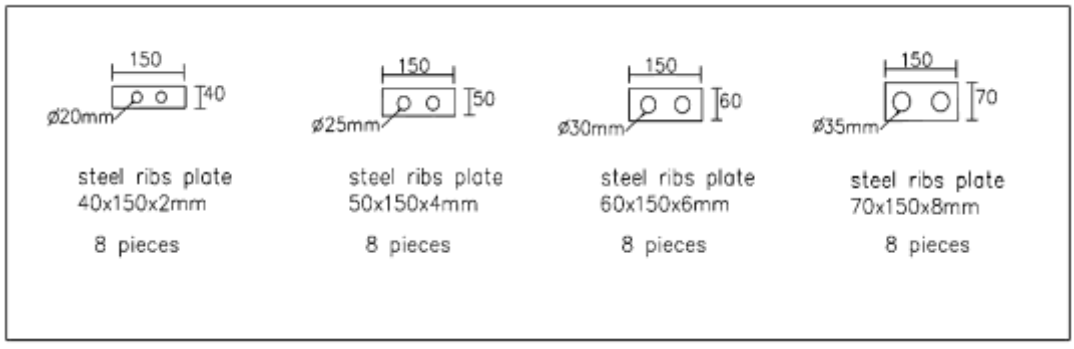

Figure 4.3: First Category (SCTG) Shear Connectors Models

4.2.2 Specimens of second category

This group consists also of four specimens double composite truss girder (DCTG) with different dimension and thickness for the concrete and perfobond ribs

shear connector, using range of thickness for the steel flange and diagonal truss member with 45° and vertical truss member in the edge of the girder, and get tested with two points of static load till the failure modes occur, Table 4.3, Table 4.4, Figure 4.4 to Figure 4.6, illustrate the specimens' details and sections dimension.

Table 4.3: Details of Second Category Specimens' Dimension

Specimens Model	Length Of model mm	T- flange Thickness mm	B-flange Thickness mm	Deck slab Thickness mm	Diagonal Length mm	Concrete Strength MPa	Truss Web Depth mm
DCTG-1	2620	6	6	70	495	35	350
DCTG-2	2620	8	8	80	495	35	350
DCTG-3	2620	10	10	90	495	35	350
DCTG-4	2620	12	12	100	495	35	350

Table 4.4: Details of Shear Connector for the Second Category Specimens

Specimens Model	Ribs Plate Spacing (mm)	Ribs Plate Hight mm	Ribs Thickness mm	Plate Hole Diameter mm	Connect Type mm	Ribs Plate hole Spacing mm	Rein. Steel bar diameter mm	Steel Strength MPa
DCTG-1	vary	5	6	20	D.W 3	50	¬ 6	235
DCTG-2	vary	60	8	25	D.W 3	60	¬ 10	235
DCTG-3	vary	70	10	30	D.W 3	70	¬ 12	235
DCTG-4	vary	80	12	35	D.W 3	80	¬ 16	235

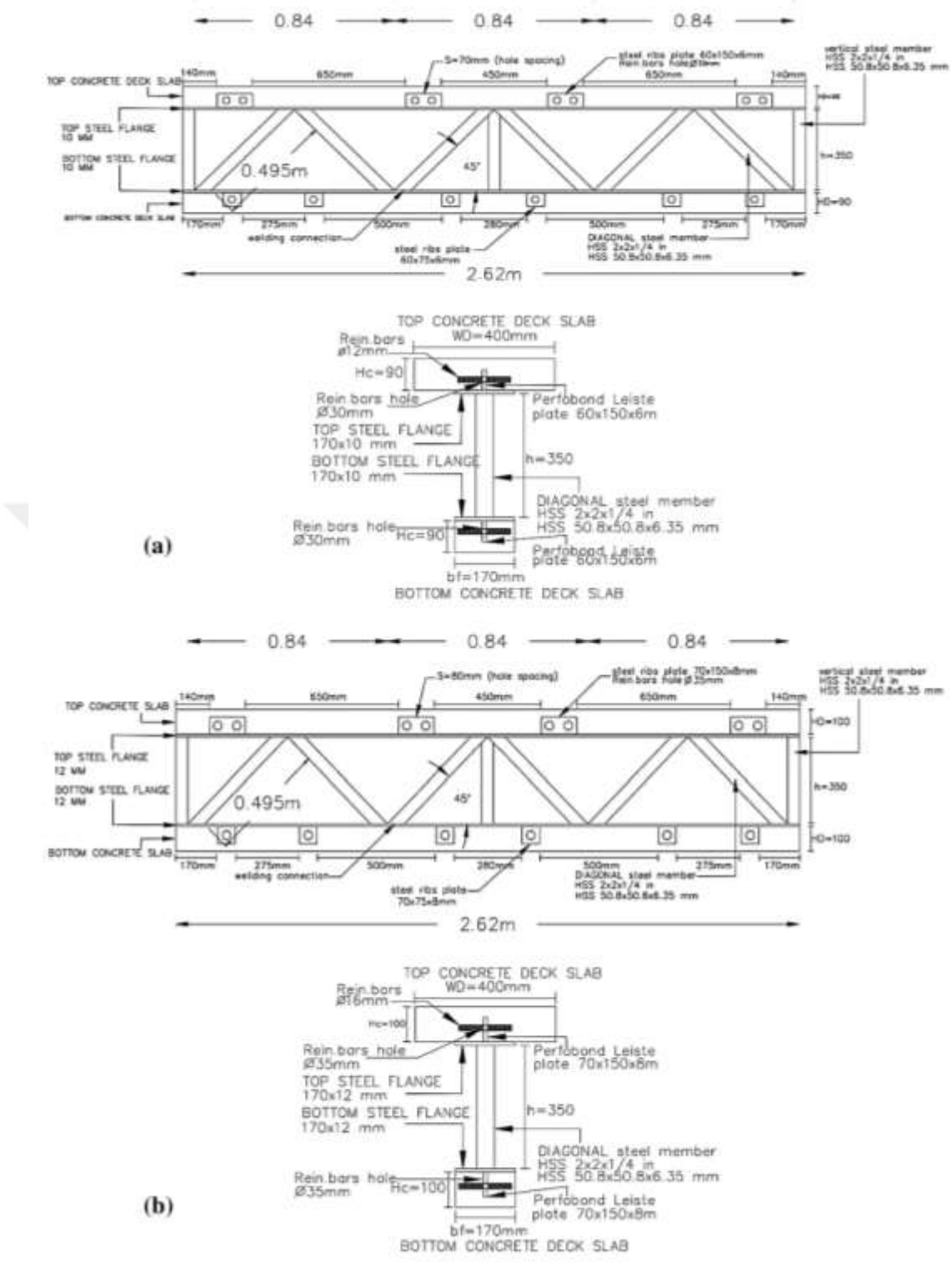

Figure 4.4: Second Category Composite Truss Girder (DCTG) models. (a) Layout of Specimen one (DCTG-1), (b) Layout of Specimen Two (DCTG-2)

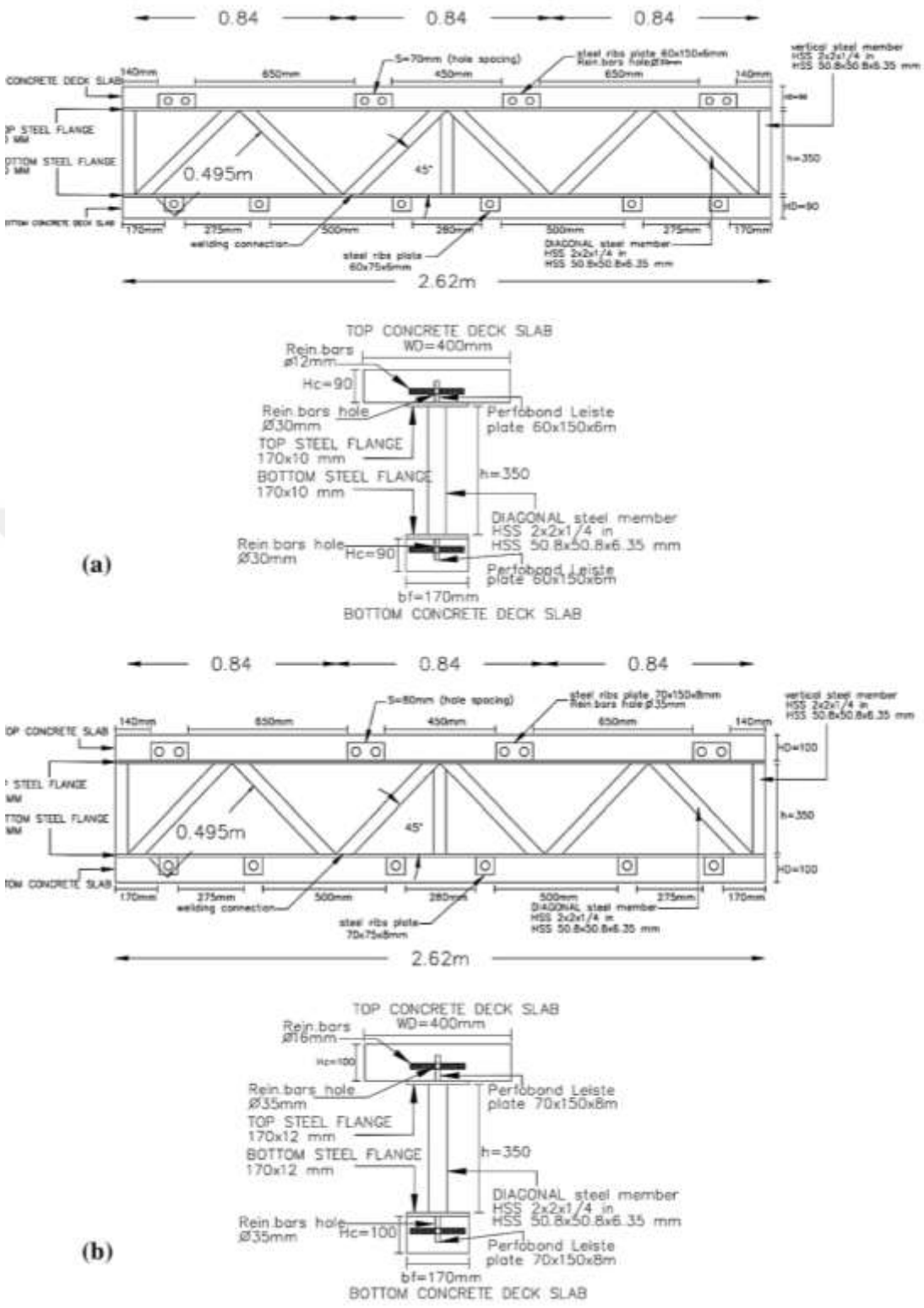

Figure 4.5: Second Category Composite Truss Girder (DCTG) Models. (a) Layout of Specimen Three (DCTG-3), (b) Layout of Specimen Four (DCTG-4)

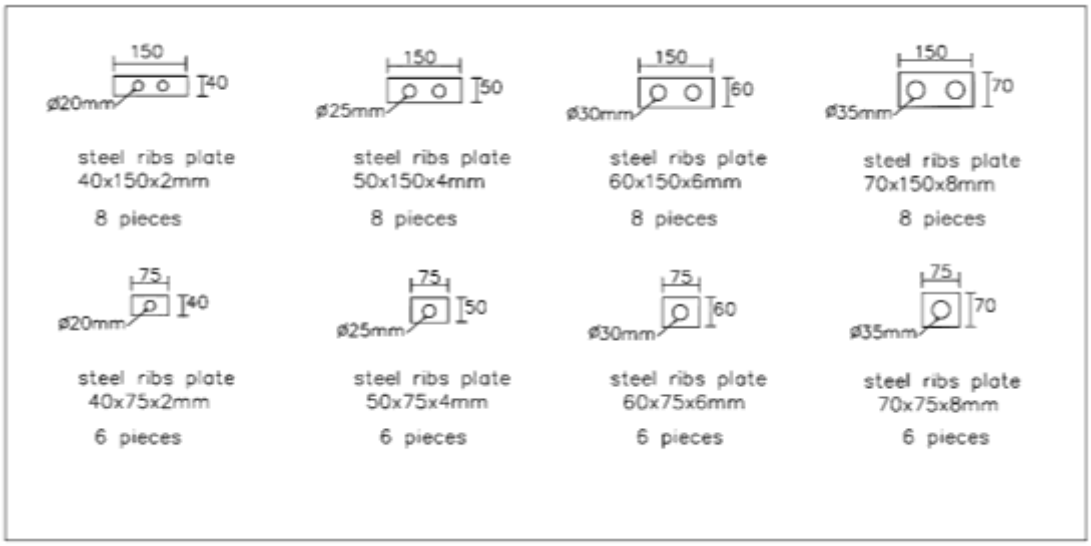

Figure 4.6: Second Category Composite Truss Girder (DCTG) Shear Connectors

4.2.3 The push – out test for perfobond ribs shear connector

According to EUROCODE 4, three specimens get tested to get results of the strength capacity and indicate data analysis of the ribs shear connector that will be used in the composite truss girder specimen, in this test used double-hole steel plates were used with different diameter for each sample, the dimension of the specimens was illustrate below in the Table 4.5 , the steel bars provided by different diameters 12 mm, 16 mm, and 20 mm, and the average dimension of the shear connector that will used on the main specimens to find the results and consider them as standard results for those samples, Figure 4.7(a),(b) and (c) illustrate the properties and dimensions.

The relative slip of the steel HSS member and side concrete was mainly measured by LVDT to avoid measurement errors during the test, the relative slip was conducted by the applied load showing at the jacking gauge, the details will be shown in Figure 4.8.

Table 4.5: Details of Perfobond Ribs Specimens for Push Out Test

Specimens Model	Ribs Plate High mm	Flange & Ribs Thickness mm	Plate Hole Diameter mm	Con. Deck slab mm	Ribs Plate hole Spacing mm	Rein. Steel bar diameter mm	Steel Strength MPa	Concrete strength MPa
PRP1	50	6	30	110	150	¬ 12	235	40
PRP2	80	10	40	140	170	¬ 16	235	40
PRP3	110	12	50	160	190	¬ 20	235	40

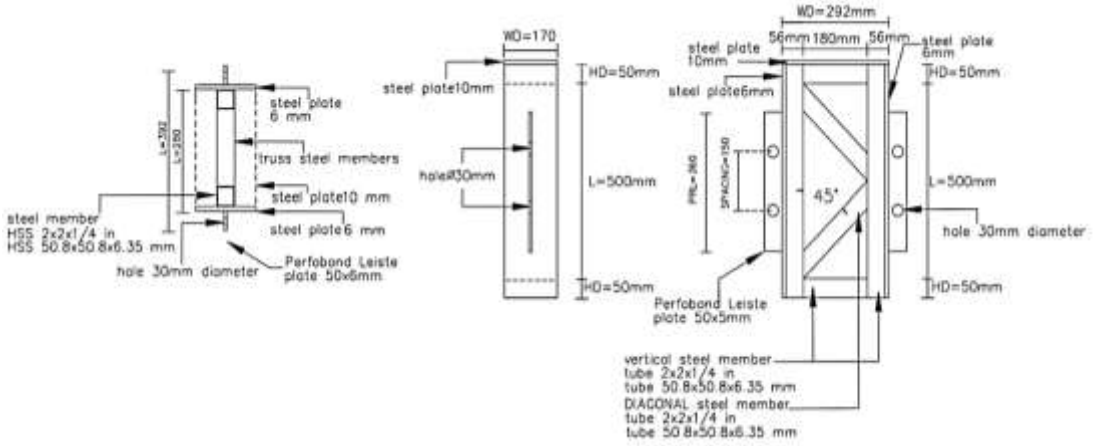

(a)

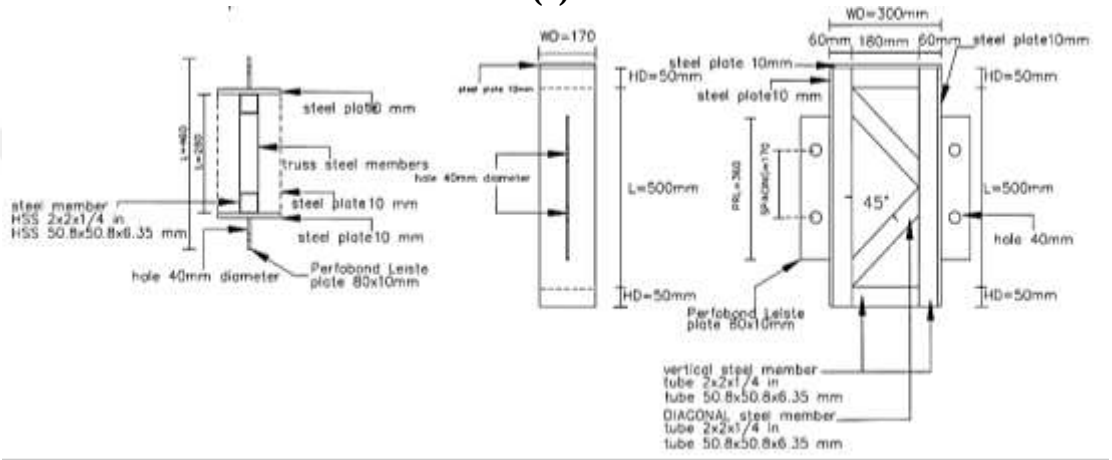

(b)

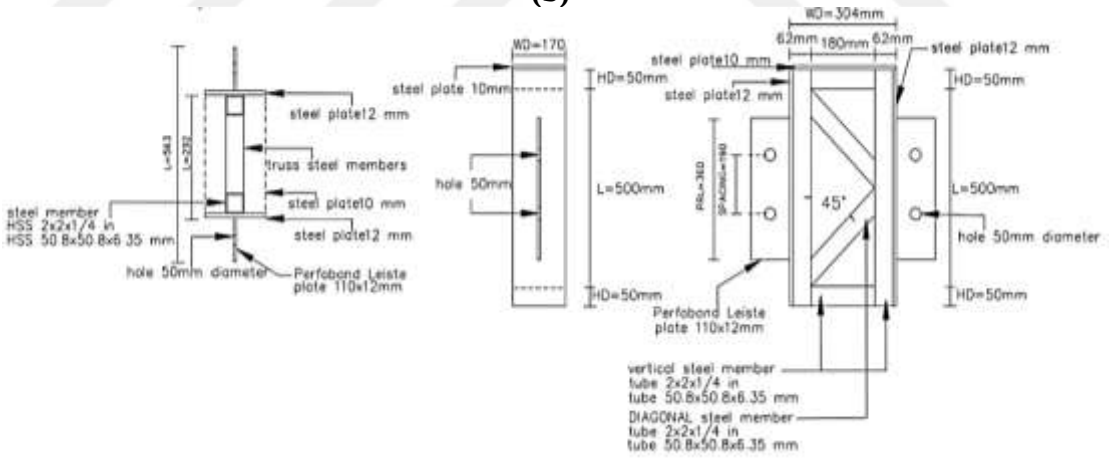

(c)

Figure 4.7: Perfobond Ribs Specimens' Dimensions for Push Out Test (a) (PRP1) Sample, (b) (PRP2) Sample, (c) (PRP3) Sample

Figure 4.8: Position of LVDT Device for the Push-Out Samples

4.3 Experimental Procedure and Specimens Fabrication

4.3.1 The push – out samples fabrication

The fabrication through several steps from cutting the steel plate and the steel HSS member type diagonals and verticals with the required dimensions, as well as the cutting progress for the perfobond ribs shear connectors.

All the connections methods get done by MEG type welding, as shown at Figure 4.9, and for the steel reinforcement of the three samples, bars with diameters of 10 mm are used with longitude spacing 100 mm and lateral 120 mm, as shown at Figure 4.10 (a) and (b).

Moreover, a three-casting wooden mold was made each one has two parts, as illustrate by details drawing in Figure 4.11 to Figure 4.14, it's get sliding inside the steel structure by the open path with width 50 mm, until the mold reaches the right position to be prepared the concrete pouring stage, for three samples required quintets about 2 m^3 of concrete get prepared for the concrete casting stage, the steps are shown in the Figure 4.15 to Figure 4.17.

Figure 4.9: Push Out Test Specimens Steel Parts Welding

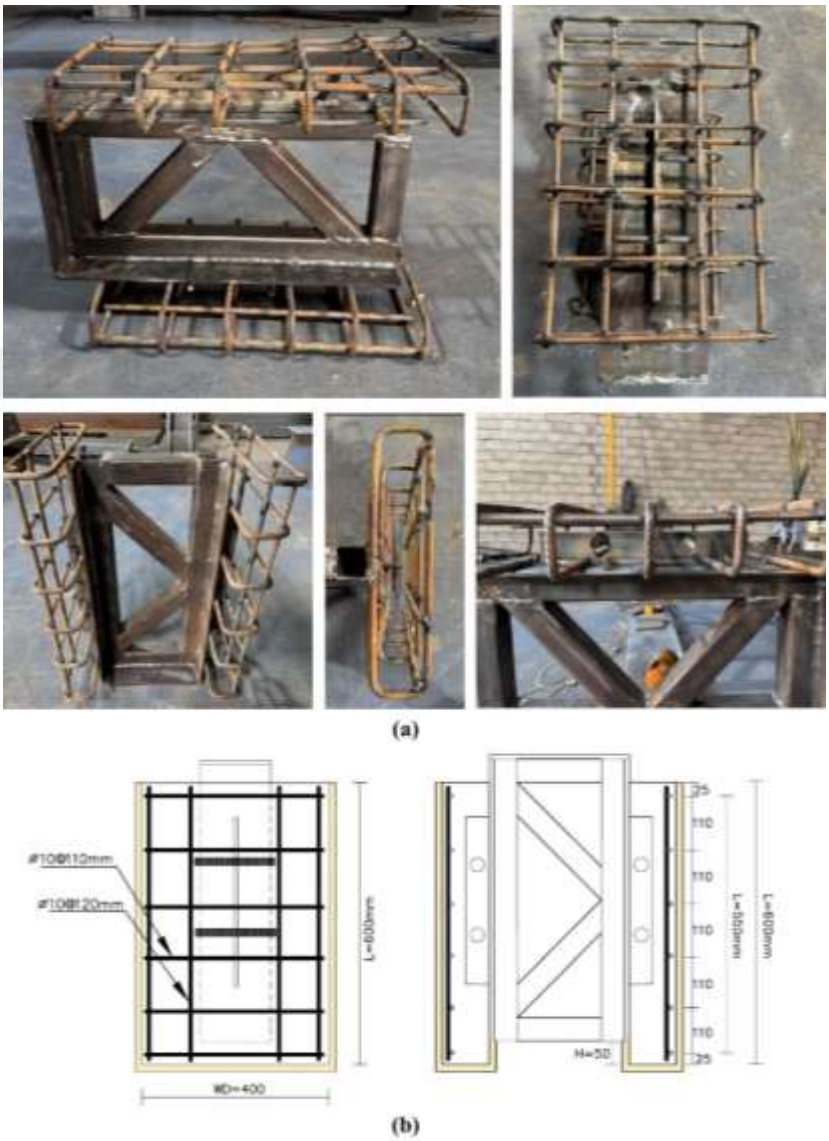

Figure 4.10: (a) Reinforcement Bars of the Push- Out Test Specimens & Perfobond Lesite (b) Reinforcement Bars of the Push- Out Test Specimens AutoCAD

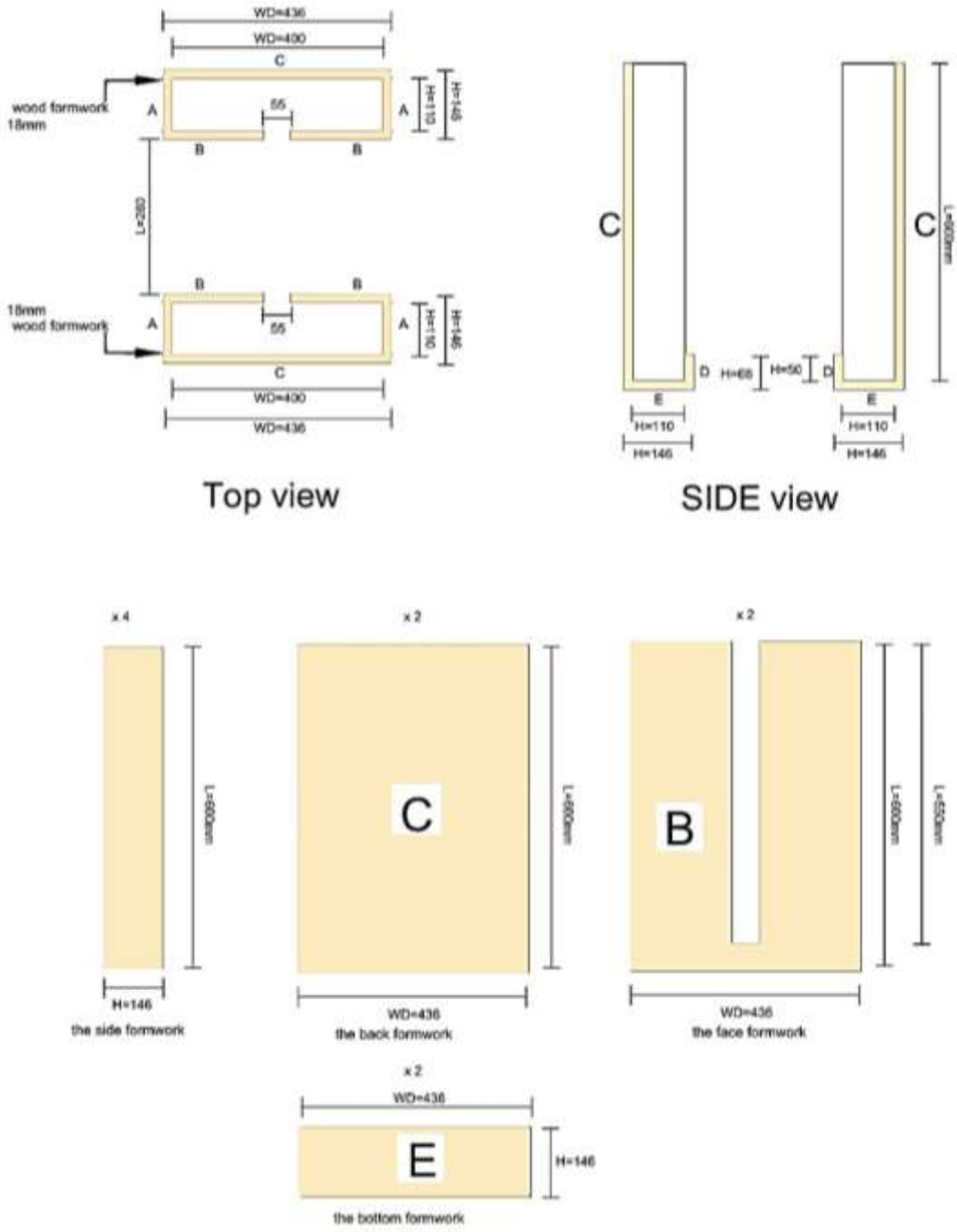

Figure 4.11: Wooden Mold of the Push-Out Test Specimen (PRP1)

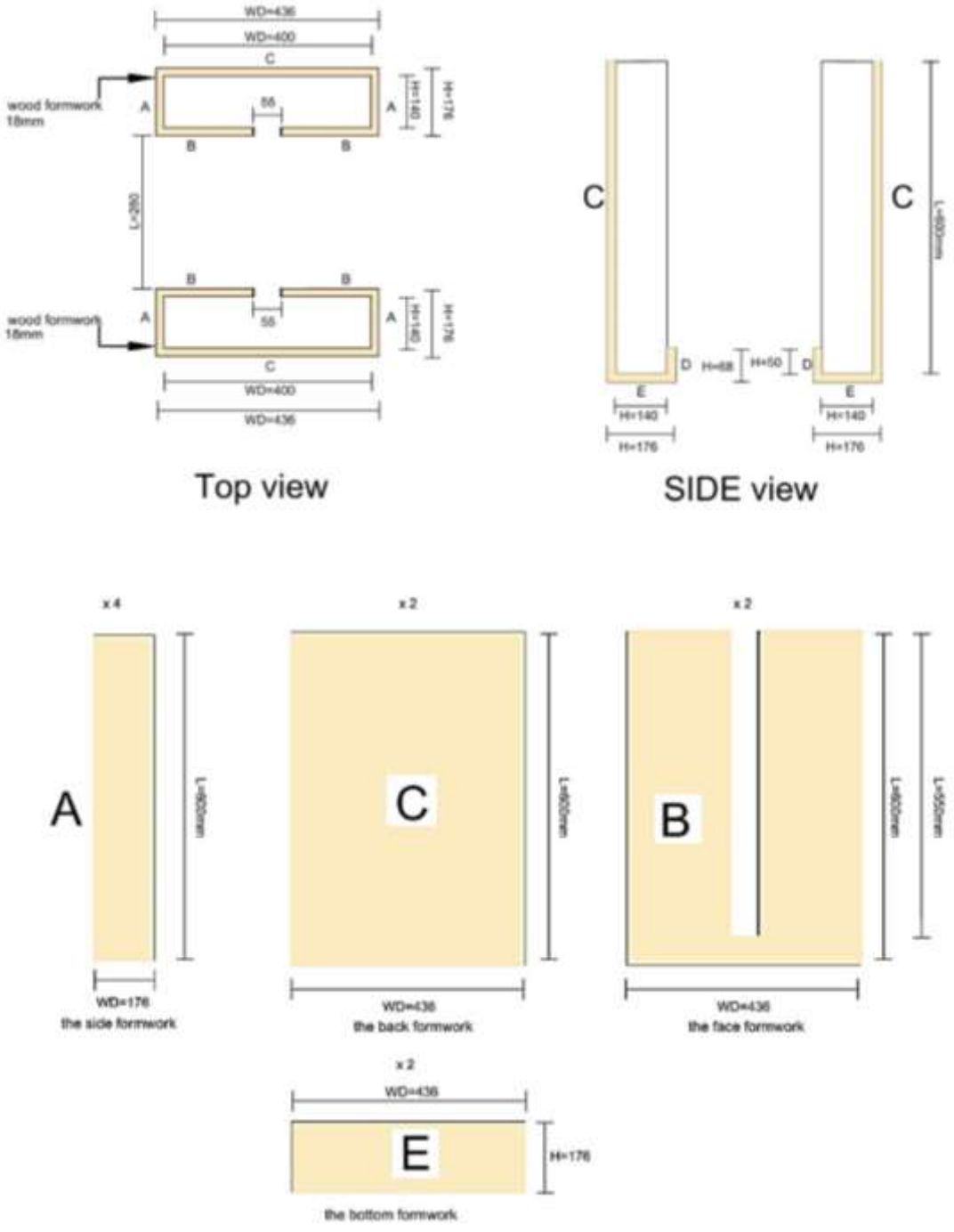

Figure 4.12: Wooden Mold of the Push-Out Test Specimen (PRP2)

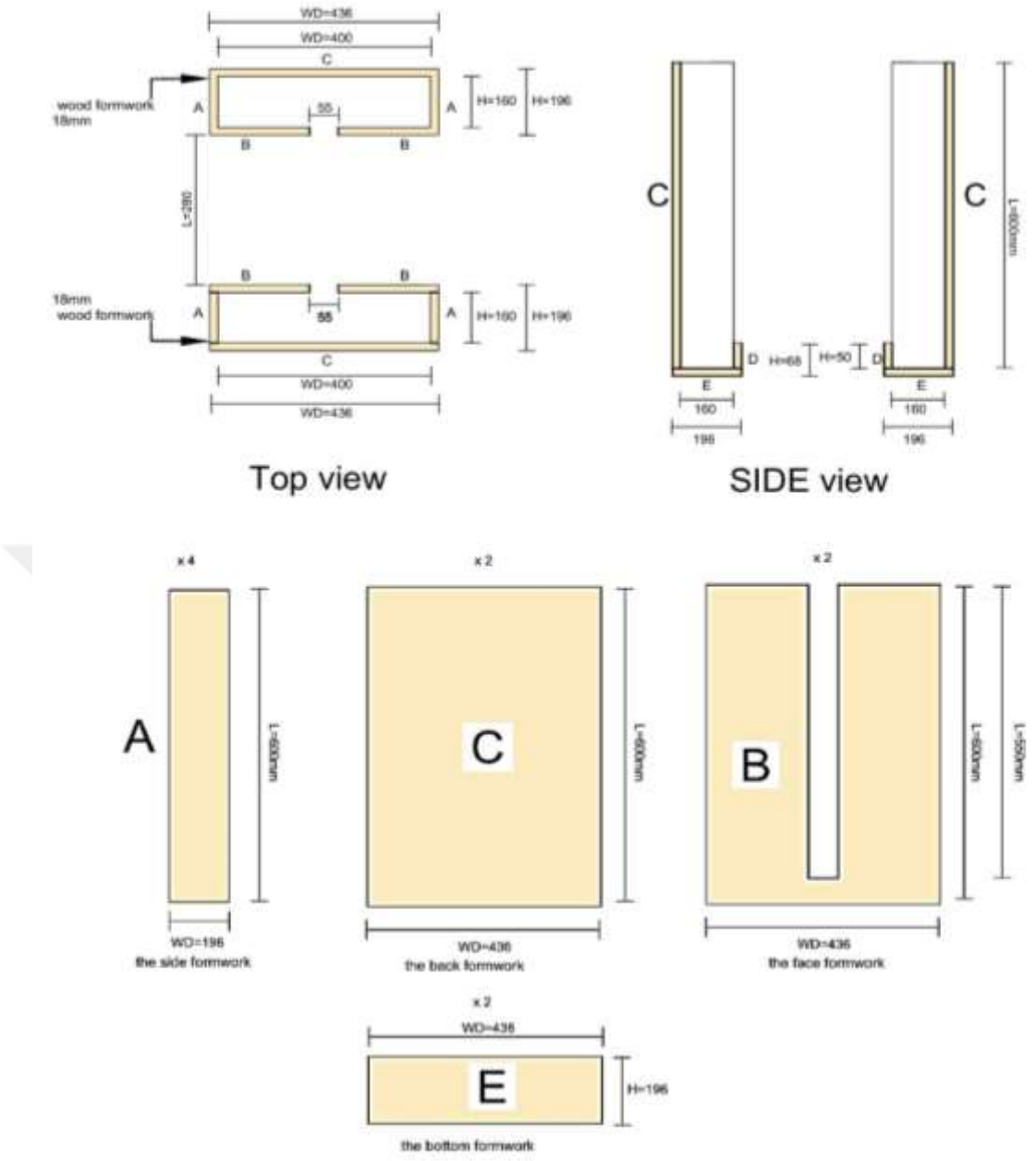

Figure 4.13: The Wooden Mold of the Push-Out Test Specimen (PRP3)

Figure 4.14: Wooden Mold of the Push- Out Test Specimens

Figure 4.15: Installation of the Wooden Casting Mold with the Samples

Figure 4.16: Concrete Pouring of the Push-Out Specimens

Figure 4.17: Final Shape of the Push- Out Specimens

4.3.2 Concrete mix proportion

In accordance with the ASTM C39 specification, concrete cylinders evaluating 15 cm in diameter and 30 cm in height were fabricated for splitting and compressive strength assessments during the casting of the concrete slab for each specimen.

The nominal concrete compressive strengths and tensile strength attained after 28 days of curing for the push-out test, Category 1 and Category 2 respectively, are detailed in Table 4.6.

Table 4.6: Mix Proportion of Concrete

Specimens Model	Design Strength (N/mm2)	aggregate size(mm)	Slump (mm)	Water Content %	Air %	Unit Cement (Kg/m3)	Unit Salinity (Kg/m3)
Push- out test	40	< 20	80 ± 25	< 55	4.5 ± 1.0	> 230	≤ 0.3
Category 1	25	< 20	80 ± 25	< 55	4.5 ± 1.0	> 230	≤ 0.3
Category 2	25	< 20	80 ± 25	< 55	4.5 ± 1.0	> 230	≤ 0.3

4.3.3 Fabrication procedure of the category one

This type refers to single composite girder connect from the top only, connect the steel top flange with the concrete deck slab by shear connector, the steel top and bottom flange made from plate 6-12 mm thickness and the vertical and diagonal truss member formed as steel tube HSS 50.8 mm x 50.8 mm x 6.35 mm, all the steel members (perfobond lesite and steel tube HSS) connect with the flanges by MIG welding of 4 mm thickness (mix of 75% argon and 25% CO2).

The perfobond ribs located to the above of top steel flange with different spacing and the hole in the steel plate made by drilling machine with required diameter, this category consist deck slab made from reinforcement concrete strength 35 MPa with effective width 400 mm and different in depth from specimen to another according to drawing 70 – 100 mm with reinforcement steel BRC bars 6¬ mm in both longitudinal and lateral ways, the depth of the cross section is 400 mm all specimens, Figure 4.18 to Figure 4.20 illustrate the manufacturing steps.

(a) (b)

Figure 4.18: Manufacturing of Category (SCTG). (a) HSS Diagonals Members Welding, (b) Cross-Section of the Truss Girder

(a)

Figure 4.19: Main Structure Body Manufacturing of Category (SCTG). (a) Side View of the Truss Girder (Steel Plate With Vertical & Diagonal HSS), (b) Side View of the Truss Girder (Welding Stage of the Bottom HSS)

Figure 4.20: Manufacturing of Perfobond Leiste of Category (SCTG). (a) Steel Plate Cutting Machine with Perfobond Leiste and Holes Bars Welding, (b) Located of the Perfobond Lesite and Reinforcement Bars at Final Stage

4.3.4 Fabrication procedure of category two

This category type refers to double composite girder connect from the top and bottom, connect the top steel flange with the concrete deck slab by shear connector, the top and bottom steel flange also made from plate 6-12 mm thickness, the cutting system of the plate was by the laser cutting machine as showing at Figure 4.21, the vertical and diagonal member formed as steel tube (HSS 50.8 x50.8 x 6.35) mm, all the members connect with the flanges by MIG welding of 4 mm thickness (mix of 75% argon and 25% CO2), the perfobond leiste connect at above the top and bottom steel flanges by welding, the hole in the steel plate made by drilling machine with required diameter, this category consist deck slab made from reinforcement concrete 35 MPa pouring with effective width 400 mm and different in depth from specimen to another 70–100 mm and bottom concrete pouring at the same way that the top

deck slab, the width of the bottom concrete as the same of steel bottom flange width, the both concrete had reinforcement steel bars 6¬ mm in both longitudinal and lateral ways, the depth of the steel cross section is 350 mm for all category specimens, Figure 4.22 to Figure 4.24 illustrates the manufacturing of category two specimens showing the final steel frame shape for eight specimens of category one and two before the concrete casting phase.

Figure 4.21: Steel Cross-Section of Category Two Specimens (DCTG)

Figure 4.22: Instillation Of Perfobond Leiste for Category Two Specimens (DCTG). (a) Bottom Perfobond Leiste Shear Connector Installation, (b) Top Perfobond Leiste Shear Connector

Figure 4.23: Holes Steel Plate Bars Instillation of Category Two Specimens (DCTG). (a) Top Holes Bars of Perfobond Leiste Shear Connector Installation, (b) Bottom Holes Bars Perfobond Leiste Shear Connector Installation

Figure 4.24: Final Stage of the Category (DCTG) and (SCTG)

4.3.5 Formwork of the Composite Truss Girder

In total 8 molds are used in the test for the main eight composite truss girder for the top concrete flanges and bottom flanges these used for the double composite girder, and 3 wooden molds are used for casting concrete stage for deck slabs of push out test specimens that will get examined as explained previously in this chapter, there molds are implemented with 18 mm in thickness of wooden plate, formed together with nails in method to achieve the required shape and dimensions of the concrete slab, Figure 4.25 to Figure 4.28 illustrate the shape and dimensions of wooden molds and installations stage.

Figure 4.25: Main Eight Specimens' Wooden Molds

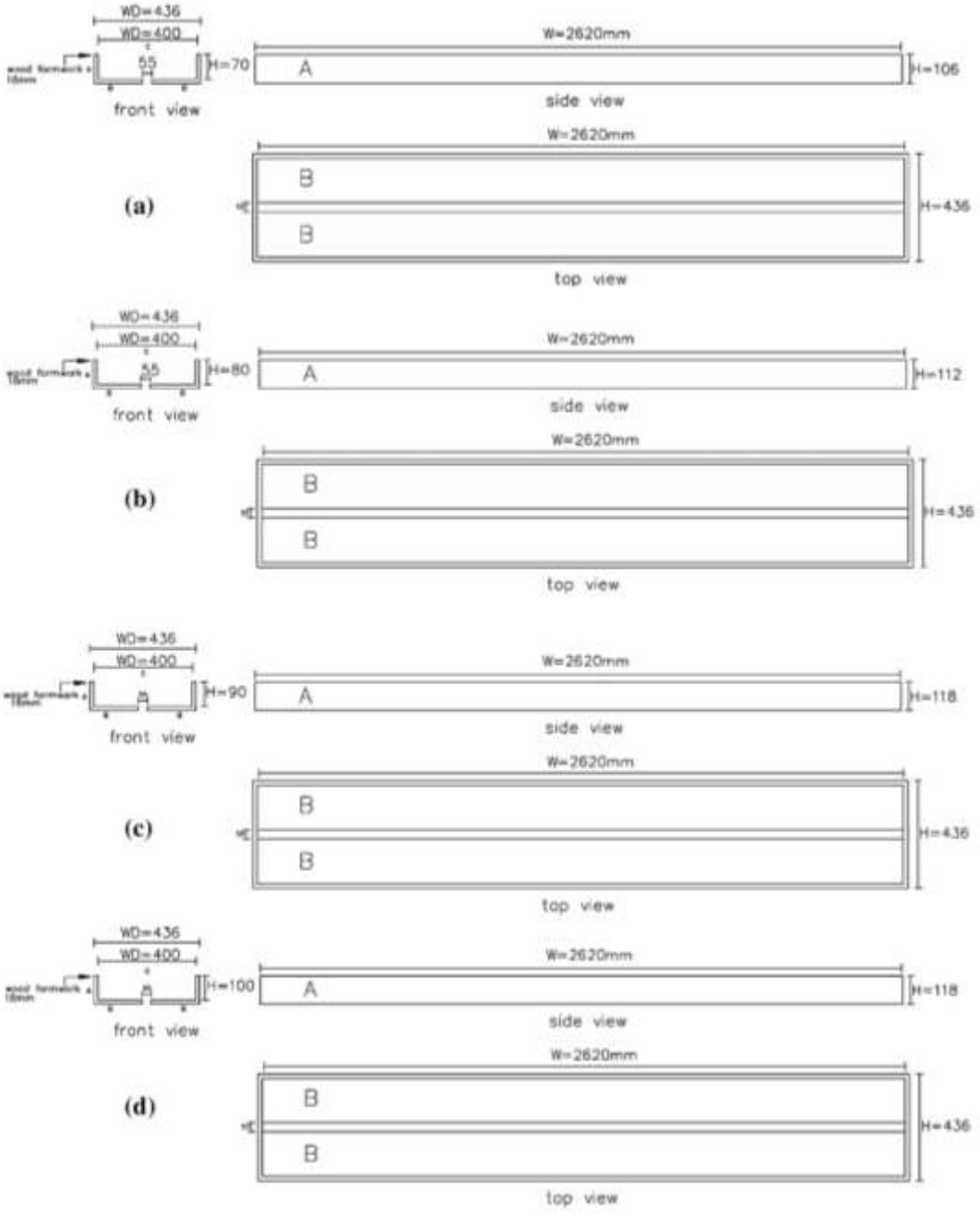

Figure 4.26: Main Eight Specimens' Top Wooden Molds Drawing Sheets and Dimensions. (a) Top Molds for the SCTG-1 and DCTG-1, (b) top Molds for the SCTG-2 and DCTG-2, (c) top Molds for the SCTG-3 and DCTG-3, (d) top Molds for the SCTG-4 and DCTG-4

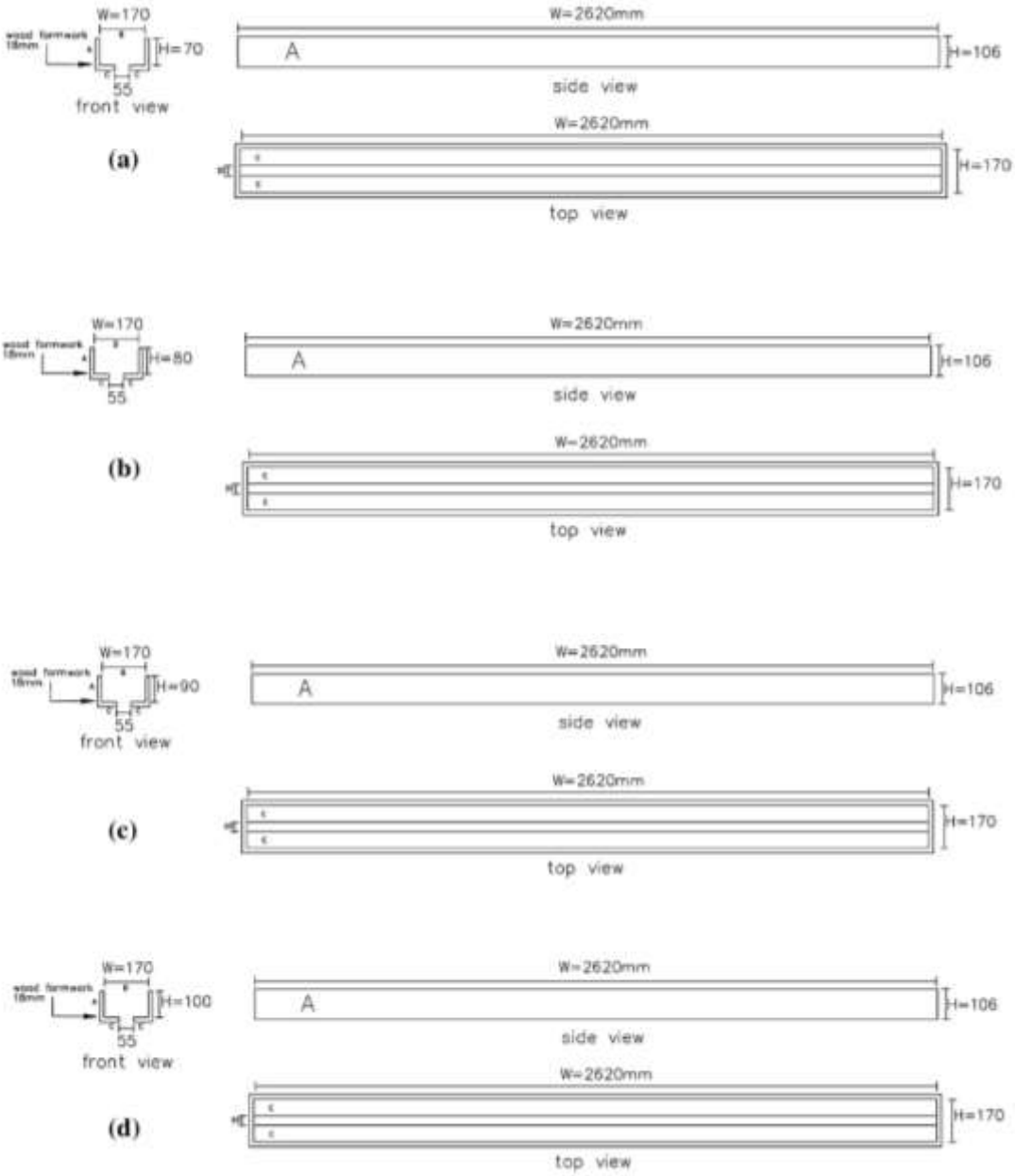

Figure 4.27: Main Eight Specimens' Bottom Wooden Molds Drawing Sheets and Dimensions. (a) Bottom Molds for DCTG-1, (b) Bottom Molds for DCTG-2, (c) for the Bottom Molds of DCTG-3, (d) Bottom Molds for DCTG-4

Figure 4.28: Main Eight Specimens' Wooden Molds site Installation. (a) Supports the Top Mold With Steel Bars By Welding, (b) Top Mold Installation, (c) Sliding the Molds to the Steel Girder, (d) Bottom Mold Installation for (DCTG), (e) Bottom and Top Mold Installation, (f) Top Mold Installation for (DCTG)

4.4 Specimens Materials Properties

All samples of materials to be used in the experiment of cement, fine aggregate, coarse aggregate, water, reinforcement steel, will check based on the AASHTO specification and steel ASTM specification and all the above materials will be thoroughly examined and we get results that show the properties of these materials through laboratory examination at the Iraqi National Center for Construction Laboratories and Consultant Lab of Technological University.

The following is general information and properties of the materials considered in the experimental work:

4.4.1 Cement

Ordinary Portland cement will be used for all experimental work specimens, all cement bags will be stored in special storages in a laboratory to avoid being affected by weather factors that affect its properties. Table 4.7 and Table 4.8 illustrate the physical and chemical properties of cement, depending on the results that have been conducted, the cement conforms to the AASHTO specification.

Table 4.7: Physical Properties of Cement

Physical properties	Test results	AASHTO Specification
Specific surface area (kg/m2) (Blaine method)	320 kg/m²	300 to 600 kg/m²
Setting time (Vicat's method)		
Initial setting time: (hrs.: min)	50 minutes	45 minutes
Final setting time: (hrs.: min)	8 hours 30 min	10 hours
Compressive strength, MPa		
At 7-day	17 MPa	Min. 15 MPa
At 28-day	28 MPa	Min. 25 MPa
Loss on Ignition	3.2 %	Max. 5%
Soundness (Autoclave method)	0.6 %	Max. 0.8 % expansion

Table 4.8: Chemical Compounds of Cement

chemical compounds	Chemical sample	Content %	Limitation of AASHTO Specification
Loss of ignition	L.O. I	2.65	Max. 3.0%
Insoluble materials	I.R	0.6	Max. 1.0%
sulfate	SO_3	2.2	Max. 3.0%
Chlorides	cl	0.04	Max. 0.06%
Tricalcium aluminate	C_3A	5.9	With Range. 5% to 15%
Magnesia	MgO	3.6	Max. 6.0%

4.4.2 Fine aggregate

The main fine material is the natural sands with maximum size 4.75 mm, these materials will be test it and evaluated it according to Iraqi specification No.45/1984 to find in which zone will be related as shown in Table 4.9 and Table 4.10 Through which the physical and chemical properties of materials are examined, The gradation of the materials included in the examination, as well as all other characteristics, indicates their conformity to the Iraqi specification and related to (zone 2).

Table 4.9: Grading of the Fine Aggregate

Sieve size mm	Cumulative Passing %	Limit of the Iraqi specification No.45/1984			
		Zone 1	Zone 2	Zone 3	Zone 4
10	100	100	100	100	100
4.75	95	90-100	90-100	90-100	95-100
2.36	85	60-95	75-100	85-100	95-100
1.18	74	30-70	55-90	75-100	90-100
0.6	32	15-34	35-59	60-79	80-100
0.3	15	5-20	8-30	12-40	15-50
0.15	5	0-10	0-10	0-10	0-15
Finer than 0.075	2	Max. 3			

Table 4.10: Chemical Compounds of Natural Sand

Properties	Test results	Limit of the Iraqi specification No.45/1984
Specific Gravity	2.8	Min: 2.60
Absorption %	1.5	Max: 2.0%
Sulfate content SO3 %	0.22	Max: for all structural elements 0.5 %

4.4.3 Coarse aggregate

Crushed gravel with maximum size 10 mm will be used in concrete mix. these materials will test and evaluated it according to Iraqi specification No.45/1984, Table 4.11 shows the physical properties of materials that get tested, the gradation of the materials included in the examination test, indicates their conformity to the Iraqi specification.

Table 4.11: Grading of the Coarse Aggregate

Sieve size mm	Cumulative Passing %	Limit of the Iraqi specification No.45/1984		
		(5-14) mm	(5-20) mm	(5-40) mm
75	100	100	Not limited	Not limited
63	100	Not limited	Not limited	Not limited
37.5	100	95-100	75-100	Not limited
20	100	35-70	95-100	100
14	100	Not limited	Not limited	90-100
10	80	10-40	30-60	50-85
5	7	0-5	0-10	0-10
2.36	3	Not limited	Not limited	Not limited

4.4.4 Additional materials

4.4.4.1 Conplast SP- 423 type G

Type of superplasticizer which properties conform to the ASTM C-494-04 specification, the recommended dosage ranges from 0.5% to 2.0 % of the weight of cement.

Conplast SP-423 is an organic polymer-based, chloride-free workability retention admixture, the chemical describes this object as brown solution, it dissolves in the water of the concrete mixture to increase the workability, cohesive and retardation, a details conplast SP- 423 material sheet located in (Appendix B)

4.4.4.2 Silica fume

It's a highly reactive pozzolan mentioned and partial cement replacement, by several physical and chemical properties that this substance contains, by this material that the durability and high strength can be obtained to concrete mix, in this research work this product must be conforms the ASTM C-1240-5 limitations, Table 4.12 illustrates the results.

The silica fume material sheet located in (Appendix B)

Table 4.12: Chemical Composition of Silica Fume Product

NO.	Compound Composition	Chemical Composition	Weight %	ASTM C-1240-5 %
1	Silica	SiO_2	90	Min. 85
2	Magnesia	Mgo	2.9	Max. 4
3	Alumina	Al_2O_3	0.22	Max. 10
4	sulfate	SO_3	0.88	Max. 1
5	Iron oxide	Fe_2O_3	1.02	Max. 5
6	Lime	CaO	0.83	Max. 6
7	Loss of ignition	L.O.I	0.86	Max. 3

4.4.5 Water

All research works for concrete mix, and all specimens get cured process with tap water without any percentage of salts that may effects on the specimens' elements.

4.4.6 Concrete Mix Design

The Ordinary Portland Cement (OPC) in the normal weigh concrete mix design will be adopted to this research to achieve compressive strength around 35 MPa for the main eight samples and 40 MPa for the three push-out samples, the mixed materials and preparties conform to the ACI 211.1-91 specifications. Table 4.13 illustrates the mixed design results.

Table 4.13: Concrete Mix Design

Mix Type	Cement Kg/m3	(gravel) Course aggregate kg/m3	(sand) fine aggregate kg/m3	Water Content kg/m3	Silica Fume kg/m3	SP kg	Modulus of Elasticity (Ec) (GPa)	Density Kg/m3	Compressive Strength (f_c') MPa
NWC	400	364.32	242.88	180	24	3.2	29.58	2298	35
NWC	400	1200	600	160	20	1.5	31.62	2400	40

Note: these results of three (150 x 300) mm cylinder test

The modulus of elasticity form = $E \approx 5000 \times \sqrt{f_c'}\ (\text{MPa})$

SP: refer to the superplasticizer additive materials

4.5 Steel Materials

4.5.1 Steel truss member and flanges

In this study, steel flanges as steel plate 170 mm x 6 -12 mm in thickness and a steel tube square HSS 50 mm x 50 mm x 6.35 mm were used for the vertical and diagonal truss member and square HSS 50 mm x 50 mm x 4 mm used as bottom member, the sections properties and dimension are illustrated in Table 4.14.

All cutting prouder will be made according to ASTM-A370-2022**,** The steel material test performed in the Iraqi National center for structural laboratories to find the mechanical properties; all the results shown in Table 4.15, the steel materials teat certificate attached to (Appendix B).

Table 4.14: Properties of HSS 2x2x1/4 in and HSS 2x2x5/32 in

Section	W Kg/m	It cm^4	r mm	A cm^2	V cm^3/m	V pl,y KN	N pl KN	M pl,y KN	I_y x 10^3 cm^4
V.M	8.0	58.03	17.6	10.25	974.19	76.592	240.776	3.86	31.86
D.M	8.0	58.03	17.6	10.25	974.19	76.592	240.776	3.86	31.86
B.M	6.4	48.36	18.4	8.18	767.74	59.495	192.291	3.23	27.80

Where: V.M is vertical HSS member, D.M is diagonal HSS member, B.M is bottom HSS member, Npl is ultimate resistance to axial force, Vpl,y is plastic limiting shear force , Mpl,y is Plastic limiting bending moment about y-axis Iy is Area moment of inertia about y-axis, R is radius of gyration about y-axis

Table 4.15: Steel Elements Mechanical Properties

Members	Poisson's ratio (ν)	Yield strength (fy) MPa	Ultimate strength (fu) MPa	Elongation %
Steel Flanges	0.3	280	407	37.7
vertical Member	0.3	511	520	6
Diagonal member	0.3	511	520	6

The steel sections are Mild Steel **(ASTM ST37)** classified as carbon structural steel.

4.5.2 Steel reinforcement

Steel BRC bars with a diameter of 6 mm are placed in the deck slab casting for the first category as well as the lower base flange casting for the second category with spacing 150 mm x150 mm c/c in both directions one layer, as shown in Figure 4.29 and Figure 4.30**,** and steel diameter of 6 mm, 12 mm and 16 mm will be used as penetrating rebar passing through the rib's palate hole for each sample.

The required test was made according to ASTM-A615-20 Standards; Table 4.16 shows the results of the steel bars test.

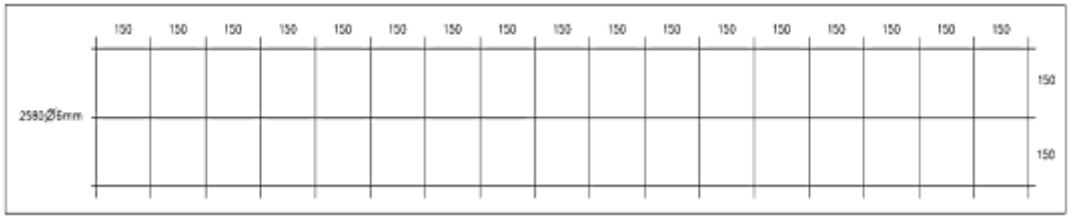

(a)

(b)

Figure 4.29: BRC 150 x150 Reinforcement Details. (a) Reinforcement Bars of the Top Concrete, (b) Reinforcement Bars of the top Concrete

Table 4.16: Steel Bars Elements Mechanical Properties

Bar size	Poisson's ratio (ν)	Yield strength (fy) MPa	Ultimate strength (fu) MPa	Elongation %
Steel Bars 10 ¬	0.3	610	690	24
Steel Bars 12 ¬	0.3	620	700	21.4
Steel Bars 16 ¬	0.3	630	718	23
Steel Bars 20 ¬	0.3	614	706	20.5

Note: reinforcement bars test results attached to (Appendix B)

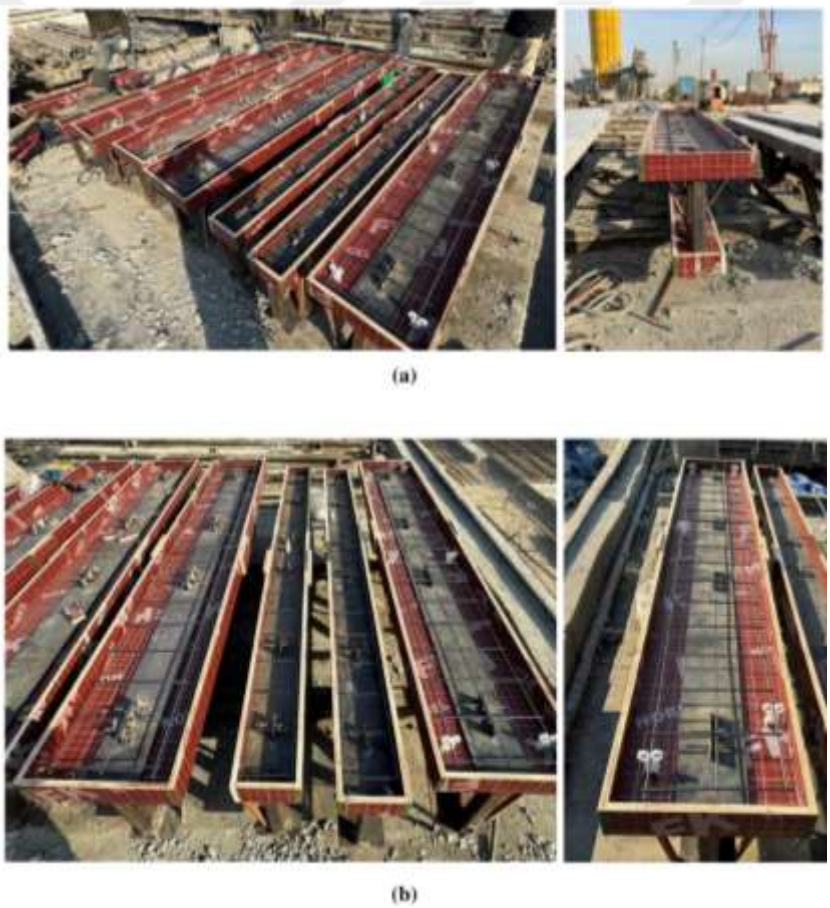

Figure 4.30: Site Reinforcement BRC installation Above the Specimen. (a) BRC Installation Forthe (SCTG) and (DCTG), (b) Addition Spacer for Cover Control for the (SCTG) and (DCTG)

4.5.3 Perfobond lesite shear connecter

The main aim is to create a real connection between the steel section and the concrete deck slab with fully transfer of shear forces, the main factor that affected on

the is the parameter of the shear connector and the spacing its part, in this experiment study we will implementation these connectors with variable parameter to study the difference of effect.

For category one, the length distribution of connectors will be on the top flange only, Table 4.2 shows the perfobond ribs parameter for (SCTG) specimens.

For category two, the length distribution will be in both the top and bottom flange, as in Table 4.4 shows the perfobond ribs parameter for (DCTG).

For both category manufacturers, carbon steel plates will be welded, and the materials will be tested according to the ASTM-A370-2022, Table 4.17 and Figure 4.31.

Table 4.17: Perfobond Leiste shear connector steel plate materials test

Member	Poisson's ratio (ν)	Yield strength (fy) MPa	Ultimate strength (fu) MPa	Elongation %
Ribs plate shear connector	0.3	280	407	37.7

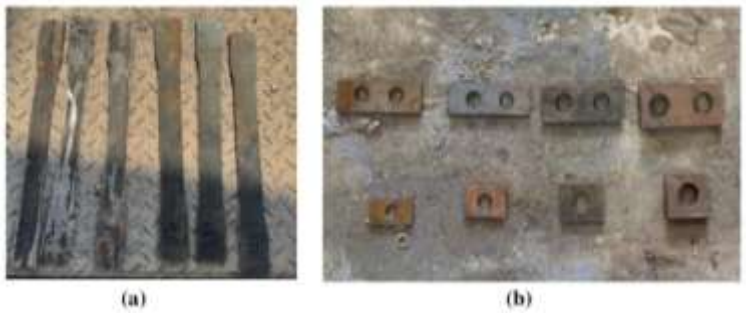

Figure 4.31: Site Reinforcement BRC Installation Above the Specimen. (a) Sampling of the Steel Plate, (b) Perfobond Lesite Samples

4.6 Mixing, Poring and Casting Procedure of Concrete

The total quantities that used to be cast on top and bottom flange about 4 m^3 get prepared and weighed by electronic mixer at Central concrete mixer.

The normal weight concrete mixing materials as the (cement, sand and gravel) put into the blender in a gradual manner with the required amount of water, the mix proses done at two times operation, the first mix time for the top concrete of the (SCTG) and bottom concrete for (DCTG) and the second time for the top concrete of the (DCTG) after 24 hours concrete get casting the specimens get flab

upset down to poring the top slab deck, Figure 4.32 to Figure 4.34 shows the casting steps for the single and double composite girders.

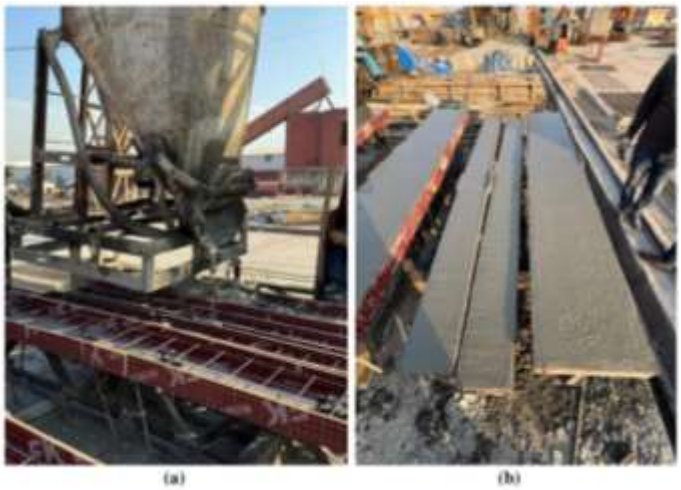

Figure 4.32: Steps of Concrete Pouring the Main Truss Girder (SCTG) and (DCTG). (a) Poring the Concrete Mix Stage, (b) Final Step of the top and Bottom Concrete

Figure 4.33: Steps of Poring and Concrete Casting of the Main Truss Girder (SCTG) and (DCTG). (a) Final Poring Shape of all Specimens, (b) Mix Distribution with Vibration Tools, (c) Concrete Casting Stage of the (SCTG)

(a)

(b)

Figure 4.34: Steps of Concrete Casting of the Main Truss Girder (SCTG) and (DCTG). (a) Concrete Casting Stage of the (DCTG), (b) Concrete Casting Stage of All Eight Specimens

4.7 Concrete Mechanical Properties

It requires 12 Cylinder inspection for the purpose of evaluating and analyzing the properties of the concrete that are used, 6 cylinders for the first concrete pouring of the push out test three sample and 6 cylinders for the main eight composite girder, Table 4.18 and Figure 4.35 illustrate the steps and properties with the research requirement and sampling for the test.

Table 4.18: Quality Concrete Control Specification

Test name	NO. of specimens	Dimension (mm)
Compressive strength f_c'	10	150 x 300
Splitting tensile strength f_{ct}	2	150 x 300

4.7.1 Compressive strength (f'_c)

This test was done according to the ASTM C39M by using the cylinder 150 mm x 300 mm to evaluate concrete due to the compressive strength properties using four specimens then take the average results of the five specimens 14 days and the other five samples at 28 days, the test done with compression machine capacity 2000 KN at engineering laboratory of Technology university.

Figure 4.35: Compressive Strength Test

4.7.2 Splitting tensile strength (f_{ct})

This parameter was performed according to ASTM C496M by using standard cylinder 150 mm x300 mm, The sample is placed horizontally, and the forces are shed to the limit of failure and the failure forces are measured for three circular samples and the rate of these samples is taken. Test results attached to (Appendix B).

Also, the formula below can be used to determine the splitting tensile strength:

$$f_{ct} = \frac{2P}{\pi LD} \tag{4.1}$$

Where: f_{ct} is split strength, P is compressive load, L is length, D is diameter.

5.7.3 Modulus of elasticity (E_c)

In the context of the elastic limit of the material, the modulus of elasticity is defined as the ratio of stress, which is defined as the force per unit area, to strain, which is defined as the deformation relative to the original length.

The line will be drawn between the two points that plot on the stress - strain curve, and the lower point (first one) which refers to the effect of crack in the initial stage and it's (0.00005), the upper point (second one) Estimated at about forty percent of the value of ultimate stress.

$$Ec= S2-S1 / \varepsilon 2 - 0.0005 \quad (4.2)$$

Where: Ec is the elastic modulus in MPa, S2 is stress at 40 percent of the ultimate load in MPa S1 is stress to the strain (0.00005) in MPa, ε2 is stress at stress S2.

4.8 Experimental Measurements and Instrumentation

There are several pieces of equipment required in this experiment study to measure the data of deflection in the specific point and the strain in the composite truss steel with concrete girder especially at the deck surface from the initial load until the failure load.

4.8.1 Strain gauges measurement

Foil strain gauges are sensors that are used to measure the relative changes in the length of a material that occurs because of the application of forces.

During this stage, the strain evaluation of each part of the steel and concrete is measured by strain gauges devices, where six devices typically a metal foil strain gauges with 120 ohms and GF equals to 2 are used such as (FLA-10-11) to measure the strain at the steel parts.

While type of (PL-60-11) was used to the concrete deck slab for top and bottom surface for each specimen, strain devices are in several places as illustrated in Figure 4.36 to Figure 4.38, and Table 4.19.

Necessary adhesive materials are used to create the required contact between the strain's gauges and the elements' part that are planned to be measured.

Table 4.19: Details of the Strain Gauges Devices

Model	Length	Gauge Factor	Plot location	Resistance
FLA-10-11	10 mm	2	steel parts	120 ohms
PL-60-11	60 mm	2	concrete deck slab	120 ohms

Figure 4.36: Strain Gauges and Adhesives Materials

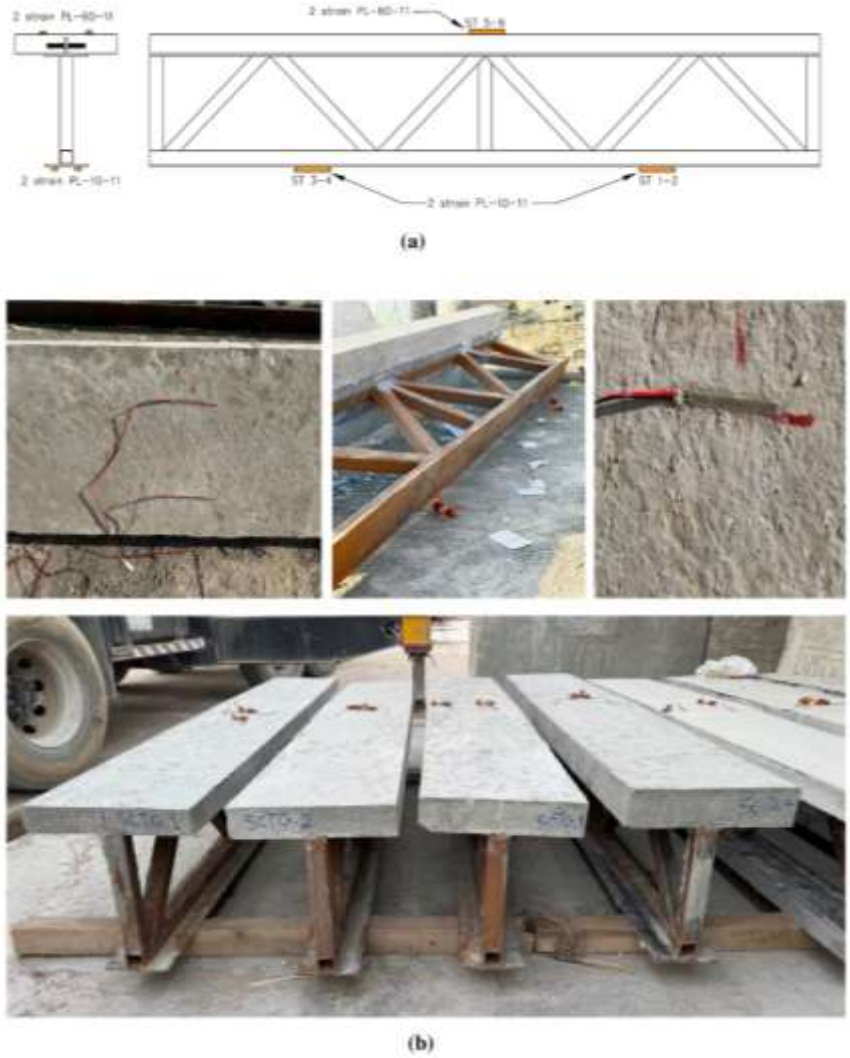

Figure 4.37: Position of the Strain Gauges for Category One Specimens (SCTG). (a) Strain Gauge Location Drawing sheet for the (SCTG), (b) Site Installation of the Strain Gauge for the (SCTG)

Figure 4.38: Position of the Strain Gauges for Category One Specimens (DCTG). (a) Strain Gauge Location Drawing Sheet for the (DCTG), (b) Site Installation of the Strain Gauge for the (DCTG)

4.8.2 Deflection and relative slip indicators

A two LVDT indicator (Linear Variable Differential Transformer) is used in the main eight specimen test for the purpose of finding deflection in the samples to be examined in the site (measure linear displacement).

Two device installation in the bottom specimen in the middle distance of the middle and edge steel support to give the data analysis of the deflection profile that will increase gradually with loading.

For measured the relative slip ratio of the composite structure by installation Two LVDT device (3 & 4) in the top for the category (SCTG) and (DCTG) between the upper steel flange and the upper concrete at the outer face to indicate the movement at the interaction faces which it's depending on the type of the perfobond lesite.

One LVDT device was used in pushing out test samples to measure the relative slip between the steel and concrete.

The LVDT work concept is to convert the voltage output from the secondary coils into a usable signal for measurement and display and gives high accuracy with low measurement errors at all stages of loading till the failure mode, as in Figure 4.39 to Figure 4.43.

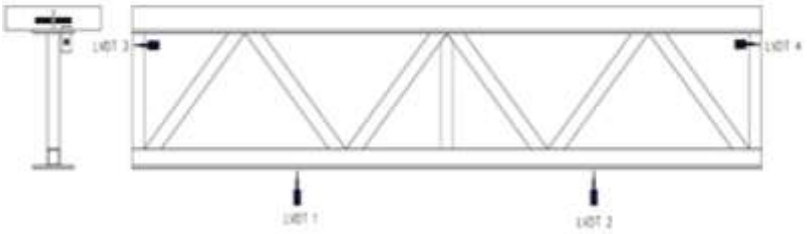

Figure 4.39: Position of the LVDT Indicator For Category One Specimens (SCTG)

Figure 4.40: Site Installation of the LVDT Indicator for Category One Specimens (SCTG)

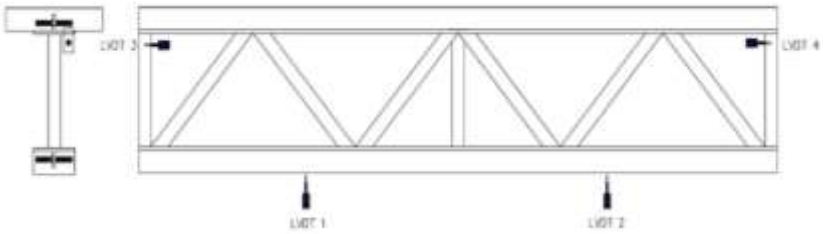

Figure 4.41: Position of the LVDT Indicator for Category Two Specimens (DCTG)

Figure 4.42: Site Installation of the LVDT Indicator for Category Two Specimens (DCTG)

Figure 4.43: Position of the LVDT Indicator for Push- Out Test Samples. (a) LVDT Installation (b) LVDT Device

4.9 Examination Steps

The main loading test of the eight main samples and the secondary test which includes the three push-out samples get performed at the site with special agreement, all specimens' categories had the same static loading and support conditions.

The sample to be examined is installation on three supports, two at both ends and one in the middle of the sample length, sample must be kept prevent from movement while the strain gauges are located as shown previously in Figure 4.36 to

Figure 4.38, as well as the two LVDT gauges to read the vertical deflection, Figure 4.39 to Figure 4.43.

The static load applied on the girder in two points of load between the middle support and the edge support to create the negative moment at the support region and the positive moment at the middle of support region.

By using the two hydraulic jacking of 3000 KN load capacity, each jack will apply load on specimen till the failure modes happened, meanwhile the sensors and devices indicated the required data that illustrate in this chapter, as shown Figure 4.44 to Figure 4.49.

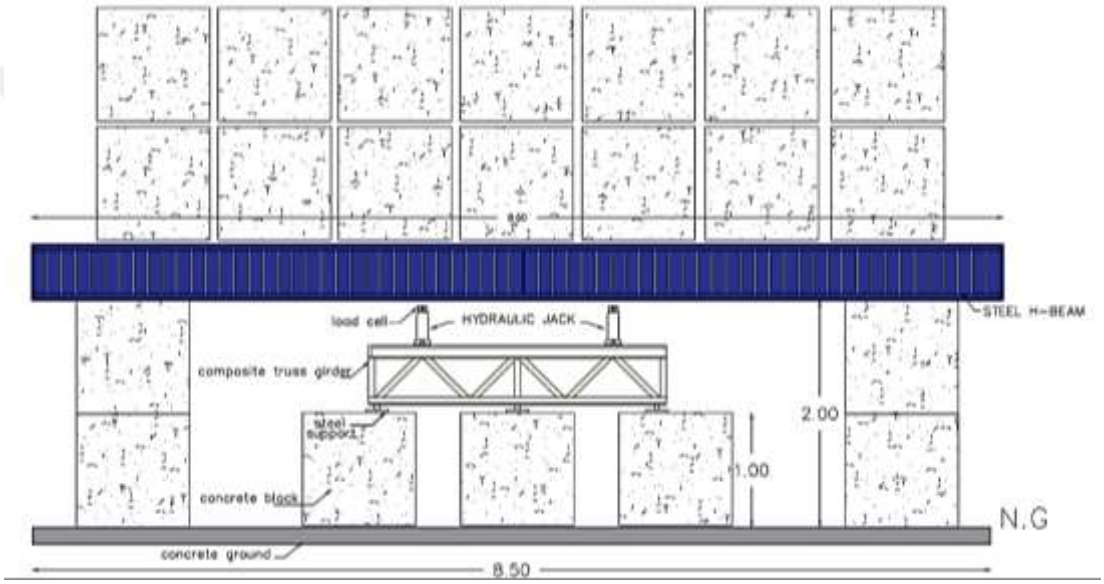

Figure 4.44: Hydraulic Machine and Load System Design Sheet

Figure 4.45: Hydraulic Jack and Load System Installation

Figure 4.46: Load Operation Setup In Universal Hydraulic Machine for Category One (SCTG)

Figure 4.47: Load Operation Setup In Universal Hydraulic Machine for Category Two (DCTG)

Figure 4.48: Hydraulic Jack and Data Logger Installation. (a) Indicated Data Analysis, (b) Data Logger Instrument

Figure 4.49: Load Hydraulic Machine for Push-Out Test. (a) Load Cell and Hydraulic Jack (b) Push-Out Samples Under Load

5. NUMERICAL MODELING AND SIMULATION USING ABAQUS CAE SOFTWARE COMPUTER PROGRAM

5.1 Introduction

The objective of using numerical modeling and simulation is to solve the complex analysis criteria of elements, especially the composite materials, while finite elements considered the most realistic solution of the more complex problem that will be used in this research.

The main reason for using ABAQUS 2023 software is its exceptional ability in the analysis of the issues about the plasticity and mechanical problems associated with this research and give the data of behavior the composite truss. It's considered as modern technology with are based on the principle of three-dimensional representation and the embodiment of the shape to be analyzed. The proposed model at this chapter prepares three-dimensional design steps for the validated samples included in the laboratory examination of the one and two categories.

5.2 Finite Element Theory

Knowing that there are several analytical approaches which is used to extract results from simple geometric models only, and to evaluate the complex structure element performance it should take in the consideration the numerical techniques due to the effective way to handle the complex structure geometries.

The finite elements analysis (FEA) nowadays considered the most relative numerical methods can be used to extract accurate analysis data.

The Abaqus program used finite element analysis to be providing the models under static load which will be presented as two points of displacement-controlled loading to the composite truss girder.

5.3 Materials characteristics and molding

5.3.1 Concrete material

Concrete can be defined using either linear elastic properties or more complex models that account for plasticity, damage, and other behaviors.

The concrete properties (tensile, strain, softening) can simulate and model the behavior of concrete with static load.

The tensile resistance characteristics of the concrete that cast surround the reinforcement bars can be used to simulate the stress transfer between the bars and concrete.

One of the ABAQUS materials features is concrete damage plasticity (CDP) used to simulate the damage Impact occurs to concrete due to increasing the load in both tension and compression and the point of plasticity failure.

In general, brittle materials such as concrete can be simulated by using the plastic models that are commonly available in Abaqus program, and the (CDP) is the perfect model that is used for this purpose especially in the phase of plasticity and it can give as accurate results of the materials response under different types of circumstances.

There are several (CDP) parameters, illustrated in Table 5.1 such as the dilatation angle (Ψ), can be about the degree of the plastic deformation in the (Kc) volume and Reflects the volume difference associated with plastic deformation of the model, and the variety values 20°- 45° which is the percent of the biaxial and the uniaxial strength (f_{b0}/f_{c0}) and represent the stresses ratio between the stress and compression, and the plastic number (K) represent the shape factor parameter which is the mount of the tension to compression and to find the response of the yield surface model, and the eccentricity of the flow rate (ε) represent how the material behaves under different stress states, especially in tension and compression, and it's defined as the ratio of the distance from the center of the yield surface to the edge of the yield surface in the direction of the compressive axis.

It reflects how much the yield surface deviates from a perfect circular shape, values for eccentricity in concrete modeling range from 0.1 to 0.3.

Lastly, the viscosity parameter (μ) which represents the material's resistance to flow under rapid loading conditions, it gives more realistic simulation to concrete behavior under static or dynamic loading and especially for sudden impact load.

Generally, the viscosity parameter values range from 0.001 to 0.1 for concrete material, the main feature of this parameter Centered around about increase the viscosity parameter can lead to more ductile behavior, that leads to the material to gradually deform with in loading increasing.

The (dc) and (dt) which are the main features of concrete, can give the inspection of the concrete damage at compression and at tension regions with values 0 - 0.5 respectively.

Table 5.1: Plasticity Parameter Values of Concrete

Concrete type	Dilation Angle (Ψ)	Viscosity (μ)	Shape factor Parameters(kc)	Eccentricity (ε)	Flow Stresses ratio (f_{b0}/f_{c0})
NWC	30	0.007985	0.667	0.1	1.16

Note: Dilation angle (Ψ) is volume expansion during plastic deformation

Viscosity (μ) is controlling the smoothness of the transition between damage states

The eccentricity (ε) and Flow Stresses ratio (f_{b0}/f_{c0}) are taken from Abaqus manual

5.3.2 Steel material definition

To simulate the elastic stage of steel materials which is behaving elastically up to yield strength which the material begins to deform plastically, the initial modulus of elasticity (E_S) take as 200,000 MPa and the poison's ratio (ν_S) take as 0.3.

For the plastic stage once the applied stress exceeds the yield strength with adopted the yield stress (f_y) values from the tensile strength as mentioned in chapter four which is For the Perfect Plasticity stage elastic perfect plastic model, and it's occurred when the stress reaches the yield strength level the material doesn't stop to be deformed even if the stress still in the same value, and the elastic perfect plastic model can simplify the analysis of structures under the deformations status without strain hardening rule, Figure 5.1.

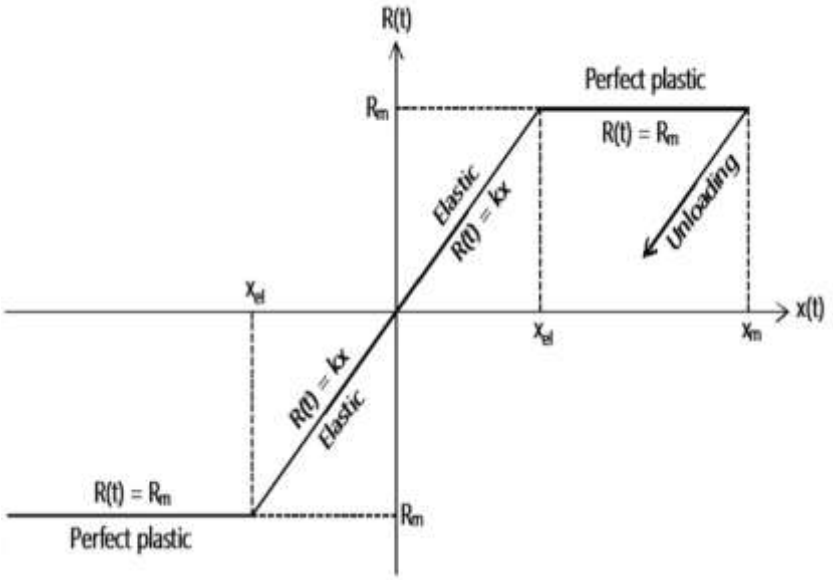

Figure 5.1: Elastic Perfect Plastic Behavior of Steel Materials

5.4 ABAQUS elements

5.4.1 Selection element types

In general, Abaqus program gives several types of elements and it's necessary to understand each element properties to choose the must proper one to simulate the required model, and it's dived to four categories as below.

5.4.1.1 Family

It is the most general way to collect many types of elements that are used for many objective models, the main features of the element's family are the geometry of each one such as, continuum solid element, shell elements, beam elements, rigid elements, membrane elements, infinite elements, truss elements and the special elements like the springs, dashpots and masses, Figure 5.2.

5.4.1.2 Number of nodes (interpolation)

Structure has many nodes and as more nodes mean greater freedom of movement (degrees of freedom) for the element, making it more flexible and capable of bending and deforming with more realism, these gives ability to estimate the behavior of every node connection response behavior.

And the node interpolation is divided into two main approaches at Abaqus program such as the first order (Linear) which works with nodes only at their

corners, like triangles with three nodes and second order (Quadratic) which refer to elements with both corner nodes and mid-side nodes, Figure 5.3.

5.4.1.3 Degrees of freedom

All the nodes have degrees of freedom (DOF) these simulate how the element will behave under any type of stress and represent fundamental physical amount such displacements (up/down, left/right) of the node, rotations, temperature.

5.4.1.4 Integration

It's a numerical method dividing the element up into many points (integration points), To find the data about the material behavior at each of these points, and for more integration points provide more accurate results.

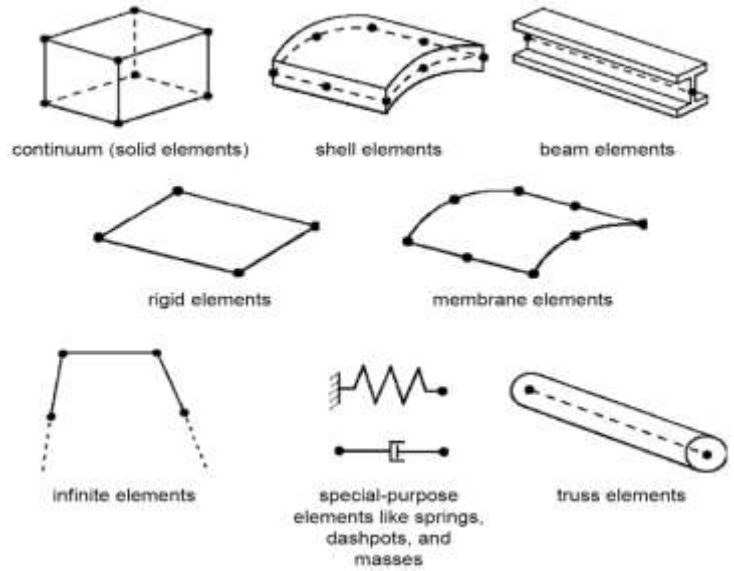

Figure 5.2: Common Element Families (ABAQUS User Manual)

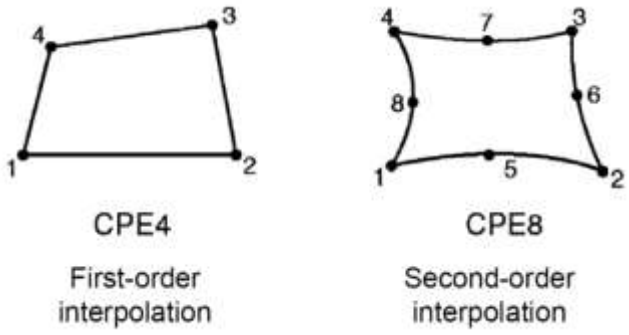

Figure 5.3: First Order & Second-Order Interpolation (ABAQUS User Manual)

5.4.2 General element dimension

This category offers a detailed overview of the element types accessible in Abaqus, when each element type is designed for various applications and should be chosen based on the analytical requirements, geometry, and material behavior such as illustration below.

5.4.2.1 Elements one dimension

One of these categories is the truss elements and used for example as Structural frameworks, cable systems or reinforcement bars, and simple tension and compression analyses, and its type (T2D2: 2-node 2D truss and T3D2: 2-node 3D truss) used to simulate the response of axial force only so it's suitable for the linear static and dynamic analyses.

The other type is beam elements and it's used to get the data of the deflections and rotations of the model due to the features of bending, axial force and shear resistance for the Structural beams, frames, and mechanical linkages analysis works, This elements types symbol as (B2D2: 2-node 2D beam, B3D2: 2-node 3D beam) and the (B3D3: 3-node 3D beam).

5.4.2.2 Elements two dimensions

One of this category is shell elements used to simulate the walled structures, automotive body panels, and tanks due to its feature of handle the bending and membrane effects and dealing with nonlinear behavior and large deformation, divided to three types such as (S4: 4-node quadrilateral shell element) and the (S8R: 8-node quadrilateral shell element) with reduced integration and last the (S3: 3-node triangular shell element).

The second category is Plane Stress Elements used to simulate the Sheet metal forming, thin-walled structures due to the features of don't assume the stress in the thickness direction and fitting the 2D modeling of thin structures, divided to three types such as (CPS4: 4-node plane stress element), (CPS8: 8-node plane stress element) and (CPS3: 3-node triangular plane stress element).

The third category is plane strain elements which are used for foundation problems and soil mechanics huge deformation due to the gives zero strains in the

thickness direction, divided to three types (CPE4) 4-node plane strain element, (CPE8) 8-node plane strain element (CPE3) 3-node triangular plane strain element.

5.4.2.3 Elements three dimension

These types of elements are used with three-dimensional models and divided into two categories:

The first solid elements are used for simulating structural analysis, thermal, and fluid dynamics analysis due to the capability of modeling complex geometries, and they're divided into four types such as (C3D8: 8-node linear hexahedral element), (C3D10: 10-node quadratic hexahedral element), (C3D4: 4-node linear tetrahedral element), (C3D10:10-node quadratic tetrahedral element).

The second continuum elements used for simulating the mechanical components, complex load conditions, and nonlinear analysis, due to the capability of modeling complex stress states with containing more node for high accurate data, and it's divided into two types such as (C3D20: 20-node quadratic hexahedral element), and (C3D6: 6-node linear triangular element).

5.4.2.4 Specialized elements

These are very important elements in Abaqus program and divided into three categories as illustrated below:

The first cohesive elements which handle the composite materials, adhesive joints, and fracture mechanics because it's ability to solve and simulate damage initiation and growth and models interface and failure between materials.

The second contact elements which are important to simulate the mechanical assemblies, clamping systems, and impact loading analysis due to the ability to of model the surface-to-surface contact.

The third thermal elements for the heat transfer in structures as well as for solids or fluids materials, divided into two types such as (T2D2) 2-node thermal conduction element and (T3D2) 2-node 3D thermal element.

5.5 Numerical Simulation of the Experiment Study Specimen

The main aim of numerical simulation is to create 3D finite elements model to find out the behavior of the experiment specimen under the static load, nine steps required in Abaqus program to simulate any specimen, as illustrated in chapter five, eight specimens will be modeled to make validation study with the experiment study.

5.5.1 Creating parts

In this phase the shape and the dimension of the specimen are obtained and all its sections such as the steel plate for flanges, the truss frame vertical and diagonal member, concrete deck slab, perfobond ribs plate shear connector, and the steel reinforcement bars for the category one and two as in Figure 5.4 and Figure 5.5.

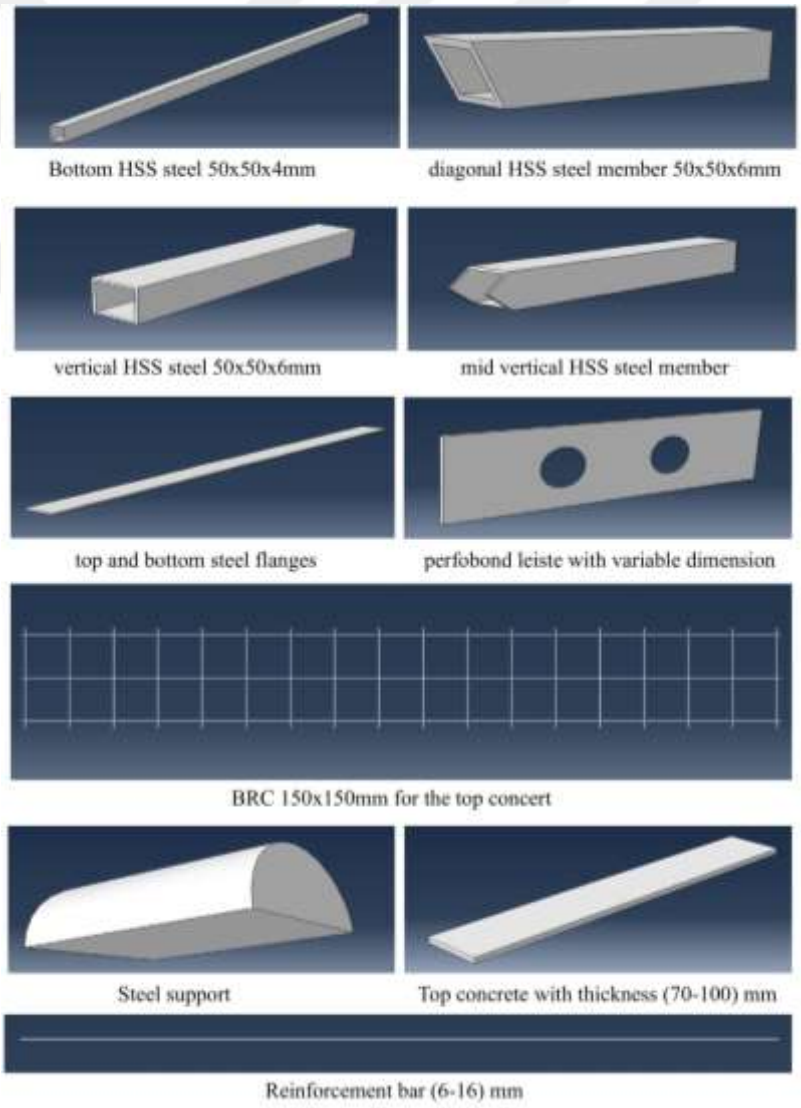

Figure 5.4: Creating Parts of the Specimens of Category One (SCTG)

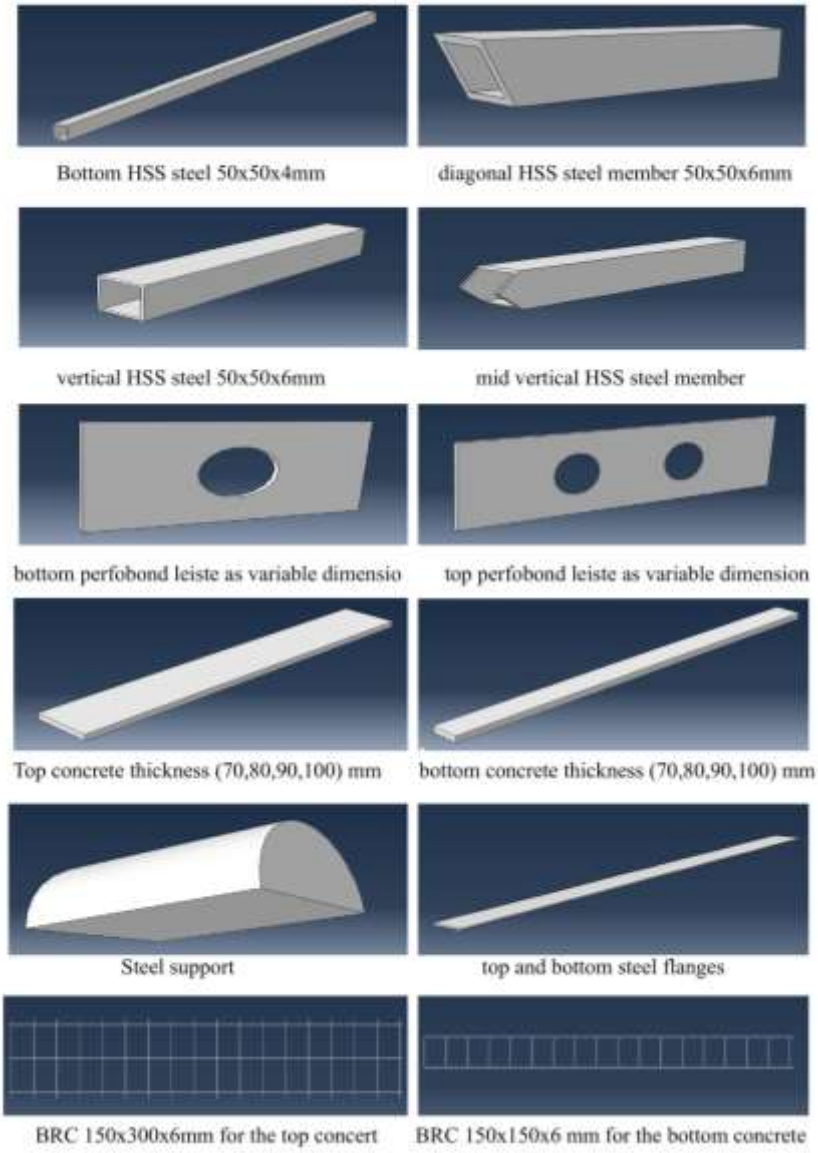

Figure 5.5: Creating Parts of the Specimens of Category Two (DCTG)

5.5.1.1 Top and bottom cords elements

The (S4R) which is the 4-node shell element with reduced integration, it's proper element to simulate the top and bottom steel plate flanges (truss chords), this element's characteristic involves having six degrees of freedom (3 translations and 3 rotations).

In Additionally, (T3D2) liner 2 node truss elements that can only resist axial loads, it has no bending stiffness, meaning it cannot carry moments, for modeling structures where members are subjected primarily to axial forces (tension and compression), such as trusses, beams, and some frames and can be defined with different cross-sectional areas and material properties.

5.5.1.2 Vertical and diagonal truss members elements

(B31) with size 10 mm was used to model the contact of the diagonals and flanges to each other, diagonal members connect the top and bottom chords and help in stabilizing the truss against lateral loads, they experience both tension and compression, this element allows for transfers the shear deformation and simulate the object as slender beams.

5.5.1.3 Welding element

All welding points in the contact members region will be shell elements (S4R) 4-node, with size 10 to 25mm to simulate all the welding work as illustrated in specimens of the experiment study at chapter five.

5.5.1.4 Steel reinforcement bars element

Several approaches can be used to model steel reinforcement bars while the most used is the embedded approach which can simulate the model by using the (T2D2) for 2D or (B31) for 3D, especially if the bars were in two layers, it must specify the properties and spacing and bars cross-sectional area for each layer, and in this study we used one reinforcement BRC layer, as shown in Figure 5.5.

5.5.1.5 Concrete slab and perfobond leiste ribs element

The (C3D8R) eight node continuum 3D brick element and reduction the integration command, the main feature is to have three degrees of freedom at each node and for all the directions, the reduced integration for the solid and shell element to reduce the solid requirement without effecting on the accuracy of the behavior analysis data.

5.5.2 Creating materials and assign sections properties

It’s required to create materials characteristics for each parts modeling from the materials button command to add the properties, in this modeling study materials as below and Table 5.2.

For the steel plate flanges will behave as an elastic stage with passion’s ratio 0.3 and young modulus 200,000 MPa, and for the steel truss frame and reinforcement bars will act as elastic perfect plastic behave elastic and plastic, for the elastic stage the young modulus (E_S) well be 200,000 MPa and Poisson ratio 0.3.

For the plastic stage the steel materials are well defined as 690 MPa, 700 MPa and 718 MPa for reinforcement bars ¬10, ¬12 and ¬16 respectively.

However, the steel flanges will be defined as 407 MPa and 520 MPa for HSS steel truss members (vertical and diagonal) respectively, and 517 MPa for the shear connector steel plate (ribs plate), these results based on the steel tensile test as illustrated in chapter five and attached to (Appendix B).

For the concrete materials type normal weight concrete (NWC), divided into two stages, first the elastic stage, young modulus of concrete (E_c) as 2.30E-09 properties data adopted as the results of experiment study test in chapter five, for the poison ratio (ν) well taken as 0.2.

Second, the plastic stage where at this stage the level of loading amount well shows up the plastic properties plasticity behavior which is defined as concrete damage plasticity (CDP) model which is had to include:

a- **Compressive behavior**: included the stress – strain curve results as shown at the experimental study for the normal weight concrete taken as 35 MPa. Figure 5.6 the details parameter attached to (Appendix B).

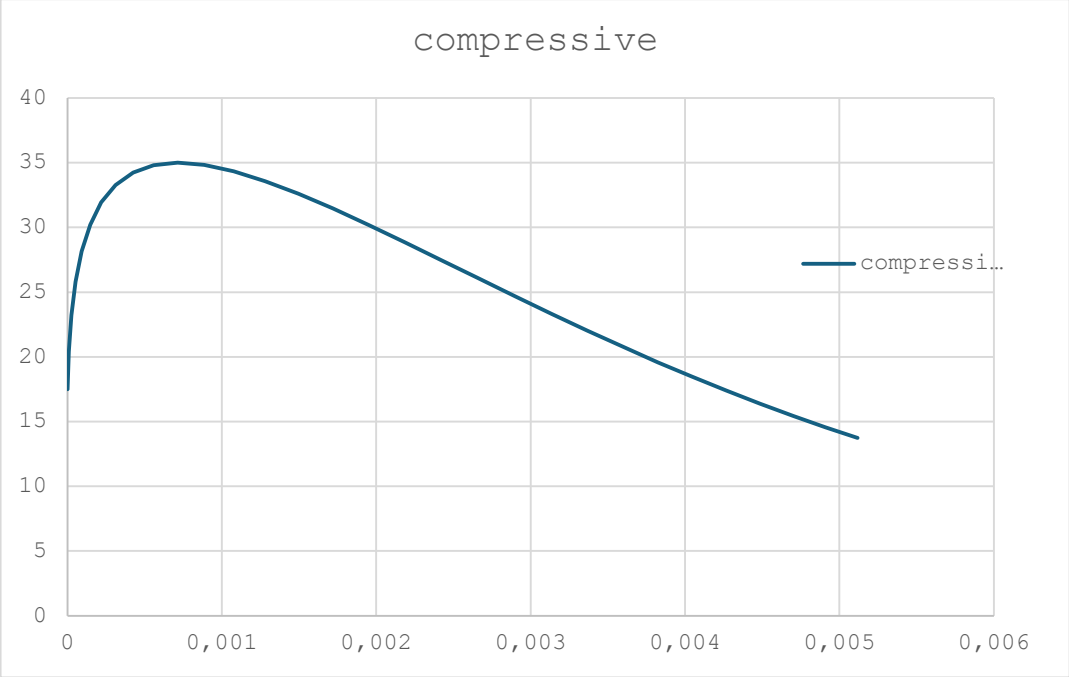

Figure 5.6: (CDP) Compression Behavior Curve

b- **Tensile behavior**: the results of the experiment study for the concrete were listed in this parameter as 4.2 MPa to have the same behavior as its response in chapter five, Figure 5.7 the details parameter shows in (Appendix B).

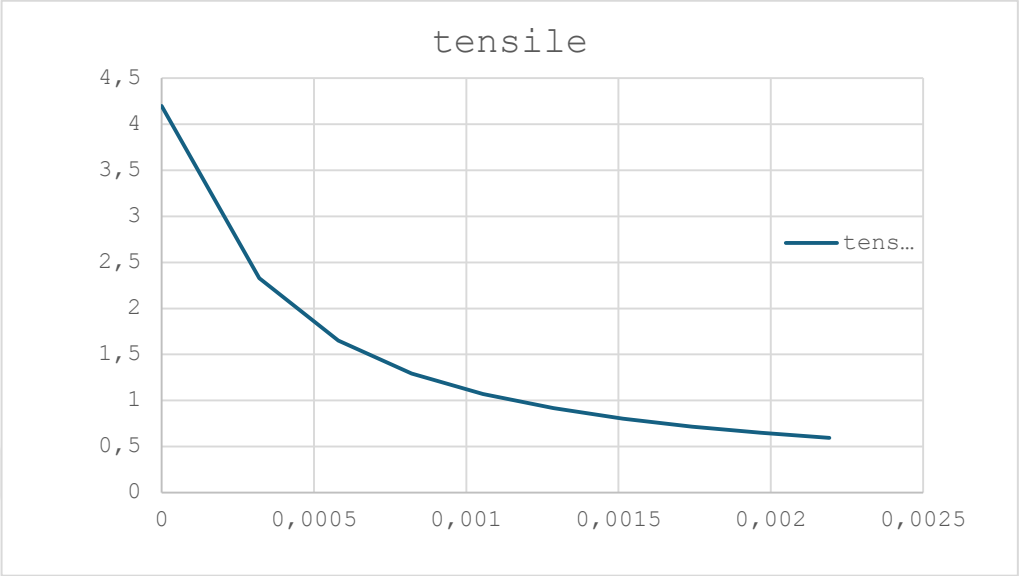

Figure 5.7: (CDP) Tensile Behavior Curve

Table 5.2: Assign the Materials and Elements for the Specimen's Parts

Section Manager

Name	Type	Material
BRC members	Truss	BRC 150X150
bars 6 mm	Truss	rein 6mm
concrete 35	Solid, Homogeneous	CDP 35
hss members	Solid, Homogeneous	steel hss
load cell	Solid, Homogeneous	steel elastic for support
ribs steel	Solid, Homogeneous	steel ribs plate
steel flange	Solid, Homogeneous	steel flange
supports	Solid, Homogeneous	steel elastic for support

Create... Edit... Copy... Rename... Delete... Dismiss

5.5.3 Assembly of specimen parts

At this step, after all parts have been creation as a single (each one alone) and creating the material and assigning them for every single one, this is step when the apply the assembling command to make sure of connect all these parts together and get the final specimen category as one sample in 3D model, as in Figure 5.8 and Figure 5.9 showing the specimens after assembly for single composite and double composite girders.

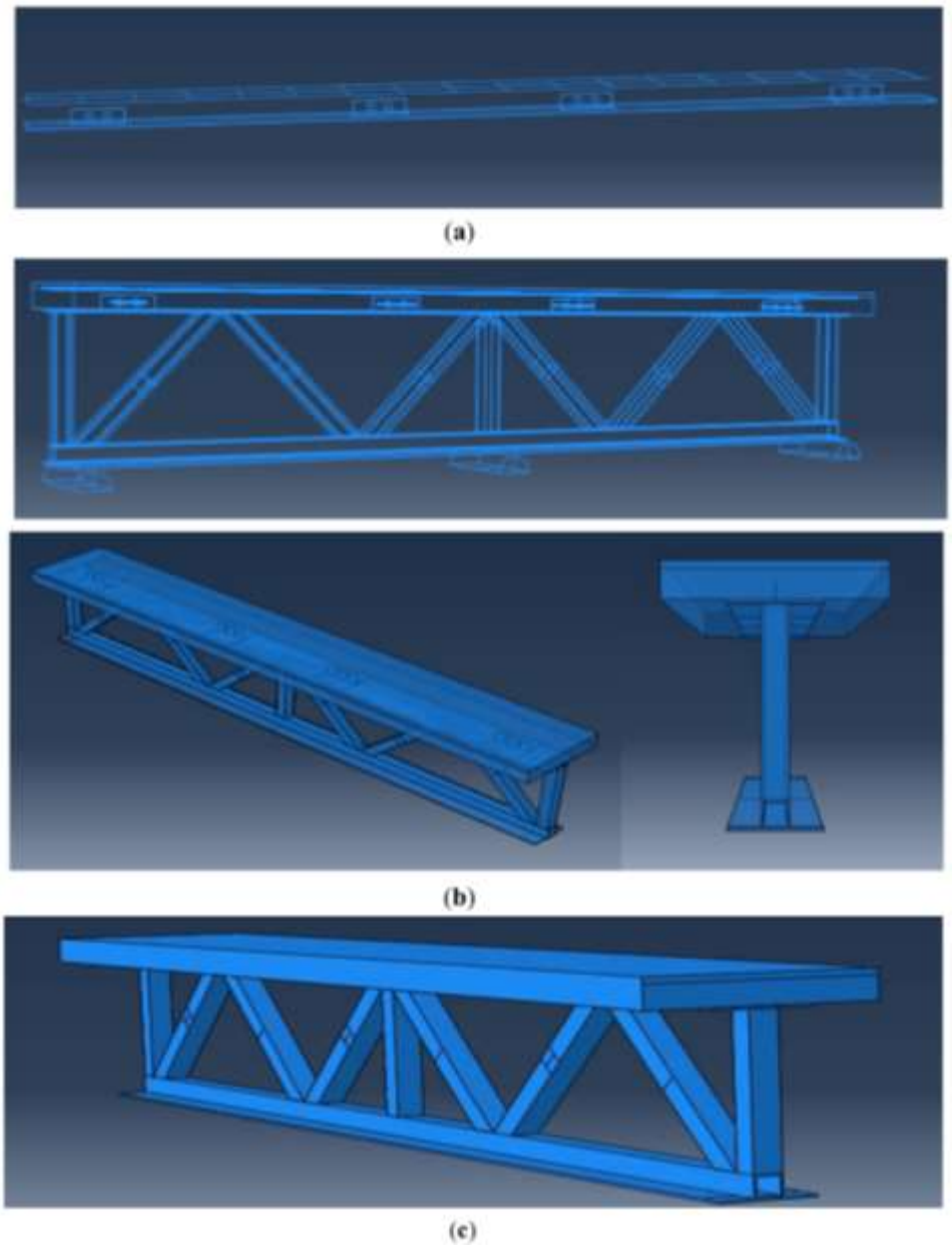

Figure 5.8: Single Composite Specimens After Assembling. (a) Top Berfobond Leiste with the BRC 300x150X6 mm, (b) Single Composite Specimen Front & Side View, (c) Front and 3D View of the Single Composite Truss Girder

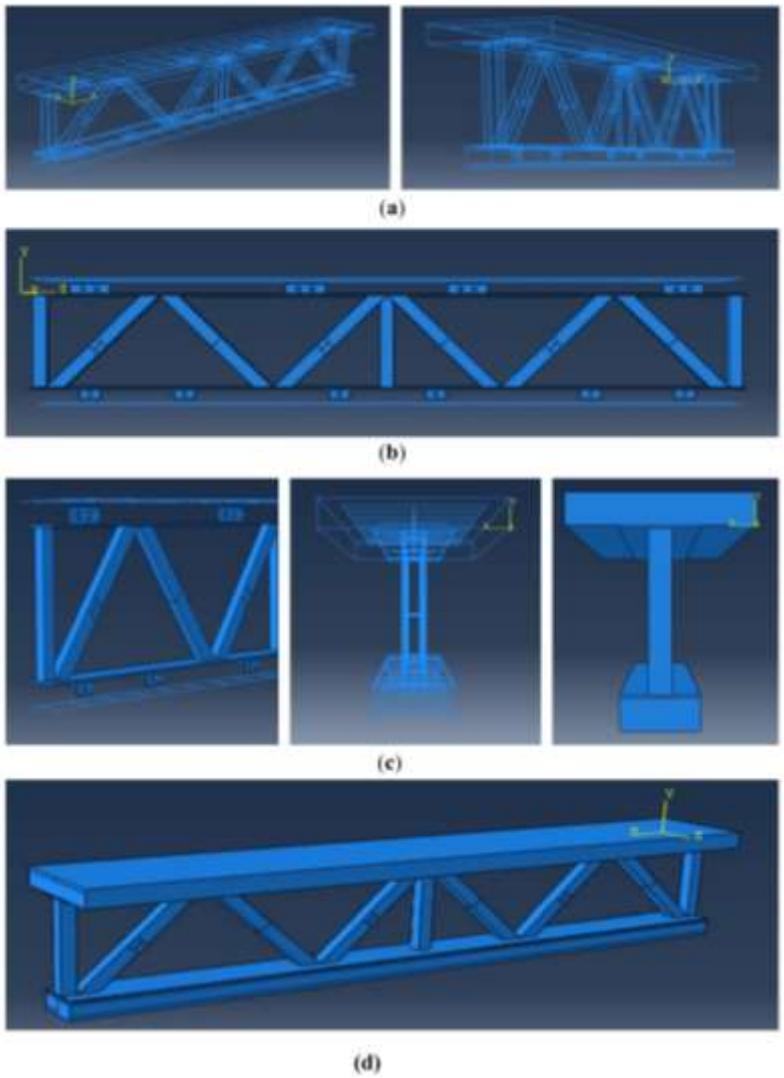

Figure 5.9: Double Composite Specimens after Assembling. (a) Top and Bottom Berfobond Leiste with the BRC 300x150X6 mm and 150x150x6mm, (b) Double Composite Specimen Side View With Shear Connectors, (c) Front View of the Double Composite Truss Girder and Plate Holes Reinforcement Bars, (d) 3D Model of the Double Composite Truss Girder

5.5.4 Define the analysis step

This step allow to define how your simulation progresses over time or in response to applied loads from the initial stage till the final stage, in this study analysis step determines as dynamic-explicit and submitting the parameters that control the simulation of model and movement and made the time period 1 sec the time of specimens test under loading, select the dynamic-explicit and specify output requests to get results during the analysis prosses (stress, strain, displacements of the contact materials and deflections), Figure 5.10

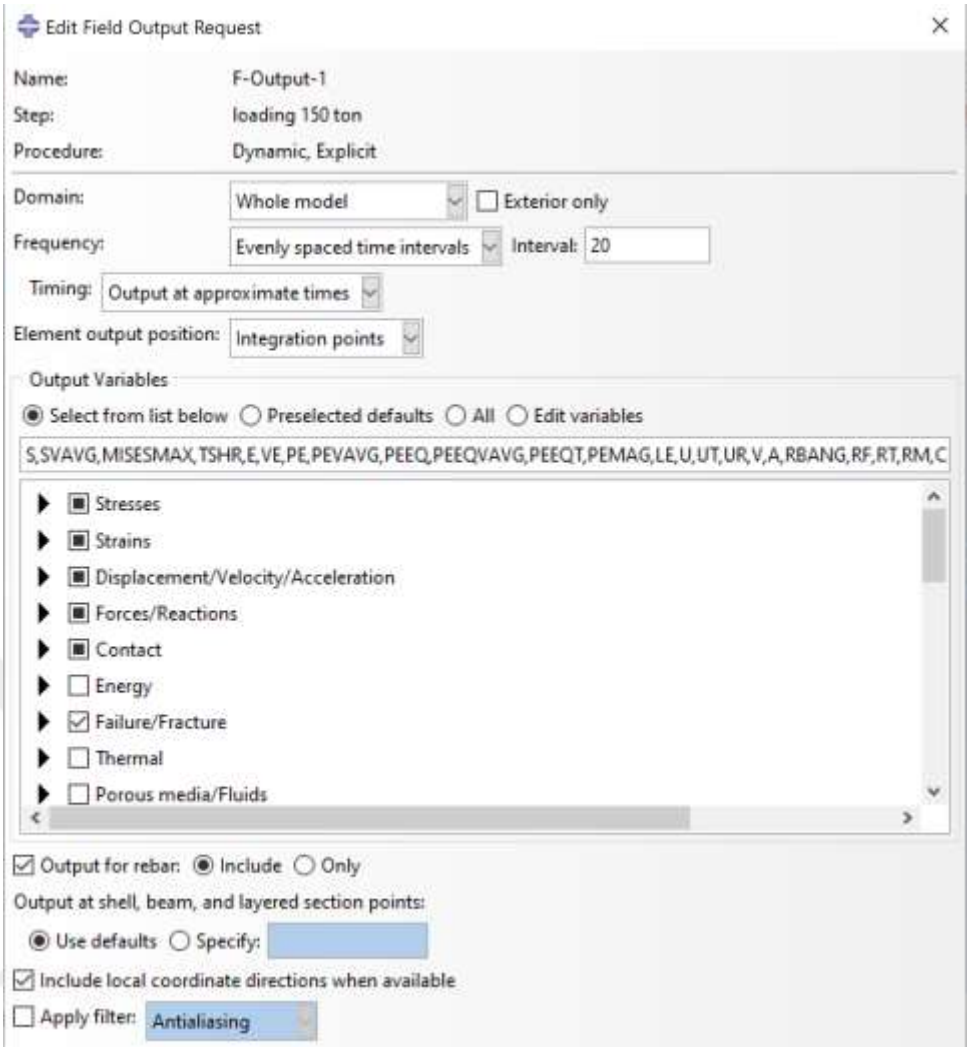

Figure 5.10: Parameters of Analysis Steps

5.5.5 Interaction of specimens parts

For the creating an interaction property modeling between the surfaces of the specimens' parts as below:

4.5.5.1 Contact as tangential behavior

As the interaction between the support (master face as red color) and the bottom girder (secondary face as pink color), select friction formulation as penalty with friction coefficient 0.35, as shown at Figure 5.11 (a) & (b).

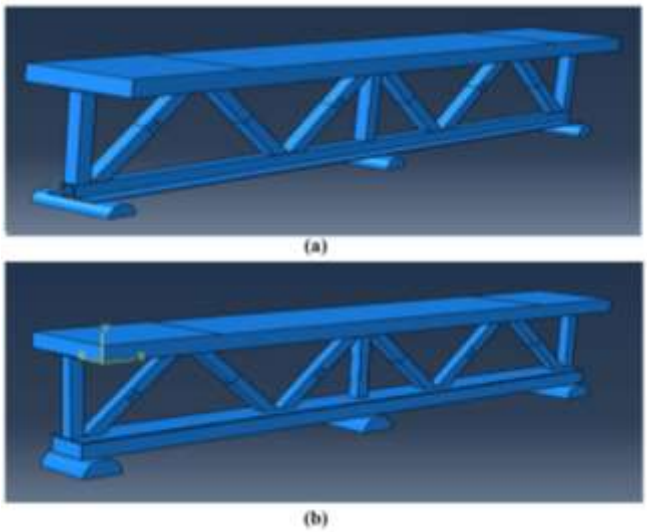

Figure 5.11: Contact as Tangential Behavior. (a)Tangential Behavior between the Bottom steel Flange With Supports (SCTG), (b)Tangential Behavior Between the Bottom Concrete With Supports (DCTG)

5.5.5.2 Normal behavior

The pressure will act as normal hard contact with allowing separation after contact, Figure 4.12 (a) & (b), for the (SCTG) and (DCTG) samples.

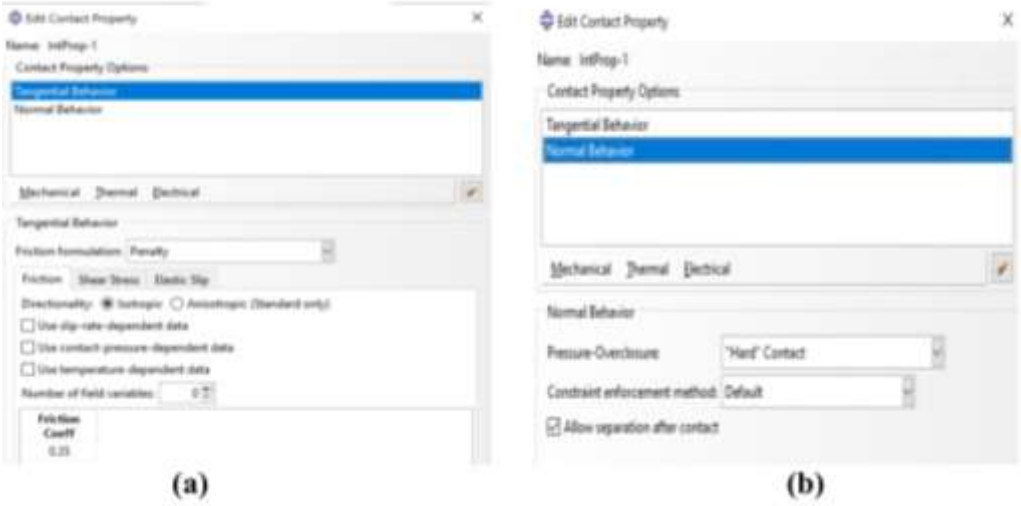

Figure 5.12: Normal Behavior. (a)Tangential Behavior Interaction Property, (b) Normal Behavior Interaction Property

5.5.5.3 Surface to surface

The interaction between the concrete surface with the steel flange surface of the truss frame simulated the normal contact.

5.5.5.4 Tie constraint type

Used for the connection between the steel flanges and the shear connector ribs, surface of steel flange treated as master surface, and the steel ribs shear connector and concrete considered as slave surface (secondary surface), as at Figure 5.13 (a), (b), (c) and (d), also for the contact of the holes bars and perfobond leiste shear connector, also for the vertical, diagonal and bottom HSS members with the steel flange, as at Figure 5.13 (e) and (f).

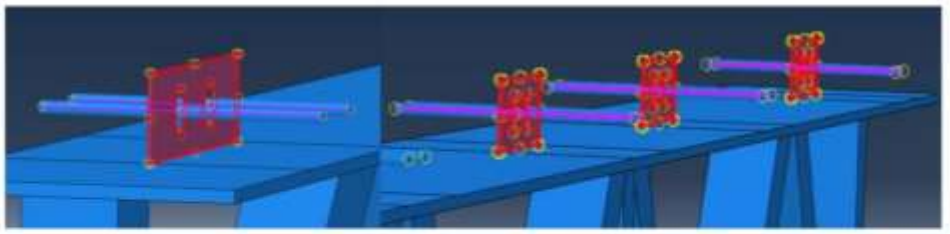

(b)

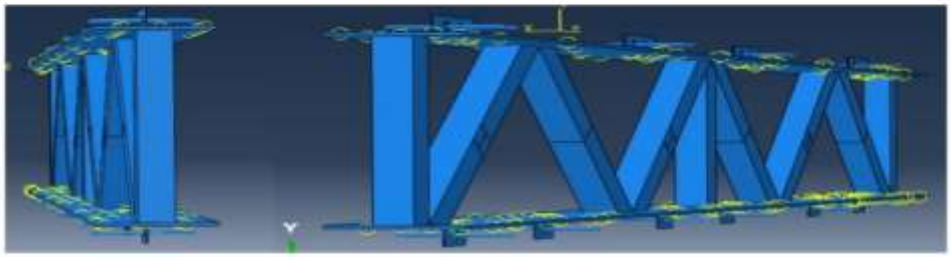

(c)

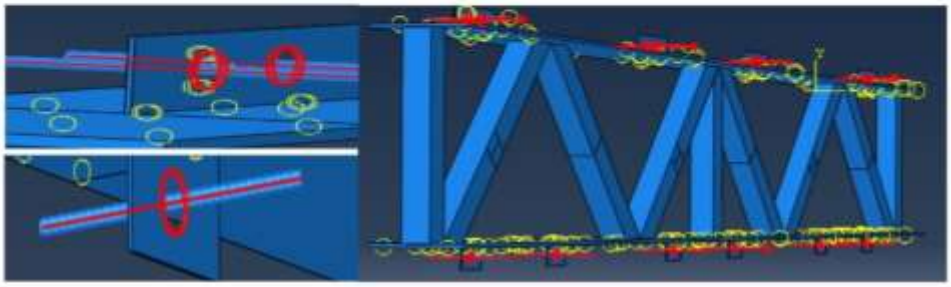

(d)

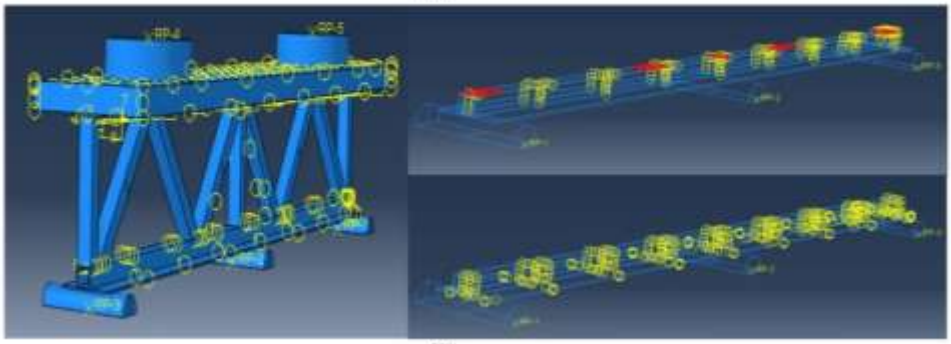

(e)

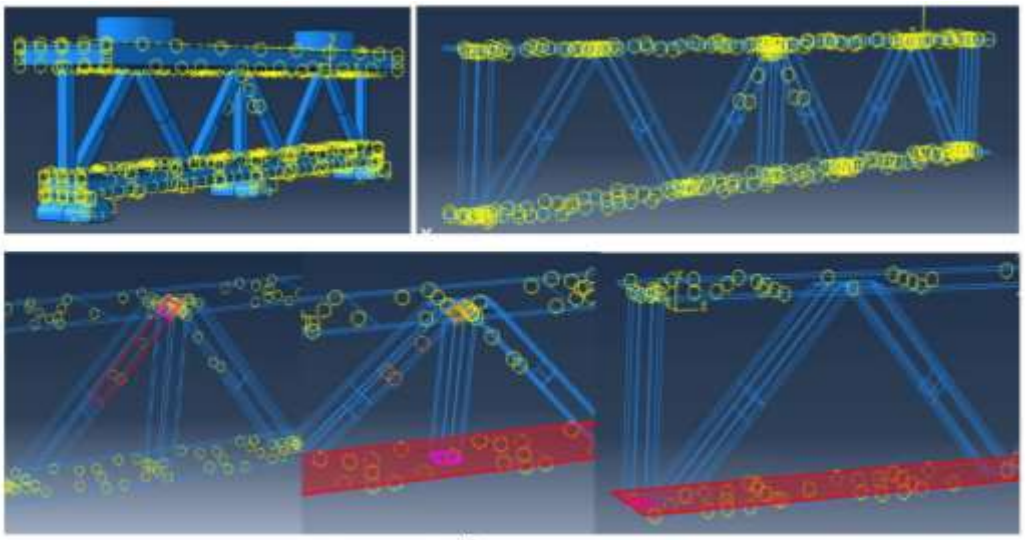

Figure 5.13: Tie Constraint Type. (a) Tie Interaction between the Steel Flange and Perfobond Lesite (SCTG), (b) Tie Interaction between the Reins Bars and Surround Perfobond Lesite (SCTG), (c) Tie Interaction between the Steel Flange and Perfobond Lesite (DCTG), (d) Tie Interaction between the Reins Bars and Surround Perfobond Lesite (DCTG), (e) Tie Interaction between the HSS Members and Steel Flanges (SCTG), (f) Tie Interaction between the HSS Members and Steel Flanges (DCTG)

5.5.5.5 Embedded region constraint

Was used for the connection between the BRC reinforcement bars with concrete and perfobond ribs shear connector and the holes rebars with concrete as shown in Figure 5.14 (a), (b), (c) and (d).

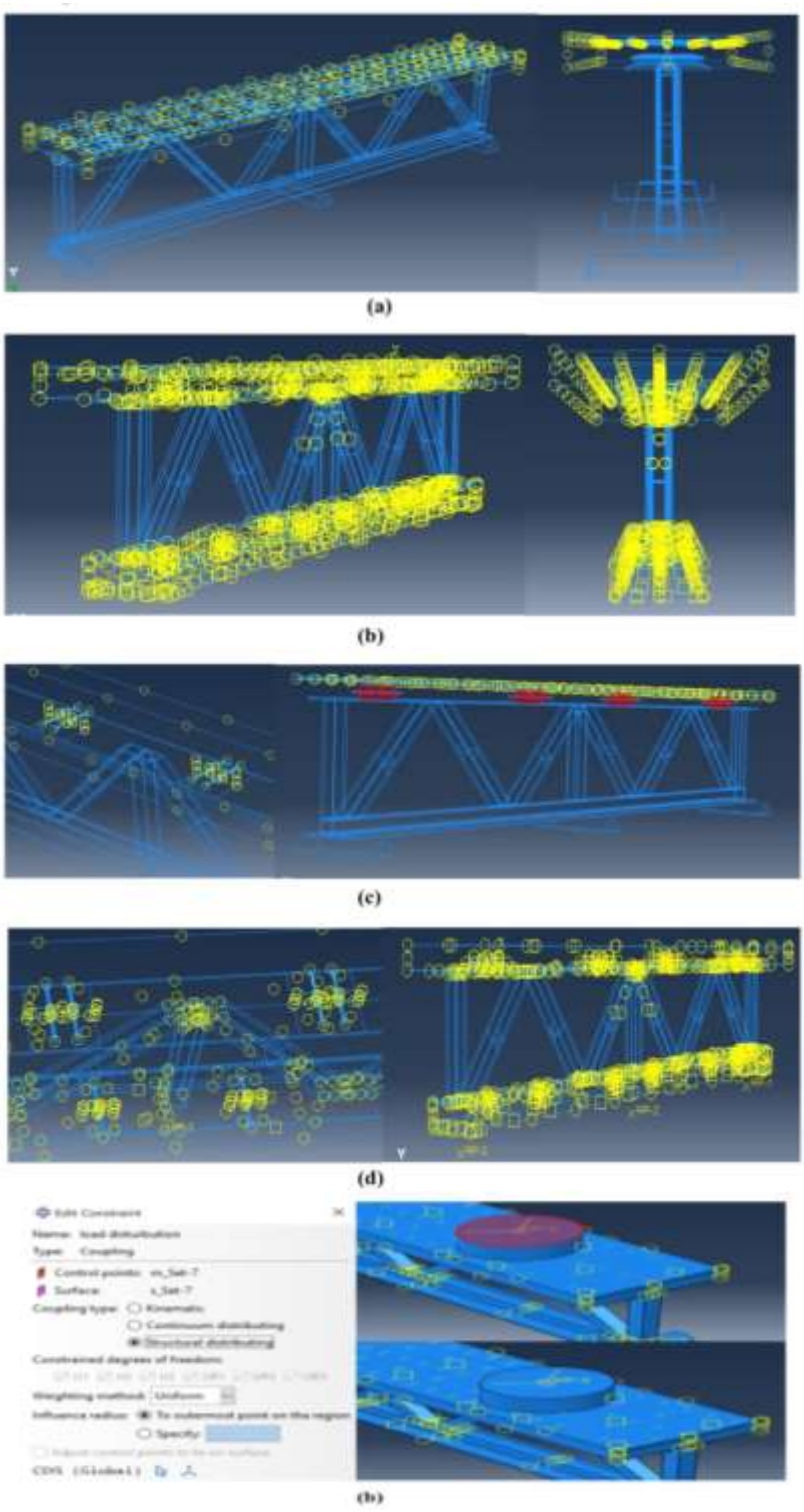

Figure 5.14: Embedded Region Constraint. (a) Embedded Interaction between the Concrete and top BRC (SCTG), (b) Embedded Interaction between the Concrete with Top and Bottom BRC (DCTG), (c) Embedded Interaction between the Concrete and Shear Connector Ribs Plate with Reinforcement Holes Bars (SCTG), (d) Embedded Interaction between the Concrete and Shear Connector Perfobond Lesite Ribs Plate with Reinforcement Holes Bars (DCTG)

5.5.6 Load modeling

It's represented as physical forces affect the behavior of the structure, in this study one type of loading is subjected to the composite girder applied to the surface of concrete slab, as two points of load with maximum 50 tons for each point of (RP.4) and (RP.5).

By creating constraint coupling as structural distributing to bond the reference points along the concrete width due to load distribution of the load cell items located at the region between the supports to find the negative bending moment at the mid support and how it's effect on the crack ratio at the top surface concrete as applied in the experiment study.

It's necessary to select the reference point in the model to simulate the load position or for simplicity we can use applied load on the surface supports as three pined supports and applied the required load amount on the surface deck slab positions, Figure 5.13(a)&(b).

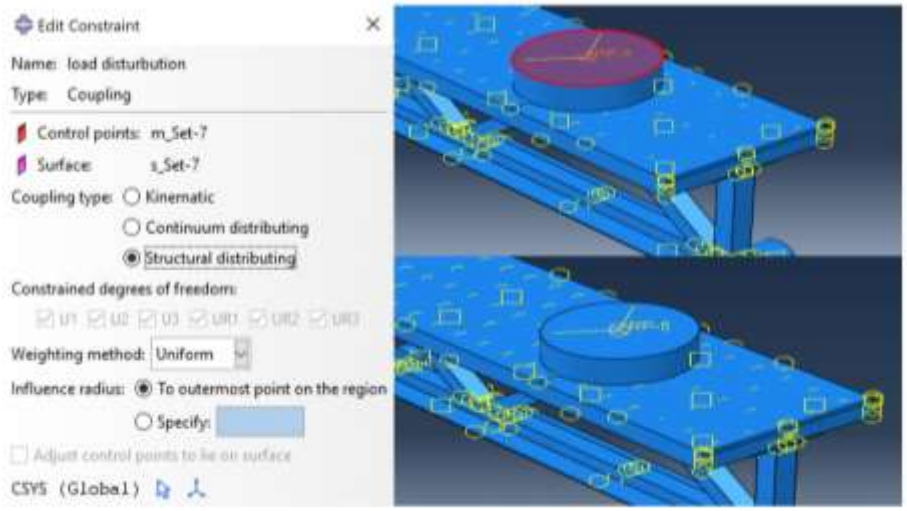

(b)

Figure 5.15: Loading Modeling. (a) Modeling of the Applied Static Load for (SCTG) and (DCTG), (b) Coupling Constrain Load Distribution of RP-4 and RP-5

5.5.7 Boundary conditions

They are essential for defining the model that interacts with its surrounding environment, they restrict the movement of nodes in your finite element model with ensuring to make the specimens model simulate and reflects real-world constraints movements.

Figure 5.16 (a) shows the boundary conditions that submit to the specimen in terms of allowing the composite truss girder to move toward the (x-axis) as bending behavior and deflection, while all lateral response as denotes to the transverse to the longitudinal axis (y-axis) and the third boundary condition as denotes to the direction parallel to the longitudinal axis (z-axis)

All the three support well defined as pinned boundary conditions when allowing part of (DOF) properties to move and restriction the others.

By creating the proper boundary condition from the Load menu and selecting the nodes or surfaces where you want to apply the boundary to setup the required condition (RP-1), (RP-2) and (RP-3).

To fix the specimens and restructure it restructured from lateral movement we need to create the out-of-plane concentrate boundary condition for the (displacement and rotation) and select the faces of the two edge surfaces, as shown at Figure 5.16 (b) and Figure 5.16 (c), shows the boundary conditions for the (SCTG) and (DCTG).

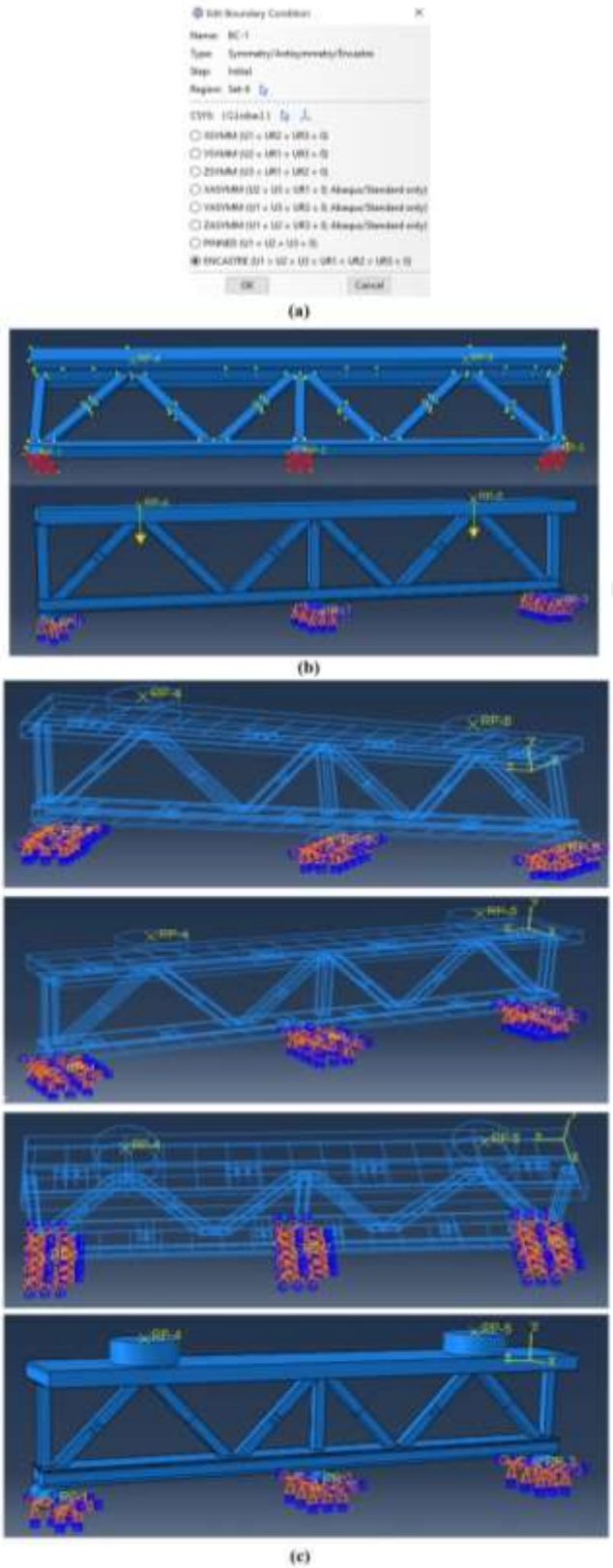

Figure 5.16: (a) Supports Boundary Conditions Parameter, (b) Modeling the Support Boundary Condition of (SCTG), (c) Modeling the Support Boundary Condition of (DCTG)

5.5.8 Meshing the specimen model

This operation is defined as the division of the sample into very small sections, which is very important for the finite element at Abaqus program, and for the auto mesh creation it's required to select the primary size which is 25 mm to achieve accurate results from the shell and solid element.

The element selects well be at this stage, so the required elements listed below:

1- **(S3R)** triangular use of the mesh shell element to mesh the steel truss HSS members as traditional reduces integration.

2- **(C3D8I)** as rectangular mesh for the concrete deck slab, shear connector palate and steel flange as incompatible modes.

3- **(T3D2)** liner truss elements will be used for the steel reinforcement rebars, it's important that for cylinder objectives to modify the meshing with medial axis to have better meshing processing as for the perfobond leiste ribs shear connector, Figure 5.17 to Figure 5.19 illustrate the submitting the elements mesh.

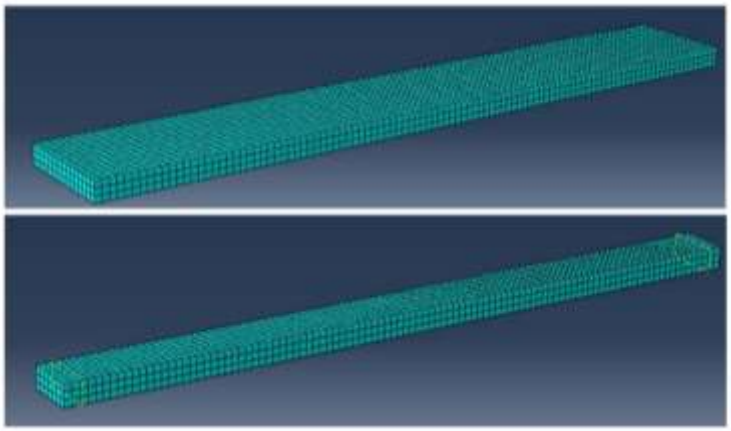

Figure 5.17: Top and Bottom Slab Meshing

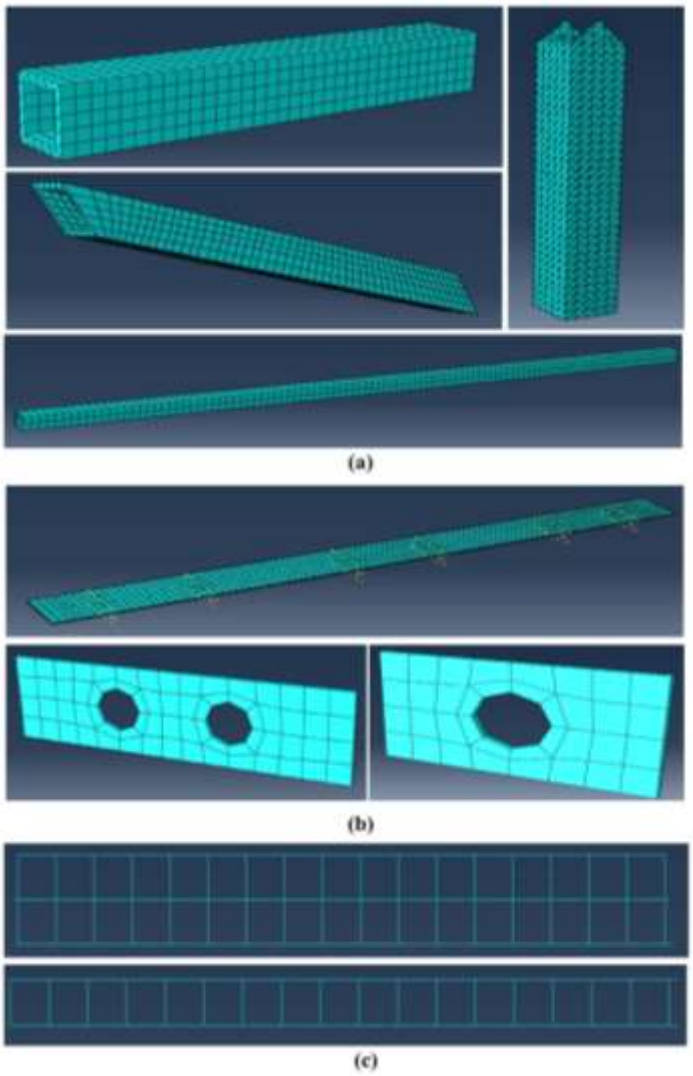

Figure 5.18: Meshing for Individual parts of the Specimens. (a) HSS Vertical and Diagonal Members Meshing, (b) Steel Flanges and Perfobond Leiste Shear Connector, (c) top and Bottom BRC Meshing

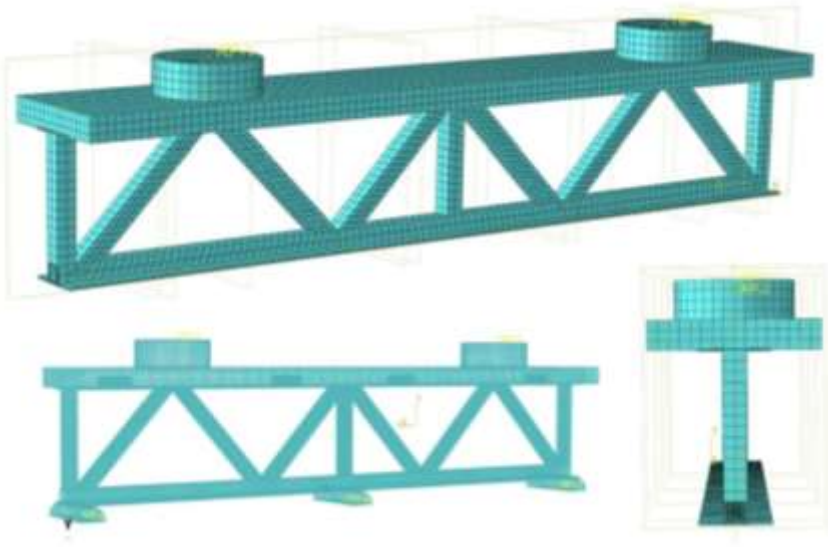

Figure 5.19: Entire Meshing of Single Composite Truss Girder (SCTG)

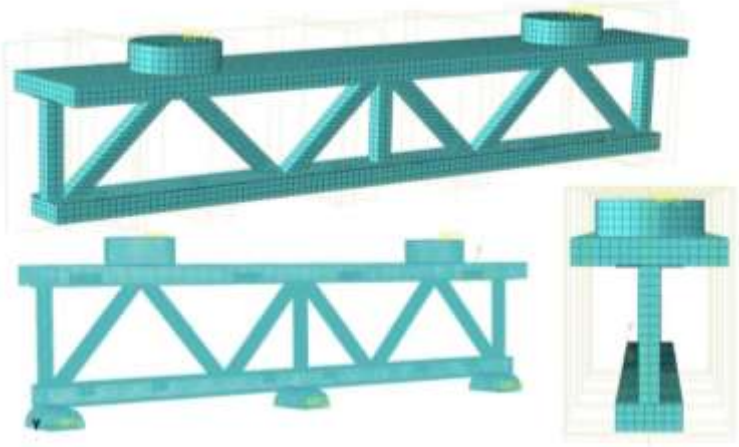

Figure 5.20: Entire Meshing of Double Composite Truss Girder (DCTG)

5.5.9 Submitting the job analysis

At this stage the analysis process of the simulate model has been done after submitting the analysis job, to achieve all results of the stress-strain, deflection, tensile and compressive values of steel and concrete materials and all the response of the main truss composite girder with the failures modes.

At Figure 5.19, which shows the list of this command, from the precision command make it from single to double explicit precision, and to get rid of a problem of many attempts errors that could happen it's necessary to change the steps cutback (IA) from 5 to 20.

Figure 5.21: Job Analysis Parameter and Properties

6. EXPERIMENTAL STUDY AND CAE ABAQUS PROGRAM RESULTS

6.1 Experimental Results and Discussions

6.1.1 Introduction

The objective is to analysis the data and make assessments of all response and mechanical behavior of the double composite truss girder compared with the single composite truss girder under the static load and all modes failures. The specimens are in two categories depending on the geometric section:

1. Single composite truss girder (SCTG)
2. Double composite truss girder (DCTG)

As illustrated in chapter five, an experimental study was performed with a certain methodology to analysis the data of these categories to study the effectiveness of the main variables on the strength and capacity of the composite girder under concentrated static load and hogging moment, and the results of concrete properties of the examination will be displayed.

Additional results will be discussion related to the specific specimen's response such as, Failure modes region and type, initial hogging moment crack regions due to load, cracks patterns and specimens state due to the ultimate load capacity, the positive and negative deflection, the slip – load relation due to the perfobond ribs vary from sample to another with the effect of the degree of interface.

The strain- load relation and the hogging moment girder resistance, the push out test results of the three-sample were used to determine the design of the shear connector for the main samples, mainly for the holes and bars diameter and spacing to get the most accurate results.

6.1.2 Push-out test

6.1.2.1 Modes of failure

In general, the expected failure modes of (PLR) connectors in this experiment study are divided into four types: first severe cracking of surround concrete, second yield of ribs steel and lead to rupture, third yield or fracture of penetrating steel bars and lastly failure in the steel truss body may occur.

Each perfobonf leiste ribs (PLR) connector failure correspondsdamagesr more failure modes in each test, where the PRP-1 sample conduct a reinforcement penetrated bar and sever concrete failure and the PRP-2 conduct the perfobond ribs plate failure and sever concrete damage at advanced stage of loading, while the sample PRP-3 shows the sever concrete damage with due to the high strength of perfobond leiste because of using bigger dimension lead to be more efficient than surround concrete, moreover, a steel structure of HSS members gets variable damages at all PRP samples.

6.1.2.2 Load and slip ratio of push out test specimens

The experiment was carried out in a method of gradual load with time until the failure occurred at ultimate load, Table 6.1**,** show the process of loading for each sample respectively, the relative slip result gets measured by using two LVDT devices located on the steel flange surface and the concrete slabs to collect the data of the movement that occur between these two elements.

Generally, load–slip curves went through four stages: elastic stage, plastic stage, strengthening stage, and failure stage, as shown in the Figure 6.1 to Figure 6.3 illustrate the phases of transition from one stage to another depending on the sample strength and deformation due to applied loading for each sample.

Table 6.1: Details of Load – Slip Measurement for Push Out Test Specimens

Sample	Safety factor γF	Ultimate Load Pu (KN)	Load p_{Rd} (kN)	Relative ξ_u slip of ultimate load (mm)	Relative ξ_{Rd} slip of design load (mm)	DUCTILITY coefficient ξu / ξuK
PRL-1	1.5	1452	725	27.1	5.2	5.21
PRL-2	1.5	1834	917	19.5	5.3	3.68
PRL-3	1.5	2145	1072	15.2	1.75	8.68

Note: P_{Rd} = design resistance of shear connectors.
γF = safety factor, often a value of 1.25-1.5

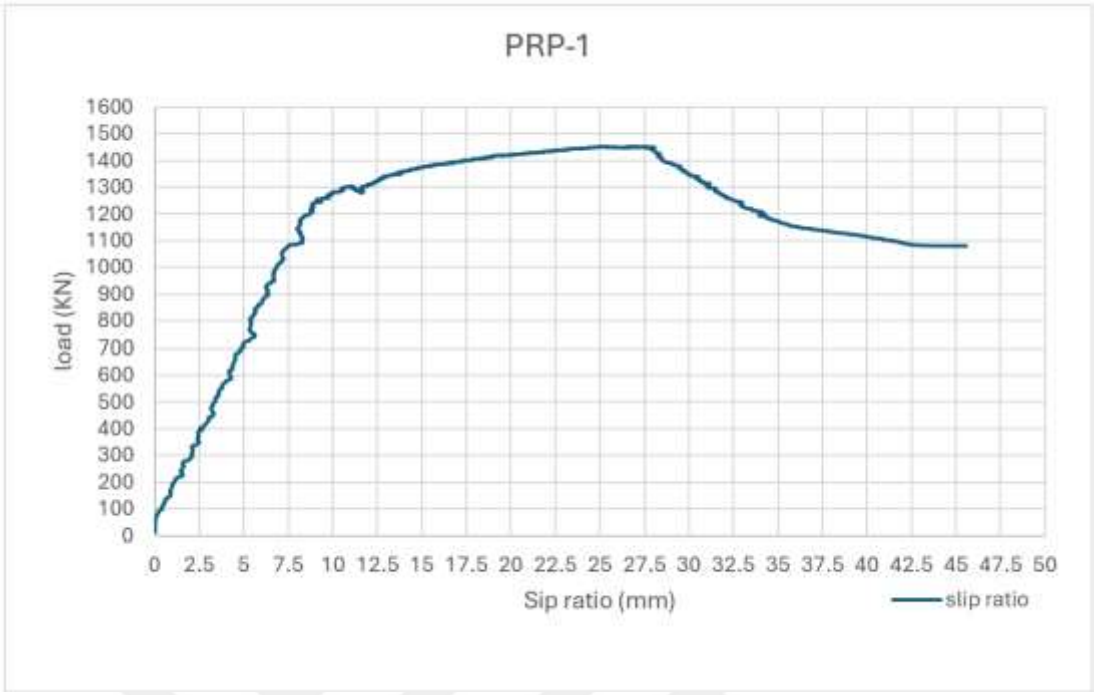

Figure 6.1: The Curve Phases of Deformations Transition for Sample (PRP-1)

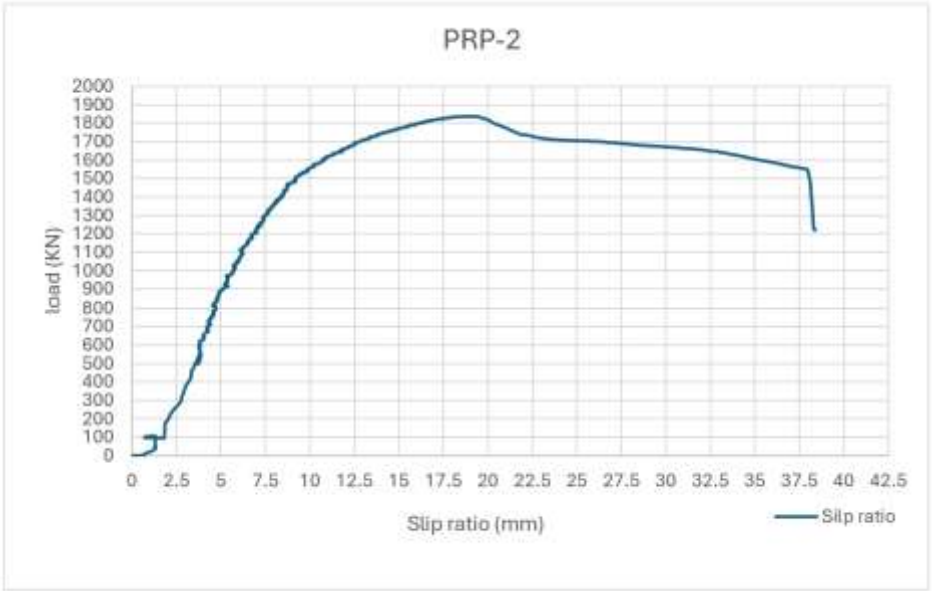

Figure 6.2: The Curve Phases of Deformations Transition for Sample (PRP-2)

Figure 6.3: The Curve Phases of Deformations Transition for Sample (PRP-3)

According to Eurocode 4, The shear connector's ductility (D) refers to its ability to withstand large deformations without failing, which is particularly important in seismic or highly variable loading conditions, which can be determined by dividing the slip value under ultimate load (ξu) over slip value under the design resistance load (ξ_{Rd}).

6.1.3 First category (SCTG) results

6.1.3.1 Modes of failure

In this study, the shape of failure that occurs for (SCTG-1) shows sever cracks in the top concrete under the hydraulic jack location due to applied load, the main failure located at the bottom HSS steel member and steel flange near the edge support, failure conduct also at mid HSS steel member due to the high compression force, for (SCTG-2) shows yield of bottom HSS steel member at the support region until rupture occurs and under mid HSS member due to the compression force in the middle support, and for (SCTG-3), very high rupture ration of HSS member at edge support region and weld failure due to high defection at sagging moment zone.

Also, for (SCTG-4), the same modes of failure of the previous samples but higher degree of damage due to the higher strength of the upper concrete part, Figure

6.4 to Figure 6.7 illustrate the states of failure of each four-specimen belonging to specimens of category one.

The strength capacity of the specimens are widely different according to the applied load stage with the fractured point, its shown that (SCTG-2) and (SCTG-1) get the higher strength with approximately 65 Ton while (SCTG-3) and (SCTG-4) was the lowest strength capacity with 52 Ton and 50 Ton respectively, and that reason is due to several factors.

The most important one is the increasing in steel flange and top concrete decreasing of the ability of the sample to bend during loading, Thus, the loads moved directly to the bottom of the sample, causing destruction to the steel section near the mid and edge steel support, where the percentage of increased tolerance between samples is estimated to 23%.

Figure 6.4: Failure Mode of the SCTG-1

Figure 6.5: Failure Mode of the SCTG-2

Figure 6.6: Failure Mode of the SCTG-3

Figure 6.7: Failure Mode of the SCTG-4

6.1.3.2 Initial crack load (p_{cr}) and the ultimate crack load (p_{ul})

Measuring the cracks with visual inspection at each load stage till the failure occurs and furthermore, the Stress distribution on concrete deck slab, to get an analysis data of the crack pattern at the initial crack load till the ultimate crack load and the period that takes from stage of (p_{cr}) and stage of (p_{ul}), as showed Table 6.2**.**

At (SCTG) samples the increase in concrete deck thickness does not affect directory on the cracking ratio reduction, especially at hogging moment region, the results show low cracks strength and initial cracks start at primary stage of loading, as shown in Figure 6.8 to Figure 6.11.

For (SCTG-1), (SCTG-2), (SCTG-3) and (SCTG-4) samples the initial cracks appearance at 31.3%, 38.6%, 66.5% and 71.7% respectively of the ultimate applied load, in other hand, the ultimate cracks which it's refer to ultimate service load begins at 75.6%, 77%, 90% and 92.2% of the full applied load.

Most of these cracks of all sample's appearance in the hogging moment region which is on the mid top concrete surface due to the high deflection in the positive moment region, at advanced loading stage the cracks appeared under the hydraulic jack zone related to concerted load.

Table 6.2: Initial Crack Load (pcr) and the Ultimate Crack Load (Pul) for (SCTG)

Specimen	F_u (KN)	D_u (mm)	Initial cracking p_{cr} (KN)	Ultimate cracking p_{ul} (KN)	Remark
SCTG-1	654	8.98	205	495	H.G.R.C
SCTG-2	658	8.7	254	507	H.G.R.C
SCTG-3	520	10.02	346	471	H.G.R.C
SCTG-4	502	9.8	360	463	H.G.R.C

Note: F_u = total ultimate applied load and D_u= total ultimate defection,
H.G.R.C = hogging moment region cracks

Figure 6.8: Crack Pattern of the SCTG-1

Figure 6.9: Crack Pattern of the SCTG-2

Figure 6.10: Crack Pattern of the SCTG-3

Figure 6.11: Crack Pattern of the SCTG-4

6.1.3.3 Load and deflection relationship

By using two LVDT senser device to collect the deflection data from the bottom cord for each panel due to the positive moment that occurs, Table 6.3 illustrates the results of the four (SCTG) specimens.

the liner response due to the applied load from the start point to the point of elastic load and the non-liner of the curve between the point of plastic load till the failure modes reached.

The results show for (SCTG-1), (SCTG-2), (SCTG-3) and (SCTG-4) that from the elastic load to ultimate load the deflection increasing 47.6%, 64.1%, 82% and 78.4% respectively, while from plastic load to ultimate load the increasing was 13.4 %, 36.8%, 47% and 59.1% respectively.

There is clearly a significant increase deflection from the initial load stage till the full loading situation, even from the plastic load stage to full load there is huge gape of unstable defection control.

The increasing at concrete and steel flanges thickness does not give the girder any ability to resist the defection, moreover, the results show that the defection at (SCTG-3) and (SCTG-4) was higher than (SCTG-1) and (SCTG-2) at final load stage while these two sample had lower deflection at elastic and plastic stages, Figure 6.12 to and Figure 6.15 illustrates the curves of deflections.

Table 6.3: Experimental Work of Load – Deflection at Bottom Cord For (SCTG)

Specimen	Experiment result					
	Elastic Load (KN)	Deflection (mm)	Plastic Load (KN)	Deflection (mm)	Ultimate Load (KN)	Ultimate Deflection (mm)
SCTG-1	523	4.70	621	7.77	654	8.98
SCTG-2	520	3.12	629	5.49	658	8.7
SCTG-3	416	1.8	505	5.31	520	10.02
SCTG-4	387	2.11	480	4.0	502	9.8

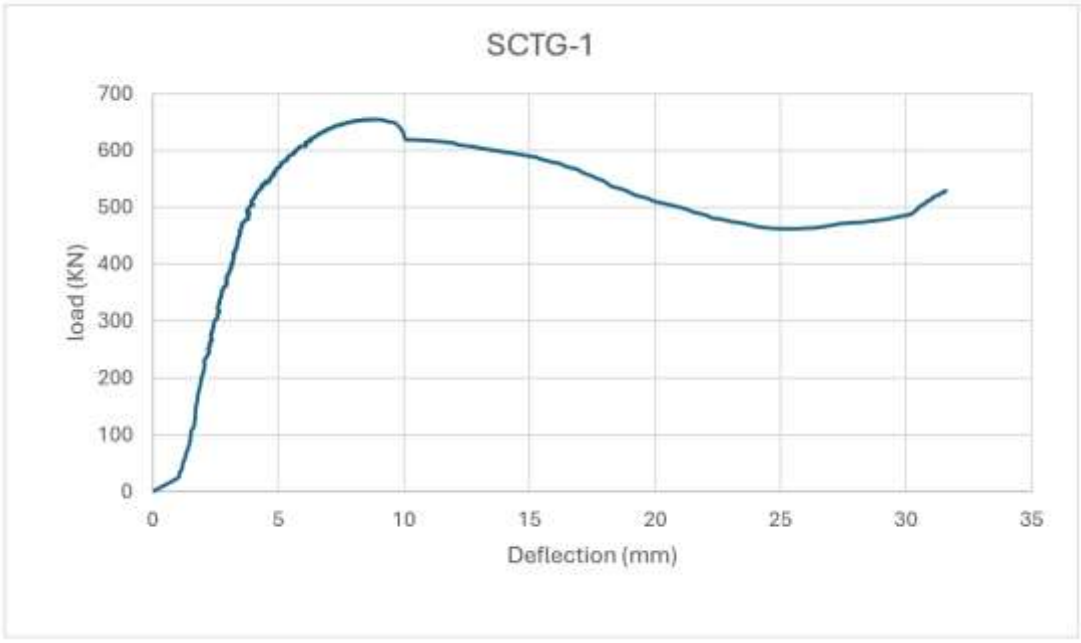

Figure 6.12: Load-Deflection of the SCTG-1

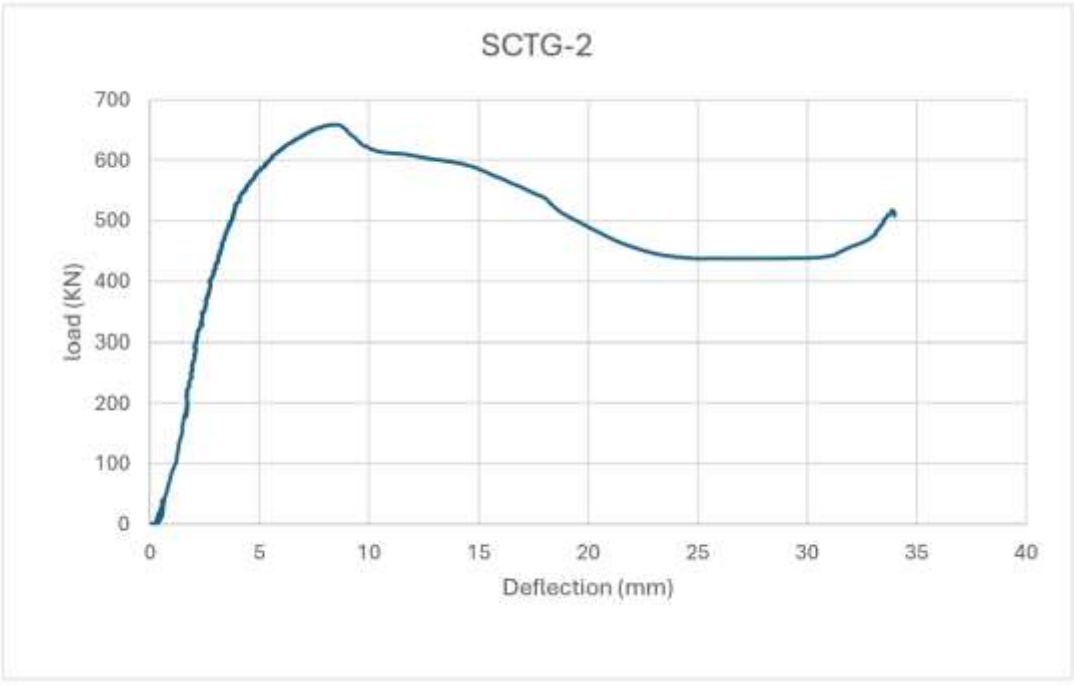

Figure 6.13: Load-Deflection of the SCTG-2

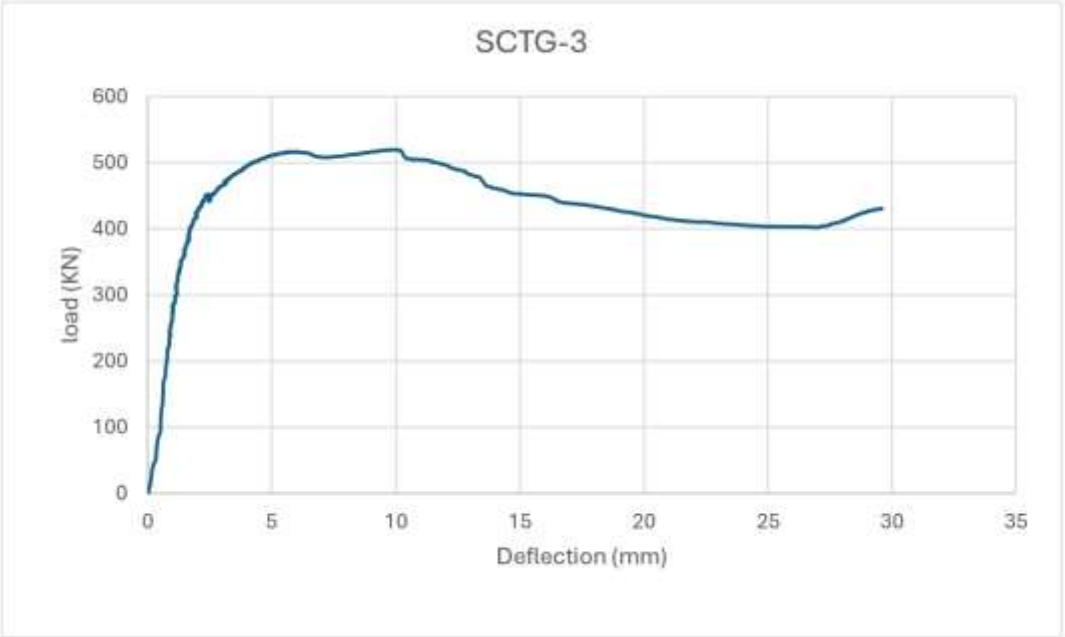

Figure 6.14: Load-Deflection of the SCTG-3

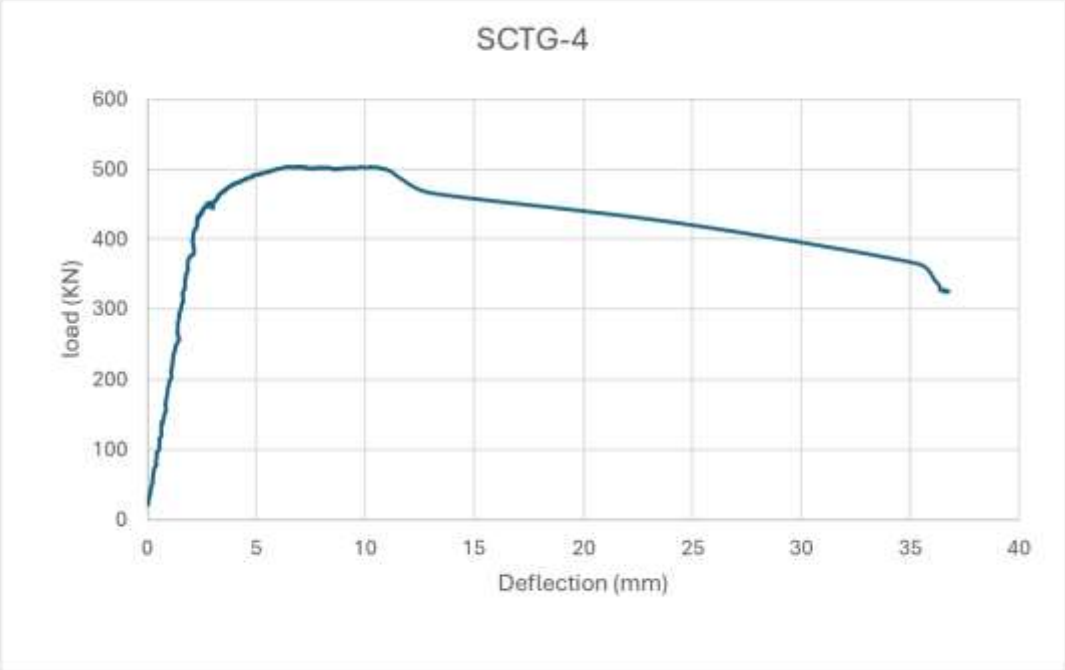

Figure 6.15: Load-deflection of the SCTG-4

6.1.3.4 Load – strain relationship

The strain is a measure of the deformation of a material which is the change in the length or size as element response due to an external force, as showing in Table 6.4 including details results of the top concrete surface (maximum negative moment) using two strain sensor with symbols (S5) and (S6), and for Table 6.5

consists results of the lower bottom steel flange (maximum positive moment) using four strain sensor symbolized as (S1), (S2), (S3) and (S4).

6.1.3.4.1 Load – strain curves of top concrete

The two sensors conduct the response of specimens at the maximum negative moment regions along the load stages, for (SCTG-1) the results show that the increase was gradual as liner path at 10.7% of ultimate load, more over the curve suddenly forward to the opposite direction and continuous increasing until it's reach the plastic strain response at 85.3% of fully applied load, the two sensor reading reached the plastic deformation at the same load stage but with variations in strain amount about 62.6% due to uneven stress distributions, Figure 6.16.

For (SCTG-2) the two sensors conduct the elastic strain at different load stages, by taking the lowest strain value as worst case, so the elastic deformation will be at 22.7% of the ultimate load while the plastic deformation takes place at 28.2%, at ultimate load the reading shows high strain increasing and decreasing of (S5) and (S6) respectively, Figure 6.17.

For (SCTG-3) the results illustrate that the final elastic deformation was reached at 19.6% mean while the plastic deformation was at 30.7% of the ultimate load, it's noticed that the surface exposed to high uneven stress distribution and the strain reading increased to high form elastic to plastic load for (S5) and (S6) as 32% and 23.3% respectively, Figure 6.18.

For (SCTG-4) sample, the result of strain with number (S5) show it's reached the elastic and plastic deformations at 16.3% and 16.5% of ultimate load respectively, meanwhile, strain (S6) shows very high reading as 72.9% and 91.4%, big gap between these two senor due to unequaled stresses and it's can be clear obvious because at plastic load of each (S5) and (S6) the strain reading 15284 x10^{-6} and 464x 10^{-6} micro strain respectively, Figure 6.19.

There are no signs of any negative effects of the strain gauge since these regions are exposed to tensile stress only.

6.1.3.4.2 Load – strain curves of bottom steel flange

The four strain sensors are divided into two sensors for each sagging region and spaced from each other by certain distance to collect the elongation.

For (SCTG-1), the results show all strain reached the same amount of elastic and plastic deformation with 80% and 96% respectively, the strain increasing from stage to other was 26.7%, Figure 6.20.

For (SCTG-2), the elastic and plastic deformation was at 27.4% and 88.7% respectively, the strain reading increased from elastic stage to final stage about 93.5%, Figure 6.21

For (SCTG-3), the curve illustrates that elastic and plastic damage starts when the load reached 43.4% and 93.4% with strain increasing at all stages till the final stage from 93.5% when the (S4) record 6656 x10^{-6}, Figure 6.22.

Lastly, about sample (SCTG-4) the elastic and plastic deformation begins at very late load stage, 85.6% and 99.4% due to high strength resistance of top concrete related to its thickness, strain (S1) record was 3947 x10^{-6}.

The results show the four strains have different values but same pattern and the high elastic and plastic percentage for bottom steel flange sensors compared to very low percentage of top concrete refer to that the upper part exposed to higher strain ratio, Figure 6.23.

Table 6.4: Experimental Load – Strain at Top Concrete for (SCTG)

Specimen		Experiment result in micro strain X 10^{-6}							
		Elastic strain Load (KN)	Strain (mm/mm)	Plastic strain Load (KN)	Strain (mm/mm)	Ultimate Load (KN)	Strain (mm/mm)	Final failure stage load (KN)	Strain (mm/mm)
SCTG-1	Strain-5	68	413	558	670	654	717	648	719
	Strain-6	67	198	540	250	654	343	648	351
SCTG-2	Strain-5	186	380	512	8294	659	15398	611	15398
	Strain-6	150	305	186	401	659	285	611	262
SCTG-3	Strain-5	149	4589	160	14303	520	14303	500	14303
	Strain-6	102	284	307	1216	520	2275	500	2270
SCTG-4	Strain-5	82	5546	83	15284	503	15284	422	15284
	Strain-6	367	365	460	464	503	398	422	375

Figure 6.16: Load- Strain Curve of Top Concrete for the SCTG-1

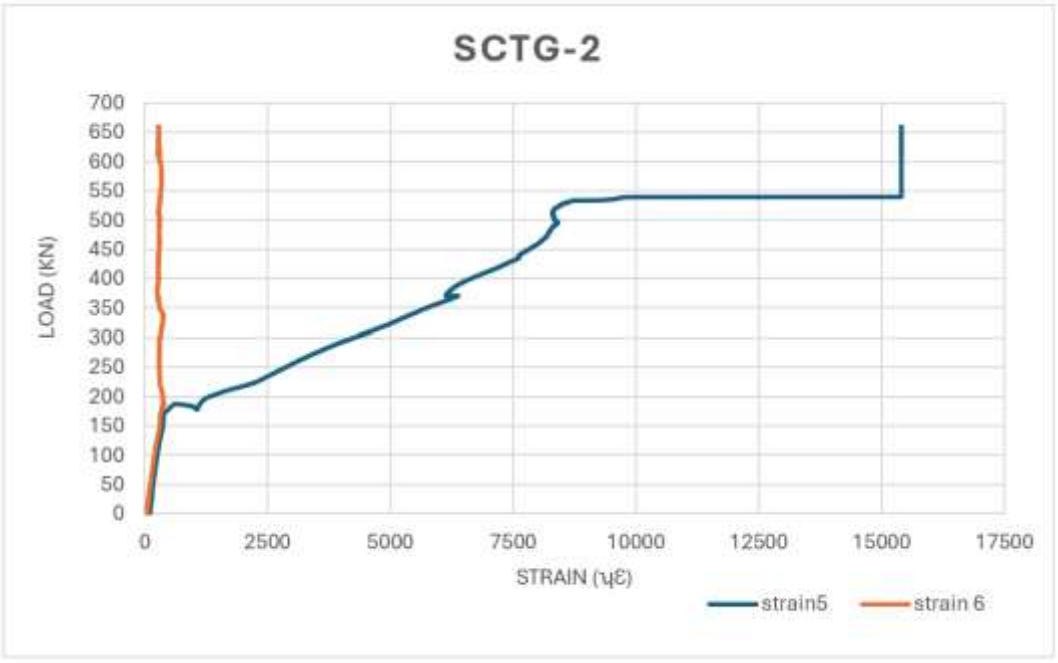

Figure 6.17: Load- Strain Curve of Top Concrete for the SCTG-2

Figure 6.18: Load- Strain Curve of Top Concrete for the SCTG-3

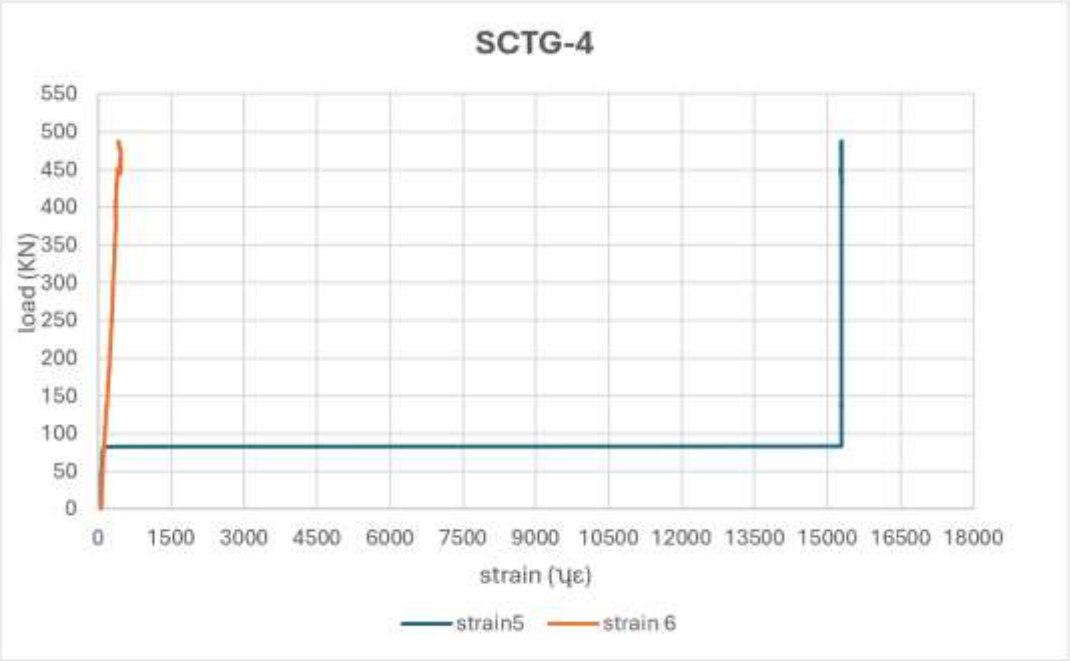

Figure 6.19: Load- Strain Curve of Top Concrete for the SCTG-4

Table 6.5: Experimental Bottom Steel Flange Load – Strain for the (SCTG) Specimens

Specimen		Experiment result in micro strain X 10^{-6}							
		Elastic deformation Load (KN)	Strain(mm/mm)	Plastic deformation Load (KN)	Strain (mm/mm)	Ultimate Load (KN)	Strain (mm/mm)	Final Failure Stage Load (KN)	Strain (mm/mm)
SCTG-1	Strain-1	524	775	630	1144	654	1399	528	1478
		523	719	635	1086	654	1266	528	1273
	Strain-2	526	738	633	1124	654	1350	528	2779
		525	941	621	1284	654	1529	528	3519
	Strain-3								
	Strain-4								
SCTG-2	Strain-1	225	288	631	1183	659	1398	515	3485
		281	332	604	1093	659	1410	515	2554
	Strain-2	184	205	610	969	659	1075	515	1339
		181	294	585	1119	659	1313	515	1415
	Strain-3								
	Strain-4								
SCTG-3	Strain-1	226	369	486	1174	520	1441	424	1559
		252	232	498	821	520	1087	424	1315
	Strain-2	250	444	500	1399	520	2129	424	4534
		250	426	512	1630	520	2206	424	6656
	Strain-3								
	Strain-4								
SCTG-4	Strain-1	431	540	500	1266	503	1428	352	3947
		438	676	492	990	503	1140	352	1792
	Strain-2	425	617	500	1256	503	1401	352	3225
		426	400	500	824	503	895	352	1919
	Strain-3								
	Strain-4								

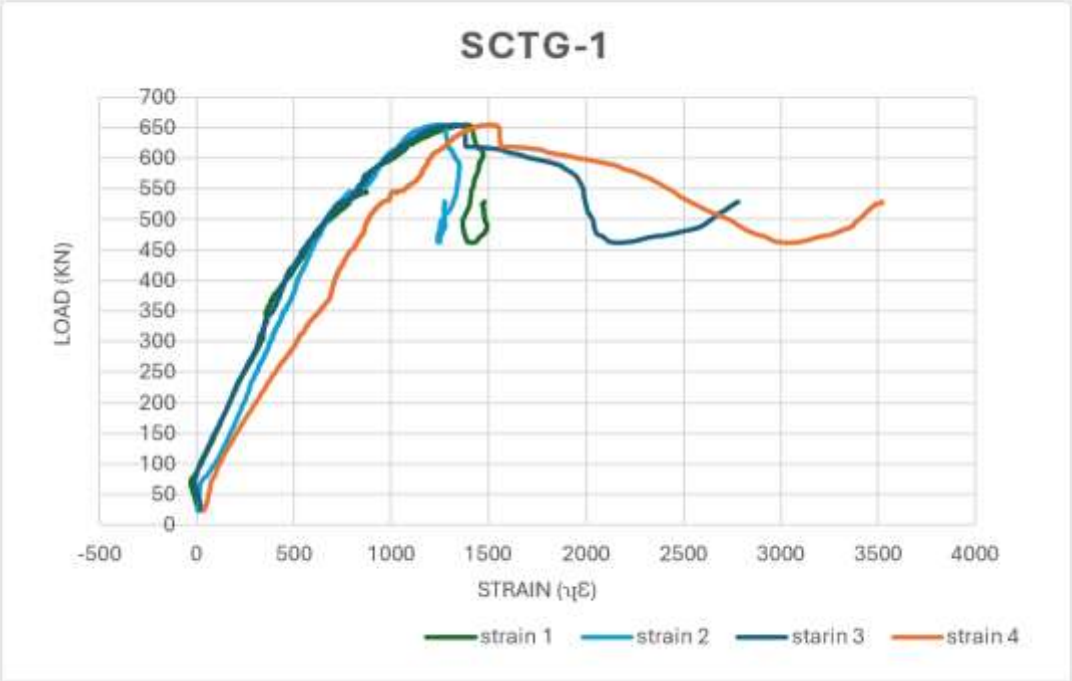

Figure 6.20: Bottom Steel Flange Load – Strain Curve for the SCTG-1

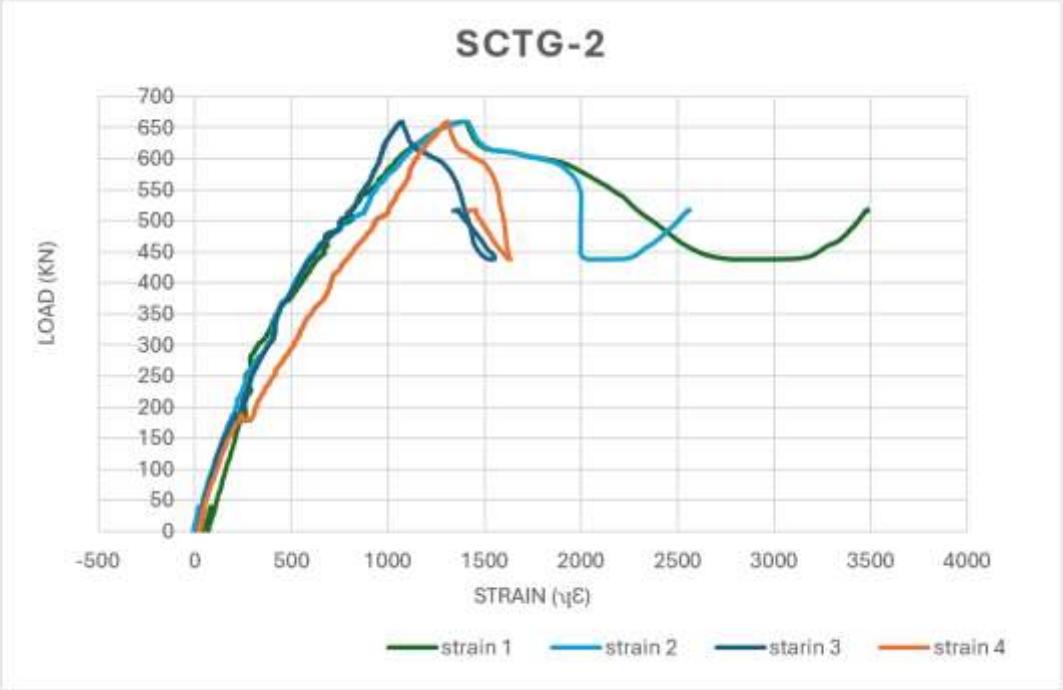

Figure 6.21: Bottom Steel Flange Load – Strain Curve for the SCTG-2

Figure 6.22: Bottom Steel Flange Load – Strain Curve for the SCTG-3

Figure 6.23: Bottom Steel Flange Load – Strain Curve for the SCTG-4

6.1.3.5 Load – Slip Relationship

By assuming full interaction, (LVDT-3) installation at left side and (LVDT-4) installation at right side of the girder, the measurement of the slip amount was made

during all load stage, as in Table 6.6 shows the details results, the positive records signs refer to the top concrete movement toward inside structure direction and steel flange to outside direction and the negative records sign means the opposite.

The sample (SCTG-1) gives variation reading amount at 81.9% of loading stage and at final load the slip occurs at lift side only, Figure 6.24.

The sample (SCTG-2) at 49.3% shows same reading pattern until the final load exposed to different slip ratio between the two edges, Figure 6.25.

The results of sample (SCTG-3) show 66% of loading it's exposed to positive slip while at 80% it's suddenly had negative slip and in final stage return to positive slip, that refers to three different curvatures, Figure 6.26.

Lastly The sample (SCTG-4) at 28.3% positive slip has occurred, and at 64% till the final load two positive and negative slip occurs at same time, that means the response was act as two curvatures cycle, Figure 6.27.

The maximum load-slip for (SCTG-1), (SCTG-2), (SCTG-3) and (SCTG-4) with records 96%, 96.8%, 66% and 22% respectively of the final load.

Table 6.6: Load -Slip for the Specimens and Shear Connector Mechanical Properties (SCTG)

Sample	Con. Strength MPa	Ultimate Load Pu (KN)	Relative ξu slip (mm)	Maximum Slip (mm)	Load P_{Rd} (kN)	Relative ξuK slip (mm)	DUCTILITY ξu/ ξuK
SCTG-1	35	654	-0.933	-1.38	588.6	-1.21	0.771
SCTG-2	35	659	-0.652	-0.652	593.1	-0.387	1.684
SCTG-3	35	520	0.376	0.347	468	0.222	1.693
SCTG-4	35	503	0.241	0.287	452.7	0.15	1.60

P_{Rd} = load at the beginning of plastic deformation According to Eurocode 4

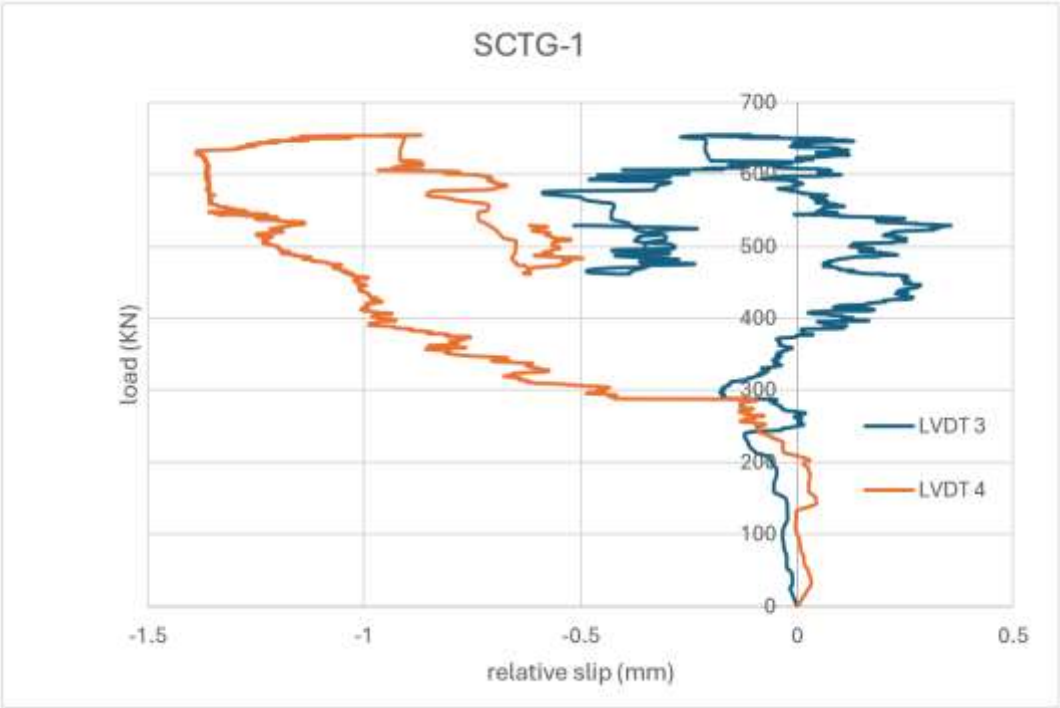

Figure 6.24: Load – Slip Curve for the SCTG-1

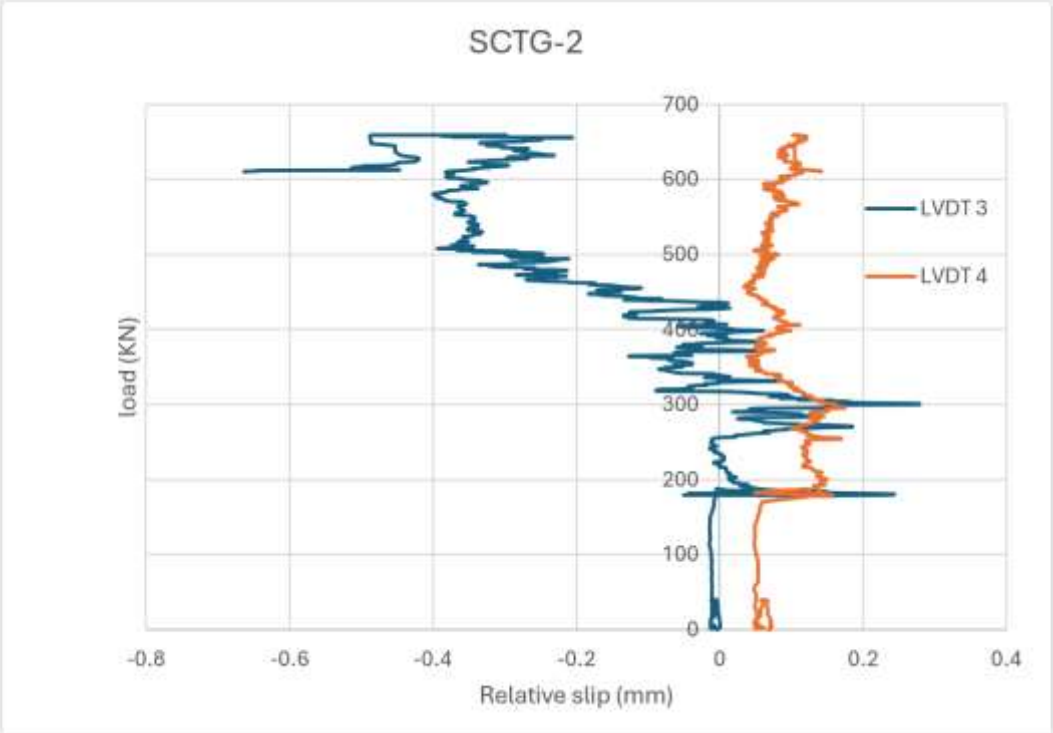

Figure 6.25: Load – Slip Curve for the SCTG-2

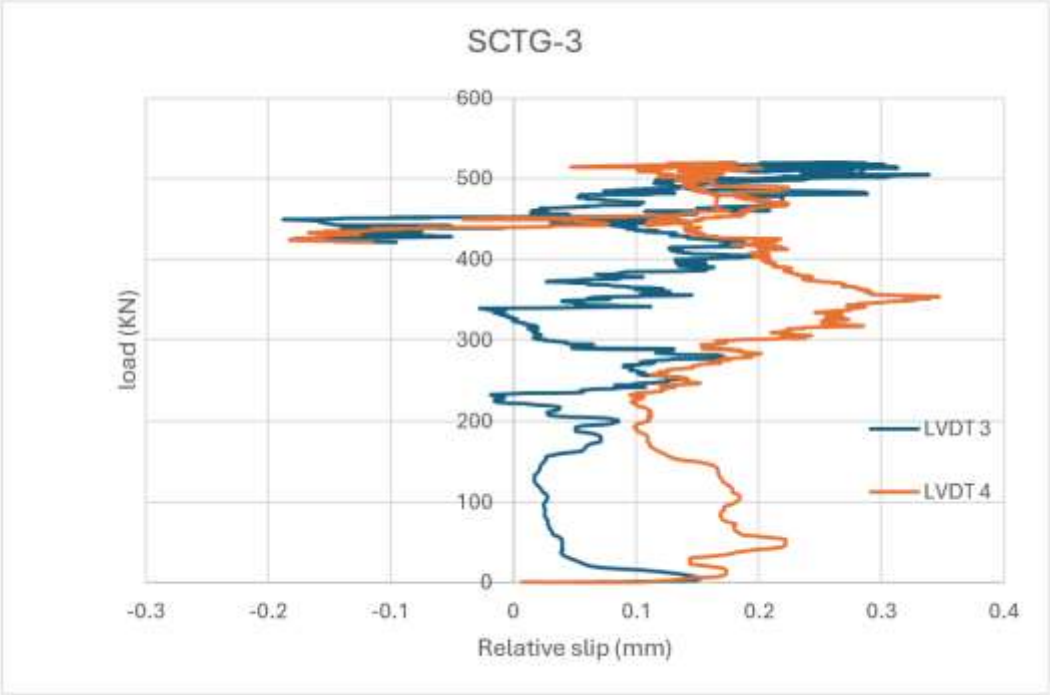

Figure 6.26: Load – Slip Curve for the SCTG-3

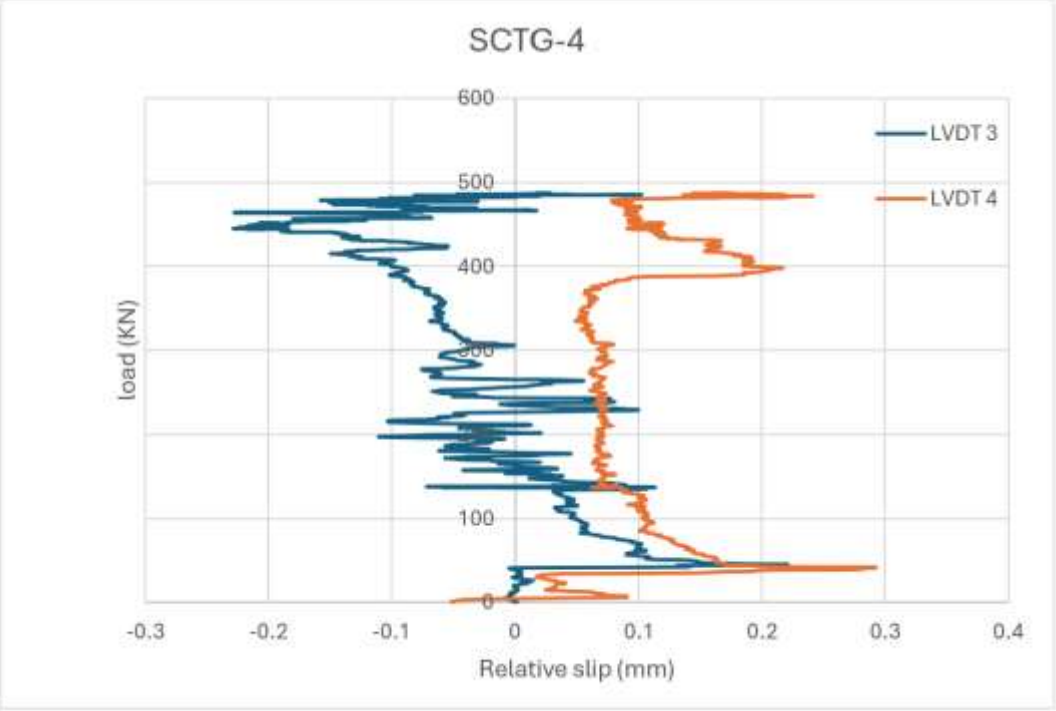

Figure 6.27: Load – Slip Curve for the SCTG-4

6.1.4 Second category (DCTG) results

6.1.4.1 Modes of failure

As mentioned at the first category results, the failure modes shape and the loading stage for the second category (DCTG) will be illustrated in this section and a compression study will be done to show the effectiveness of the Double composite action which refers to the addition lower concrete against the single composite samples.

Each specimen will be corresponding to one or more failure modes in each test, Figure 6.28 to Figure 6.31 illustrate the states of failure of each specimen belonging the results show that for the (DCTG-1) it's suffered a failure condition of the advanced type at bottom concrete with steel flange due to the high compassion stress generated the shear force effect on the section, moreover, concrete detachment from the perfobond leiste shear connector cause the uplift of the steel flange which conduct a shear connector failure in this region.

For (DCTG-2) the same mode shape of the previous sample but in less failure amount, the fractured points start at the lower cord especially at mid bottom concrete cause shear failure and HSS steel member weld get few fractured, all three support regions get damaged at the same time, for the (DCTG-3) the results show high failure at the bottom concrete cord with steel flange separation due to failure of shear connector, while full fractured of the diagonal HSS member from the bottom, for (DCTG-4) shows bottom concrete failure at edge near the steel support, while the mid region give good failure resistance due to the thickness of concrete with good interaction with shear connectors.

The strength capacity of (DCTG) was higher than the (SCTG) samples by 13%, when this category (DCTG-1), (DCTG-2), (DCTG-3) and (DCTG-4) get strength results as 71 tons, 61 tons 71 tons and 75 tons respectively.

Figure 6.28: Failure Mode of the DCTG-1

Figure 6.29: Failure Mode of the DCTG-2

Figure 6.30: Failure Mode of the DCTG-3

Figure 6.31: Failure Mode of the DCTG-4

6.1.4.2 Initial crack load (p_{cr}) and ultimate crack load (p_{ul})

Cracks indicated by the visual inspection method, the results for this category (DCTG) show in Table 6.7**,** including elastic and plastic load to indicate the load level at which the initial cracks appear until the final cracks appear helps to understand how (DCTG) effects the delay in the appearance of the initial cracks on maximum moment zones.

For (DCTG-1), (DCTG-2), (DCTG-3) and (DCTG-4) samples initial cracks appear at hogging moment region (H.M.R.C) which is on the surface of top concrete structure due to generated of high negative moment, the results show that cracks appearance in 44.1%, 61.1%, 66% and 69.3% of the ultimate applied load of

respectively each samples, and the ultimate service cracks start at 91.1%, 94.9%, 96.6% and 96.8% respectively from the ultimate load.

It's obvious that the initial carks appeared at intermediate stages of the loading stage, unlike the (SCTG) samples that appeared at the primary loading stage, moreover, the ultimate service cracks appeared at very advanced loading stage while the (SCTG) samples results show it's appeared at intermediate to advanced stages, the type of cracks that appeared of the advanced type in the region of negative momenta, where their occurrence was delayed by bottom concrete which is represent the double composite, cracks ratio and pattern shape illustrate in Figures 6.32 to Figures 6.35.

Table 6.7: Initial Crack Load (pcr) and the Ultimate Crack Load (pul) for (DCTG)

Specimen	F_u (KN)	D_u (mm)	Initial cracking p_{cr} (KN)	Ultimate cracking p_{ul} (KN)	Remark
DCTG-1	725	7.80	320	661	H.M.R.C
DCTG-2	613	5.26	375	582	H.M.R.C
DCTG-3	716	6.14	473	692	H.M.R.C
DCTG-4	754	4.6	523	730	H.M.R.C

Note: F_u and D_u= ultimate load and corresponding ultimate displacement

Figure 6.32: Initial and Ultimate Cracks Pattern of the DCTG-1

Figure 6.33: Initial and Ultimate Cracks Pattern of the DCTG-2

Figure 6.34: Initial and Ultimate Cracks Pattern of the DCTG-4

Figure 6.35: Initial and Ultimate Cracks Pattern of the DCTG-4

6.1.4.3 Load–Deflection Relationship

By using two LVDT senser devices to collect the deflection data from the bottom cord connect with the surface of the bottom concrete at maximum positive moment regions or sagging moment, Table 6.10 illustrates the results.

The results show for (DCTG-1), (DCTG-2), (DCTG-3) and (DCTG-4) from the elastic load to ultimate load that the deflection increasing 14.1%, 27.3%, 14% and 14.3% respectively, on other hand, from plastic load to ultimate load the deflection increasing was 7.6%, 23.1%, 5.2% and 2.1% respectively.

This previous result gives clear vison about the samples response at several stages, by comparison the (DCTG) with (SCTG) it's clear obvious the effect of double composite on decreasing defection ratio for all samples even if the (DCTG) samples exposed to higher loads.

It's can notice that the defection ratio from the initial load stage till the full loading was moderately situation that led to have a specimen with high stable defection control, even from plastic load stage to full load the increasing was very low percentage, and the most important features about (DCTG) samples it's had high elastic load illustrated as a straight line as show in Figure 6.36 to and Figure 6.39 illustrates the curves of deflections.

Table 6.8: Experimental Workload – Deflection at Bottom Cord for (DCTG)

Specimen	Experiment result					
	Elastic Load (KN)	Deflection (mm)	Plastic Load (KN)	Deflection (mm)	Ultimate Load (KN)	Ultimate Deflection (mm)
DCTG-1	659	6.7	691	7.2	725	7.80
DCTG-2	621	5.30	639	5.61	665	7.3
DCTG-3	636	5.28	701	5.82	716	6.14
DCTG-4	649	3.94	747	4.5	754	4.6

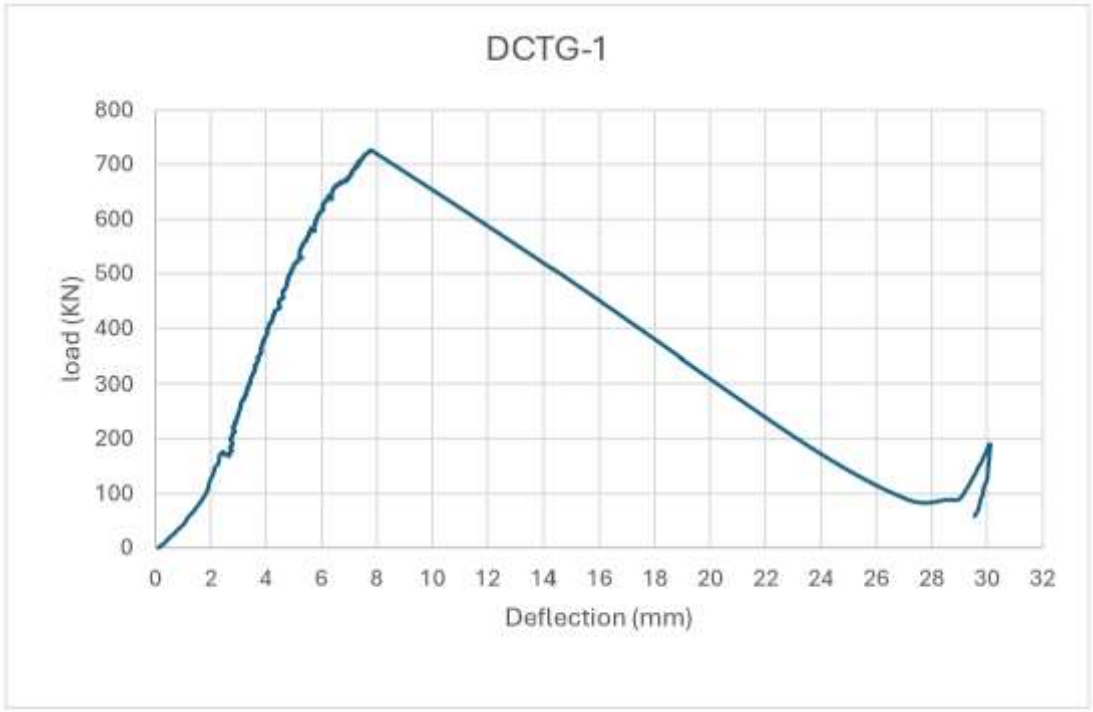

Figure 6.36: Load-Deflection Curve of the DCTG-1

Figure 6.37: Load-Deflection Curve of the DCTG-2

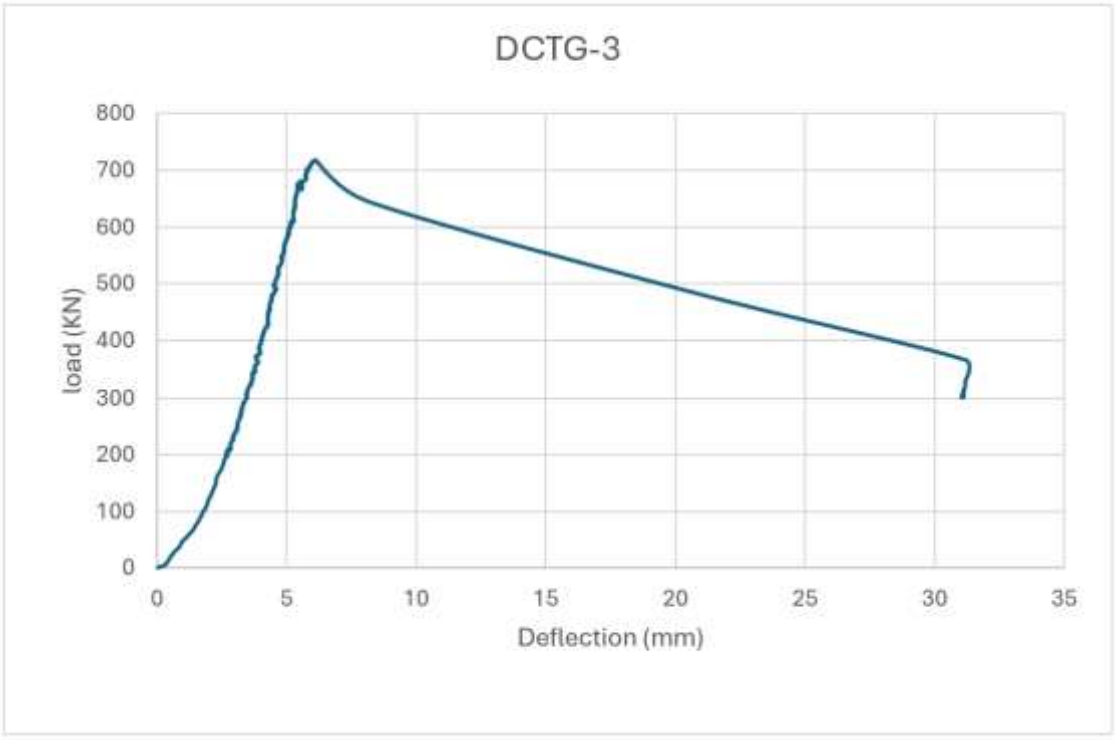

Figure 6.38: Load-Deflection Curve of the DCTG-3

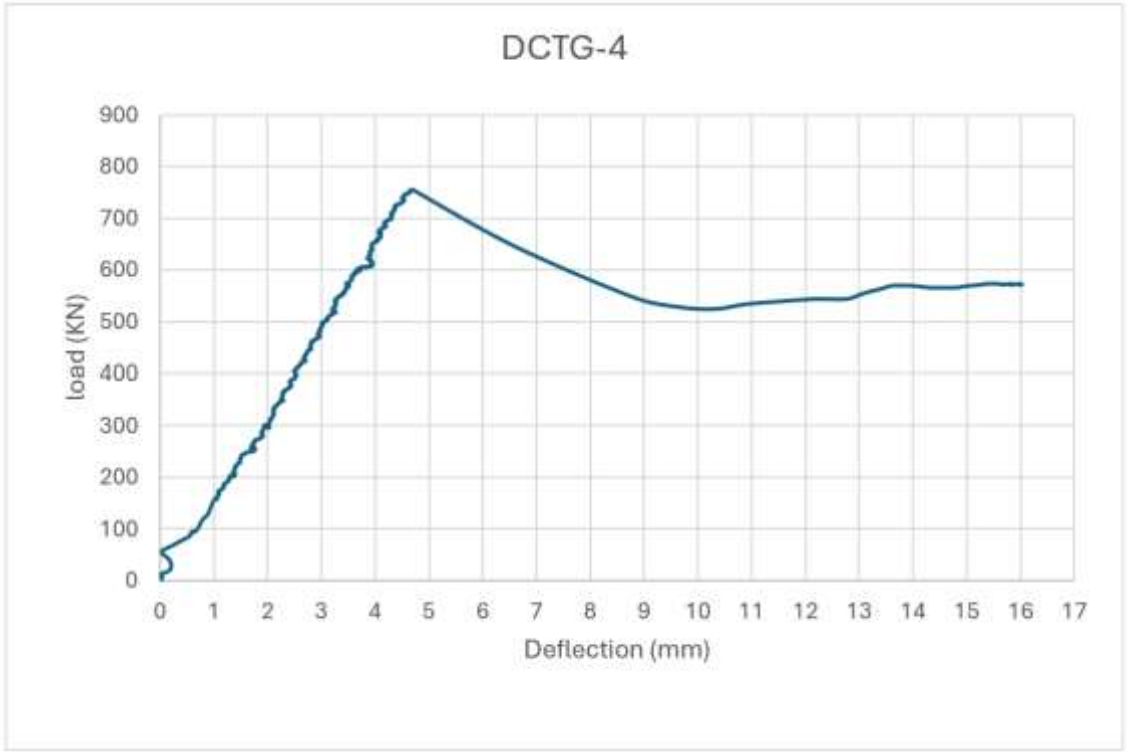

Figure 6.39: Load-Deflection Curve of the DCTG-4

6.1.4.4 Load – strain relationship

By adhesive six strain gauge in each specimen to conduct the data of stresses point at the mid top concrete part which refers to hogging moment region, and for the

bottom concrete at positive moment region to record the sample response, Table 6.9 and Table 6.10 illustrated the details data.

6.1.4.4.1 Top concrete load – strain curves

Sample (DCTG-1) the elastic deformation load was conducted at (61.5%), (14.6) while plastic deformation was in 89.1% and 16% from the ultimate loading for strain (S5) and (S6) respectively, it's worth mentioning that (S6) reading was higher than (S5) due to its exposed to high crack zone, Figure 6.40.

While (DCTG-2) was having same strain pattern but different values, for the two strain sensor (S5) and (S6) reached the elastic deformation at the same load stage about 17.5%, but for the plastic deformation was recorded at 61.6% and 75.9% from the ultimate load, at final stage the concrete surface exposed to reflected compression stress related the sample curvature response and that's can be clear obvious with the negative results sign, Figure 6.41.

for (DCTG-3) sample the reading was normal for the first load stage but the strain (S5) at 27% loading stage conducts high strain reading and counting as the same amount till the final load, for more details, the elastic strain was for (S5) and (S6) at the same level while plastic deformation was variable at 28% and 94.7% respectively, Figure 6.42.

For (DCTG-4) girder the elastic strain deformation takes place at (S5) before (S6) as 25.8% and 35.4% while the plastic deformation shows up at very closed load level of the strain sensor at 72.9% and 78.9%, Figure 6.43.

Moreover, the last sample had the most accurate strain data when it had the same strain increasing pattern till the final load, and that gave evidence about the initial cracks that showed up at very advanced load stage.

6.1.4.4.2 Bottom concrete load – strain curves

To find the strain mount of the below concrete of the double composite truss girder, four strain gauges were used, each two located in the positive moment region collecting the required data of the maximum strain.

At bottom surface of (DCTG-1), the plastic strain of the worst sensor records case was in (S1) where the ultimate cracks are being propagated and grow at load

stage 20.1% meanwhile (S2), (S3) and (S4) were at 76.1%, 83.1% and 75.1% respectively, Figure 6.44.

For (DCTG-2), the four sensors were at same pattern, plastic deformation (S1) and (S2) were at 84.2%, on other hand the (S3) and (S4) were at 63.4%, that is good enough if compared with the results of the upper part, Figure 6.45.

Where the sample (DCTG-3) plastic strain was for (S1), (S2) and (S3) was at 85.2%, 84.2% and 73.9% while the strain (S4) conducts the high strain ratio in earlier load stage with 52%, Figure 6.46.

Lastly for (DCTG-4) all sensors curve was as adequate pattern at 33.1% of the ultimate load, after that suddenly values get variation, the results show that the bottom surface exposed to very high tensile stress along the loading stages while low stress was on the top concrete surface, Figure 6.47.

In average, all strain sensor reading of the (DCTG) samples show It has more stability and a good fit between the load and the readability of the strain sensor compared to the (SCTG) samples when it’s show very high stress reading and variation amount at the same load stage due to unstable and uneven load distribution on the surface.

The results show that when the stress reaches high level on the top concrete surface it’s act in the opposite way for the bottom concrete surface, when results show low strain level, and that’s depend on the variation of the curvature degree of the composite girder.

Table 6.9: Experimental Load – Strain of Top Concrete for (DCTG)

Specimen		Experiment result in micro strain X 10^{-6}							
		Elastic strain Load (KN)	Strain (mm/mm)	Plastic strain Load (KN)	Strain (mm/mm)	Ultimate Load (KN)	Strain (mm/mm)	Final failure stage load (KN)	Strain (mm/mm)
DCTG-1	Strain-5	446	214	646	296	725	314	507	208
	Strain-6	106	103	116	8806	725	8808	507	8808
DCTG-2	Strain-5	120	170	410	244	665	-56	566	-128
	Strain-6	117	293	505	90	665	40	566	54
DCTG-3	Strain-5	102	59	197	5301	717	5301	301	5301
	Strain-6	103	206	679	2894	717	2574	301	2099
DCTG-4	Strain-5	159	40	551	131	755	184	549	217
	Strain-6	268	246	593	379	755	392	549	258

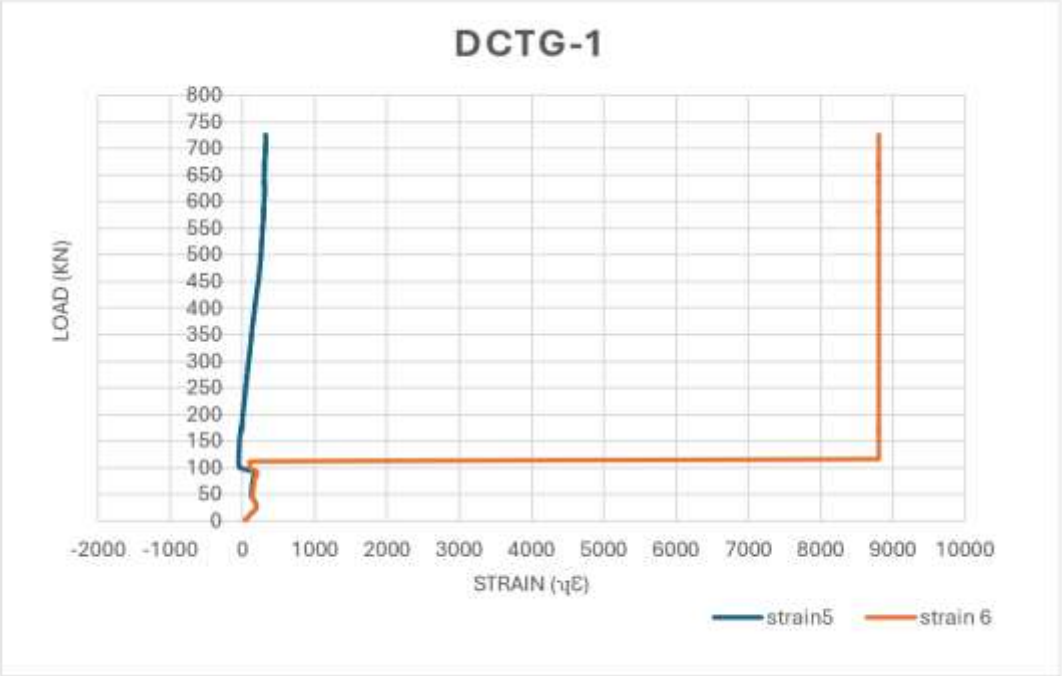

Figure 6.40: Load- Strain Curve of Top Concrete for the DCTG-1

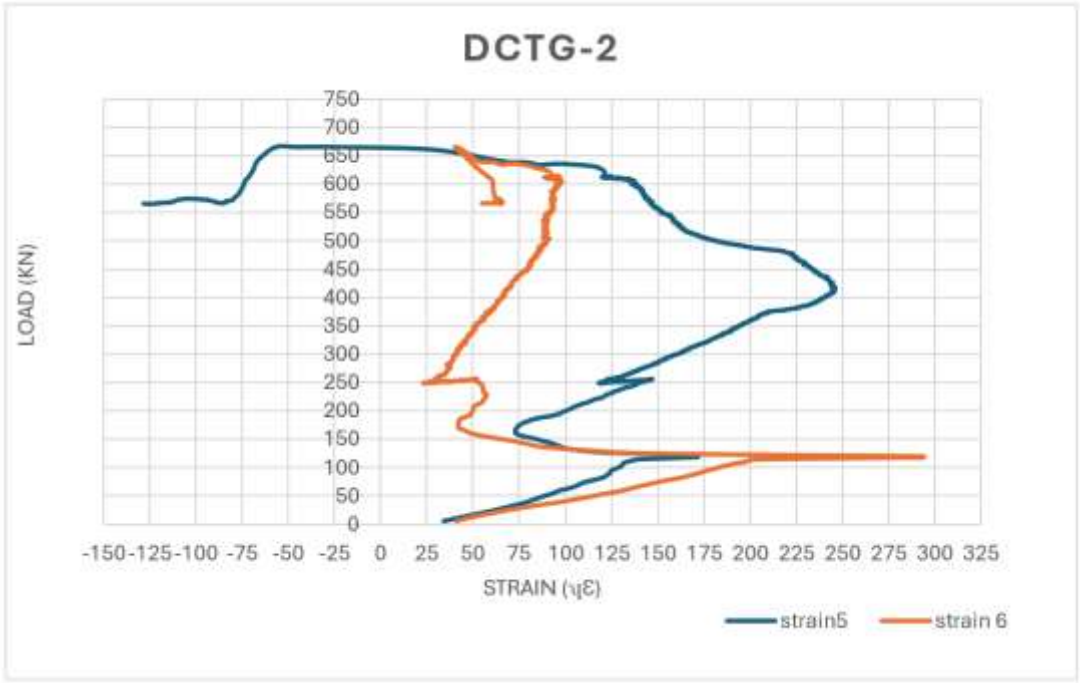

Figure 6.41: Load- Strain Curve of Top Concrete for the DCTG-2

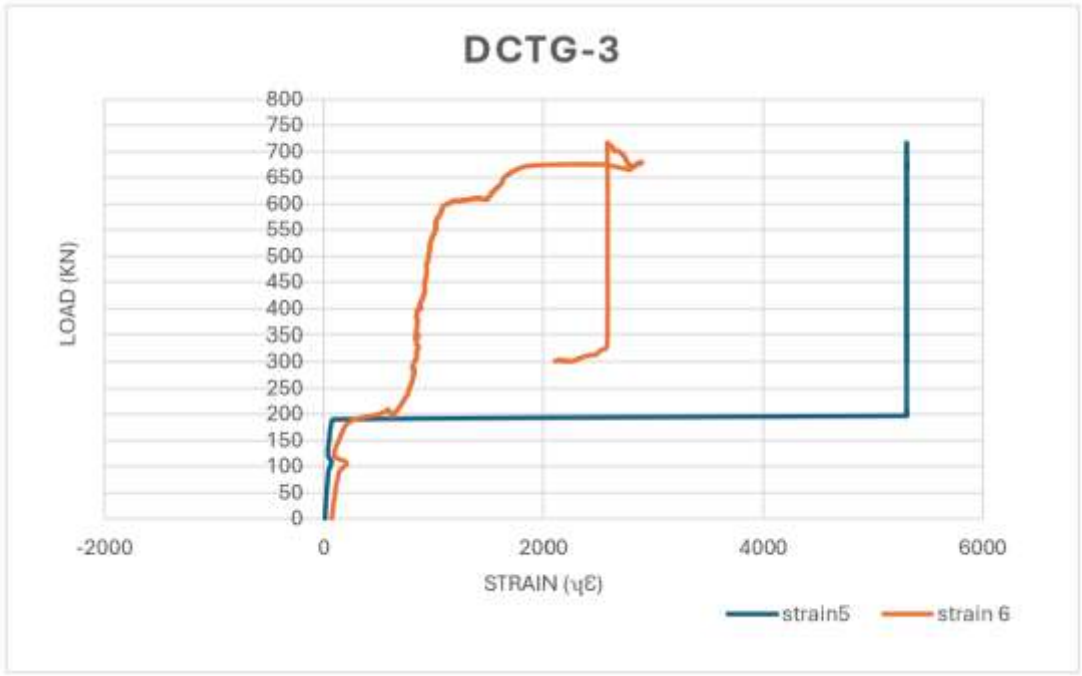

Figure 6.42: Load- Strain Curve of Top Concrete for the DCTG-3

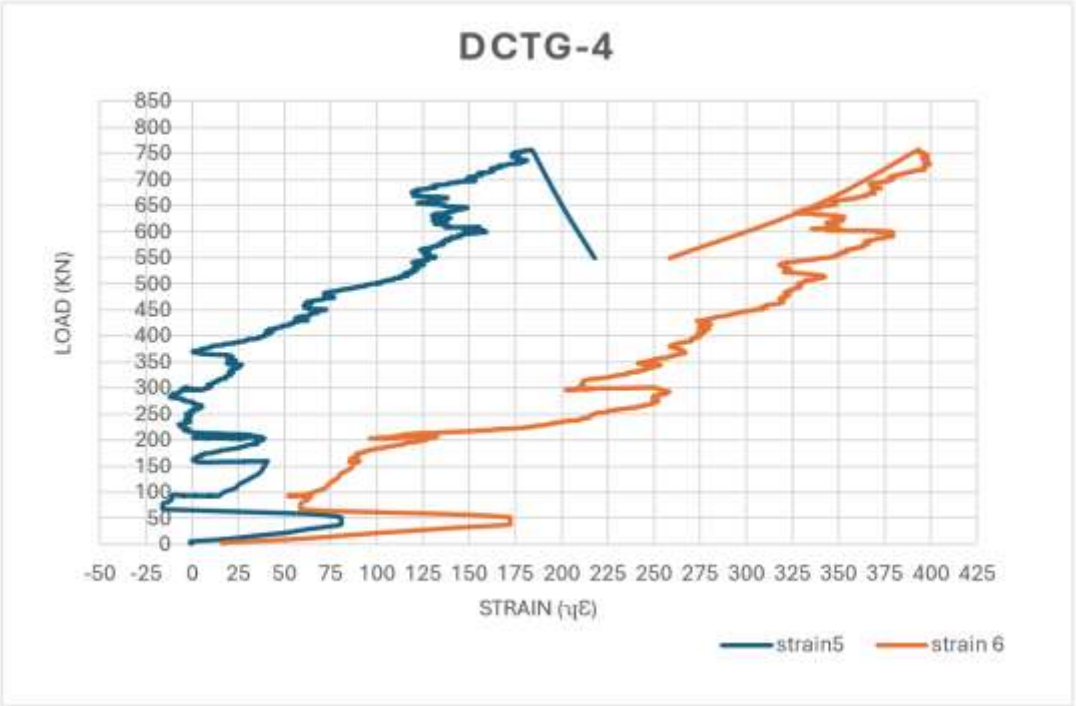

Figure 6.43: Load- Strain Curve of Top Concrete for the DCTG-4

Table 6.10: Experimental Load – Strain of Bottom Concrete for the (DCTG) Specimens

Specimen		Experiment result in micro strain X 10^{-6}							
		Elastic Load (KN)	Strain (mm/mm)	Plastic Load (KN)	Strain (mm/mm)	Ultimate Load (KN)	Strain (mm/mm)	Final failure stage load (KN)	Strain (mm/mm)
DCTG-1	Strain-1	100	269	152	1327	725	12643	507	12643
	Strain-2	220	1666	552	1781	725	1718	507	1400
	Strain-3	400	2543	603	2495	725	2477	507	2479
	Strain-4	225	903	545	1067	725	1071	507	1044
DCTG-2	Strain-1	126	196	560	193	665	158	625	84
	Strain-2	124	209	570	200	665	376	625	355
	Strain-3	365	365	427	393	665	469	625	472
	Strain-4	256	213	422	256	665	277	625	276

Table 6.12: (Cont.) Experimental Load – Strain of Bottom Concrete for the (DCTG) Specimens

Specimen		Experiment result in micro strain X 10^{-6}							
		Elastic Load (KN)	Strain (mm/mm)	Plastic Load (KN)	Strain (mm/mm)	Ultimate Load (KN)	Strain (mm/mm)	Final failure stage load (KN)	Strain (mm/mm)
DCTG-3	Strain-1	204	293	611	336	717	150	644	161
	Strain-2	321	1021	604	1177	717	795	644	811
	Strain-3	333	2427	530	2551	717	543	644	542
	Strain-4	197	1897	374	2980	717	904	644	900
DCTG-4	Strain-1	462	842	476	908	755	9114	647	9114
	Strain-2	397	1041	541	2889	755	7770	647	7770
	Strain-3	250	729	481	6051	755	6173	647	6016
	Strain-4	159	-57	250	337	755	88	647	113

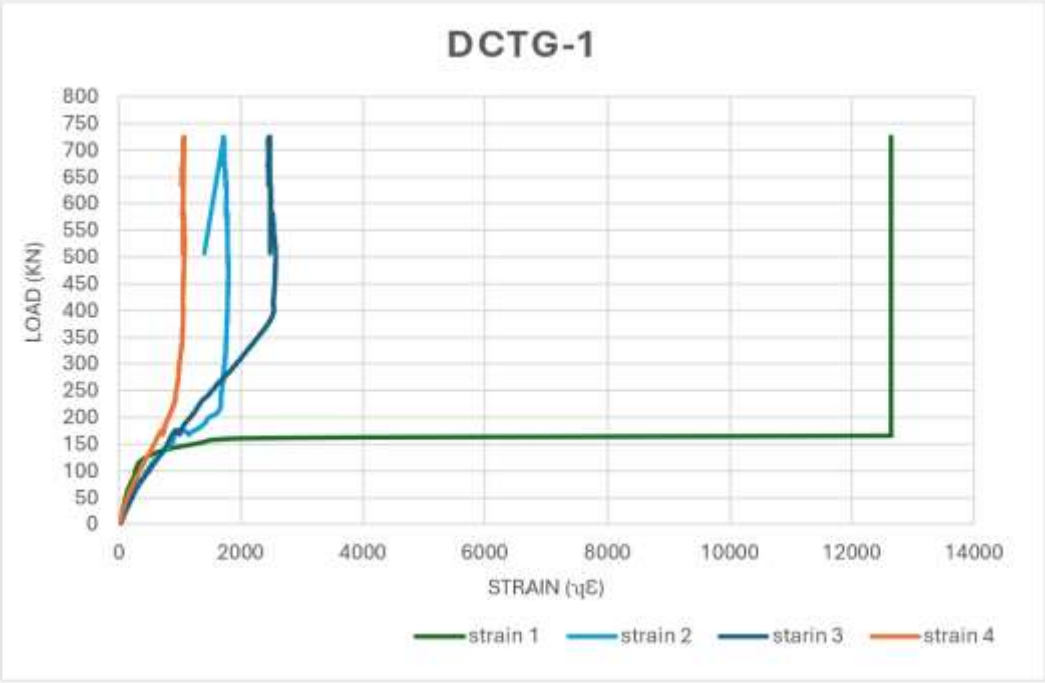

Figure 6.44: Load – Strain for Bottom Concrete for the DCTG-1

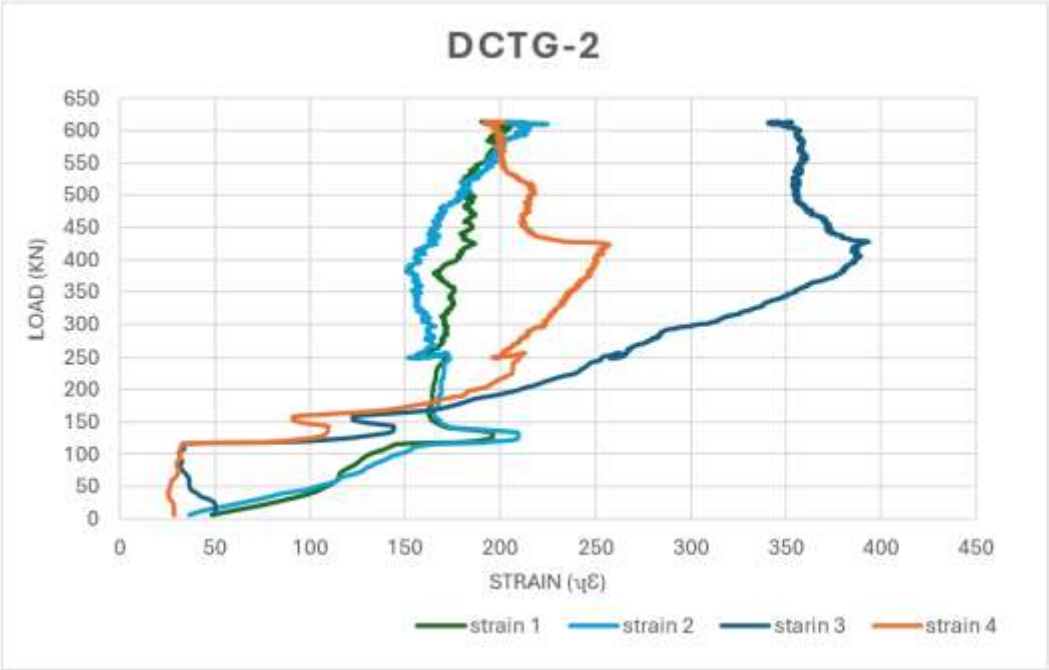

Figure 6.45: Load – strain for bottom concrete for the DCTG-2

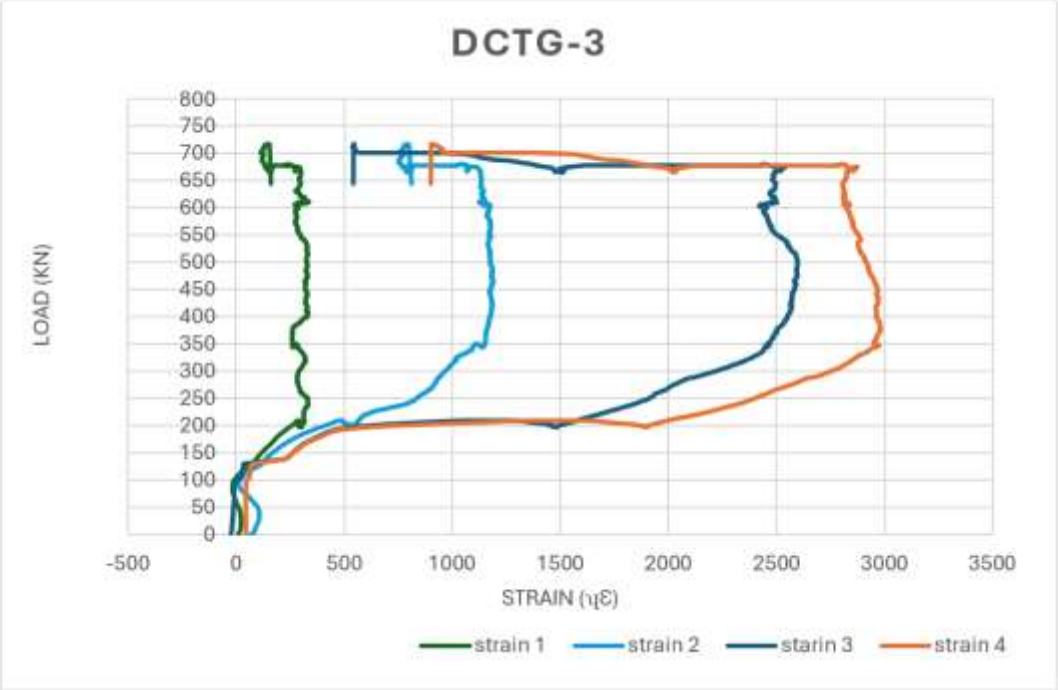

Figure 6.46: Load – Strain for Bottom Concrete for the DCTG-3

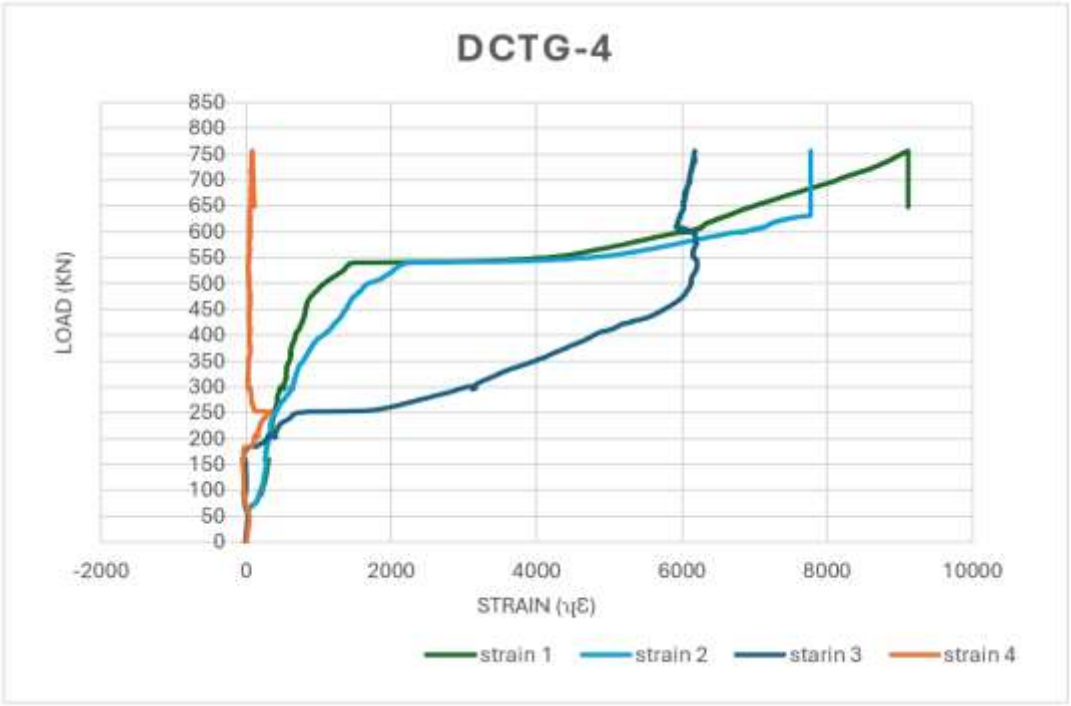

Figure 6.47: Load – Strain for Bottom Concrete for the DCTG-4

6.1.4.5 Load – Slip Curves

Assuming full interaction between steel and deck slab, and the measurement of the slip amount at the edge of the specimen also with each load stage, Table 6.13 shows the required details**,** to reduce errors in the test, the relative slip is an averaged from four LVDTs.

The results revealed that (DCTG-1) sample had negative signs due to pulling the LVDT sensor that occurs due to increasing the gap between the concrete and steel flange, so at 23% each LVDT had certain direction, Figure 6.48.

While the (DCTG-2) had two degrees of curvature due to the reflect in result sign during the loading process, the maximum elastic slip of all tested samples occurs at this sample at 24.4% of the ultimate load, Figure 6.48.

For (DCTG-3) had the same slip pattern situation, so at 81% of loading the LVDT with number (S2) lead to be at positive region, and at final stage all sensors record exceptionally low slip ratio, Figure 6.49.

Lasty (DCTG-4), show the minimum elastic and plastic slip ratio of all the samples, even the maximum slip was low compared to others, Figure 6.50.

The maximum slip for (DCTG-1), (DCTG-2), (DCTG-3) and (DCTG-4) records at 62%, 81%, 24.4% and 73.9% of each sample final load respectively, which is elastic slip and decreeing at final load stage.

Table 6.11: Details of Load -Slip for the Specimens (DCTG)

Sample	Con. Strength MPa	Ultimate Load PU (KN)	Relative ξu slip. (mm)	Maximum Slip (mm)	Load P_{Rd} (kN)	Relative ξuK slip. (mm)	DUCTILITY ξu / ξuK
DCTG-1	35	725	-0.609	-1.08	652.5	-0.804	0.75
DCTG-2	35	665	-0.160	0.53	645.3	-0.196	0.81
DCTG-3	35	717	0.193	0.28	598.5	-0.077	29.23
DCTG-4	35	755	-0.152	0.27	679.5	-0.0052	35.9

Note: P_{Rd} = load at the beginning plastic deformation of ultimate load

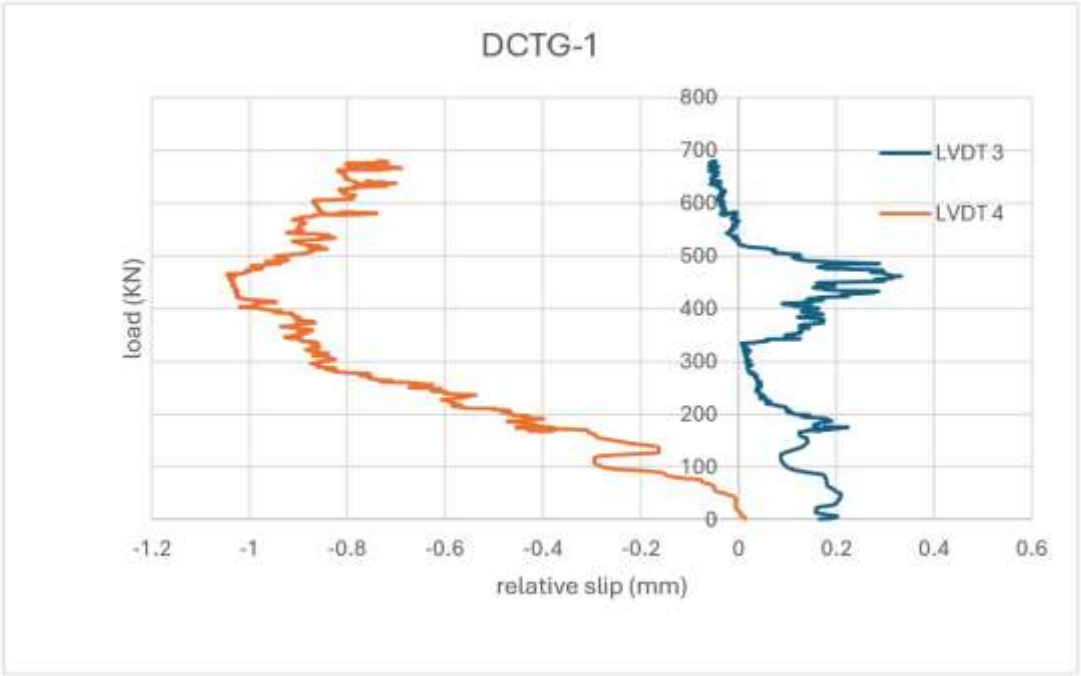

Figure 6.48: Load – Slip Curve for the DCTG-1

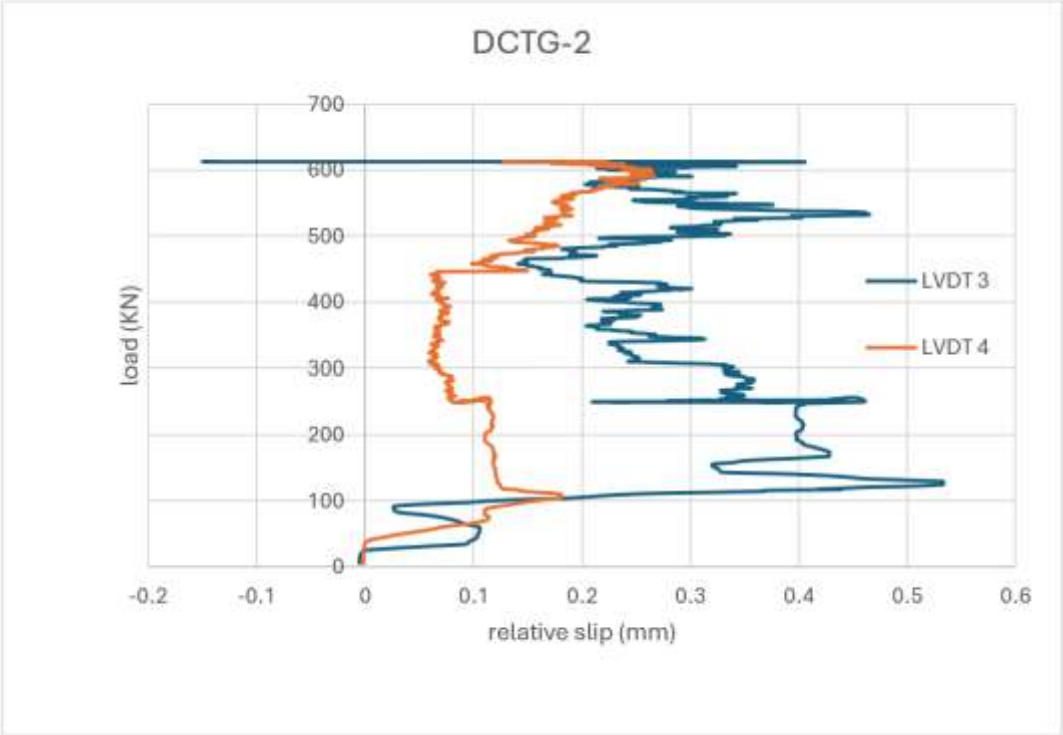

Figure 6.49: Load – slip curve for the DCTG-2

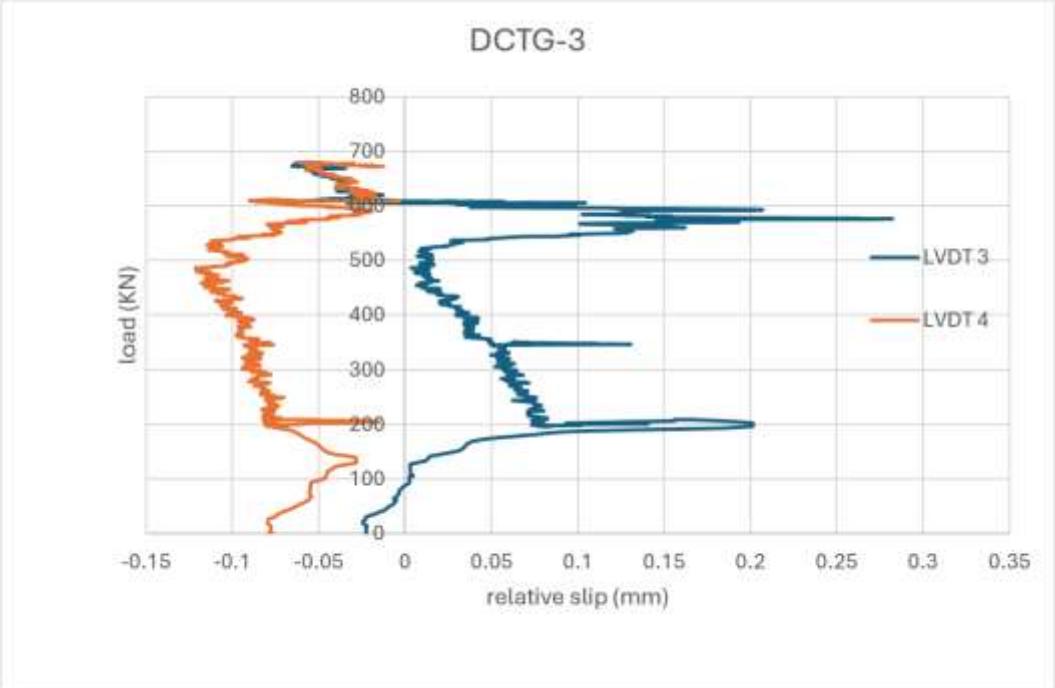

Figure 6.50: Load – slip curve for the DCTG-3

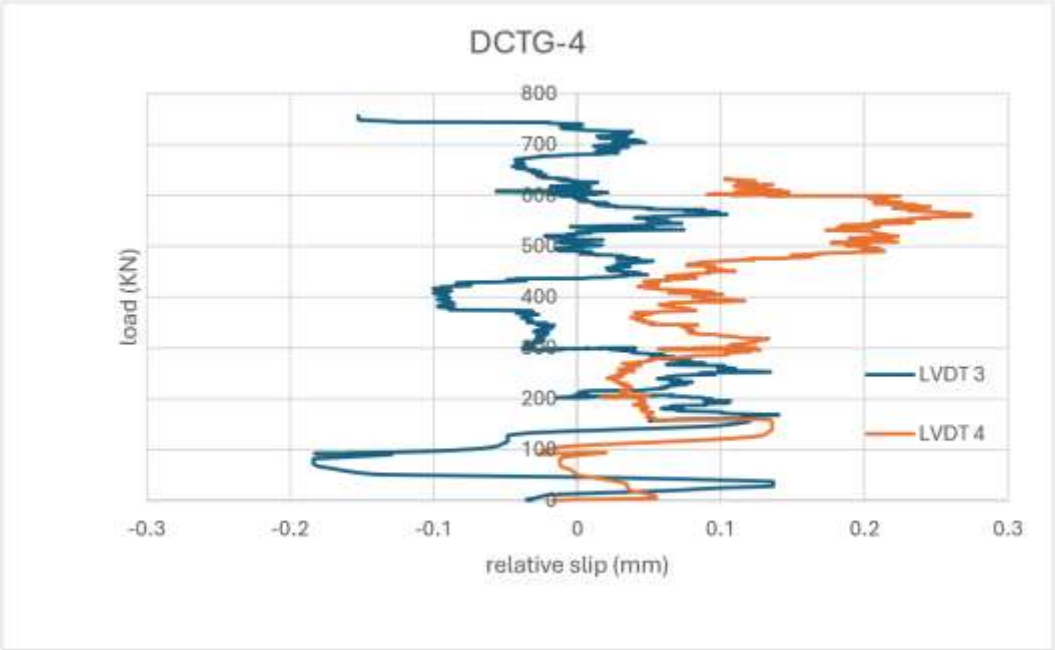

Figure 6.51: Load – Slip Curve for the DCTG-4

6.2 CAE Abaqus Program Results and Validation

6.2.1 Introduction

The results of this section will express the behavior of all eight specimens of the single composite girder (SCTG) and double composite girder (DCTG) after simulating with modeling program under static load, these data will be comparison with the experiment test results to made validation study after getting all specimens modeling exactly as the actual experiment test with the same check condition to verification the analysis method.

6.2.2 Verification of the finite element's models

The comparison process will be between the two groups, the main focus will be on Precipitation check results for the these specimens that simulate the actual response of entire length of the composite truss girder and the effect of the concentrated load on the deformation behavior such as the deflection ratio due to load increasing, the capacity of the single and double composite girder, stress- stain deformation curve for and find the elastic and plastic girder strength, the concrete cracks pattern and the modes of failure along the specimens well be investigated.

6.2.3 First category specimens' program analysis

6.2.3.1 Modes of failure

The results of the simulating model show the failure which occurred to every sample, as illustrated in Figure 6.52 and Figures 6.53, which is compared to the experimental test results, The performance of these two tested was give the same girder strength and exact failure shape situation as its explained in chapter five, moreover, the numerical analysis gives more accurate details due to optimal test and materials conditions, also it's give us the samples failure situation even behand the experiment actual load test.

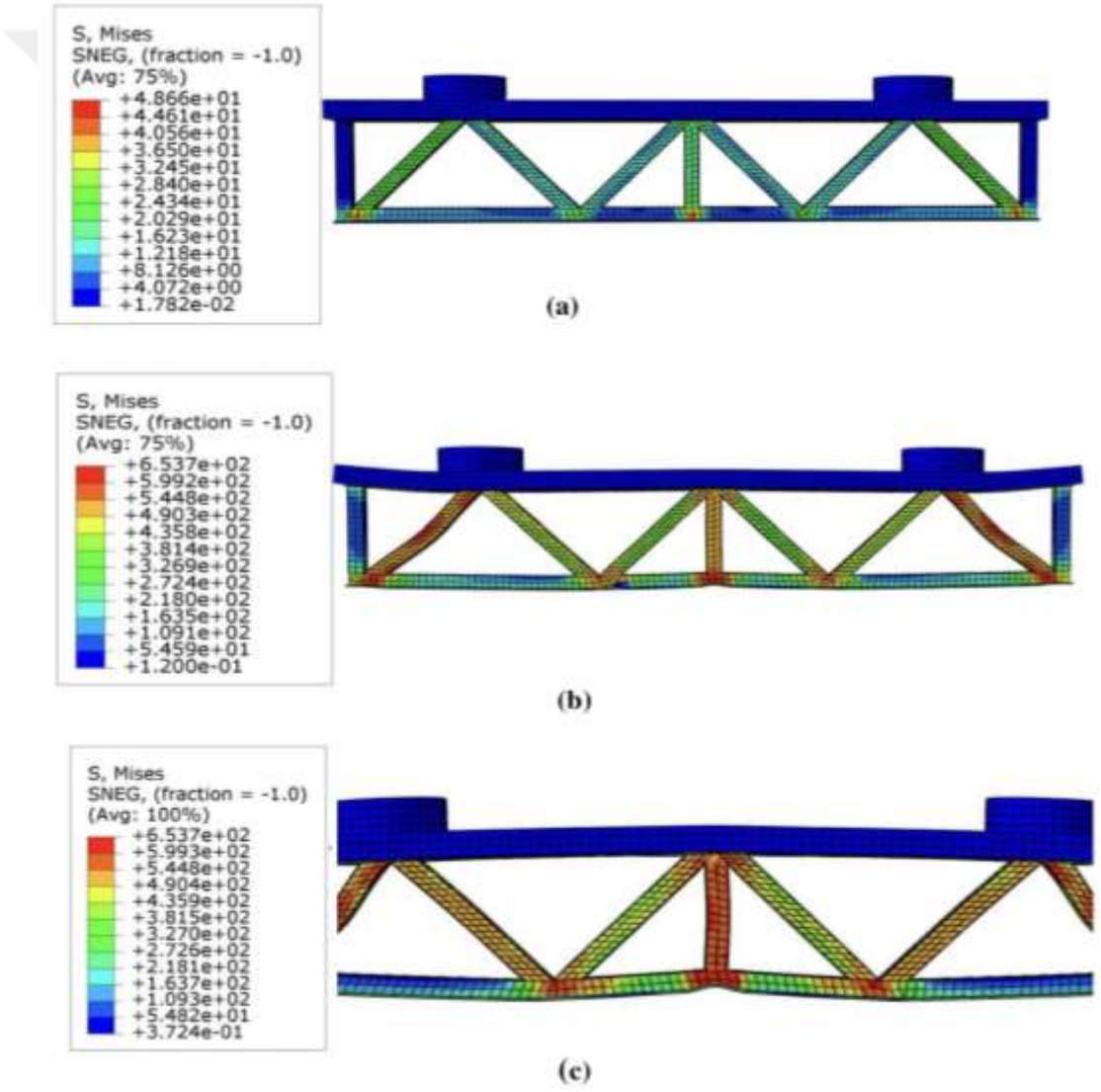

Figure 6.52: Abaqus simulating Failure mode for the SCTG specimens. (a) tensile and compression stress distribution initial loading stage, (b) tensile and compression stress distribution half loading stage, (c) damage mode at ultimate load

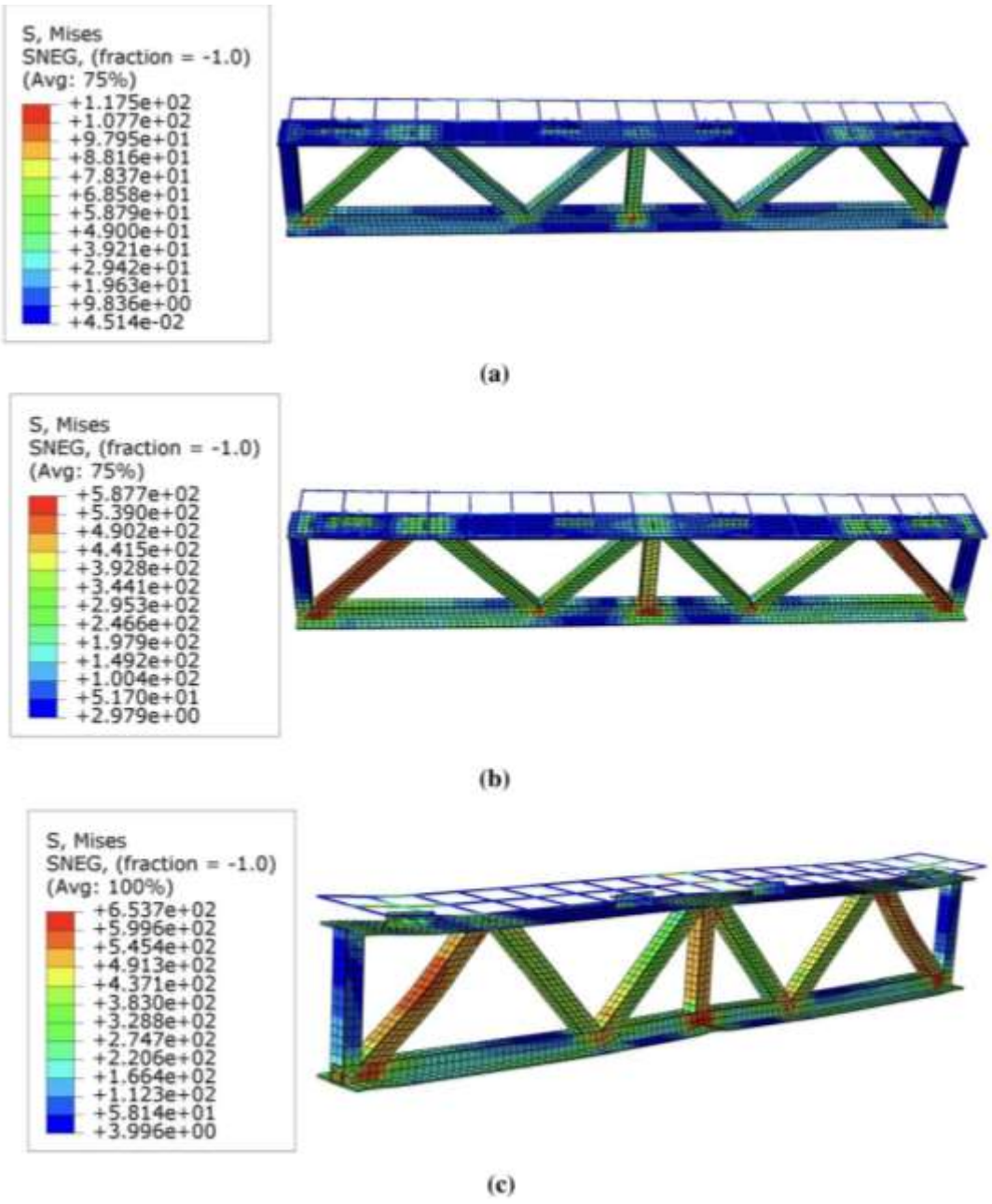

Figure 6.53: Abaqus simulating steel yielding for the SCTG specimens. (a) steel yielding at initial loading stage, (b) steel yielding at half loading stage, (c) steel yielding at ultimate loading stage

For the ultimate load capacity, the Table 6.12 illustrates the specimens load capacity details for the experiment and simulating of all first category specimens until the failure takes place, it can notice that the difference in results between the experiment and Abaqus modelling between 3.6% to 5.1% for the SCTG-1 and SCTG-2, this toleration percentage seems to be acceptable if we took into account the amount of variables in this model.

While the percentage was between 19.4% to 25.1% for SCTG-3 and SCTG-4 and the reason for this difference was due to these samples getting damaged early at the experiment test to some reason related to steel materials or welding.

Additionally, the single composite truss girder simulate model results shows that from the initial till the final stage load stage the stress get distribute equally in the begging in the truss frame until it's get increasing specially at the diagonal HSS member at the edge and the medium vertical HSS, till the failure has occurs in the under cord at the bottom of each of these members which is obvious clear with red color, while the green areas sever from tensile stress with lower ratio, the simulation results show that after the actual ultimate load that applied in the experiment test the diagonal HSS exposed to high buckling damage.

Table 6.12: Experimental and Simulate Results Load – Strength Capacity for (SCTG)

Specimen	Experiment result		Theoretical results		Ultimate strength Discrepancy Ratio %
	Plastic deformation (KN)	Ultimate strength (KN)	Plastic deformation (KN)	Ultimate strength (KN)	
SCTG-1	621	654	561	622	5.1%
SCTG-2	629	658	582	634	3.6%
SCTG-3	505	520	595	643	19.4%
SCTG-4	480	502	605	671	25.1%

6.2.3.2 Load - deflection relationships

In this part the deflection results of the model that built up with the software program will be illustrated, It's can note than there are relative convergence of results between laboratory experiments and software modeling, taking into account that the results of the program tend to be more accurate because the conditions for modeling took all the sample situation as best as possible such as the strength of concrete and the properties of steel, down to the optimal interaction bond between steel and concrete, which was considered a fully interaction.

position of deflection node was at the first quarter of the spacemen length, the collected results found the discrepancy ratio ranges between 2.3% to 6.5% for the single composite truss girder from the experiment and numerical analysis for all four specimens, Table 6.15.

It can be noticed the deflection get increasing after the point of fracture failure when the bond of concrete and steel get lost, in general, all the samples gave an approximate result, since the main factor of resistance to deflection was ratio of the moment of inertia for the composite girder, where at the beginning the curve show elastic deformation in perfobond leiste where deflection increasing slowly, Figure 6.54 to Figure 6.57.

Table 6.13: Experimental and Simulate Results Load – Deflection for the (SCTG)

Specimen	Experiment result		Theoretical results		Deflection discrepancy ratio %
	Ultimate Load (KN)	Deflection (mm)	Ultimate Load (KN)	Deflection (mm)	
SCTG-1	654	8.98	622	9.2	2.3%
SCTG-2	658	8.7	634	9.31	6.5%
SCTG-3	520	10.02	643	9.7	3.1%
SCTG-4	502	9.8	671	10.1	2.9%

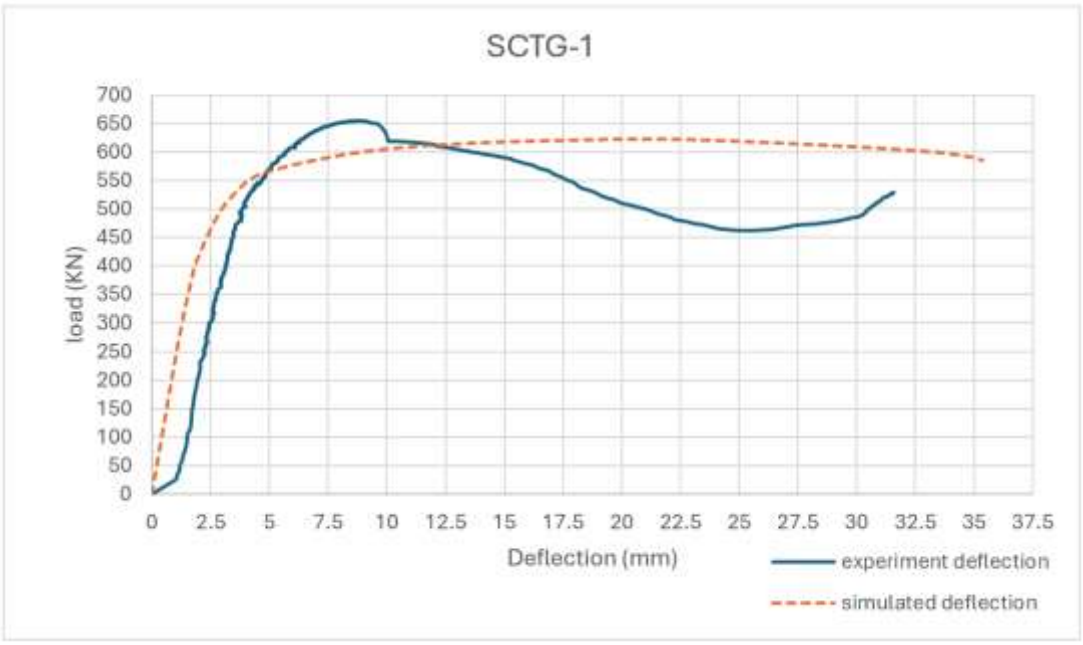

Figure 6.54: Load – Deflection of Simulate and Experiment Test for the SCTG-1

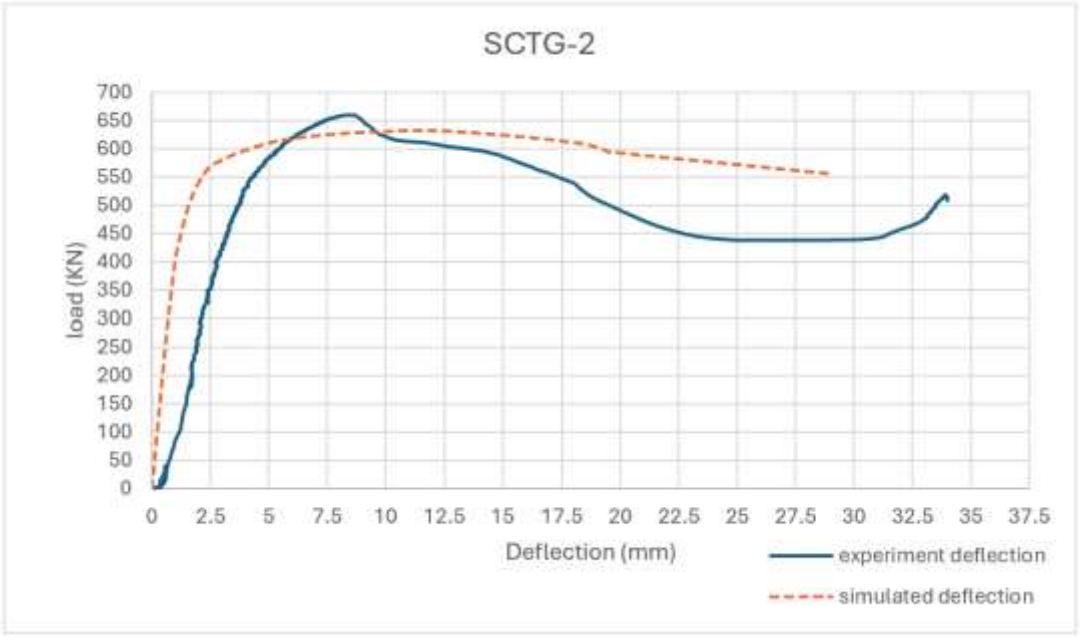

Figure 6.55: Load – Deflection of Simulate and Experiment test for the SCTG-2

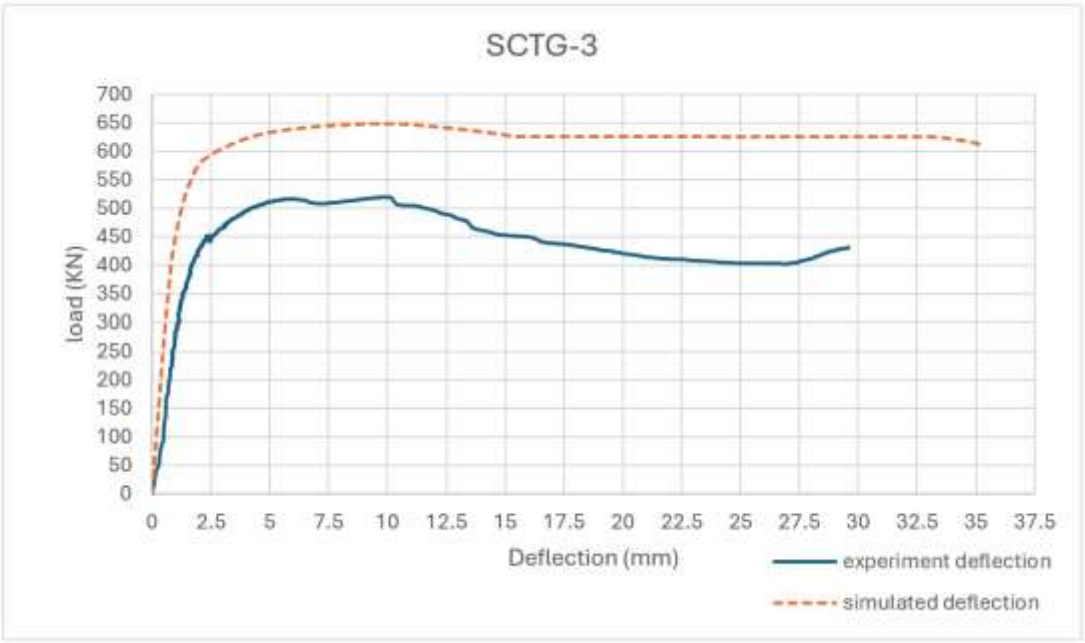

Figure 6.56: Load – Deflection of Simulate and Experiment Test for the SCTG-3

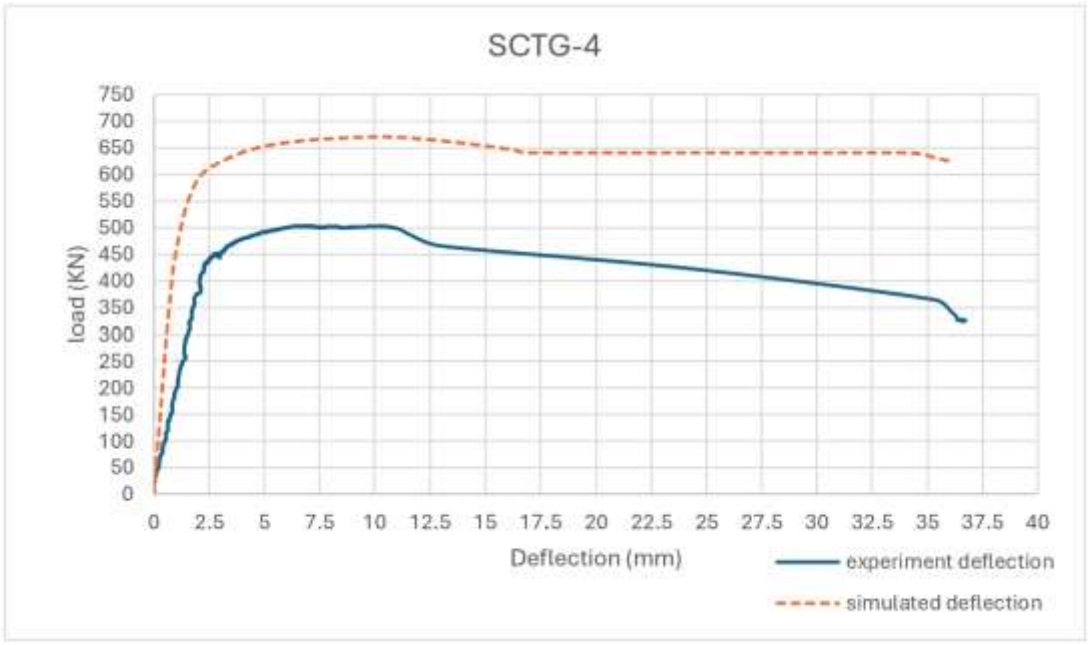

Figure 6.57: Load – Deflection Of Simulate and Experiment Test for the SCTG-4

6.2.3.3 Load - strain results

For the experiment work it takes six strain gauges at different positions to collect analysis data for each sample, at the top deck slab with strain samples (S5 and S6) and for bottom concrete flange or at the bottom steel flange (S1 and S2) for left and (S3 and S4) for right side especially focusing on the main predicting strain regions , Therefore, the focus was on the same places in the numerical analysis to extract its own data from Abaqus software program, the results gets compared with the results of laboratory examination, due to unevenly stress distributed at the surface the strain sensor gives different record, for that reason the average records well be produced to comparison study as shown in Figures 6.58 to Figures 6.62 illustrating the comparison and differences of the modeling and the experimental work.

Referring to SCTG-1 sample, the strain difference values between experiment tests than simulating test by Abaqus program reached approximately around 9% for top surface and 7.3% for the bottom surface and its acceptable percentage.

While for other samples it was 2.5% & 1% for SCTG-2, and 4% & 2% for SCTG-3, and 4% & 6.2% for SCTG-4 as for top and bottom concrete respectively, which is considered low discrepancy ratio according to very complex model including wide variables.

All the results of simulated models by the software program will be the most accurate results, as well as depending on the ability to simulate exact materials and all the parameters to give the same response of the experiment test.

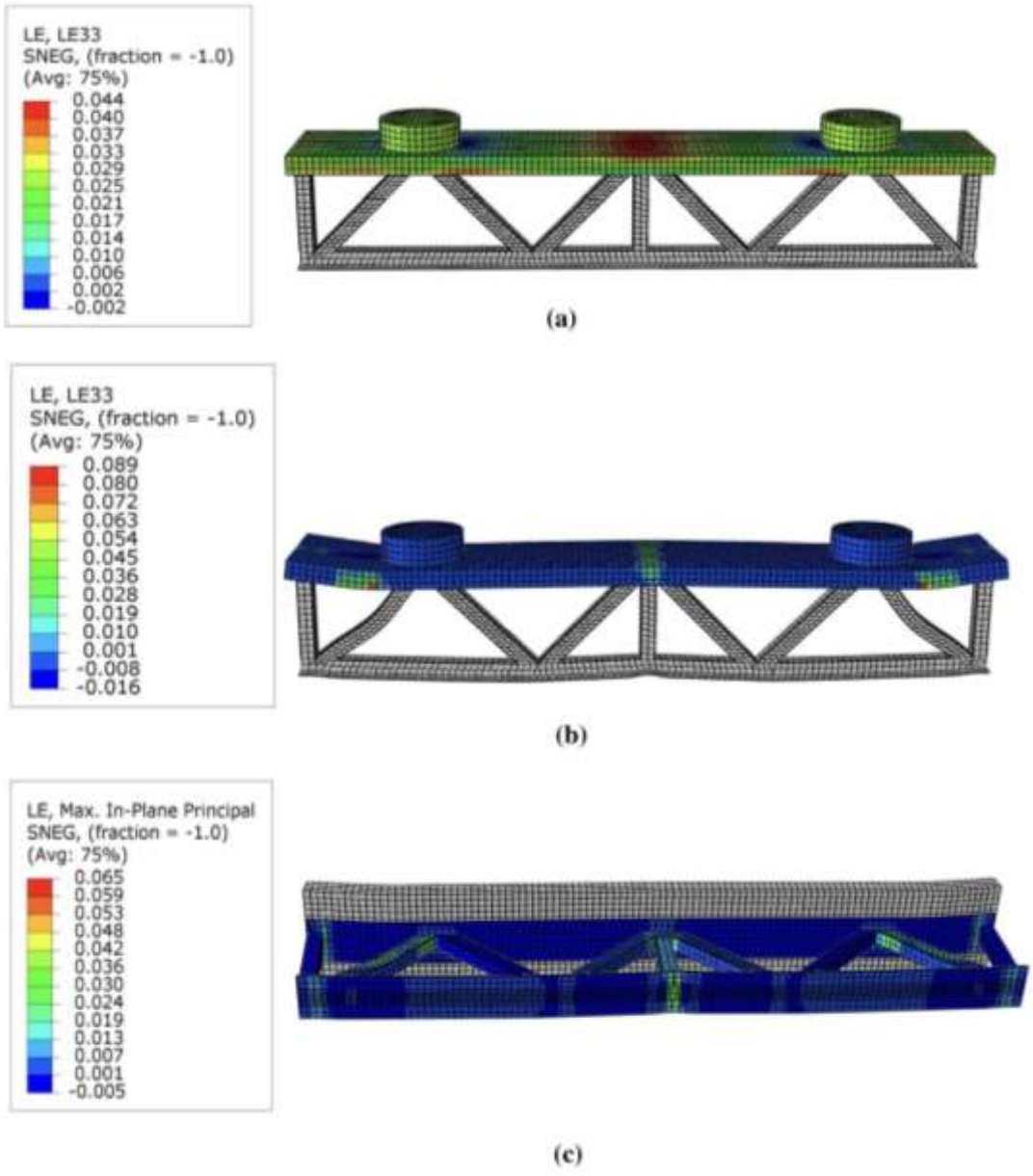

Figure 6.58: Stain Distribution on the Top And Bottom Surface of (SCTG) Specimens (A) Top Surface Strain Distribution At Half Load (B) Top Surface Strain Distribution At Full Load (C) Bottom Surface Strain Distribution At Full Load

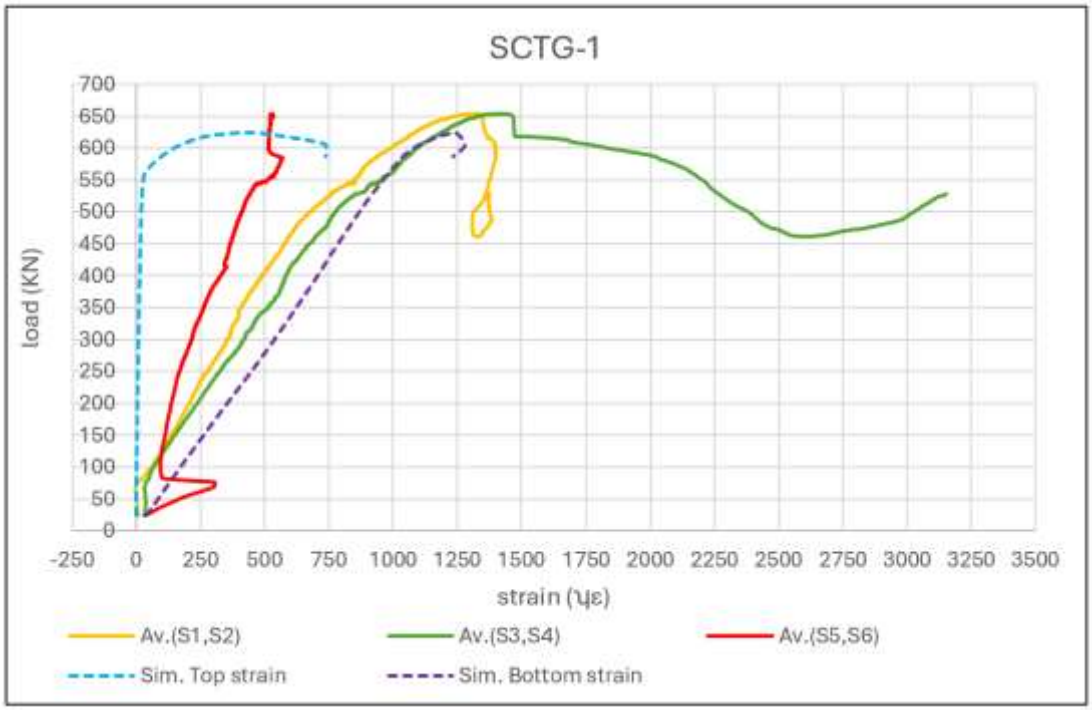

Figure 6.59: Stain Curve of Experiment and Numerical Simulation SCTG-1

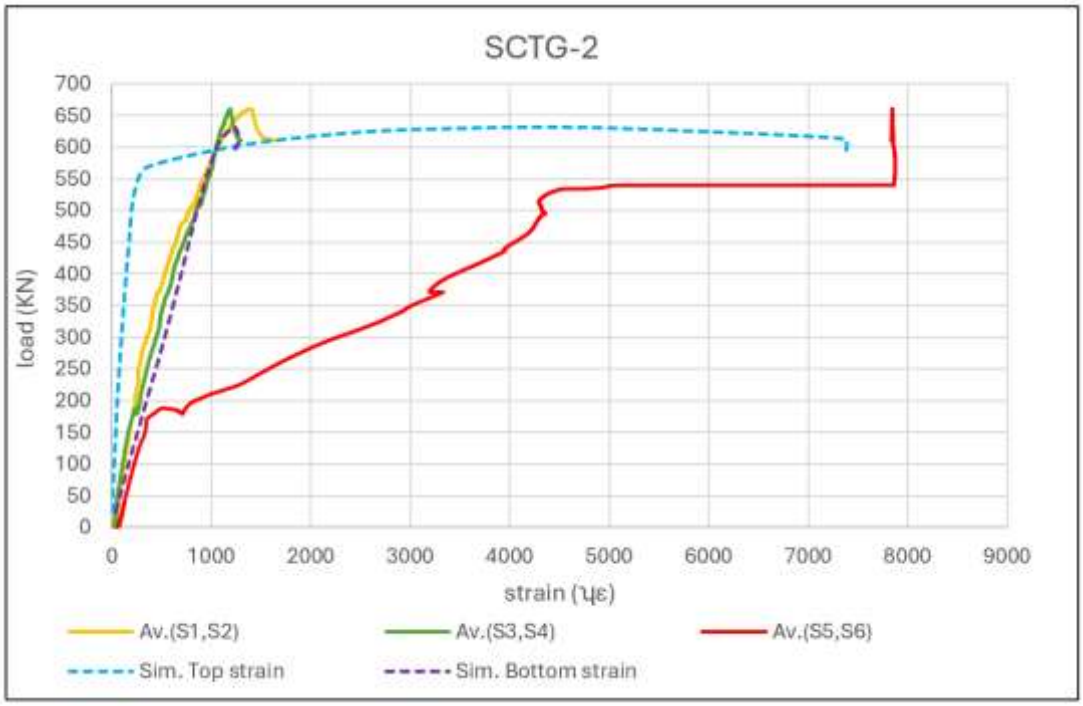

Figure 6.60: Stain Curve of Experiment and Numerical Simulation SCTG-2

Figure 6.61: Stain Curve Of Experiment and Numerical Simulation SCTG-3

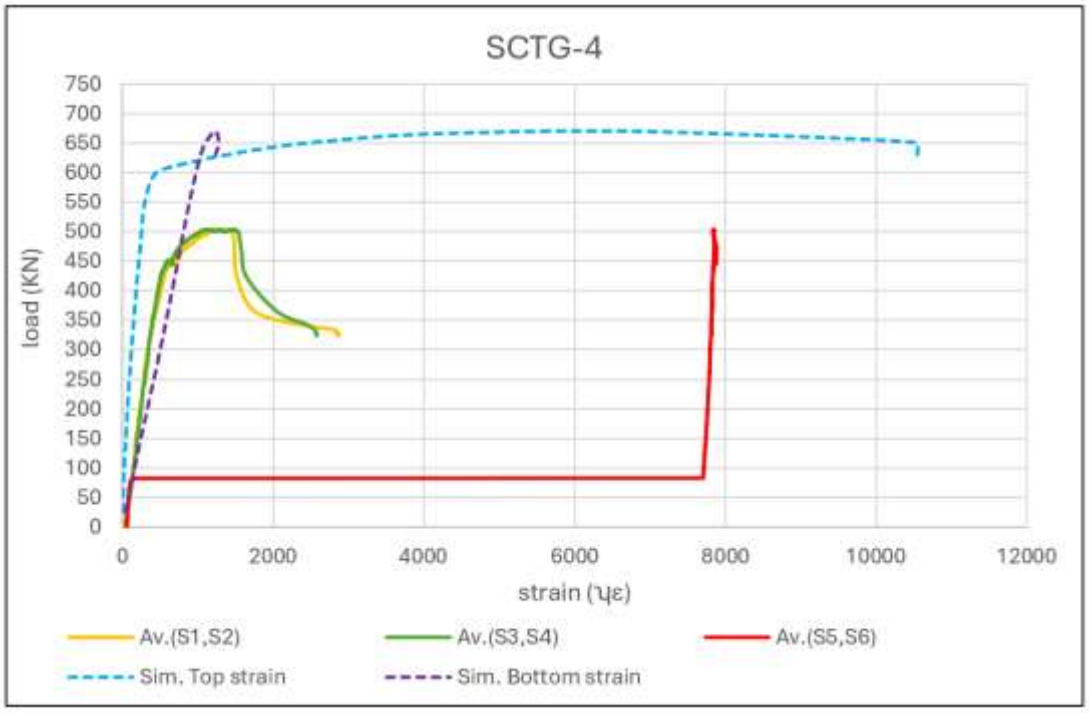

Figure 6.62: Stain Curve of Experiment and Numerical Simulation SCTG-4

6.2.3.4 Load - Slip results

To compare the results for this topic, a point is defined in the simulated model on the edge end of the concrete segment as (node-1) the same situation for the steel flange as (node-2), the movement between these two nodes can be explained as slip ratio, Figure 6.63, illustrated the slip location.

By comparing the simulated results with the actual slip in the experiment study it had a low discrepancy percentage around 12.3% to 27.5% which considered to be acceptable, Table 6.16 and Figure 6.63 to Figure 6.68.

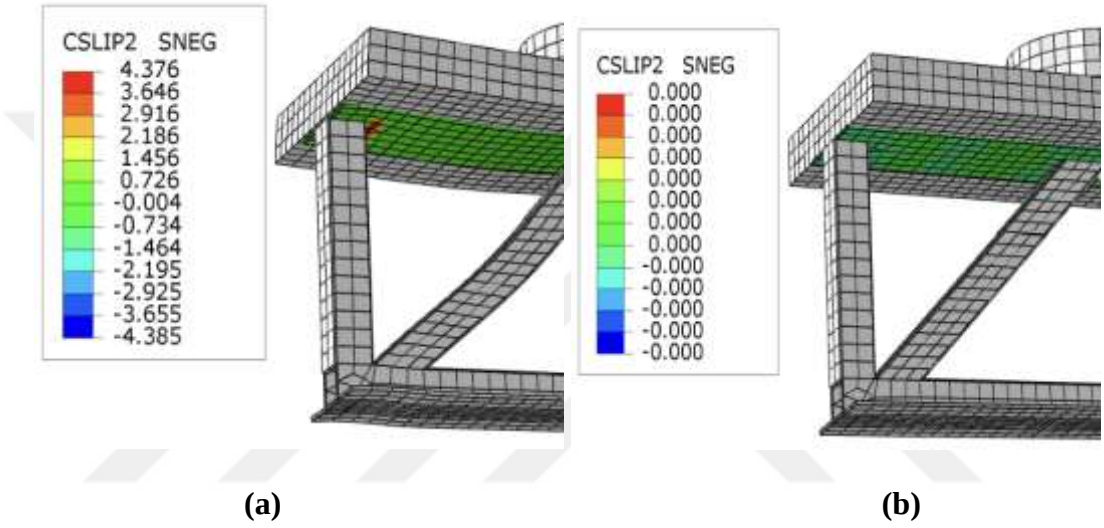

(a) **(b)**

Figure 6.63: Slip Location Between Top Concrete and Steel Flange for SCTG Samples. (a) Before Loading Status (b) Full Loading Status

Table 6.14: Load -Slip For the Specimens and Shear Connector Mechanical Properties (SCTG)

Sample	Experiment results			Simulated results		Discrepancy ratio %
	Con. Strength MPa	Ultimate Load Pu (KN)	Maximum Slip (mm)	Ultimate Load (kN)	Maximum Slip (mm)	
SCTG-1	35	654	-1.38	622	1.21	12.3%
SCTG-2	35	659	-0.652	634	0.54	17.1%
SCTG-3	35	520	0.347	643	0.42	17.3%
SCTG-4	35	503	0.29	671	0.21	27.5%

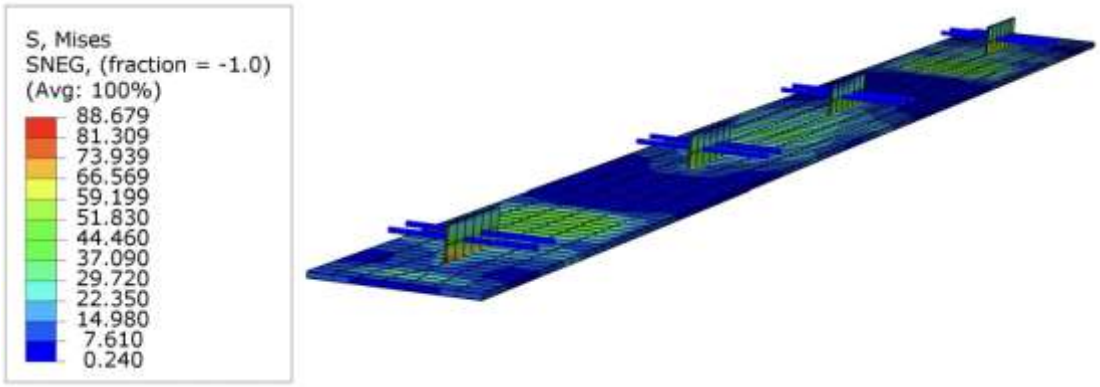

(a)

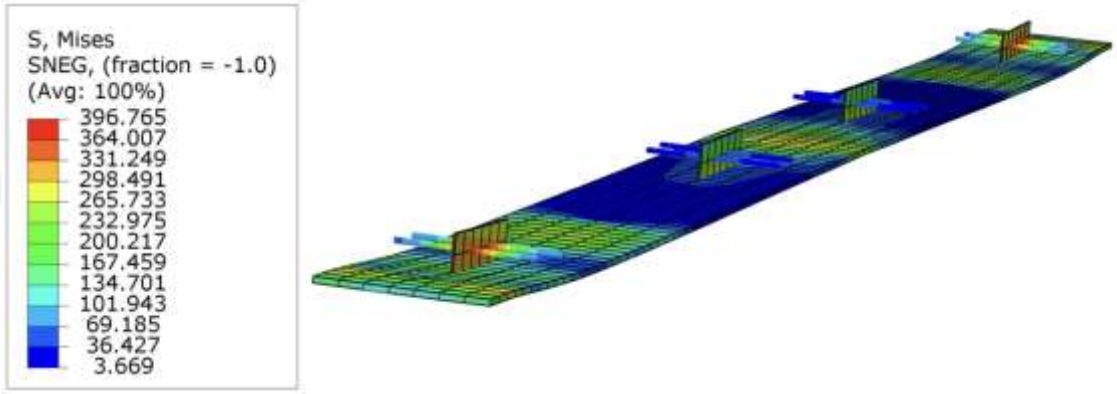

(b)

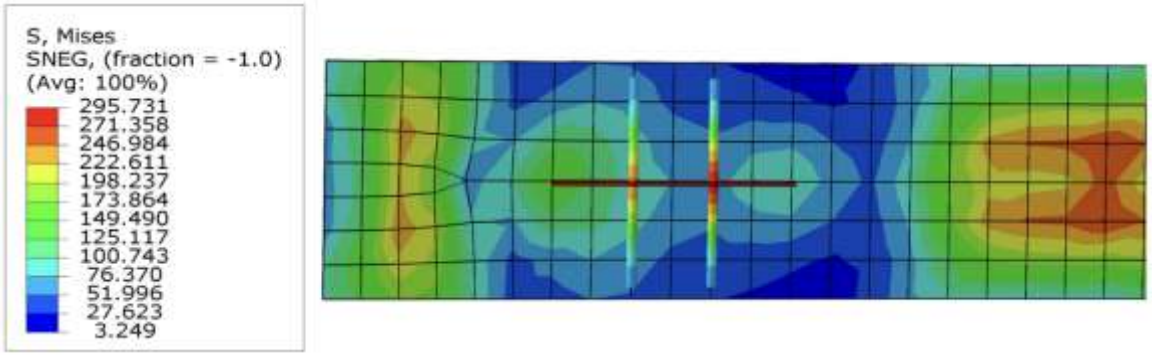

(c)

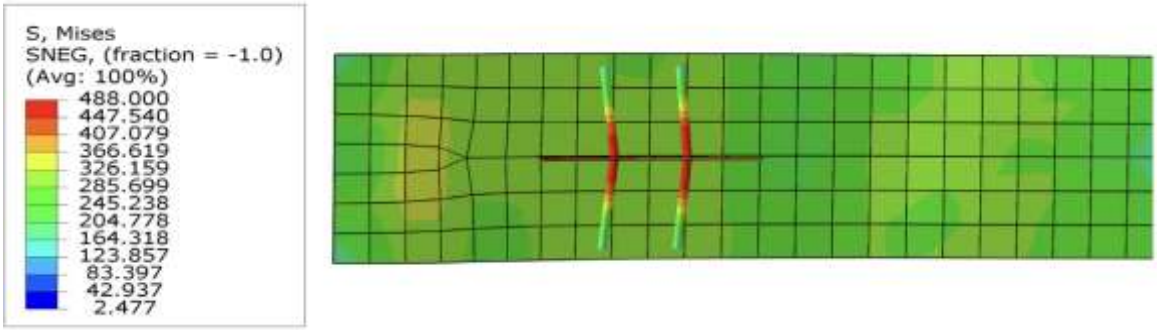

(d)

Figure 6.64: Perfobond Leiste Shear Connectors Deformation Due To Slip Action. (SCTG) (a) Perfobond Leiste Deformation At Half Load, (b) Perfobond Lesiste Defermation At Full Load, (c) Perfobond Leiste Acting At Half Load, (d) Perfobond Leiste Acting At Full Load

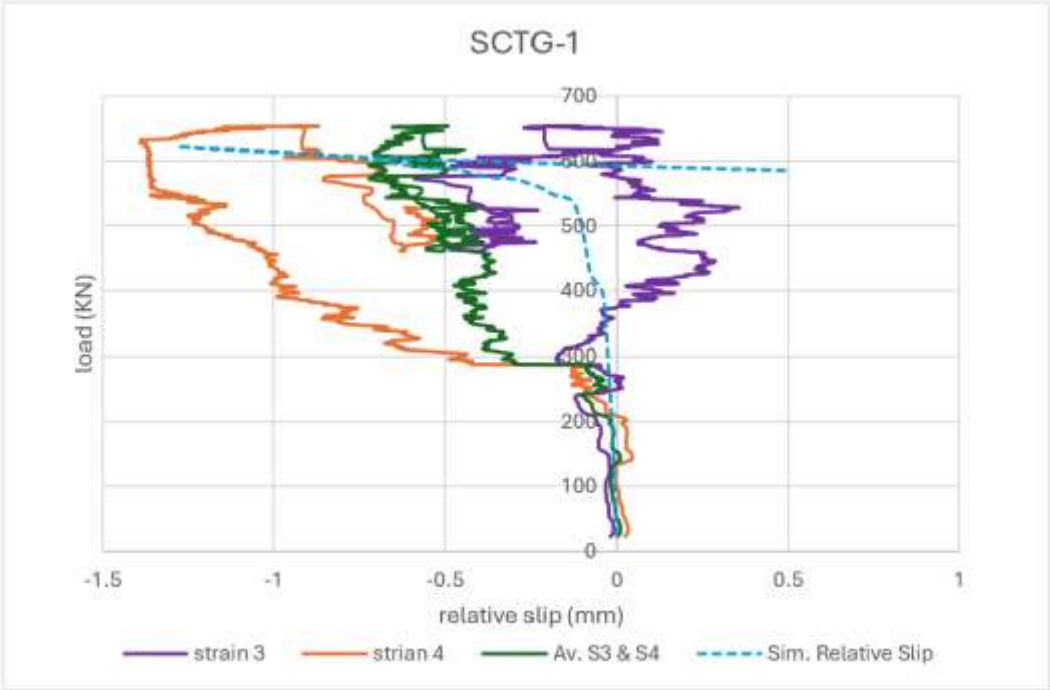

Figure 6.65: Load-Slip of the Experiment and Numerical Simulation SCTG-1

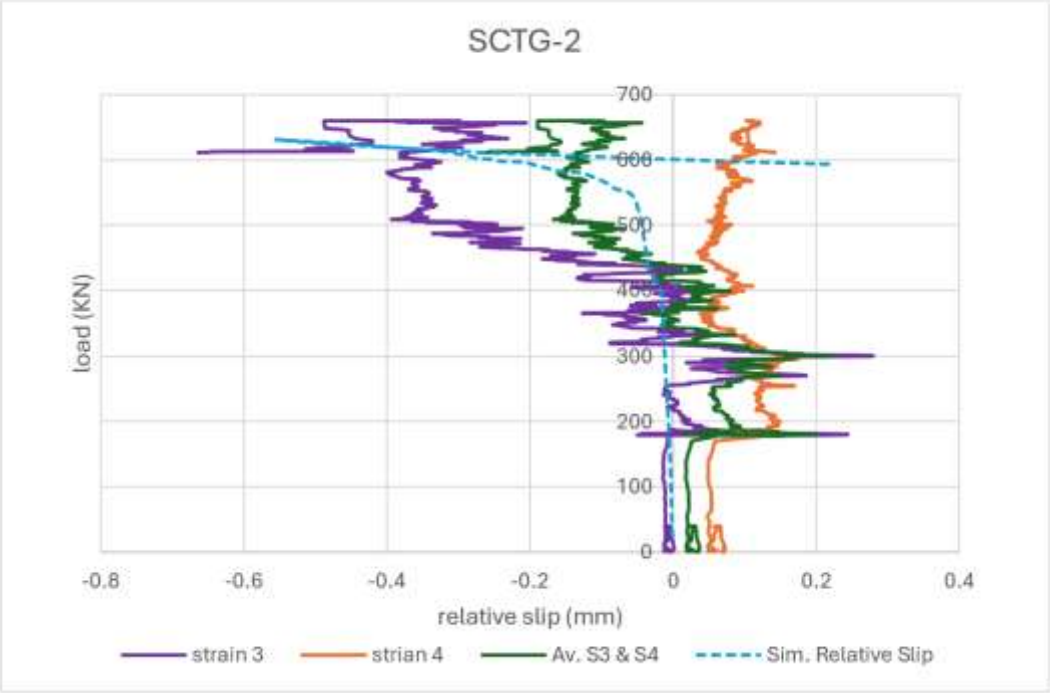

Figure 6.66: Load-Slip of the Experiment and Numerical Simulation SCTG-2

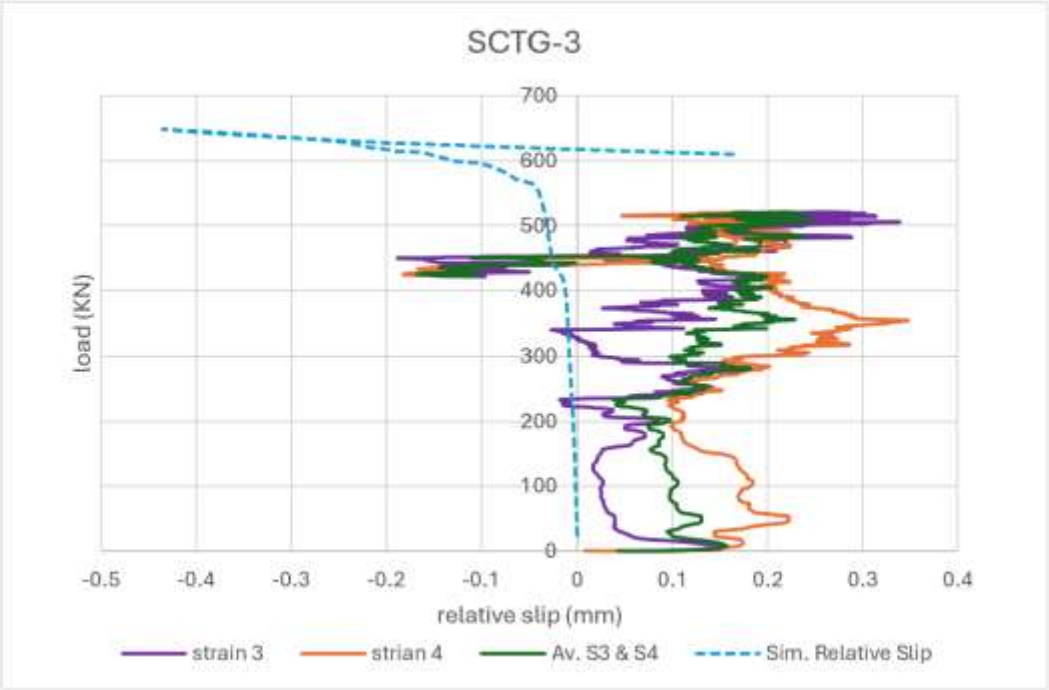

Figure 6.67: Load-Slip of the Experiment and Numerical Simulation SCTG-3

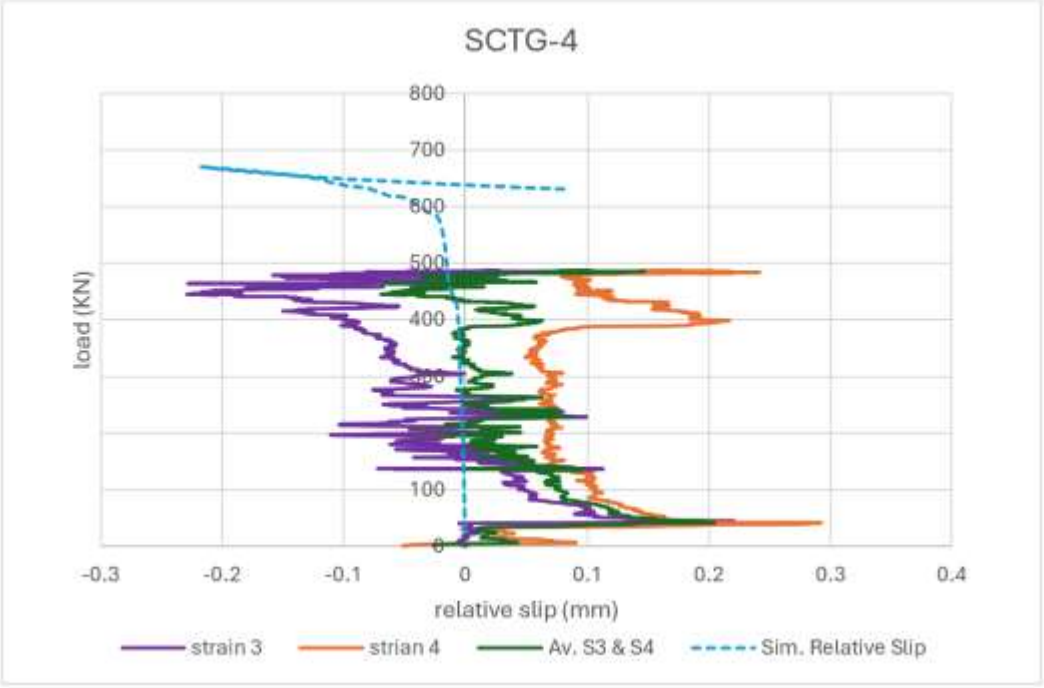

Figure 6.68: Load-Slip of the Experiment and Numerical Simulation SCTG-4

6.2.4 Seconds category specimens' program analysis

6.2.4.1 Modes of failure

For the ultimate load capacity, Table 6.17 illustrates the specimens load capacity details for the experiment and simulating for the category two specimens until the failure takes place, it can notice that the difference in results between the experiment and Abaqus modelling between 4.7% to 14.3%.

At the double composite truss girder simulate model the stress results show that from the initial till the final stage load stage the distribute equally in the begging in the truss HSS members frame until it gets increasing especially at the diagonal HSS member at the edge and the medium vertical HSS, the failure occurs in the lower cord at the bottom of each of these members.

The compression shear force failure occurs under the mid vertical HSS leading to uplift of the bottom steel flange from the bottom concrete referring also to the shear connector failure which reveals different strength capacity values from sample to another and becomes the most effect featured on the composite girder capacity, Figure 6.69 to Figure 6.70 illustrate the stages of the mode of failures.

Table 6.15: Experimental and Simulate Results Load – Strength Capacity for (DCTG)

Specimen	Experiment result		Theoretical results		Ultimate strength Discrepancy Ratio %
	Plastic deformation (KN)	Ultimate strength (KN)	Plastic deformation (KN)	Ultimate strength (KN)	
DCTG-1	691	725	711	761	4.7%
DCTG-2	639	665	690	776	14.3%
DCTG-3	701	716	731	785	8.7%
DCTG-4	747	754	755	801	5.8%

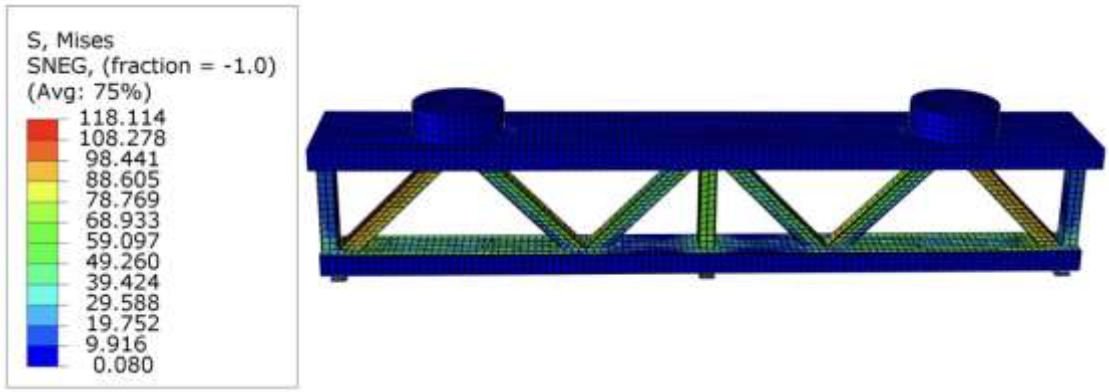

(a)

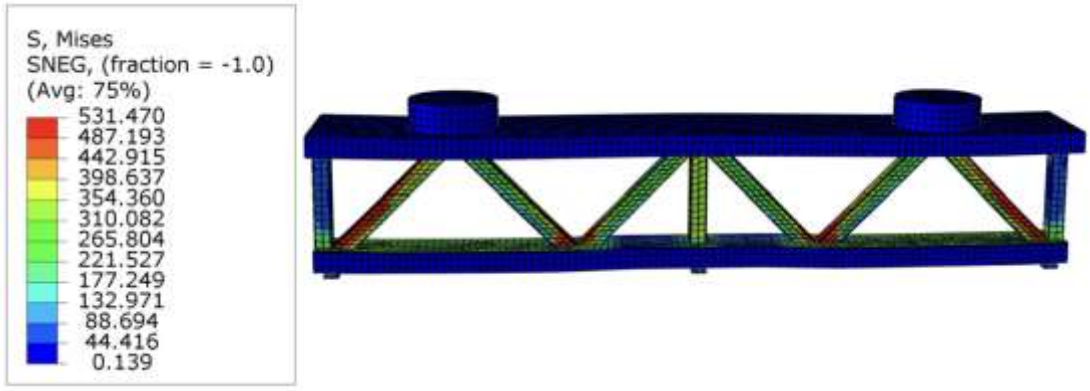

(b)

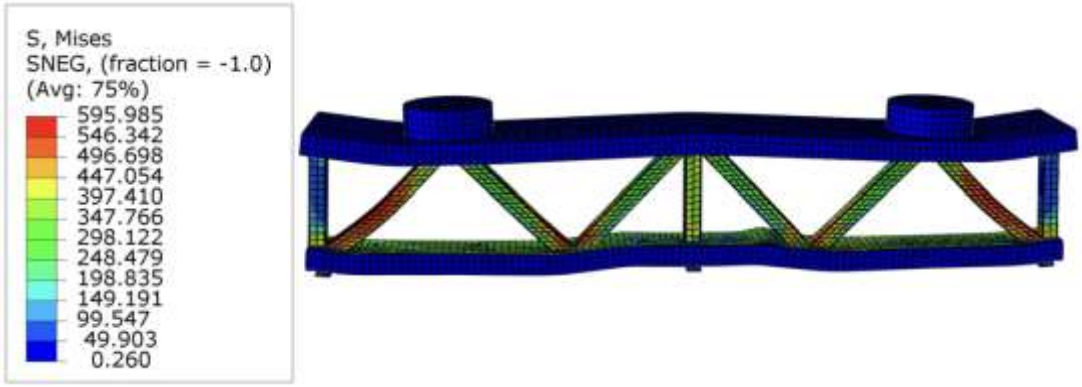

(c)

Figure 6.69: Abaqus Simulating Failure Mode of the DCTG Specimens (a) Tensile and Compression Stress Distribution Initial Loading Stage (b) Tensile and Compression Stress Distribution Half Loading stage (c) Damage Mode At Ultimate Load

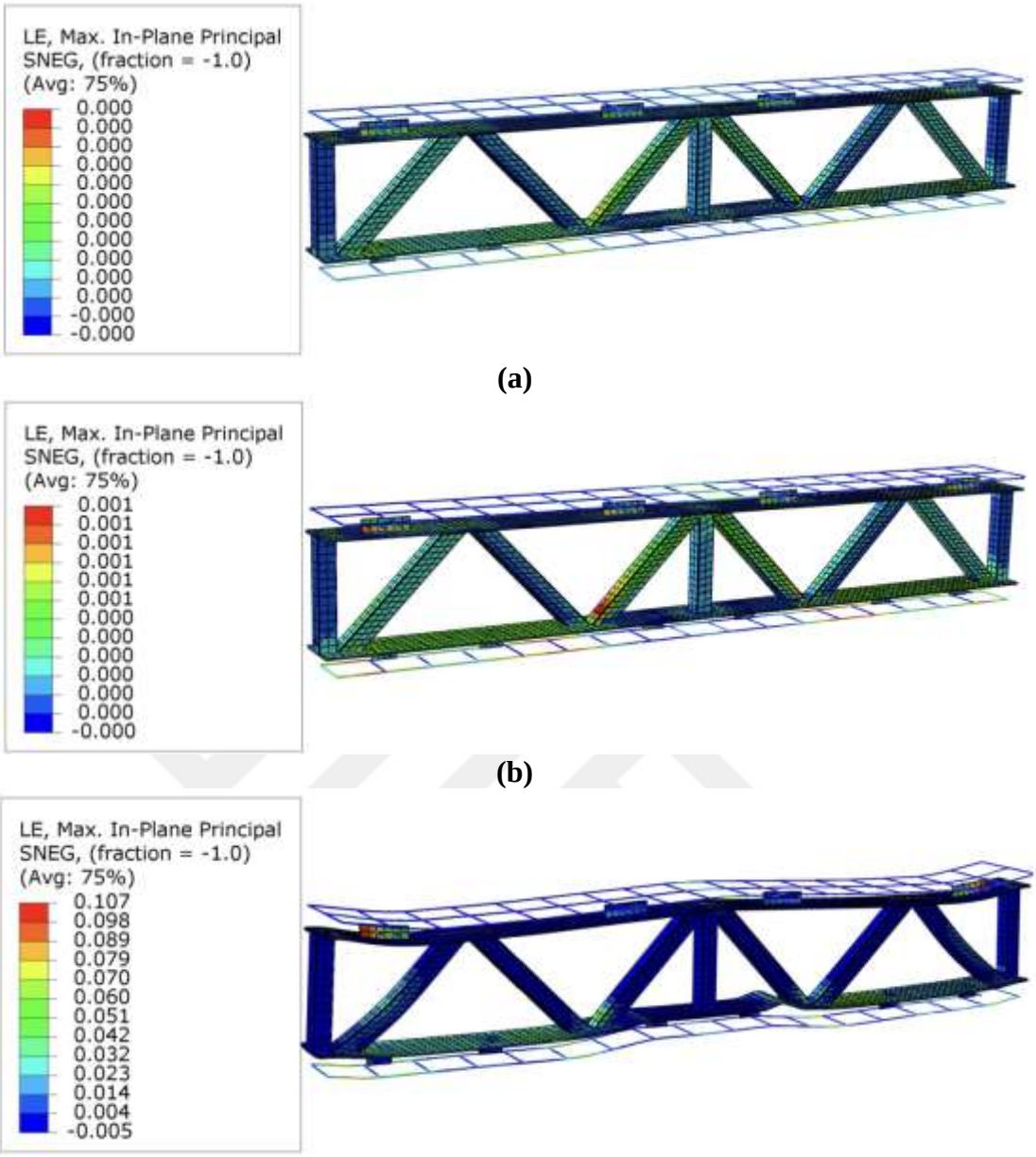

Figure 6.70: Abaqus Simulating Steel Yielding of DCTG Specimens (a) Steel Yielding at Initial Loading Stage (b) Steel Yielding at Half Loading Stage (c) Steel Yielding at Ultimate Loading Stage

6.2.4.2 Load - deflection relationship

This analysis data can be accessed with the assessment and considered acceptable with the deflection discrepancy ratio 2.6% to 10.1%, all the slight differences can be considered due to the nature of the existence of relative differences between theoretical calculations and experiment application.

For this category the results show that the deflection response for all (DCTG) samples was lower than (SCTG) samples, and this improvement in the properties and

behavior of samples is considered one of the good properties added to this category, especially if the load was higher at (DCTG) than (SCTG) by 18.3% and deflection percentage was less by average 31%.

As illustrated in Table 6.16, the deflection ratio decreased from (DCTG-1) to the (DCTG-4) with range 37.6% which is good enhancement features.

It's clear that these deflections values are mainly affected by the thickness of the concrete and steel flanges at this category unlike the case of the first category, where it behaves asymptotically with these properties, as shown in Figure 6.71 to Figure 6.74.

Table 6.16: Experimental and Simulate Results Load – Deflection for the (DCTG)

Specimen	Experiment result		Theoretical results		Deflection discrepancy ratio %
	Ultimate Load (KN)	Deflection (mm)	Ultimate Load (KN)	Deflection (mm)	
DCTG-1	725	7.80	761	8.21	4.9%
DCTG-2	665	7.3	776	7.11	2.6%
DCTG-3	716	6.14	785	5.88	4.2%
DCTG-4	754	4.6	801	5.12	10.1%

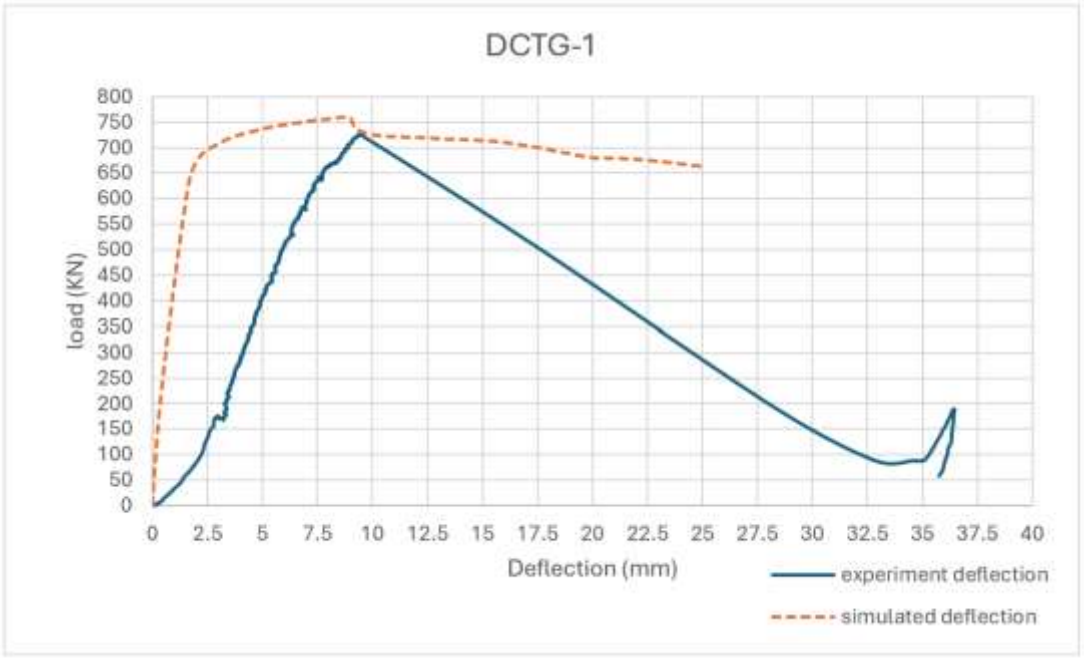

Figure 6.71: Load - Deflection of Simulate and Experiment Test for the DCTG-1

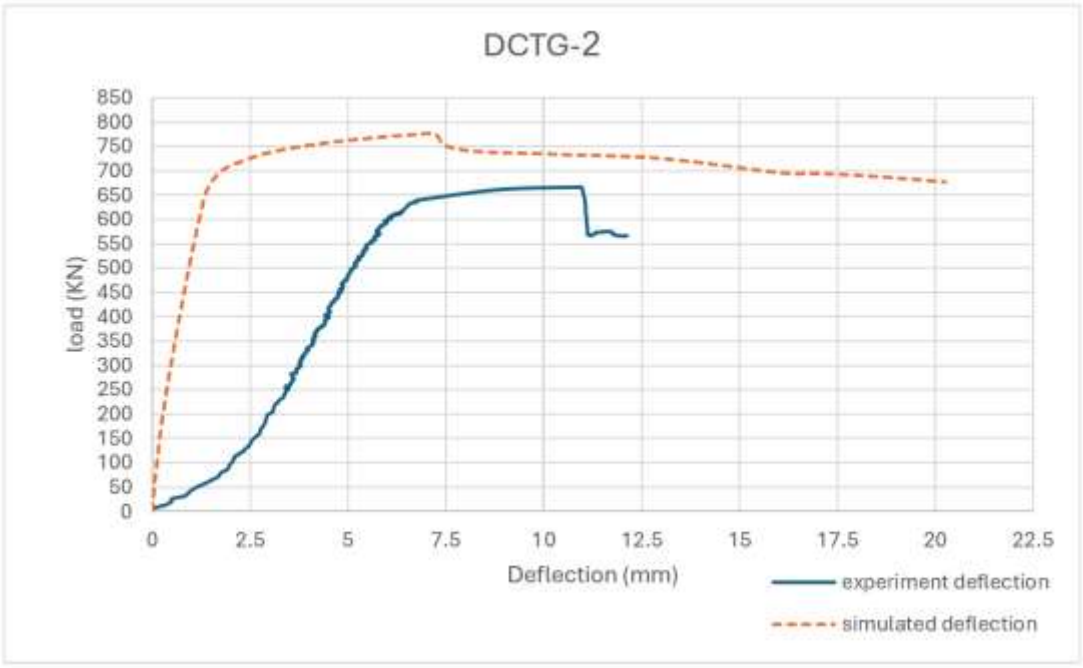

Figure 6.72: Load - Deflection of Simulate and Experiment Test for the DCTG-2

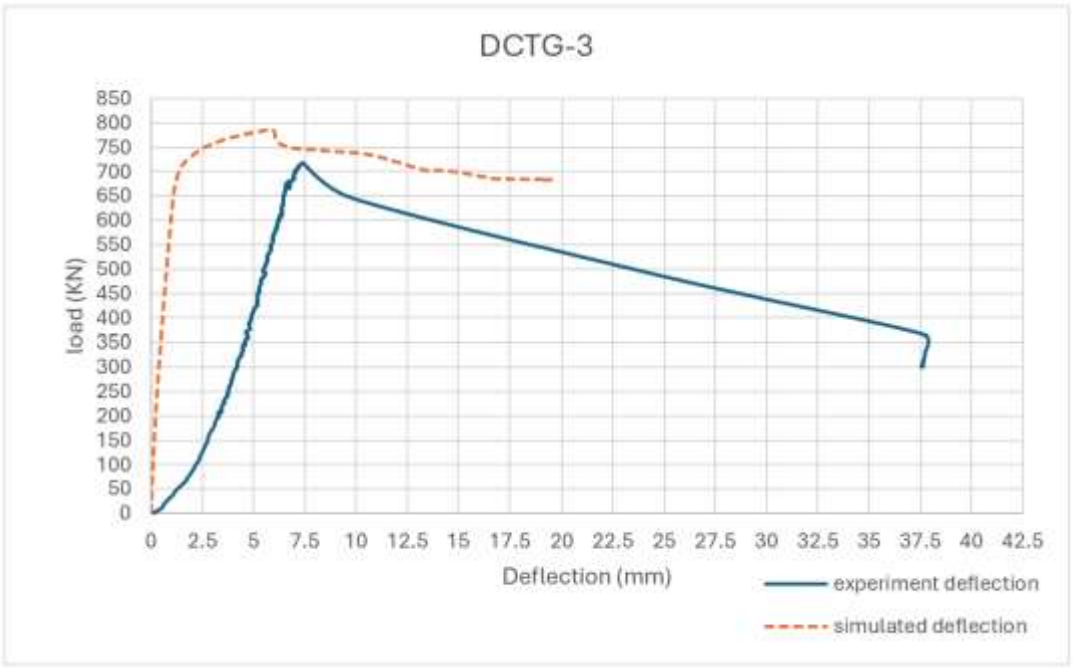

Figure 6.73: Load - Deflection of Simulate and Experiment Test for the DCTG-3

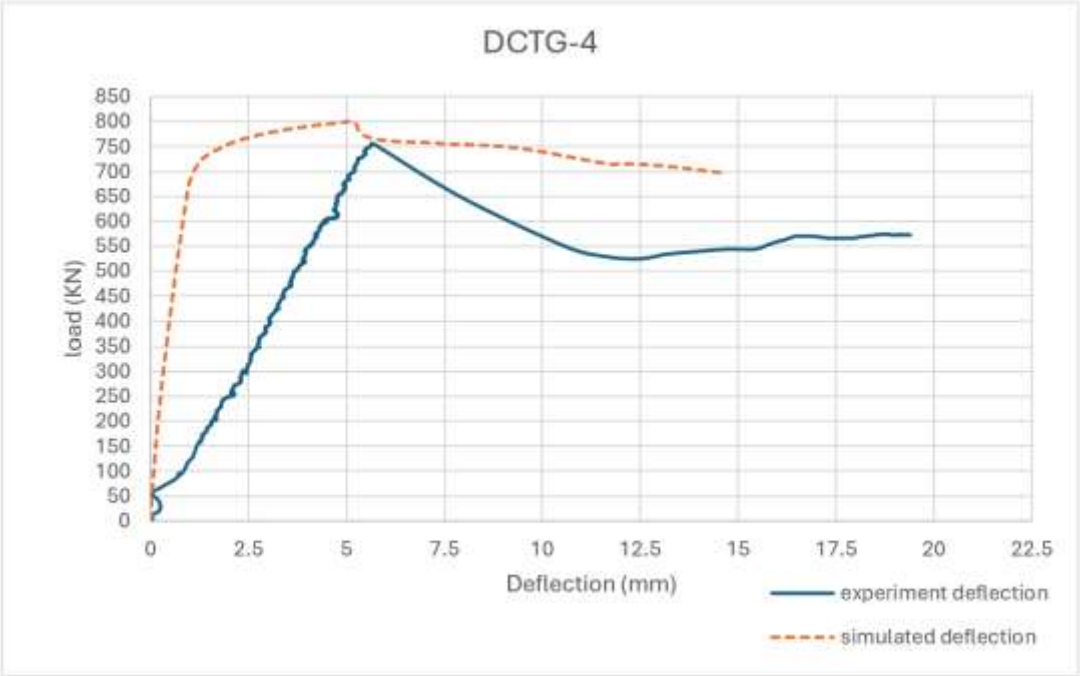

Figure 6.74: Load – deflection of Simulate and Experiment test for the DCTG-4

6.2.4.3 Load - strain results

As mentioned previously, this section includes comparing study of the experiment work with six strain gauges with samples (S5 and S6) at the top concrete and for bottom concrete (S1 and S2) for left side and (S3 and S4).

Therefore, as usual the results were taken for the same of the strain positions in practical experiment, to extract its own data from Abaqus software program and compare the results with the results of laboratory examination.

And due to the stress at the surface not evenly distributed when every strain sensor gives different record so for that reason the average record well be produced to comparison study, as well as for the load-strain response at the Figures 6.76 to Figures 6.79 illustrating the comparison and differences according to the increasing and decreasing strain value for each samples depending on the applied load of the modeling and the experimental work.

Referring to the strain values, the records at ultimate load was around 12%, 4%, 13.6% and 7% at the top concrete and 7.1%, 14%, 5% and 3% at the bottom concrete for (DCTG-1), (DCTG-2), (DCTG-3), and (DCTG-4) respectively, as validation of the experiment test with simulating by Abaqus and tend to be acceptable percentages.

For the strain distribution as shown at Figures 6.75, it can explain that the stresses increasing at the bottom concrete at the edge until the failure get occurs acting as the response of the experimental test, moreover, the strain ratio at the top concrete was decreasing and the plastic deformation at the hogging moment region was conducted at the 90% of the ultimate load, meanwhile, all sagging moment suffer from high stresses from the early load stage.

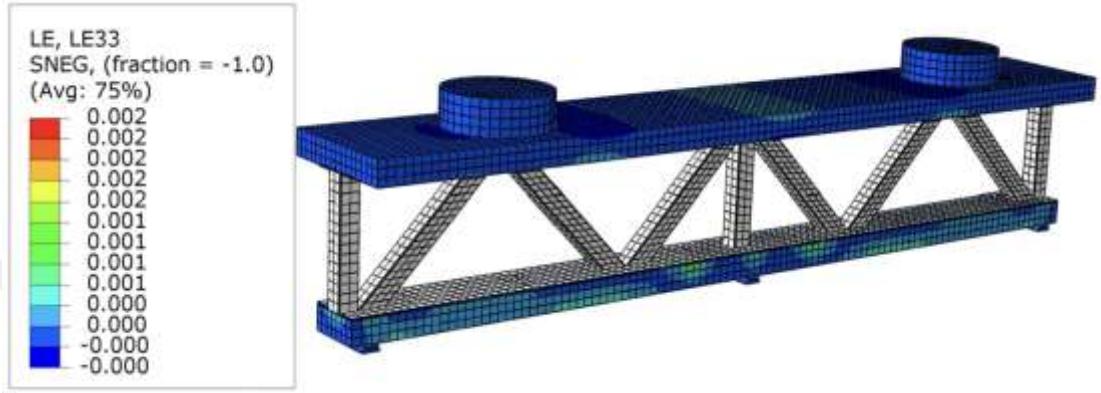

(a)

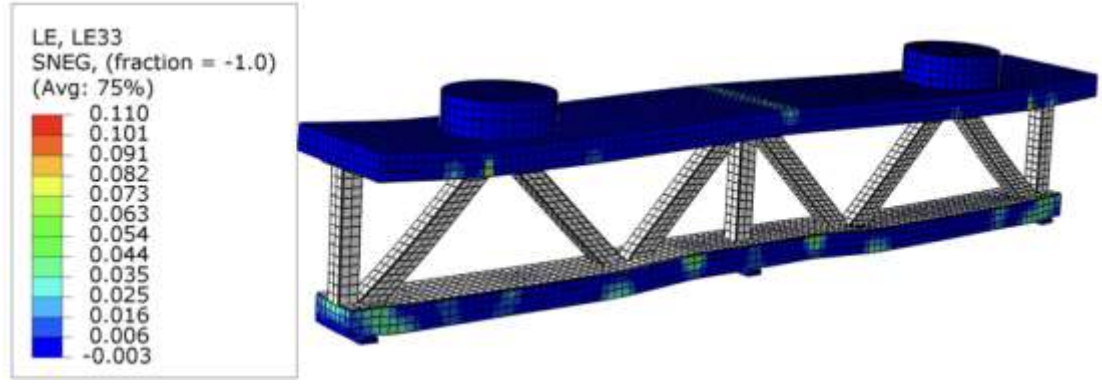

(b)

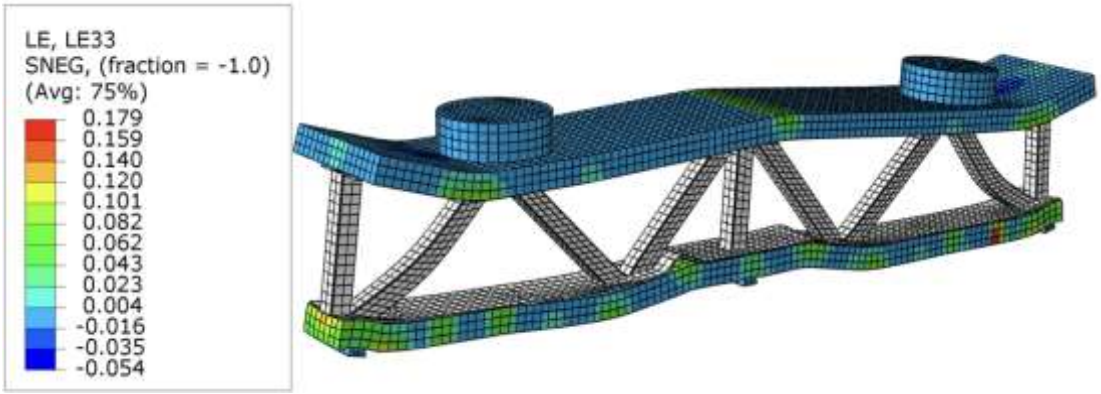

(c)

Figure 6.75: Stain Distribution on the Top and Bottom Surface of (DCTG) Specimens (a) Top And Bottom Surface Strain Distribution At Half Load (b) Top And Bottom Surface Strain Distribution At Full Load (c) Top And Bottom Surface Strain Distribution At Full Load

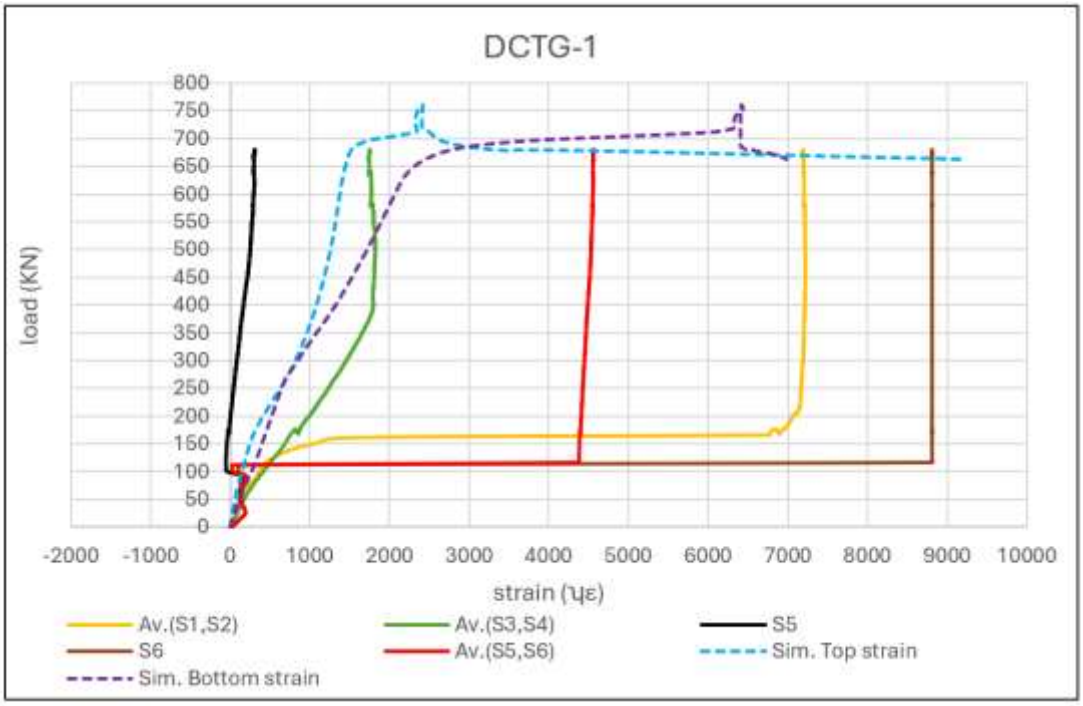

Figure 6.76: Stain Curve of Experiment and Numerical Simulation DCTG-1

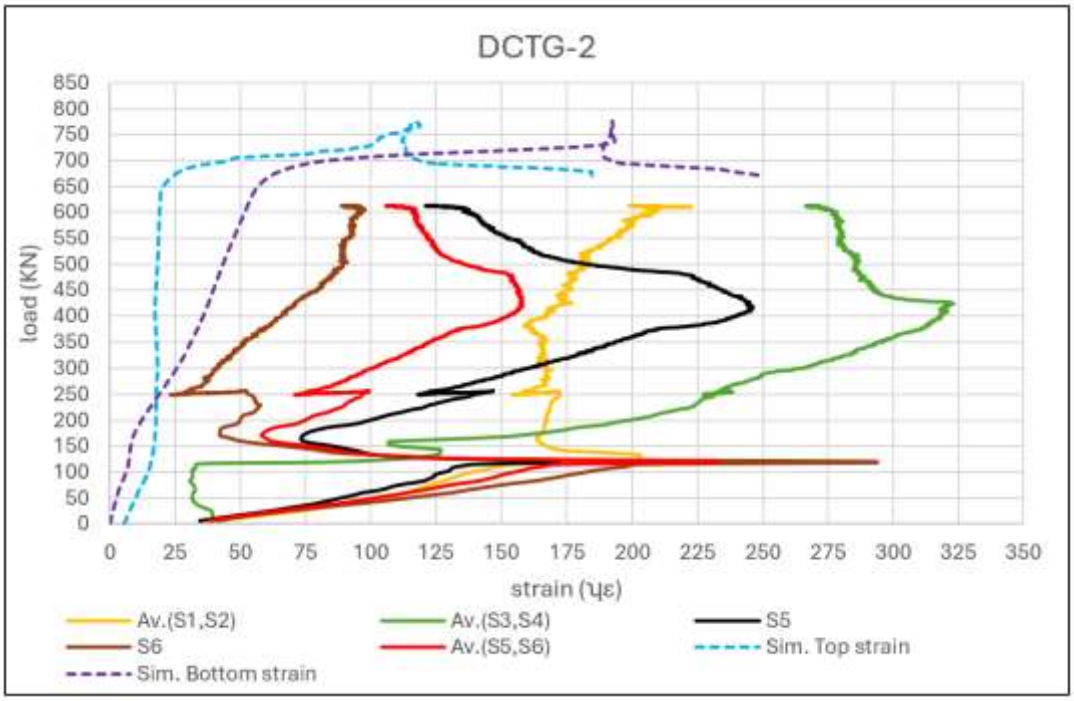

Figure 6.77: Stain Curve Of Experiment and Numerical Simulation DCTG-2

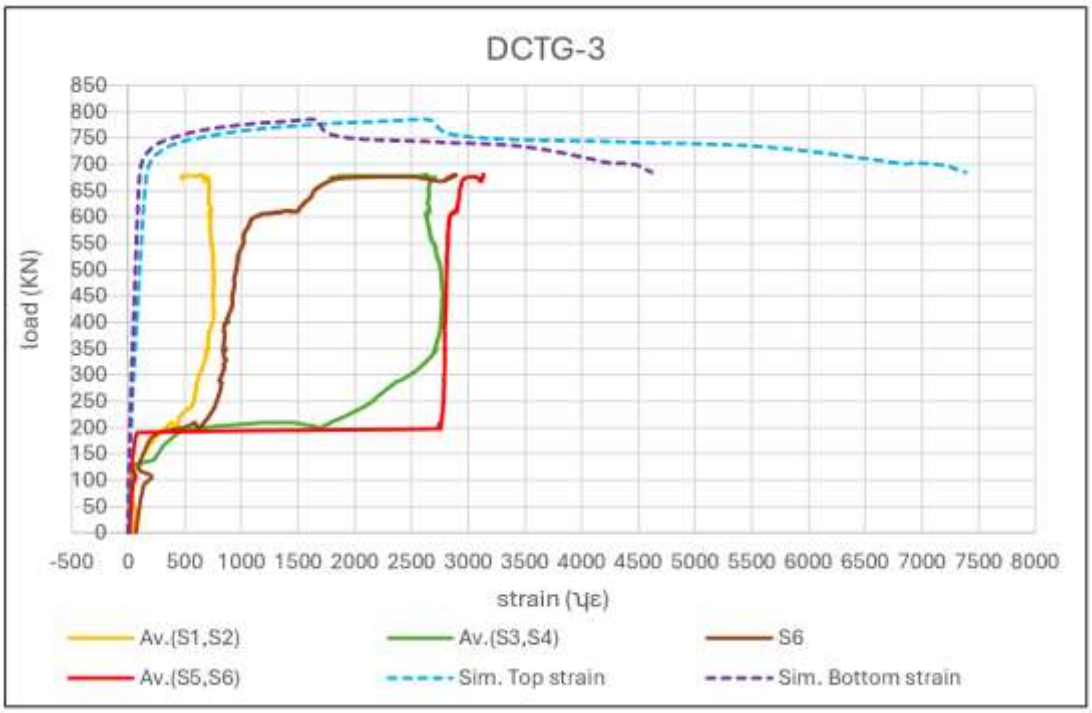

Figure 6.78: Stain Curve of Experiment and Numerical Simulation DCTG-3

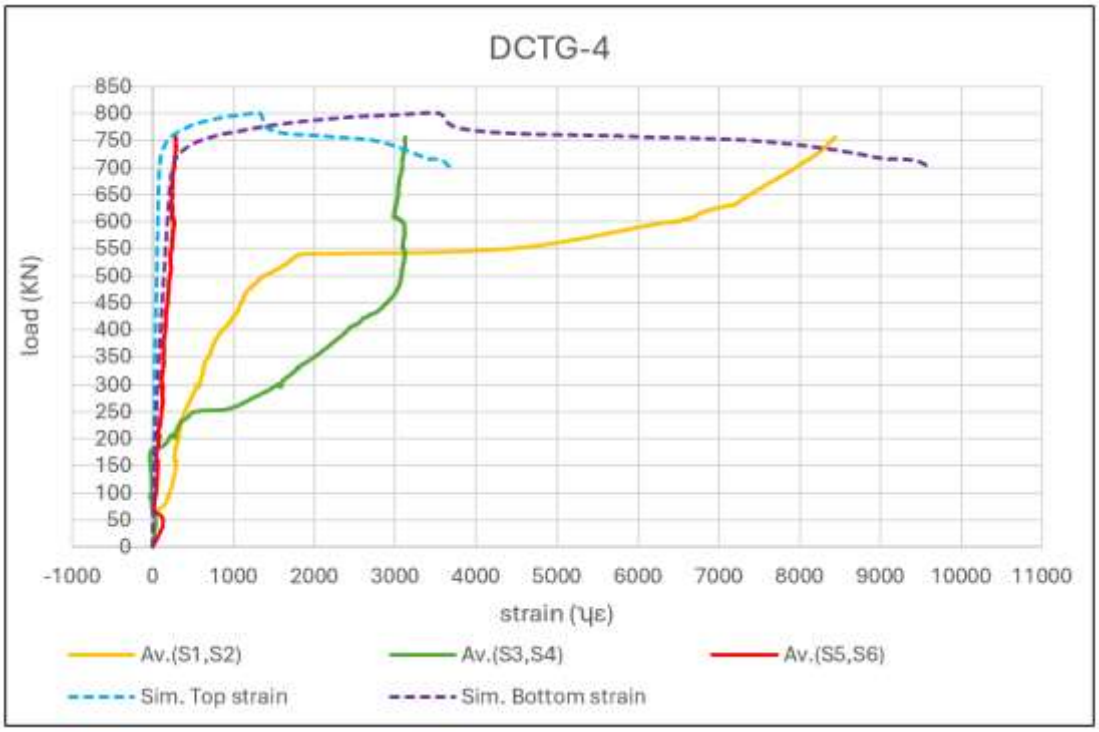

Figure 6.79: Stain Curve of Experiment and Numerical Simulation DCTG-4

6.2.4.4 Load - slip results

As mentioned previously, a point is defined in the simulated model on the edge end of the concrete segment as (node 1) the same situation for the steel flange

as (node 2), the movement between these two nodes can be explained as slip ratio, Figure 6.80, illustrated the slip location.

By comparing the simulated results with the actual slip in the experiment study it had low discrepancy percentage with range 6% to 22% which it could be accepted, Table 6.17 and Figure 6.81 to Figure 6.87 illustrated the results.

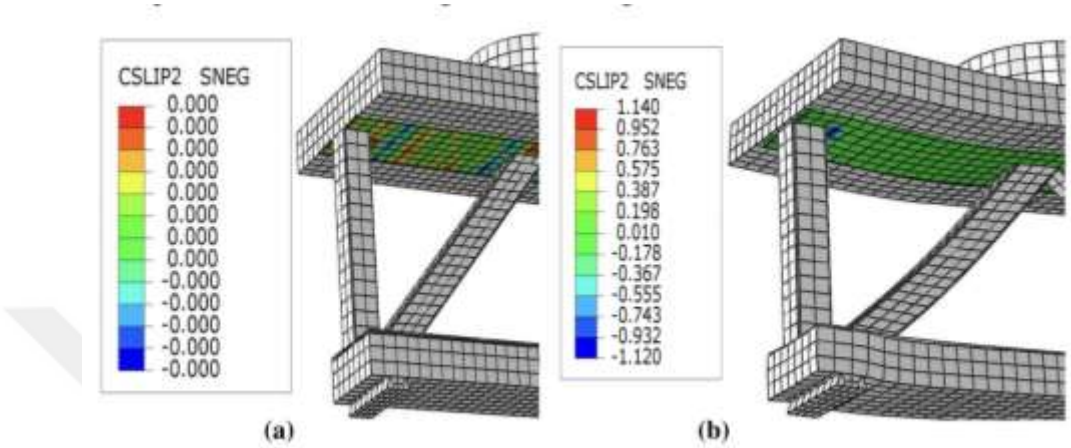

(a) **(b)**

Figure 6.80: Slip Location between Top Concrete and Steel Flange. (a) Before Loading Status, (b) Full Loading Status

Table 6.17: Load -Slip for the Specimens and Shear Connector Mechanical Properties (DCTG)

Sample	Experiment results			Simulated results		Discrepancy ratio %
	Con. Strength MPa	Ultimate Load Pu (KN)	Maximum Slip (mm)	Ultimate Load (kN)	Maximum Slip (mm)	
DCTG-1	35	725	-1.08	761	-1.15	6%
DCTG-2	35	665	0.53	776	-0.64	17%
DCTG-3	35	717	0.28	785	-0.32	12.5%
DCTG-4	35	755	0.27	801	-0.21	22%

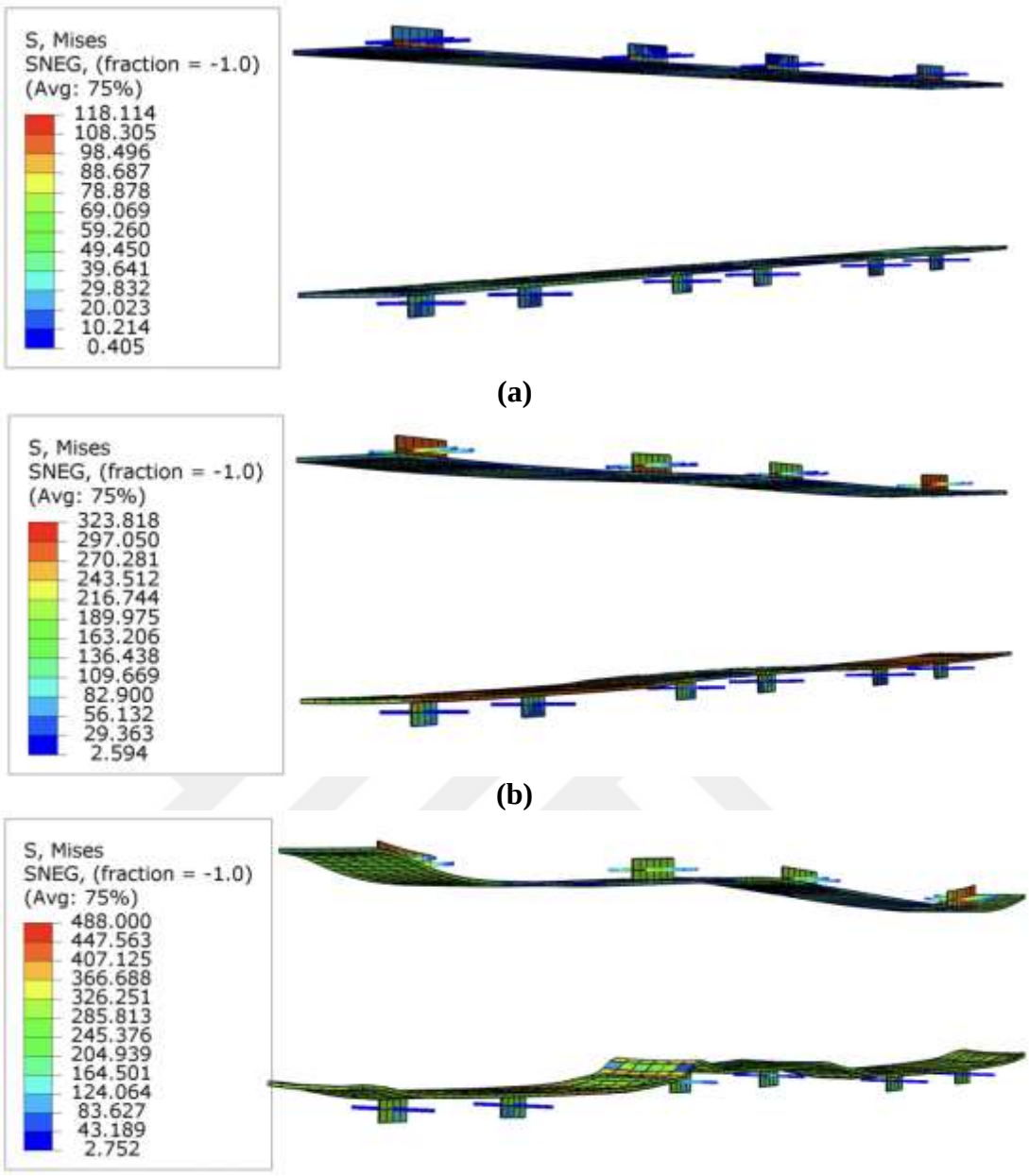

Figure 6.81: Perfobond Leiste Shear Connectors Response due to Slip Action (DCTG) (a) Perfobond Leiste Deformation At First Loading Stage (b) Perfobond Lesiste Defermation At Half Load (c) Perfobond Leiste Acting At Full Load

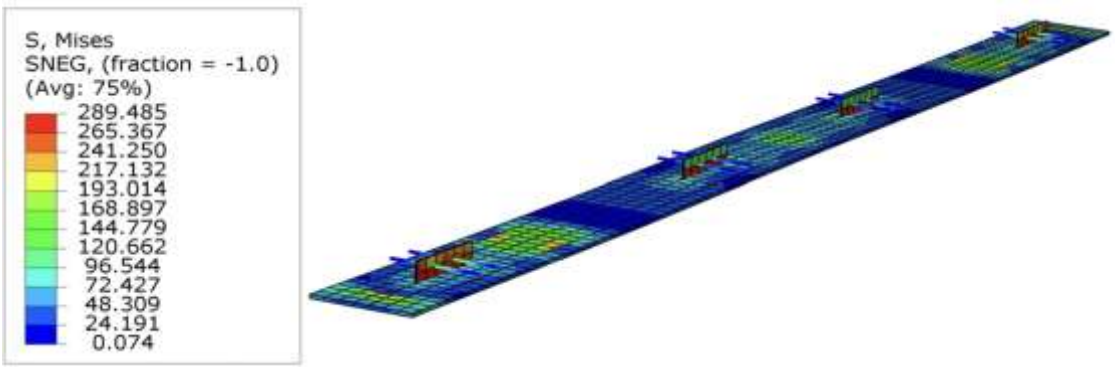

(a)

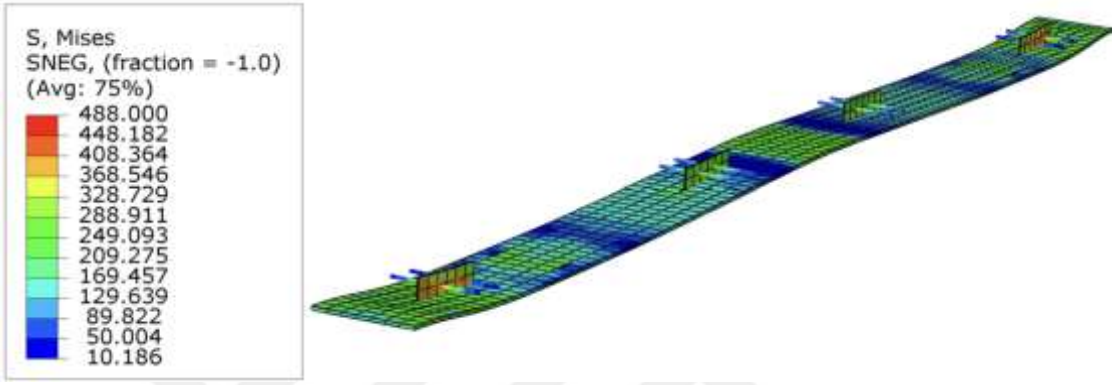

(b)

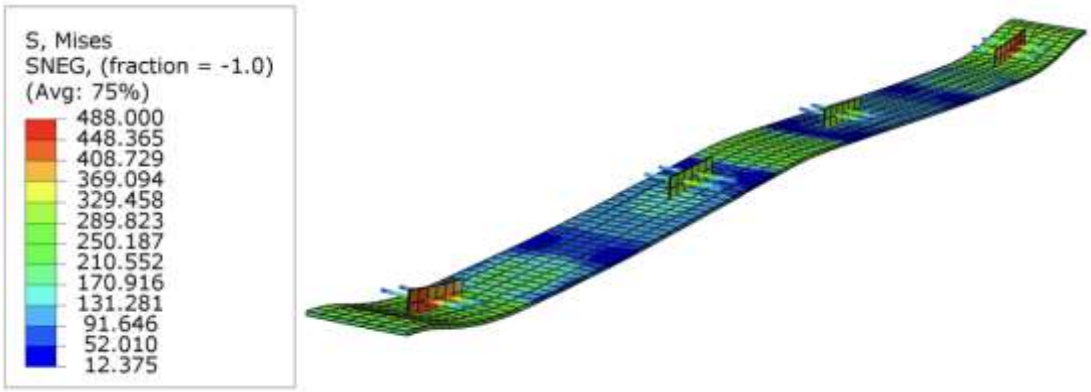

(c)

Figure 6.82: Perfobond Leiste and Rein. Bars Acting at Top Steel Flange Due to Slip Action (DCTG). (a) Perfobond Leiste Acting at First Loading Stage, (b) Perfobond Leiste Acting at Half Load Stage, (c) Perfobond Leiste Acting at Full Load Stage

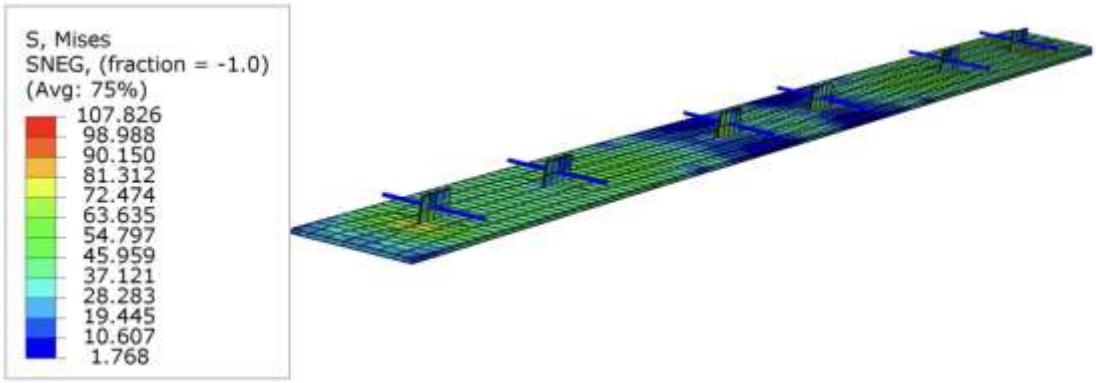

(a)

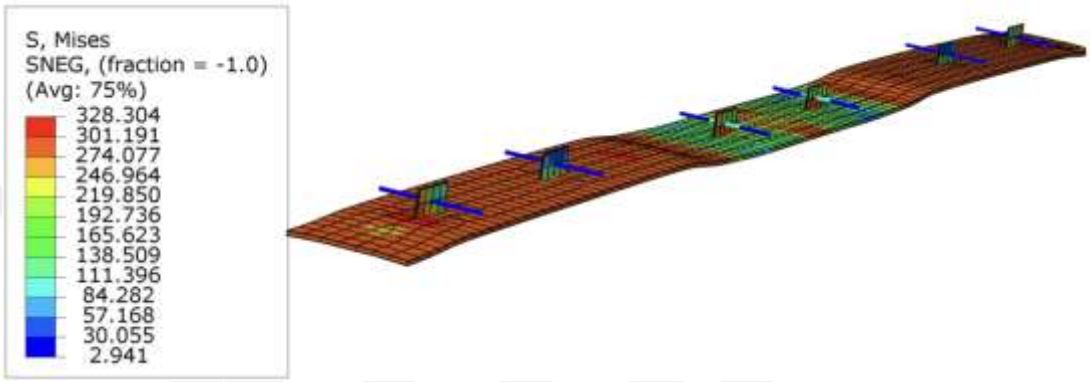

(b)

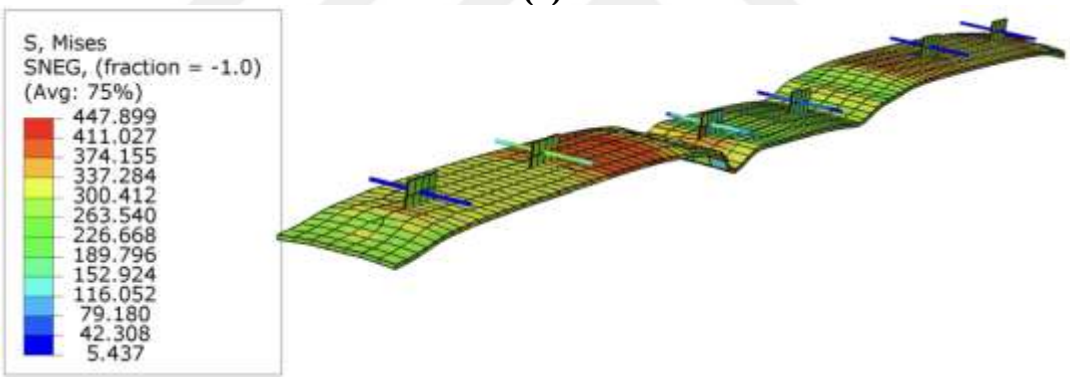

(c)

Figure 6.83: Perfobond Leiste and Rein. Bars Acting at the bottom flange due to slip action (DCTG). (a) perfobond leiste acting at the First Loading Stage, (b) Perfobond Leiste Acting at Half Loading Stage, (c) Perfobond Leiste Acting at the Full Loading Stage

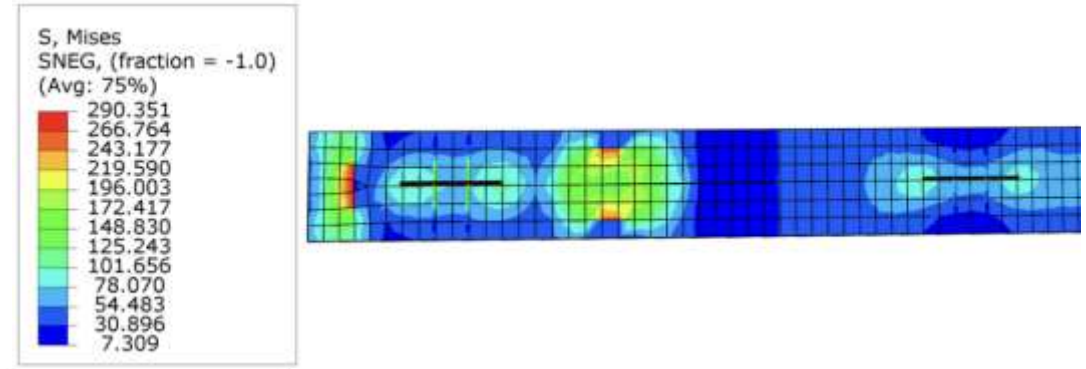

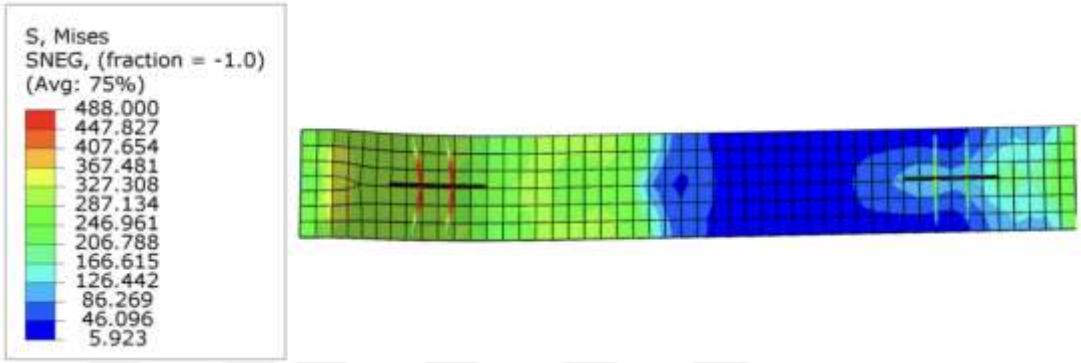

(a)

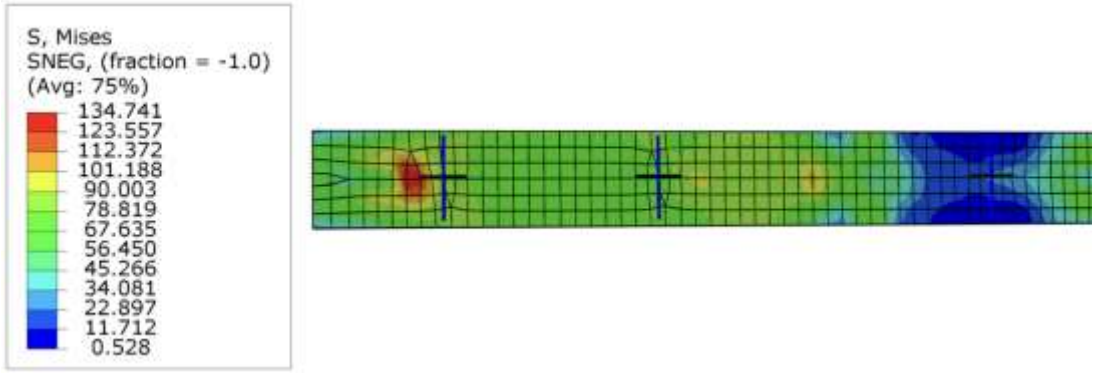

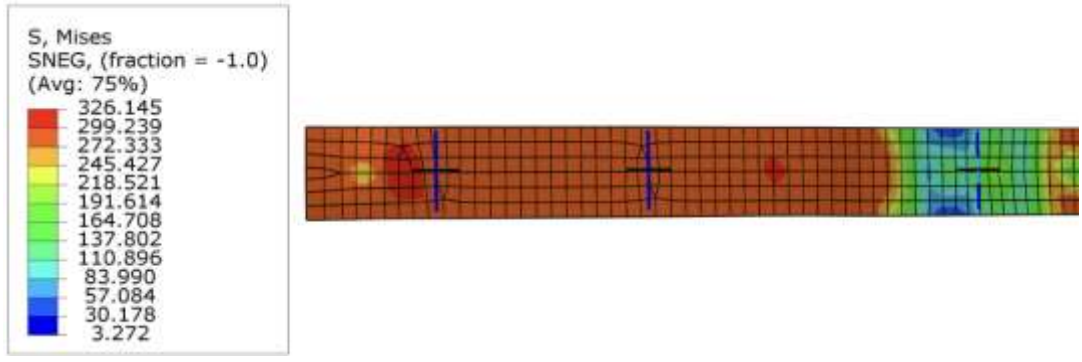

(b)

Figure 6.84: Perfobond Leiste and Rein. Bars Deformation Due to Slip Action (DCTG). (a) Top Perfobond Leiste Deformation at the first and Full Loading Stage, (b) Bottom Perfobond Leiste Deformation at the First and Full Loading Stage

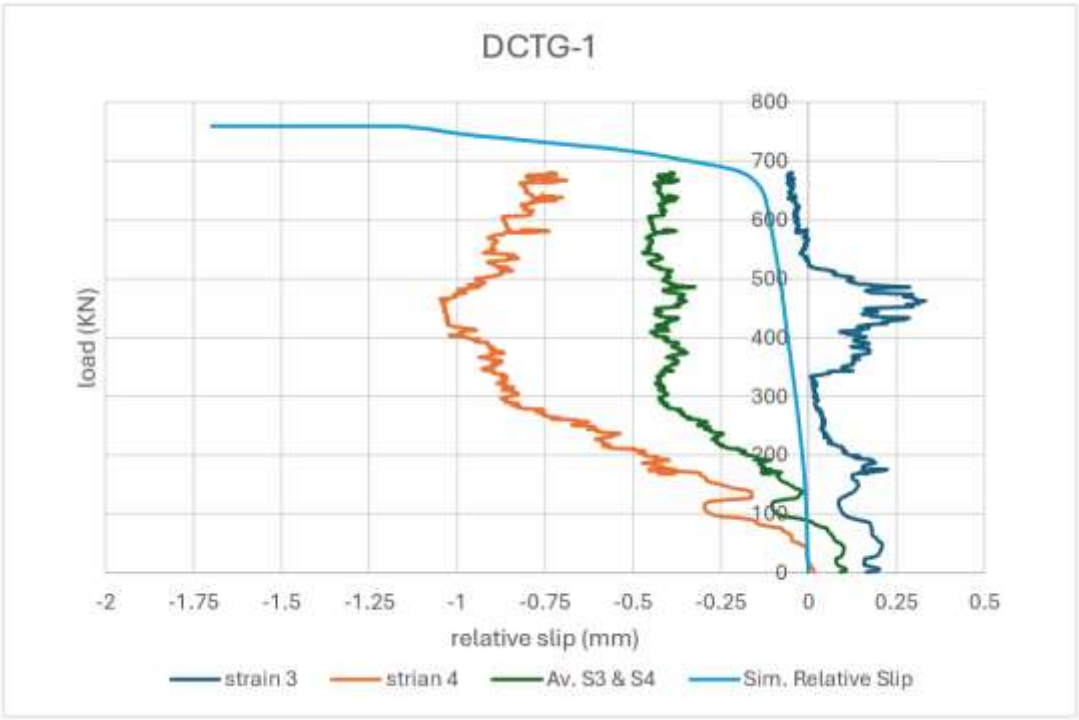

Figure 6.85: Load-Slip of the Experiment and Numerical Simulation DCTG-1

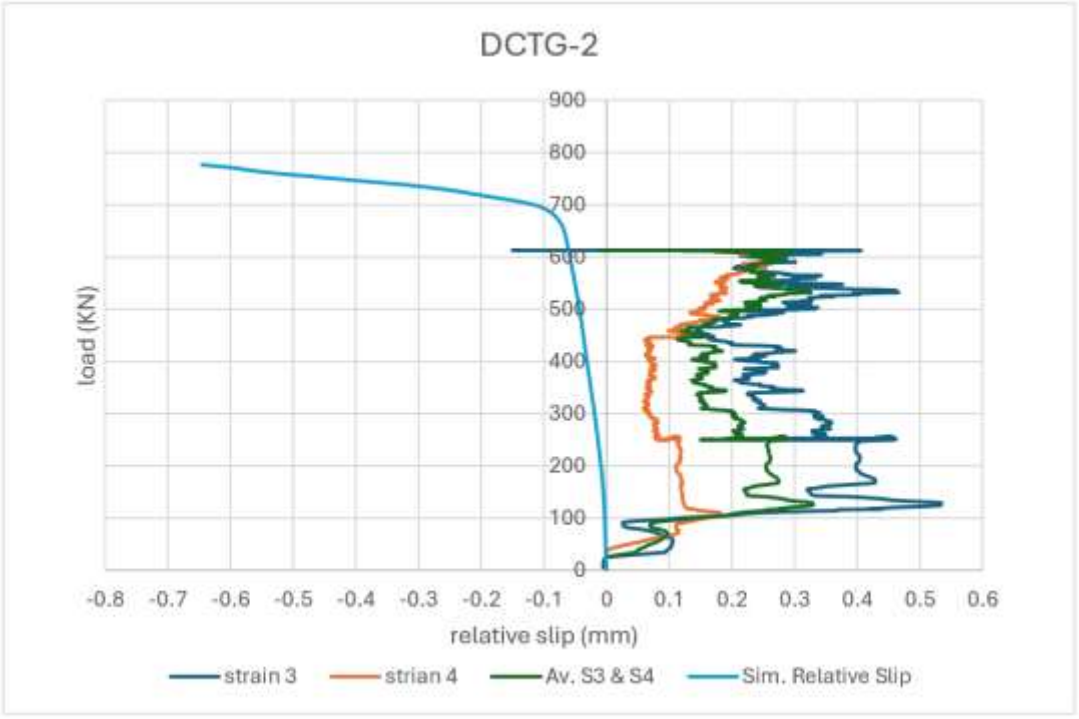

Figure 6.86: Load-Slip of the Experiment and Numerical Simulation DCTG-2

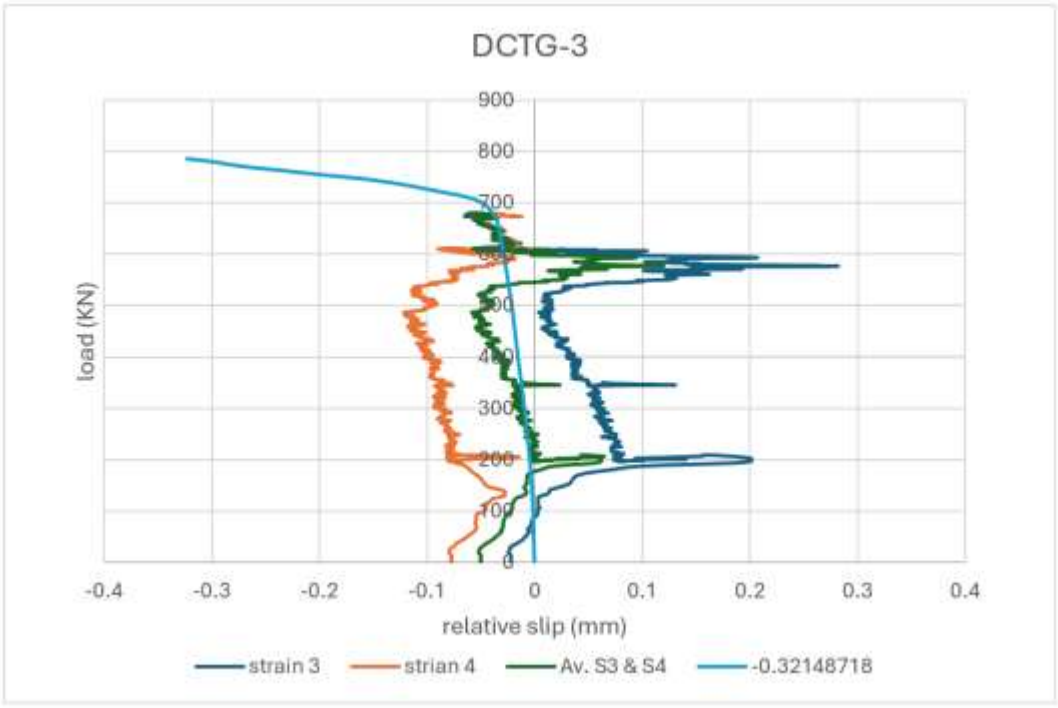

Figure 6.87: Load-Slip of the Experiment and Numerical Simulation DCTG-3

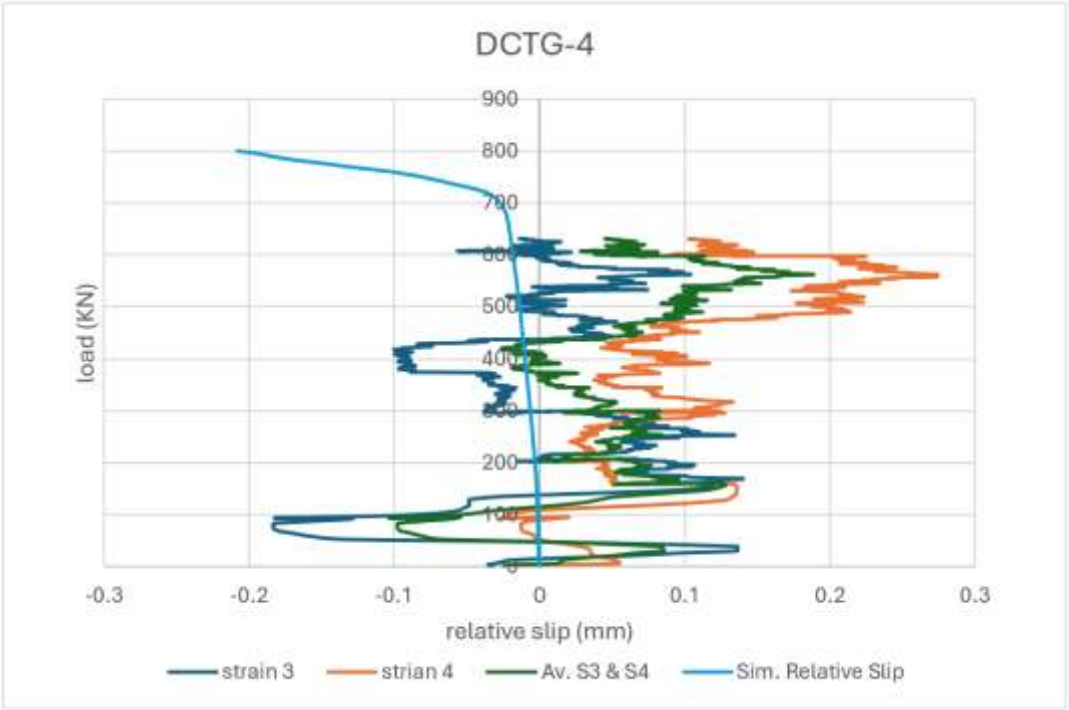

Figure 6.88: Load-Slip of the Experiment and Numerical Simulation DCTG-4

7. CONCLUSIONS AND RECOMMENDATIONS

7.1 Summary

This research study aims to investigate the mechanical response consist of the strength capacity, deflection ratio, the shear connector slip resistance, cracks pattern related to initial and ultimate cracks and strain-stresses distributions of eight composite truss girder divided to two main categories, the first one consist of four single composite truss girder and the second contain four double composite truss girder that assumed to be used for long continuous spans bridges, and how it is will behave under the hogging moment force which it reaching the maximum values at the mid support pier.

Perfobond leiste was used as shear connectors for bonding process between concrete and steel flange, studying the variables of the slip ratio through loading stages, for instance, push-out test for three samples was made to conduct the behaviors of perfobond leiste to create preliminary information data that used for design appropriate shear connectors for the main composite truss girder.

Obtained this type of continuous long composite girder will allow the structure designers to implementation the low weight structure with low budget and higher structure strength and durability compared to the normal prestressed or post-tension concrete girders with very heavy weight reaching hundreds of tons, especially when these typical long continuous bridge span suffered from advanced cracks at the concrete deck slab due to generated high hogging moment at mid support regions.

The results of this study are illustrated in detail in chapter six, which consists of an experiment field test and validates the results with simulated model by Abaqus software program.

7.2 Conclusions

Based on the results that are obtained from the investigation research study including experiment and numerical analysis studies the following can be concluded:

1- The proposed method of finite elements analysis appears to be valid for evaluating the response of Composite truss girder under static load.

2- Strain sensors show less stress values at the top concrete surface (hogging moment region) for the double composite than the single composite girders by 42.7%, while the bottom surface (sagging moment region) for the two categories exposed to high stress values.

3- Regarding to the deflection values of the double composite girder was less than in single composite by 31% which it's get effected by delay the full interaction losing point between the top concrete and steel flange due to multiply the ratio of interaction by the bottom perfobond leiste shear connectors Contribution, moreover, the elastic and plastic defection resistance for (SCTG) was at 79% and 95.7% respectively, while the results show improvement for (DCTG) when these deformation was at 89% and 97.1% respectively.

4- In terms of load-slip ratio the results conduct decreasing of the slip values from first perfobond leiste shear connectors to the fourth type by 79.2% and 75% for the (SCTG) and (DCTG) specimens respectively, meanwhile, these slip values gets decreased within 18.7% in the double composite (DCTG) than the single composite (SCTG) with high ductility range, which is refer to long phase of plastic deformation before reaching the fractured point, these causes by decreasing the shear flow over the top shear connectors by contribution of the bottom shear connector line at (DCTG) specimens, the details result showing improvement in the ductility for (DCTG-3) & (DCTG-4) by 90% over than (DCTG-1) & (DCTG-2), while the second category (SCTG) was showing low ductility ratio for all perfobond leiste samples.

5- Increasing the thickness of the concrete and steel flange layers contributed to an increase in the moment of inertia of the composite girder, leading to improvement the deflection resistance, moreover, the double composite feature at (DCTG) specimens enhanced the deflection resistance from (DCTG-1) to (DCTG-4) by average 37.6%, while it continues increasing at (SCTG) girders.

6- The period of load-elastic cracks deformation ratio (initial cracks) at the double composite girder was beginning at higher load stage than the single composite with overall average 60% and 49% respectively of the ultimate load, that's leading to delay the period of the plastic cracks deformation (ultimate cracks) to advanced loading stage which is increasing the girder cracks resistance by 11.1% especially at the hogging moment regions, when the results Illustrated and conduct plastic cracks for (DCTG) and (SCTG) at 94% and 82.9% of the ultimate load.

7- Results conducted that the girder's strength capacity at (DCTG) specimens was higher than (SCTG) within 13%, where the maximum bearing load capacity for (DCTG-4) girder was 75 tons and for the (SCTG-4) was 65 tons.

8- In general, results revel that the double composite truss girder (DCTG) gives more enhancement response than single composite truss girder according to all features, such as elastic and plastic defamation resistance values, these improvement including delay the initials and ultimate cracks, decreasing the slip ratio, influence positively on the deflection values and less strain distribution on the concrete surface that prevent cracks and saving the deck slab bridge from the water and external environments effect.

7.3 Recommendation

1- Study the effect of lateral torsional buckling and the flexural under static and dynamic loading for universal composite truss girders.

2- Study the fatigue test of the double composite truss girder under cyclic loading.

3- Implementation of low relaxation prestressed concrete strands for all composite truss specimens.

4- Validation study of using stud shear connectors and perfobond lesite ribs steel plate.

5- Study the effect of the steel truss frame height on the girder strength capacity and girder response.

6- Design and analysis entire composite truss girder of continuous bridge using bridge software analysis program.

REFERENCES

[1] **(AASHTO)** American Association of State Highway and Transportation Officials, 17th edition 2002).

[2] **ACI 318- 2014** American Concrete Institute Code

[3] **AISC**. Steel construction manual, 14th edit

[4] **Chanakya Arya,** Design of Structural Elements**,** Concrete, steelwork, masonry and timber designs to British Standards and Eurocodes, Third Edition

[5] **Ehab Ellobody**, Finite Element Analysis And Design Of Steel And Steel Concrete Composite Bridges, Second Edition

[6] **Pedro V, Sebastiao A, Luciano R, Marley M, Luis A**. Modeling Steel and Composite Structures 1st Edition - May 23, 2017

[7] **AASHTO LRFD Bridge Design Specifications**, 4th Edition, 2007

[8] **Eurocode 4,** "Design of Composite Steel and Concrete Structures": ENV1994-1-1: Part 1.1: General rule and rules for buildings.

[9] **Weiwei Lin Teruhiko Yoda**. Bridge engineering, classification design loading and analysis methods, 2017.

[10] **Johnson, R.P.,** Composite structures of steel and concrete, beams, slabs, columns, and frames for building, 3rd edition, Granada, 2004

[11] **Johnson R.P. and Buckby R.J.,** "Composite Structures of Steel and Concrete: Volume 2: Bridges", Second edition, Collins, 1986.

[12] **Johnson R.P. and Hope-Gill M.C.,** "Tests on Three Three-Span Continuous Composite Beams", Proc.Inst.Civ.Engrs., Part2, Vol.61, , pp. 367-381, June 1976.

[13] **Zellner, W.** Recent designs of composite bridges and a new type of shear connectors. In Composite Construction in Steel and Concrete; American Society of Civil Engineers: New York, NY, USA, 1987; pp. 240–252.

[14] **Ansourian P.** Experiments on Continuous Composite Beams", Proc.Inst.Civ.Engrs., Part 2, Vol.71, , pp. 25-51, December 1981.

[15] **Zhang, Q.; Pei, S.; Cheng, Z.; Bao, Y.; Li, Q**. Theoretical and experimental studies of the internal force transfer mechanism of perfobond rib shear connector group. J. Bridge Eng. 2017, 22, 0000997.

[16] **Wenqing W, ,Jinxi D, Liang C, Dan L and Xiaoyi Z.** Experiment Analysis on Crack Resistance in Negative Moment Zone of Steel–Concrete Composite Continuous Girder Improved by Interfacial Slip, materials, 2022, DOI.org/10.3390/ ma15238319

[17] **Qinghua Zhang; Donglin Jia; Yi Bao, S.M. ASCE; Zhenyu Cheng; Yizhi Bu; and Qiao Li .** Analytical Study on Internal Force Transfer of Perfobond Rib

Shear Connector Group Using Nonlinear Spring Model, Journal of Bridge Engineering,Vol. 22, No. 10, 2017 DOI:10.18057/IJASC.2021.17.4.8

[18] **Wu, F.; Liu, S.; Xue, C.; Yang, K.; Feng, Y.; Zhang, H.** Experimental Study on the Mechanical Properties of Perfobond Rib Shear Connectors with Steel Fiber High Strength Concrete, Materials, 2021, Doi.org/10.3390/ma14123345

[19] **Oehlers, D. J., & Bradford, M**. Composite Steel and Concrete Structural Members: Fundamental Behavior, Pergamon Press, (1995).

[20] **Wang, X.; He, Q.; An, Z.; Liu, G.; Wen, X.; Wang, Y.; Zhong, Z.** Experimental Study of Perfobond Rib Shear Connector under Lateral Force, Applied Sciences, 2021 DOI.org/10.3390/app11199088

[21] **Shuangjie Z, Chen Z, Yangqing L.** Analytical Model for Load–Slip Relationship of Perfobond Shear Connector Based on Push-Out Test, materials,2018, DOI.org/10.3390/ma12010029.

[22] **Weiwei lin, Teruhiko yoda.** Mechanical behaviors of composite girders subjected to hogging moment experimental study, structural engineering, vol 28, no2, 29s-42s, 2011.

[23] **R.P. Johnson.** designer guide to Eurocodes of Composite Steel and Concrete Structures EN 1994-1-1 " ICE Publishing, second edition,2011.

[24] **David Collings.** Steel-concrete Composite Bridges, Designing with Eurocodes, ICE Publishing, second edition, 2013.

[25] **Fritz Leonhardt**. Bridges Aesthetics and Design, MIT Press Series in Structural Mechanics,1984

[26] **Kang, J.Y., Park, J.S., Jung, W.T. and Keum, M.S.** Evaluation of the Shear Strength of Perfobond Rib Connectors in Ultra High-Performance Concrete. Engineering, 2014 doi.org/10.4236/eng.2014.613089

[27] **British standard** BS 5400 Loading, part 2

[28] **F Alsharari, A el-sisi, Mohammed M, Hani S, A El-Zohairy**. Effect of the Progressive Failure of Shear Connectors on the Behavior of Steel-Reinforced Concrete Composite Girders, Buildings, 2022 doi.org/10.3390/buildings12050596

[29] **Chengquan W , Jun X, Yonggang S, Jiqing J.** Research on the Mechanical Behavior of a Steel–Concrete Composite Link Slab on a Simply Supported Girder Bridge, Metals 2022. doi.org/10.3390/met12091410

[30] **Chengfeng X, Zhou F, Fangwen W, Laijun L, Lanqing H and Xuan C.** Research on the Shear Behavior of Composite Shear Connectors, Buildings, 2022

[31] **Chisung L ,Seung H, Jae Y, Sun J , Moon L and Kang K**, Shear Behavior of Concrete Encased Steel Truss Composite Girders, Appl Sci, 2021 doi.org/ 10.3390/app11041569

[32] **Yiyan C, Jucan D, Tianhua X**. Composite box girder with corrugated steel webs and trusses– A new type of bridge structure, Engineering Structures, 2018.

[33] **Bu, J.; Cao, W.; Wang, X.; Zhang, L.** Experimental Research on the Mechanical Properties of MURSP-Type Steel-Concrete Composite Beams in Negative-Moment Region. Buildings 2023 doi.org/ 10.3390/buildings13041095

[34] **Peng, K.; Liu, L.; Wu, F.; Lei, S.; Cao, J.; Fan, X.; Wang, X.** Experimental and Numerical Evaluation on the Performance of Perfobond Leiste Shear Connectors in Steel–SFRCC Composite Beams, Materials, 2022 doi.org/10.3390/ma15207237

[35**] Fan, Z.; Wu, F.; He, L.; He, R.; Zeng, K.; Liu, Z.** Experimental Investigation on the Mechanical Performance of Steel-ECC Composite Girders with Corrugated Webs under Negative Moment. Materials 2022, doi.org/10.3390/ ma15196539

[36] **Yongjian Liu, Zhihua Xiong, Yalin Luo, Gao Cheng, Ge Liu, Jian Yang.** Double-composite rectangular truss bridge and its joint analysis, Journal of Traffic and Transportation Engineering (English Edition), Volume 2, Issue 4, 2015, Pages 249-257, ISSN 2095-7564, doi.org/10.1016/j.jtte.2015.05.005.

[37] **Song A, Xu H, Wan S, Luo Q.** Analytical Model of Crack Width in Hogging Moment Regions of Steel-Concrete Composite Beams Under Fatigue Loading, Frontiers in Materials, 2022. doi: 10.3389/fmats.2022.859687

[38] **Hope Gill And Johnson.** Tests on three three-span continuous composite beams, Proc. Instn Cio. Engrs, Part 2, 1976, 61, June, 367-381

[39] **Vinicius de Oliveiraa , Adriano de Carvalhob , Alexandre Rossic , Felipe Piana Vendramell Ferreirac , Carlos Humberto Martinsb.** ELASTIC AND INELASTIC ANALYSES OF COMPOSITE CELLULAR BEAMS IN HOGGING MOMENT REGIONS, Thin-Walled Structures, December 2022, Doi: 10.1016/j.tws.2022.110513

[40] **El-Zohairy, A.; Mustafa, S.; Shaaban, H.; Salim, H.; Allawi, A.A.** Numerical Modeling and Analysis of Strengthened Steel–Concrete Composite Beams in Sagging and Hogging Moment Regions. CivilEng 2023, 4, 483–505. doi.org/ 10.3390/civileng4020028

[41] **A. Hamoda, K.M.A. Hossain, K. Sennah, M. Shoukry, Z. Mahmoud.** Behaviour of composite high performance concrete slab on steel I-beams subjected to static hogging moment, Engineering Structures, Volume 140, 2017, Pages 51-65, doi.org/10.1016/j.engstruct.2017.02.030.

[42] **Long, G.; Zhou, R.; Ma, H.; Xin, G.; Emadi, S.; Shi, X.** Experimental and Numerical Study on UHPC–RC Decks within Hogging Moment Region. Appl. Sci. 2022, doi.org/10.3390/ app122211446

APPENDICES

Appendix A.1: Theoretical Design and Analysis of bridge superstructure

Appendix A.1.1: Design Criteria

Appendix A.1.1.1: Bridge Geometry

The case study will illustrate a long span bridge with 300 m which is 50 m for each span, the bridge will be implemented along a wide valley, the high of the bridge surface level to the bed level of the valley approximately around 20 m, the main design will focus on the superstructure of the bridge.

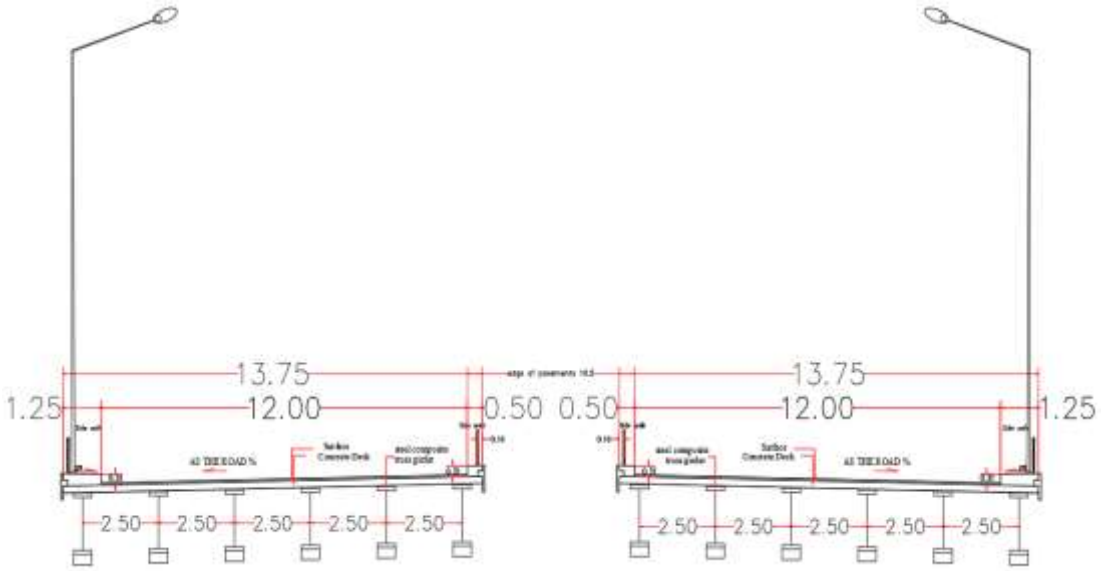

Figure A.1: Composite Truss Bridge Section

The superstructure consists of a 12 m wide carriageway with 1.25 m sidewalk, the type of girder will be double composite truss steel girder with Perfobond Leiste shear connector in both top and bottom flange.

The girder web truss will be warren type, where the chords carry the bending in tension and compression and the diagonals carry the shears, also in tension and compression and the vertical members carry only panel loads, The connection between the truss and web will be by welding methods, Figure A.2 showing The design will be for each two continuous spans for 100 m as continuous span.

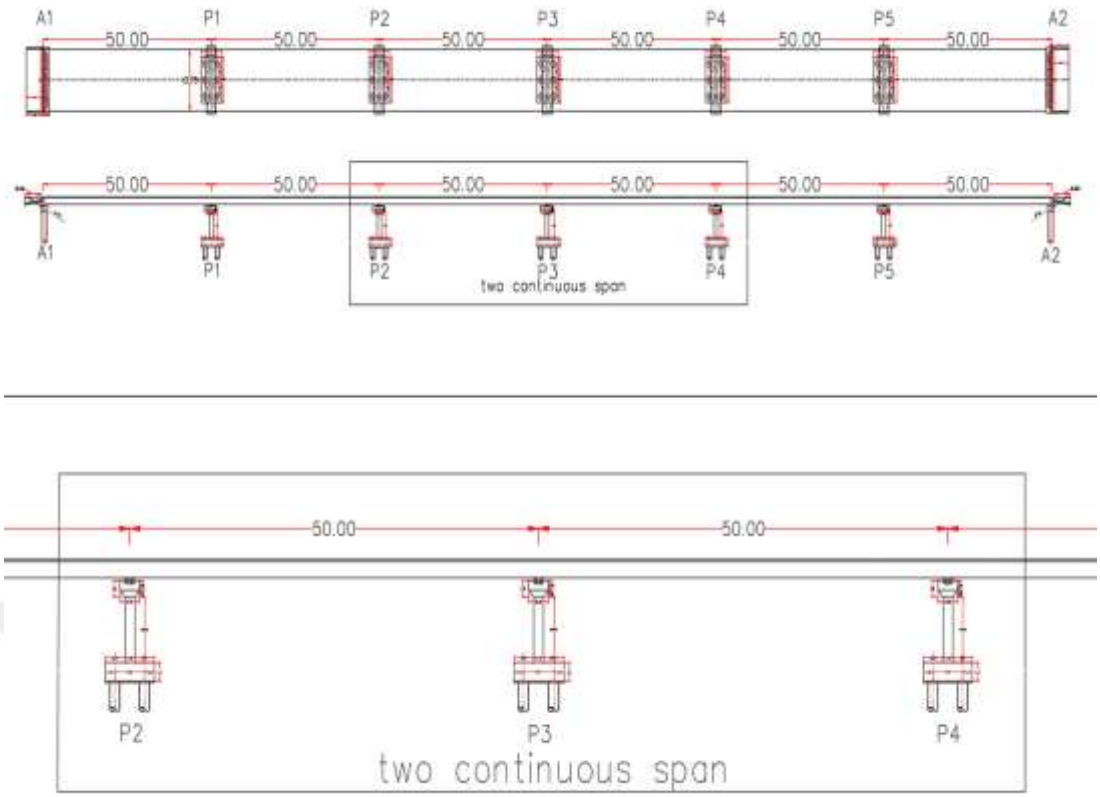

Figure A. 2: Bridge Side View and Two Continuous Spans

Appendix A.1.1.2 Specification of Materials

1.Steel Reinforcement ASTM A615 (Grade 60): yield strength fy=420 MPa

2. Steel truss members ST35 fy=350MPa (EN 10025)

3. Compressive Strength of Concrete: 40 MPa (Girders, Deck Slab).

4. Compressive Strength of Concrete: 35 MPa (for Curb Stone, Shoulder, New jersey Barrier).

Appendix A.1.2 loading

Appendix A.1.2.1 Dead load

The following unit weights of construction materials shall be used in computing dead load applied to different parts of the bridge structure, Table A.1.

Table A.1: Construction Materials Density

Material	Density
Structural steel or cast steel	78.5 kN/m3
Cast iron	72.5 kN/m3
Plain concrete	23.0 kN/m3
Reinforced concrete	24.0 kN/m3
Asphaltic concrete	22.5 kN/m3

All structures will be designed to carry an additional dead load (curb to curb) of 0.75kN/m2.

By assuming the concrete deck slab thickness = 0.2 m and asphalt layer = 0.06 m

And assuming flange width of the steel truss beam = 60 cm and girder c/c = 2.5 m

kN/m per girder

Minimum $h_{\min} = 1.2\left(\frac{S+3000}{30}\right)$ deck slab = ft **AASHTO table 8.9.2**

S= c/c = 2.5m = 8.202 ft

S= (2.5 c/c – 0.7 girder flange width) + 0.2 deck slab = 2 m = 6.561ft

= 1.2 (S +10/30) = 1.2(6.561+10/30) = 0.662 ft = 0.20 m ≤ 0.2 m then ok

take slab deck 0.20 m

Surface wearing is asphalt = 12 x 50 x 0.06 x 22.5 = 810 kN for one span

(0.06 x 2.5 c/c x 22.5) = 3.375 kN/m per girder

Concrete slab = 13.75 x 50 x 0.2 x 24 = 3300 kN for one span

(0.20 x 2.5 c/c x 24) = 12 kN/m per girder

concrete sidewalk = (1.25+0.5) x 50 x 0.32 x24 = 672 kN for one span

(0.32 x 1.75 x 24)/6 = 2.24 kN/m per girder

Steel hand railing and lighting posts = 5.25 KN/m x 50 x 2 = 525 KN for one span

(5.25/6) = 0.875 kN/m per girder

Total dead load for two spans length 100 m will be:

= (810 + 3300 + 672 + 39.2) = 4,821.2 KN per span

= (3.375 + 12 + 2.24 + 0.875) = 18.49 kN/m per girder

By Analysis the uniform distribution load with robot structural analysis program:

(B.M)hog bending moment per girder due to the dead load = 5778.13 KN/m

(B.M)sag bending moment per girder due the dead load = 3250.13 KN/m

(S.F) maximum shear force per girder due to the dead load = 577.81 KN

Figure A.3: Bending Moment Due to Dead Load

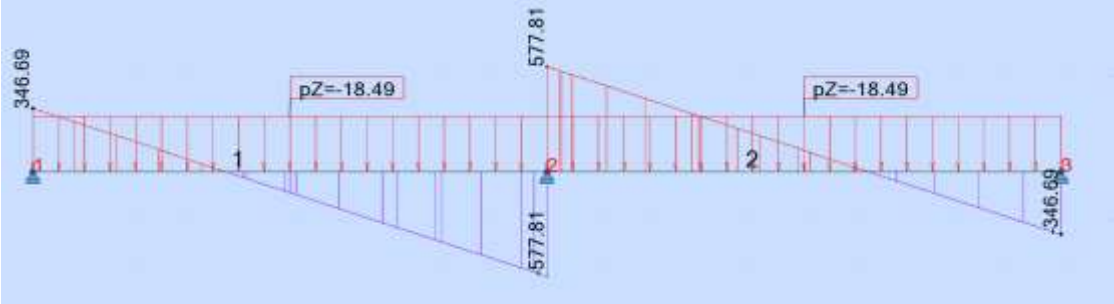

Figure A.4: Shear Force due to Dead Load

A.1.2.2 Live load

A.1.2.2.1 Civilian live load According to AASHTO LRFD

A.1.2.2.1.1 Truck design Live Load (HL-93) total weight 325kN

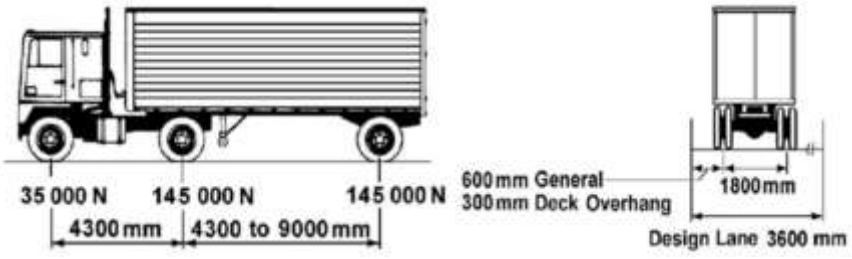

Figure A.5: Truck design Live Load (HL-93)

First due to the Bending Moment (B.M.)

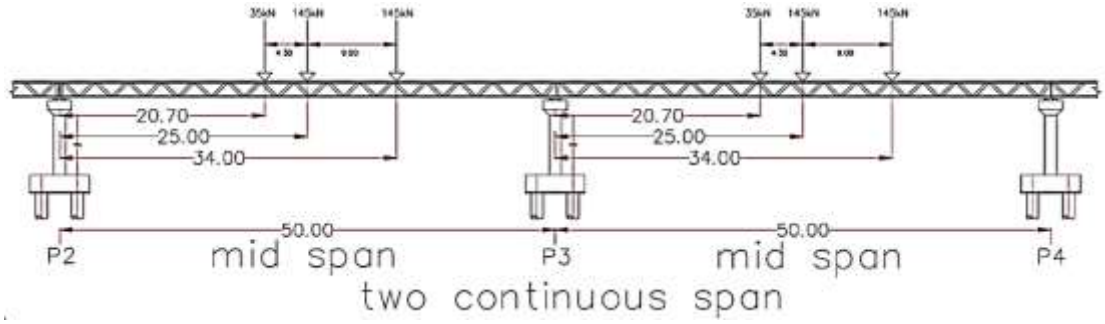

Figure A.6: Truck design live load at mid span

- (B.M.) at center of girder at mid span using robot structural analysis program, the second point of truck load will be at the center of the span.

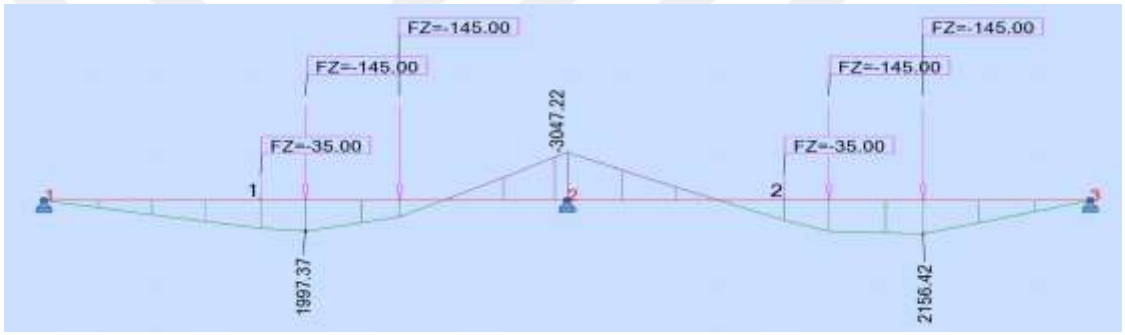

Figure A.7: Bending Moment Due to HL-93 Truck Live load at Mid Span

Figure A.8: Reactions Due to HL-93 Truck Live Load at Mid Span

(B.M.)hog per Lane = 3047.22 kN.m

The lane width for civilian load is 3.00 m **AASHTO LRFD 2017**

Distributing Factor (D.F) = Spacing of girder /3 = 2.5m / 3m = 0.833

B.M. girder= (B.M.) per lane x D.F.

B.M. girder = 3047.22 x 0.833 = 2,538.334 kN.m

Impact is 1.33 as per AASHTO LRFD 2017 clause § 3.6.2.1 and applied only for truk or tandem of HL93 loads, but not for design lane, pedestrian loads.

B.M. per girder = 2,538.334 kN.m x 1.33 = 3,375,984 kN.m

Load factors according to AASHTO Sec. 3.4 per girder will be (1.5)

(B.M.)hog per girder = 3,375,984 kN.m x 1.5 = 5,063,976 kN.m

(B.M.)sag per Lane = 1997.37 kN.m

The lane width for civilian load is 3.00 m **AASHTO LRFD 2017**

Distributing Factor (D.F) = Spacing of girder /3 = 2.5m / 3m = 0.833

B.M. girder= (B.M.) per lane x D.F.

B.M. girder = 2156.42 x 0.833 = 1,796.297 kN.m

Impact is 1.33 as per AASHTO LRFD 2017 clause § 3.6.2.1 and applied only for truk or tandem of HL93 loads, but not for design lane, pedestrian loads.

B.M. per girder = 1,796.297 kN.m x 1.33 = 2,389.076 kN.m

Load factors according to AASHTO Sec. 3.4 per girder will be (1.5)

(B.M.)sag per girder = 2,389.076 kN.m x 1.5 = 3,583.614 kN.m

Second due to Shear Force (VL.L.)

The first point of truck load will be at 1.5 from support p3 of the span 1 & 2

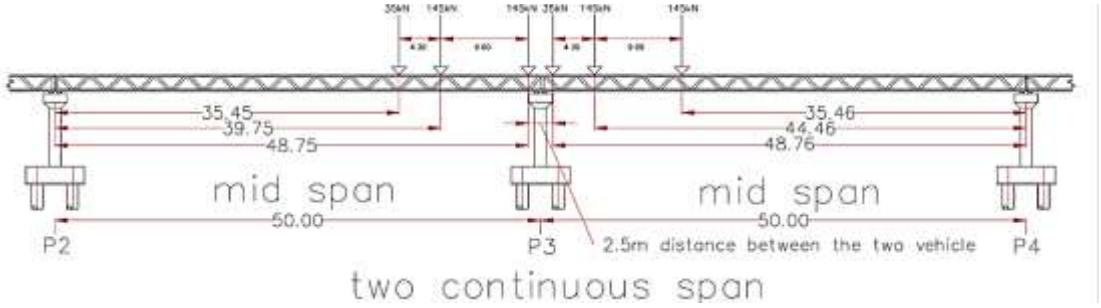

Figure A.9: Truck Design Live Load at Support p3

(B.M.) when the loading near to support (p3) using robot structural analysis program.

Figure A.10: Bending Moment Due to HL-93 Truck Live Load at Mid Support

Maximum (VL.L) with Reactions near support p3 using robot structural analysis program.

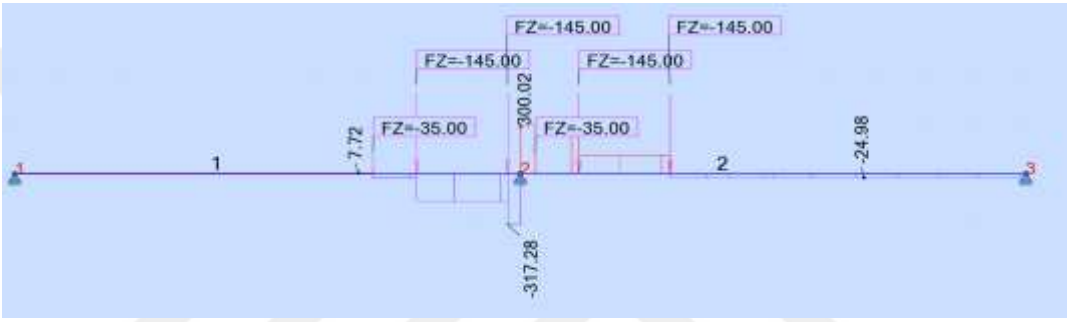

Figure A.11: Reactions Due to HL-93 Truck Live Load at Mid Support

The reaction on each support (p2) = 7.72 KN

The reaction on each support (p4) = 24.98 KN

The reaction on support (p3) = 617.30 KN

Maximum shear force will be taken as (317 kN) per lane

The lane width for civilian load is 3m according to AASHTO LRFD 2017

Distributing Factor (D.F) = Spacing of the girder /3 m= 2.5m / 3m = 0.833

(Shear Force) per girder = (Shear Force) per lane x D.F

(Shear Force) per girder = 317 kN x 0.833 = 264.061 kN

A.1.2.2.1.2 Tandem Design LiveLoad

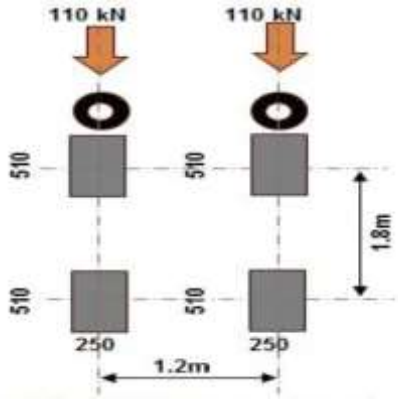

Figure A.12: Tandem design Live Load (HL-93) tire plane

First due to the Bending Moment (B.M.)

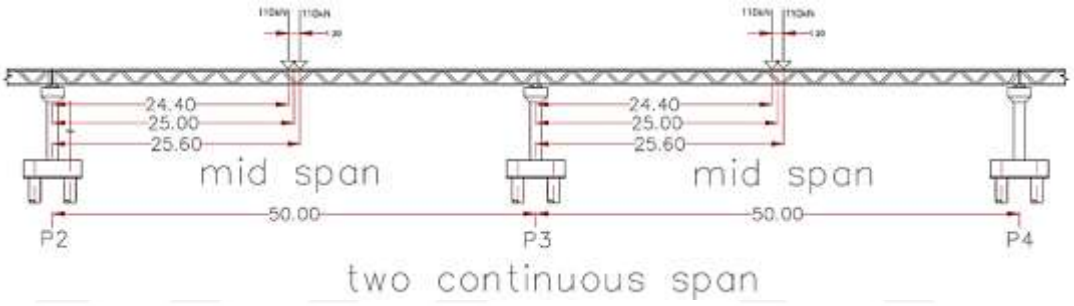

Figure A.13: Tandem Design Live Load at Mid Span

- (B.M.) at center of girder at mid span using robot structural analysis program

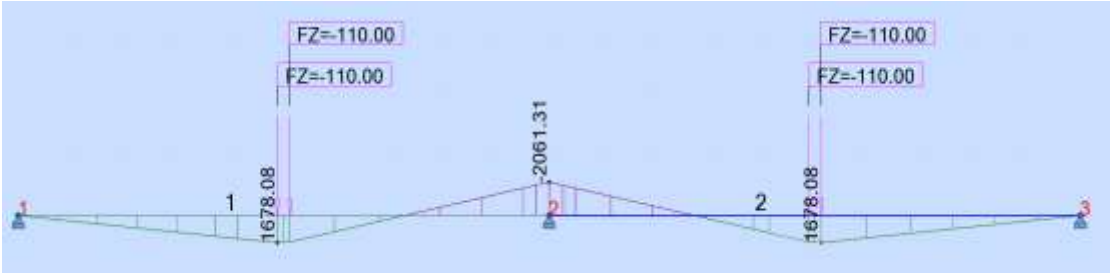

Figure A.14: Bending Moment as Tandem Design Live Load At Mid Span

Figure A.15: Shear Force as Tandem Design Live Load at Mid Span

(B.M.)hog per Lane = 2061.31 kN.m

The lane width for civilian load is 3.00 m **AASHTO LRFD 2017**

Distributing Factor (D.F) = Spacing of girder /3 = 2.5m /3m = 0.833

B.M. girder= (B.M) per lane x D.F.

B.M. girder = 2061.31 x 0.833 = 1,717.071 kN.m

Impact is 1.33 as per AASHTO LRFD 2017 clause § 3.6.2.1 and applied only for trukand tandem of HL93 loads, but not for design lane, pedestrian loads.

B.M. girder = 1,717.071 kN.m x 1.33 = 2,283.704 kN.m

Load factors according to AASHTO Sec. 3.4 per girder will be (1.5)

(B.M)hog per girder = 2,283.704 kN.m x 1.5 = 3,425,556 kN.m

(B.M)sag per Lane = 1678 kN.m

The lane width for civilian load is 3.00 m **AASHTO LRFD 2017**

Distributing Factor (D.F.) = Spacing of girder /3 = 2.5m /3m = 0.833

B.M. girder= (B.M.) per lane x D.F.

B.M. girder = 1678 x 0.833 = 1,397.774 kN.m

Impact is 1.33 as per AASHTO LRFD 2017 clause § 3.6.2.1 and applied only for trukand tandem of HL93 loads, but not for design lane, pedestrian loads.

B.M. girder = 1,397.774 kN.m x 1.33 = 1,859 kN.m

Load factors according to AASHTO Sec. 3.4 per girder will be (1.5)

(B.M)sag per girder = 1,859 kN.m x 1.5 = 2,788 kN.m

Second due to Shear Force (VL.L.)

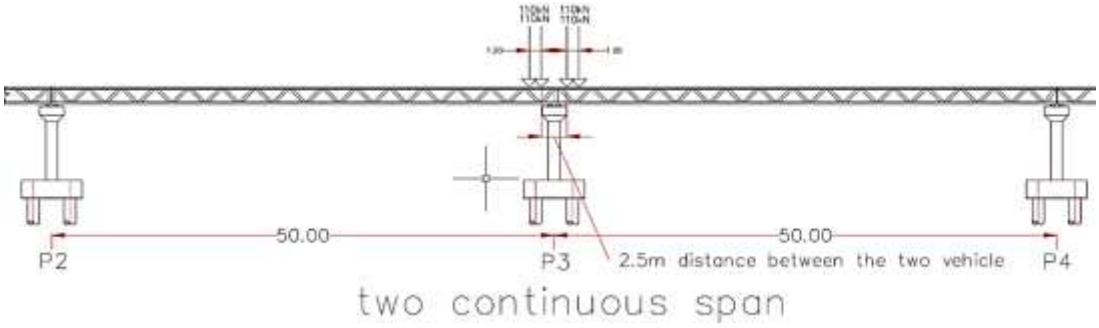

Figure A.16: Tandem Design Live Load At Support p3

- Reactions with maximum (VL. L) using robot structural analysis program

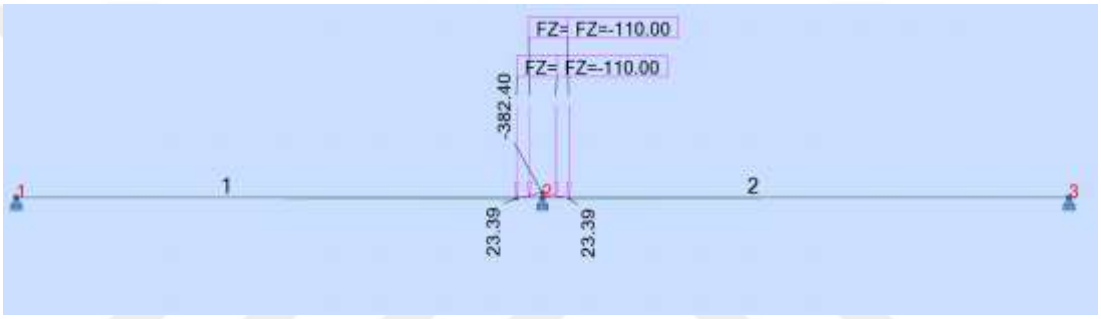

Figure A.17: Bending Moment as Tandem Design Live Load at Support p3

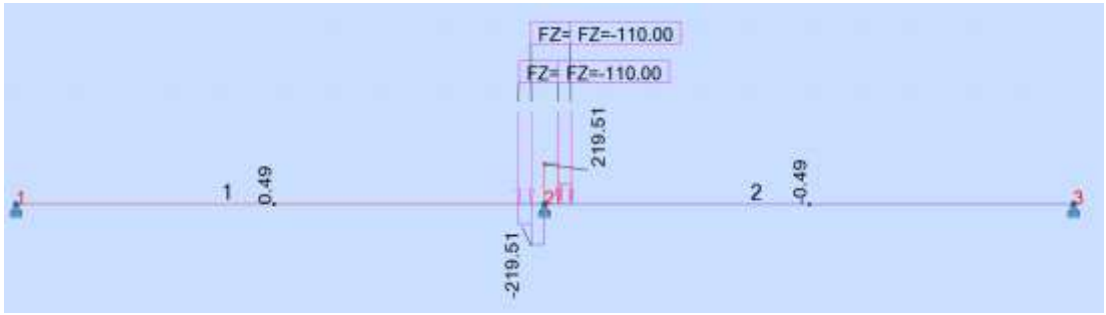

Figure A.18: Shear Force as Tandem Design Live Load at Support p3

The reaction on each support (p2) = 0.49 KN

The reaction on each support (p4) = 0.49 KN

The reaction on support (p3) = 439.02 KN

Maximum shear force will be taken as (219.51 kN) per lane

The lane width for civilian load is 3m according to AASHTO LRFD 2017

Distributing Factor (D.F.) = Spacing of the girder /3 m= 2.5m /3m = 0.833

(Shear Force) per girder = (Shear Force) per lane x D.F.

(Shear Force) per girder = 219.51 kN x 0.833 = 182.851 kN

A.1.2.2.1.3 Design Lane Live load

Design lane consists of uniformly distributed load of 9.3 kN/m design lane load is assumed to be uniformly distributed over a width of (3.0m).

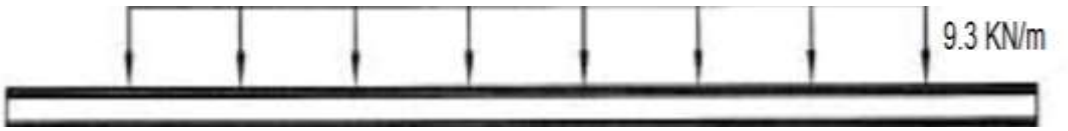

Figure A.19: Typical Design Lane Live load

- (B.M.) at center of girder at mid span using robot structural analysis program

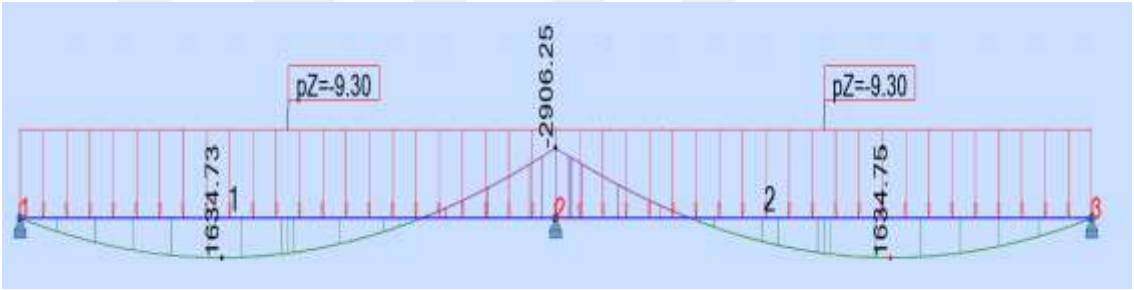

Figure A.20: Bending Moment Design Lane Live load

(B.M.)hog per Lane = 2906.25 kN.m

The lane width for civilian load is 3.00 m **AASHTO LRFD 2017**

Distributing Factor (D.F.) = Spacing of girder /3 = 2.5m /3m = 0.833

B.M girder= (B.M.) per lane x D.F.

(B.M)hog girder = 2906.25 x 0.833 = 2,421 kN.m

(B.M)sag per Lane = 1634.73 kN.m

The lane width for civilian load is 3.00 m **AASHTO LRFD 2017**

Distributing Factor (D.F.) = Spacing of girder /3 = 2.5m /3m = 0.833

B.M girder= (B.M.) per lane x D.F.

(B.M)sag girder = 1634.73 kN.m x 0.833 = 1,361 kN.m

- Reactions with maximum (VL.L) using robot structural analysis program

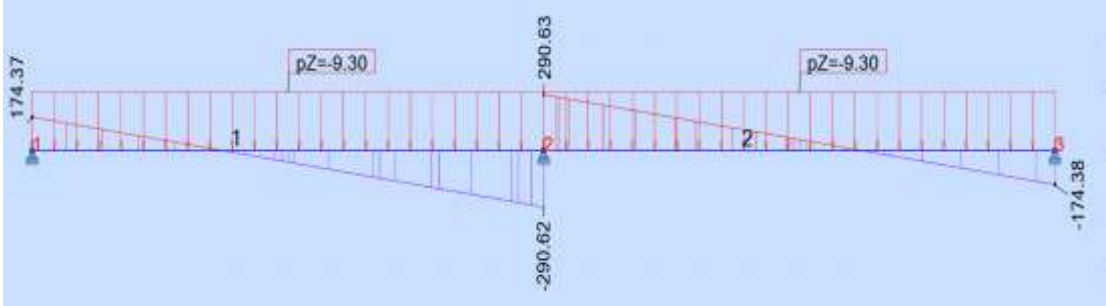

Figure A. 21: Shear Force Design Lane Live load

The reaction on each support (p2) = 174.37 KN

The reaction on each support (p4) = 174.38 KN

The reaction on support (p3) = 581.25 KN

Maximum shear force will be taken as (291 kN) per lane

The lane width for civilian load is 3m according to AASHTO LRFD 2017

Distributing Factor (D.F) = Spacing of the girder /3 m= 2.5m /3m = 0.833

(Shear Force) per girder = (Shear Force) per lane x D.F

(Shear Force) per girder = 291 kN x 0.833 = 242.403 kN

HL-93 is the maximum of the two of these:

First Design Tandem + Design Lane or Design Truck + Design Lane

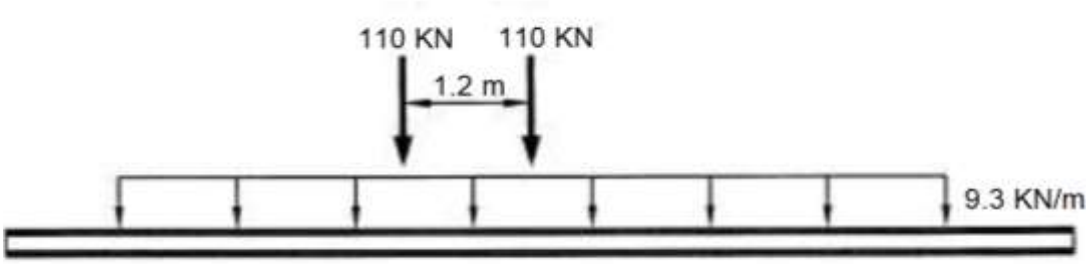

Figure A.22: HL-93 Truck Live Load and Lane Live Load

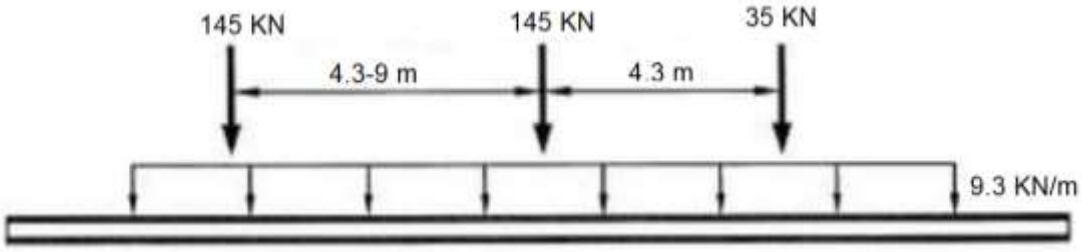

Figure A.23: HL-93 Tandem and lane Design Live Load

Bending moment, the truck load = 5,063,976 kN.m

Shear force truck load = 264.061 kN

Bending moment tandem load = 3,425,556 kN.m

Shear force tandem = 182.851 kN

Bending moment design live load = 2,420.906 kN.m

Shear force tandem load = 242.403 kN

Then use truck load + lane load

Maximum bending moment = 5,063,976 kN.m + 2,420.906 kN.m = 7,484,882 kN.m

Maximum shear force = 264.061 kN + 242.403 kN = 506.464 kN

A.1.2.2.1.4 Pedestrian load (PL)

A pedestrian load of 3.6 KN/m^2 shall be applied to all sidewalks

3.6KN/m^2 x 1.75 m = 6.3 KN uniform load per span

Figure A.24: Bending Moments due to Pedestrian Load

Figure A.25: Shear Force Due to Pedestrian Load

The bending hogging moment with robot structural analysis = 1968 kN.m

Distributing Factor (D.F.) = Spacing of the girder /3 m= 2.5m /3m = 0.833

(B.M) per girder = (Shear Force) per lane x D.F.

(B.M)hog per girder = 1968 kN.m x 0.833 = 1,639.344 kN.m

The bending sagging moment with robot structural analysis = 1107 kN.m

Distributing Factor (D.F.) = Spacing of the girder /3 m= 2.5m /3m = 0.833

(B.M) per girder = (Shear Force) per lane x D.F.

(B.M)sag per girder = 1107 kN.m x 0.833 = 922.131 kN.m

The shear with robot structural analysis = 196 KN

Distributing Factor (D.F.) = Spacing of the girder /3 m= 2.5m /3m = 0.833

(S.F) per girder = (Shear Force) per lane x D.F.

(S.F) per girder = 196 kN x 0.833 = 163.268 kN

A.1.2.2.2 Civilian live load According to BS 5400 with Iraqi Specifications

As The Vehicle loads (moving loads) For Road and Bridge, 1978" (civil and military live loads)

A.1.2.2.2.1 (UDL and KEL loading)

Table A.2: Iraqi Standard for Road and Bridges

CARRIAGEWAY WIDTH	NO. OF LANES
ABOVE 16 FEET (4·88m.) UP TO & INCLUDING 24 FEET (7·31m.)	2
" 24 " (7·31m.) " " " 36 " (10·97m.)	3
" 36 " (10·97m.) " " " 48 " (14·63m.)	4
" 48 " (14·63m.) " " " 60 " (18·29m.)	5

The carriageway of the bridge = 12 m table 3.1 the number of lanes = 4

The lane width = 3 m ≥ 2.3 m

For 50m loaded span, for transverse slabs per linear meter of 3.05m lane and designed lane of the bridge = 3 m

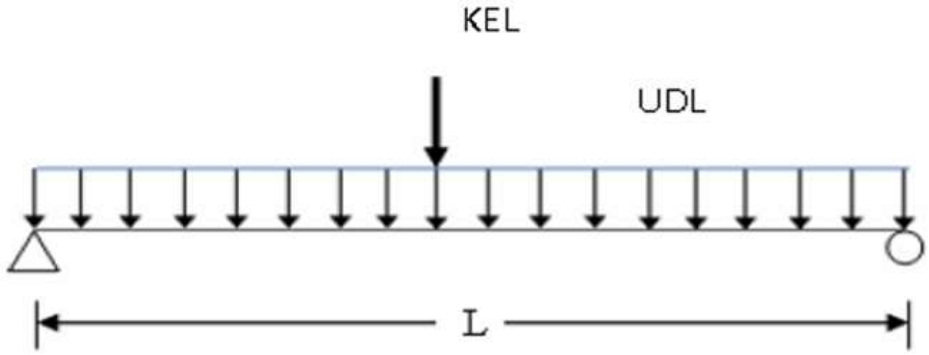

Figure A.26: Civilian Loading (KEL: Knife Edge Load / UDL: Uniformly Distributed Load)

UDL = 2360 kg/m per lane = 23.6 kN/m per lane

Modified UDL = 23.6 kN/m x 3 /3.05 = 23.213 kN/m per lane

UDL per Girder (spacing = 2.5 m) = UDL x spacing / lane width

UDL per Girder = 23.213 x 2.5 m/3 m= 19.344 kN/m per girder

KEL= 4018 kg/3m (lane width) = 1339 kg /m (see table in page 4 from (ISHL)

KEL = 13.39 kN/m (assume 1,000 kg= 10 kN)

KEL = 13.39 kN/m x Lane width =13.39 kN/m x 3m= 40.17 kN per lane

KEL per Girder= 40.17 kN x 2.5 m/3 m = 33.475 kN per girder

Sidewalk live loading = 3.91 KN/m2 x 1.75 m = 6.842 kN/m uniform loading per lane

Sidewalk live loading per girder = 6.842 kN/m x 2.5 m/3m = 5.701 kN/m per girder

Total uniform loading per girder = 19.344 kN/m + 5.701 kN/m = 25.045 kN/m

Using robot structural analysis to find bending moment to due uniform load

The maximum (B.M)hog due to UDL and S.W loading = 7812 KN.m per girder

The maximum (B.M)sag due to UDL and S.W loading = 4394.44 KN.m per girder

The maximum (B.M)hog due to KEL loading = 313.83 KN.m per girder

The maximum (B.M)sag due to KEL loading = 261.52 KN.m per girder

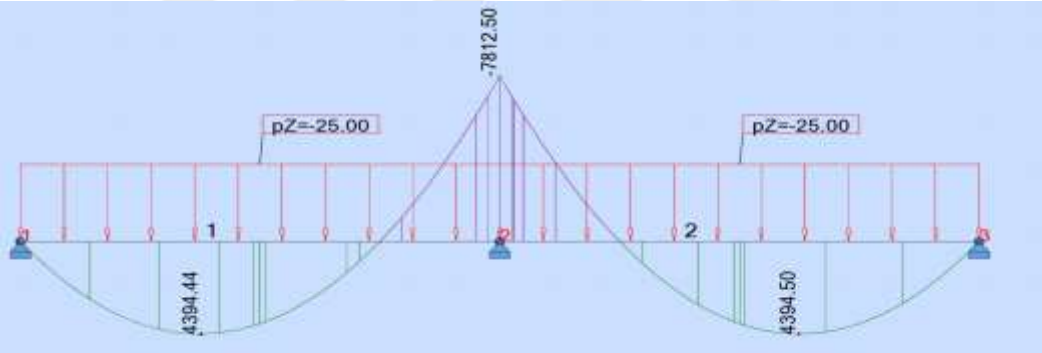

Figure A.27: UDL and Sidewalk Bending Moment Per Girder

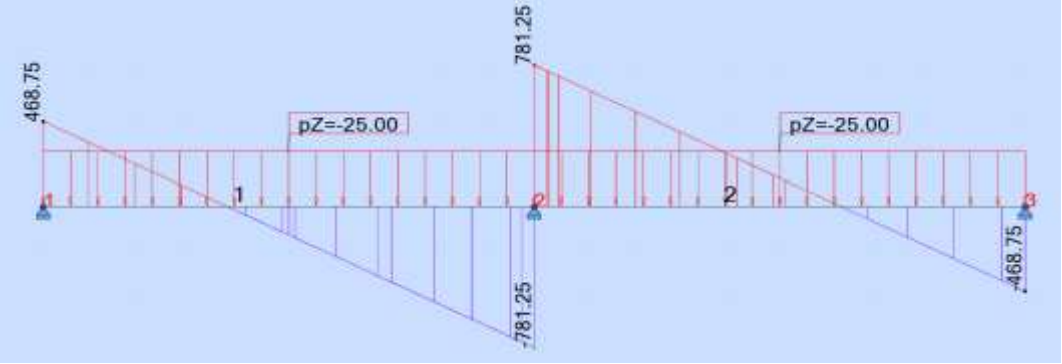

Figure A.28: UDL and Sidewalk Shear Force Per Girder

Figure A.29: KEL Bending Moment Per Girder

Figure A.30: KEL Shear Force Per Girder

A.1.2.2.2.2 Military load

The military load classification to two types as illustrated in **Figure A.31**.

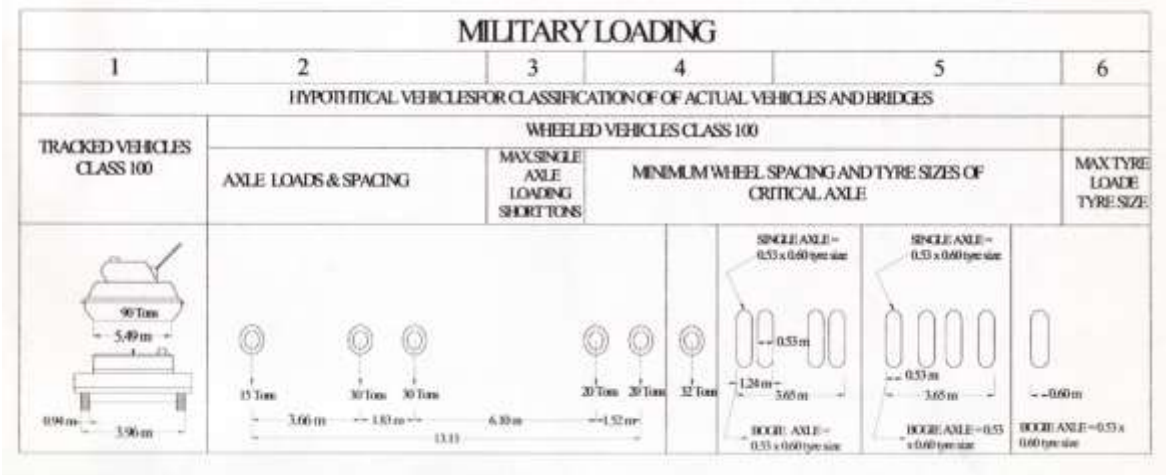

Figure A.31: Military Loading Classification

A.1.2.2.2.2.1 Tracked class 100 live load (tank 900 KN)

First due to the Bending Moment (B.M.)

The worst case will be when this Tank is in the middle of the span.

The Tank has 2 tracks, so each track will have 900/2= 450 kN.

The distributed load per track will be 450 kN/5.49 m = 81.97 kN/m

The reaction on each support (p2, p4) = 5P/16 = 140.625 KN

The reaction on support (p3) = 11P/8 = 618.75 KN

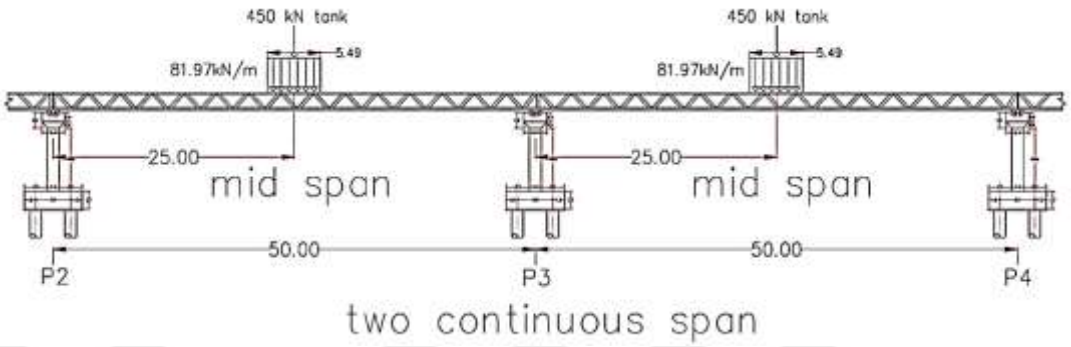

Figure A.32: Tank Load Distribution at Mid Spans

- (B.M.) at center of girder at first mid span using sky civ analysis program

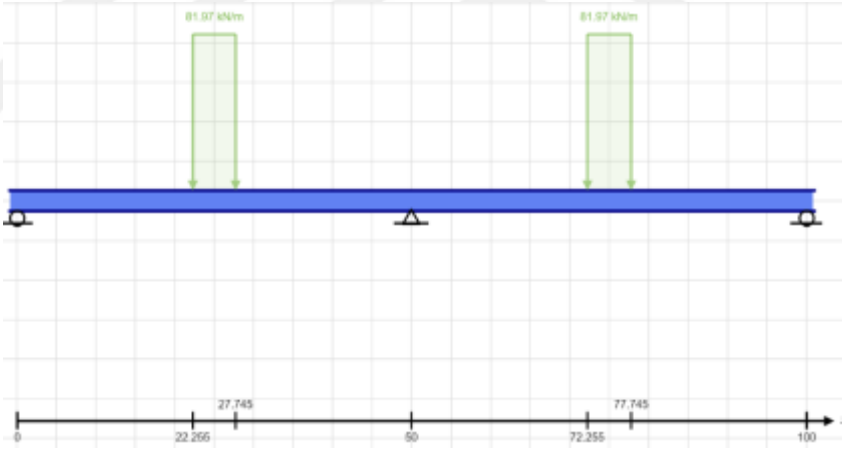

Figure A.33: Load Distribution with the Bridge Spans

Table A.2: Track Class 100 Analysis Results at mid Spans

Support at	X	Y	Mx
0	0 kN	140.969 kN	0 kN-m
100	0 kN	140.969 kN	0 kN-m
50	0 kN	618.093 kN	0 kN-m

Force Extremes

Result	Max	Min
Bending Moment	3194.697 kN-m	-4201.939 kN-m

(B.M.)hog at first mid span = 4201.939 kN.m

Since we have 2 tracks then (B.M.) two tracks= 2 x 4201.939 = 8,403.878 kN.m per lane. The lane width for military load is 4.5m (Page 9 from ISHL).

Distributing Factor (D.F.) = Spacing of girder /4.5 = 2.5 / 4.5 = 0.555

(B.M.) girder = (B.M.) per lane x D.F.

(B.M.) girder = 8,403.878 x 0.555 = 4,664.152 kN.m

Impact Factor = 0.21 (Table Page 10 from (ISHL)). Table 3.1

For tracked load, the Impact Factor is divided by 2 (note 5 page 9 from (ISHL))

Impact Factor = 0.21/2 = 0.105

(B.M.) girder = 4,664.152 x 1.105 = 5,153.888 kN.m

According to Iraqi Specifications (ISHL)-pg. 11 item 3-B, increase allowable stresses by 1.3 (longitudinal load)

(B.M.)hog girder = 5,153.888 x 1.3 = 6,700 kN.m

(B.M.)sag at first mid span = 3194.697 kN.m

Since we have 2 tracks then (B.M.) two tracks= 2 x 3194.697= 6,389.394 kN.m per lane. The lane width for military load is 4.5m (Page 9 from ISHL).

Distributing Factor (D.F.) = Spacing of girder /4.5 = 2.5 / 4.5 = 0.555

(B.M.) girder = (B.M.) per lane x D.F.

(B.M.) girder = 6,389.394 x 0.555 = 3,546.113 kN.m

Impact Factor = 0.21 (Table Page 10 from (ISHL)). Table 3.1

For tracked load, the Impact Factor is divided by 2 (note 5 page 9 from (ISHL))

Impact Factor = 0.21/2 = 0.105

(B.M.) girder = 3,546.113 x 1.105 = 3,918.454 kN.m

According to Iraqi Specifications (ISHL)-pg. 11 item 3-B, increase allowable stresses by 1.3 (longitudinal load)

(B.M.)sag girder = 3,918.454 x 1.3 = 5,093.990 kN.m

Table A.3: Impact Factor In Iraqi Standard for Road and Bridges

	SPAN IN METRES	0	2	6	10	20	30	40	50	60	80	100 OR MORE
REINFORCED CONCRETE & MASONRY STRUCTURES	ALL PARTS OF ROAD BRIDGE SUPER-STRUCTURE	·40	·39	·37	·36	·32	·28	·24	·12	0	0	0
	DITTO WITH 0·5 M. COVER OR ARCHES	·30	·29	·27	·26	·22	·18	·16	·08	0	0	0
STEEL TRUSS & GIRDER BRIDGES	ALL PARTS OF ROAD BRIDGE SUPER-STRUCTURE	·60	·55	·45	·36	·32	·28	·24	·21	·18	·14	·10

Note:

The impact factor is applied only to the military load to one line

The impact for tracked vehicle= ½ impact factor for wheeled vehicle

Shear Force (VL.L.) Calculations

The worst case will be when this Tank is in the middle of the span.

The Tank has 2 tracks, so each track will have 900/2= 450 kN.

The distributed load per track will be 450/5.49= 81.97 kN/m

The Tanks are near the support P3

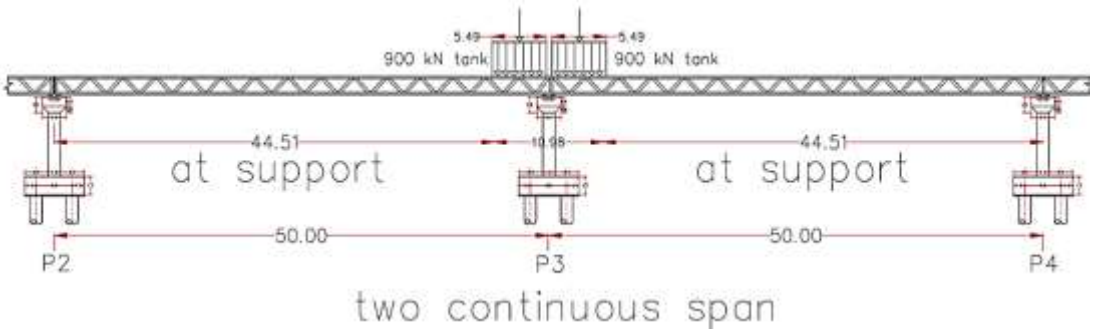

Figure A.34: Tank Load Distribution at Supports

The reaction on each support (p2, p4) = 2.638KN

The reaction on support (p3) = 894.754 KN

- (B.M.) at center of girder at first mid span using sky civ analysis program

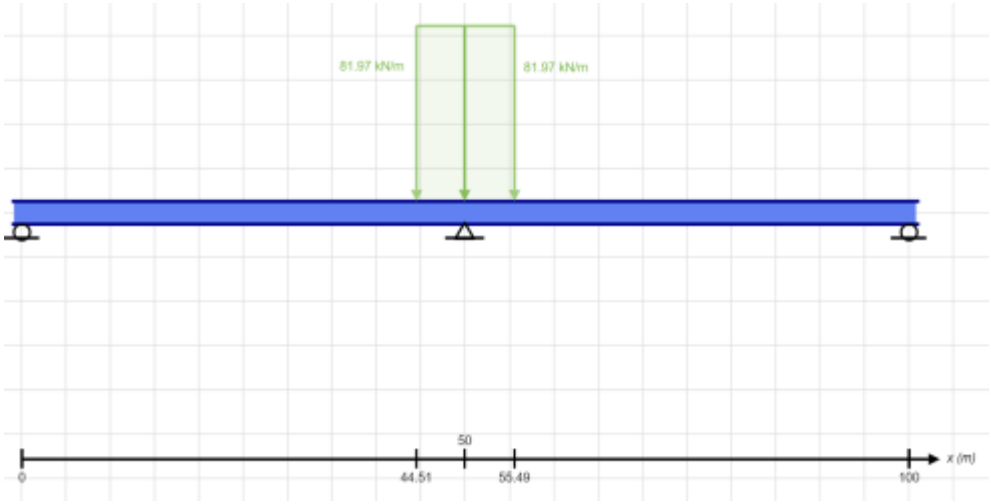

Figure A.35: Load Distribution with the Bridge Spans

Table A.4: Track Class 100 Analysis Results at mid Support

Support at	X	Y	Mx
0	0 kN	2.638 kN	0 kN-m
100	0 kN	2.638 kN	0 kN-m
50	0 kN	894.754 kN	0 kN-m

Force Extremes

Result	Max	Min
Bending Moment	117.428 kN-m	-1103.38 kN-m

Maximum shear force will be taken as (447.377 kN)

(Shear Force) one track = 447.377 kN

Since we have 2 tracks then (Shear Force) two tracks= 2 x 447.377 KN = 894.754 kN per lane.

The lane width for military load is 4.5m (note 3 Page 9 from (ISHL)).

The width of the Tank is 3.96 m.

Distributing Factor (D.F.) = Spacing of the girder /4.5 m= 2.5 / 4.5 = 0.555

(Shear Force) girder = (Shear Force) per lane x D.F.

(Shear Force) girder = 894.754 kN x 0.555 = 496.588 kN

Impact Factor = 0.21 (Table Page 10 from (ISHL)). Table 3.1

For tracked load, the Impact Factor is divided by 2 (note 5 page 9 from (ISHL))

Impact Factor = 0.21/2 = 0.105

(Shear Force) girder = 496.588 kN x 1.105 = 548.729 kN

According to Iraqi Specifications (ISHL)-pg. 11 item 3-B, increase allowable stresses by 1.3 (longitudinal load)

(Shear Force) girder = 548,729 x 1.3 = 713,347 kN.m

A.1.2.2.2.2.2 Military wheeled vehicles class 100 live load

From Table in page 9 – Column 2 from (ISHL), one can see that the Military wheeled has 5 axles.

The total weight is = 136.6+272.2+272.2+181.4+181.4 = 1,043.8 kN

The total length is 3.66+1.83+6.10+0.52 = 12.13m

Bending Moment (B.M.) Calculations

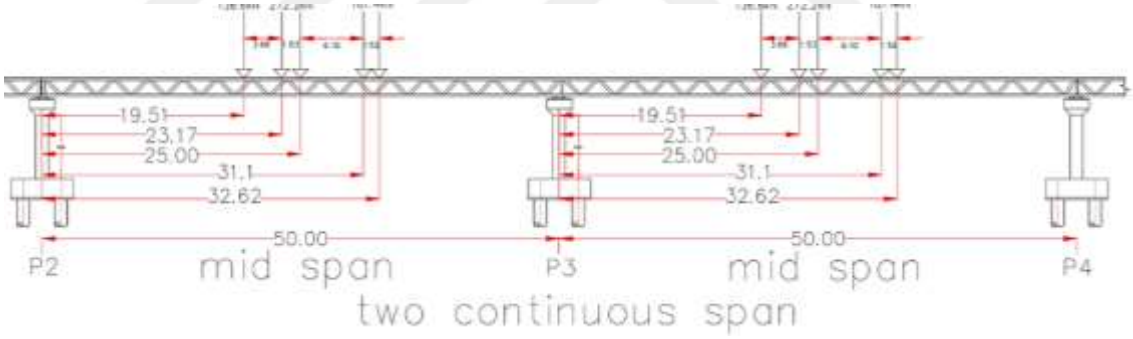

Figure A.36: Military Wheeled Vehicles Load Distribution at Mid Span

- (B.M.) at center of girder at first mid span using robot structural analysis program

Figure A.37: Load Distribution with Bending Moment

(B.M.)hog per Lane = 9816.62 kN.m

The lane width for military load is 4.27m (see note 3 Page 9 from (ISHL)).

Distributing Factor (D.F.) = Spacing of girder /4.27 = 2.5 / 4.27 = 0.555

B.M. girder= (B.M.) per lane x D.F.

B.M. girder = 9,816.62 x 0.555 = 5,448.224 kN.m

Impact Factor = 0.21 (see Table Page 10 from (ISHL)).

B.M. girder = 3,692.809 kN.m x 1.21 = 6,592.351 kN.m

According to Iraqi Specifications (ISHL) (pg. 11 item 3-B), increase allowable stresses by 1.333 so

(B.M.)hog girder max allowable stresses = 4,468.298/1.333 = 4,945.499 kN.m

(B.M.)sag per Lane = 6653.71 kN.m

The lane width for military load is 4.27m (see note 3 Page 9 from (ISHL)).

Distributing Factor (D.F.) = Spacing of girder /4.27 = 2.5 / 4.27 = 0.555

B.M. girder= (B.M.) per lane x D.F.

B.M. girder = 6653.71 x 0.555 = 3,692 kN.m

Impact Factor = 0.21 (see Table Page 10 from (ISHL)).

B.M. girder = 3,692 kN.m x 1.21 = 4,468 kN.m

According to Iraqi Specifications (ISHL) (pg. 11 item 3-B), increase allowable stresses by 1.3 (longitudinal load)

(B.M.)sag girder = 4,468 x 1.3 = 5,808 kN.m

Shear Force (VL.L.) Calculations

It can be noticed that is the critical case for shear forces where the two vehicles near to the support P2, with 2m distance between the wheeled vehicles as shown in **figure 3-38**.

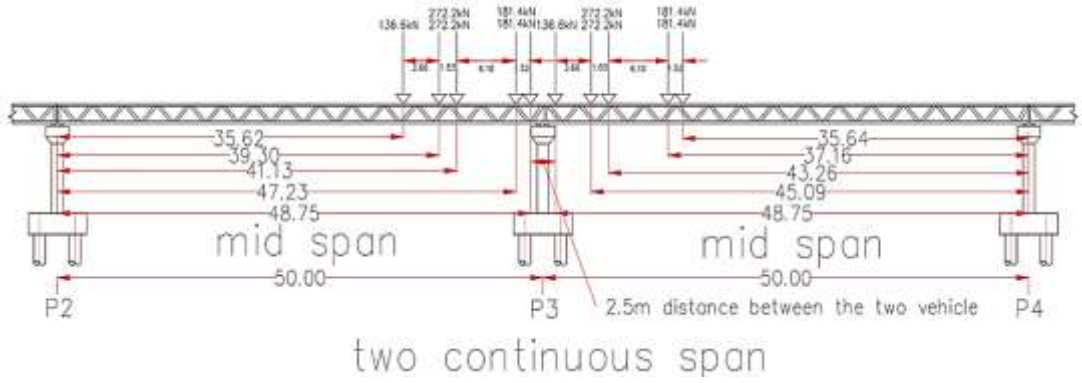

Figure A.38: Military Wheeled Vehicles Load Distribution at Supports

- Shear Force diagram analysis using robot structural analysis program

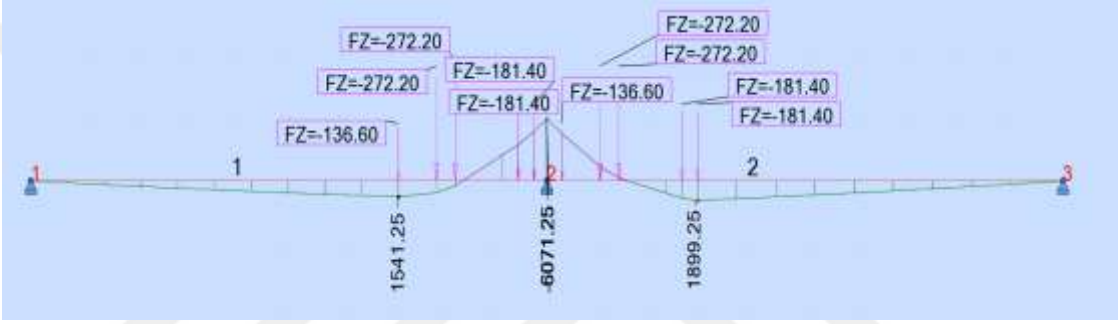

Figure A.39: Load Distribution with Bending Moment

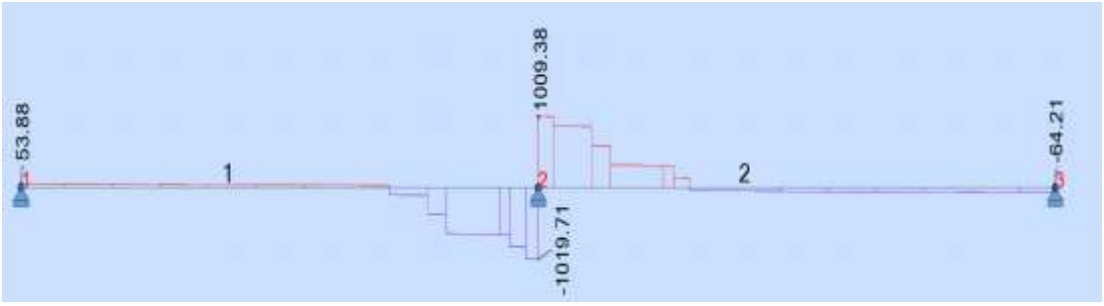

Figure A.40: Load Distribution with Supports Reactions

The reaction on support p1 = 53.88 KN

The reaction on support p2= 2,029.09 KN

The reaction on support p3 = 64.21 KN

Maximum shear force will be taken at support 2 =1015 kN for one lane

The lane width for military load is 4.5m (note 3 Page 9 from (ISHL)). Please note that the width of the Tank is 3.96 m.

Distributing Factor (D.F.) = Spacing of girder /4.5 = 2.5 / 4.5 = 0.555

(Shear Force) girder= (Shear Force) per lane x D.F.

(Shear Force) girder = 1015 x 0.555 = 563.325 = 563 kN

Maximum Shear Force at support = 563 kN per girder

Impact Factor = 0.21 (see Table Page 10 from (ISHL)).

(Shear Force) girder = 563 kN x 1.21 = 681.23 kN

According to Iraqi Specifications (ISHL) (pg. 11 item 3-B), increase allowable stresses by 1.3 (longitudinal load)

(Shear Force) girder = 681.23 x 1.3 = 885.599 kN.m

A.1.3 Details Bending Moment and Shear Force Results

Table A.5: Details Loading Results of Dead Load

Dead load of self-weight		
Bending moment (B.M)	HOG	5778.13 KN.m per girder
	SAG	3250 KN.m per girder
Shear force (V.L)	577.81 KN per girder	

Table A.6: Details Loading Results According to AASHTO

AASHTO live load			
Truck load	B.M	HOG	5,063,976 kN.m per girder
		SAG	3,583.614 kN.m per girder
	V.L	264.061 kN per girder	
Tandem load	B.M	HOG	3,425,556 kN.m per girder
		SAG	2,788 kN.m per girder
	V.L	182.851 kN per girder	
Design lane load	B.M	HOG	2,420.906 kN.m per girder
		SAG	1,361 kN.m per girder
	V.L	242.403 kN per girder	
Pedestrian load (PL)	B.M	HOG	1,639.344 kN.m per girder
		SAG	922.131 kN.m per girder
	V.L	163.268 kN per girder	
Maximum bending moment (Hogging) = truck load + design lane load + PL			9,124,226 KN.m
Maximum bending moment (sagging) = truck load + design lane load + PL			3,585,897 KN.m

Table A.7: Details Loading Results According to BS and Iraqi Standards

BS 5400 and Iraqi standards specifications for loading			
UDL load and S.W	B.M	HOG	7812 KN.m per girder
		SAG	4394.44 KN.m per girder
	V.L	781 KN	
KEL load	B.M	HOG	313.83 KN.m per girder
		SAG	261.52 KN.m per girder
	V.L	23 KN	
Track military load	B.M	HOG	6,700 kN.m per girder
		SAG	5,094 kN.m per girder
	V.L	713,347 kN.m per girder	
Wheeled military load	B.M	HOG	4,945.499 kN.m per girder
		SAG	5,808 kN.m per girder
	V.L	885.599 kN.m per girder	
Maximum (B.M)Hog = track load + UDL and KEL load			14,825.83 kN.m
Maximum (B.M)sag = wheeled load + UDL and KEL load			10,463.96 kN.m

Maximum hogging moment = 14,825.83 + 5778.13 = 20,603.96 ► 20,604 KN.m

Maximum sagging moment = 10,463.96 + 3250 = 13,713.96 ► 13,714 KN.m

Maximum shear force at support p3 = 577.81 + 781+ 23 + 885.599 = 2,267 KN.m

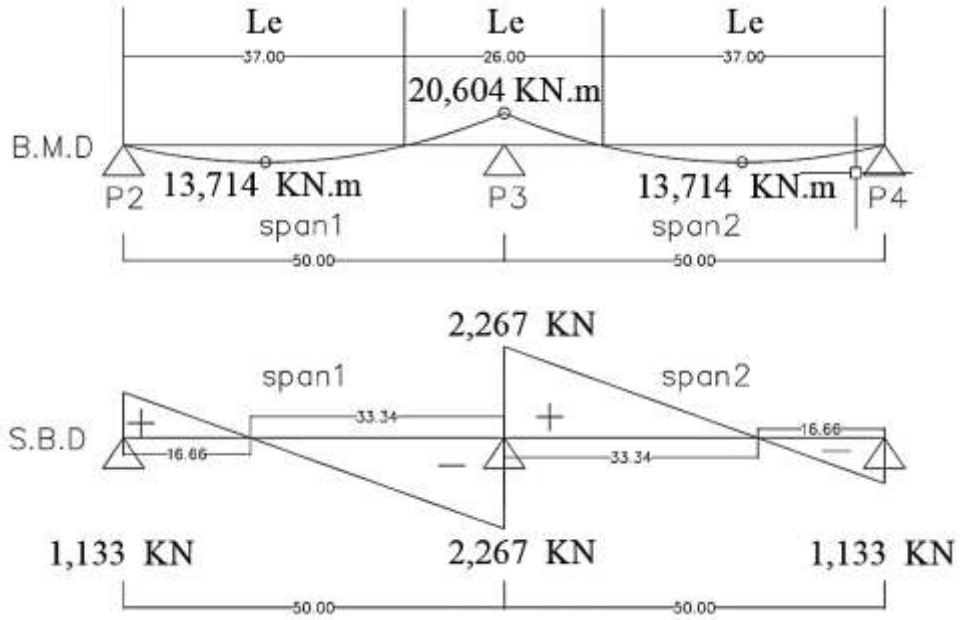

Figure A.41: Maximum Bending Moment and Shear Diagram per Continuous Girder

A.1.4 Factored load and stability

The minimum Depth of Composite Beam Portion

0.027L for continuous spans **Table 2.5.2.6.3-1 AASTO LRFD**

Overall Depth of Composite Beam

0.032L for continuous spans **Table 2.5.2.6.3-1 AASTO LRFD**

The Span/Depth Ratio of Composite Beam = L/D = 12 to 20 **Eurocode 4 code**

L for span = 50 m/2.5 m= 20

0.027(50) = 1.35 depth of the steel section only

0.032(50) = 1.6 depth of the composite girder

So, assuming all depth of composite member = 2.5 m

The deck slab = 0.2 m ► 2 – 0.20 = 1.80 m depth of the steel section

For serviceability limit state cases factored load**:**

Maximum hogging moment = 14,825.83(1.6) + 5778.13(1.4) = 31.811 KN.m

Maximum sagging moment = 10,463.96(1.6) + 3250(1.4) = 21,292 KN.m

Maximum shear force at support p3 = 577.81(1.4) +(781+23+885.599) (1.6) = 3,484 KN.m

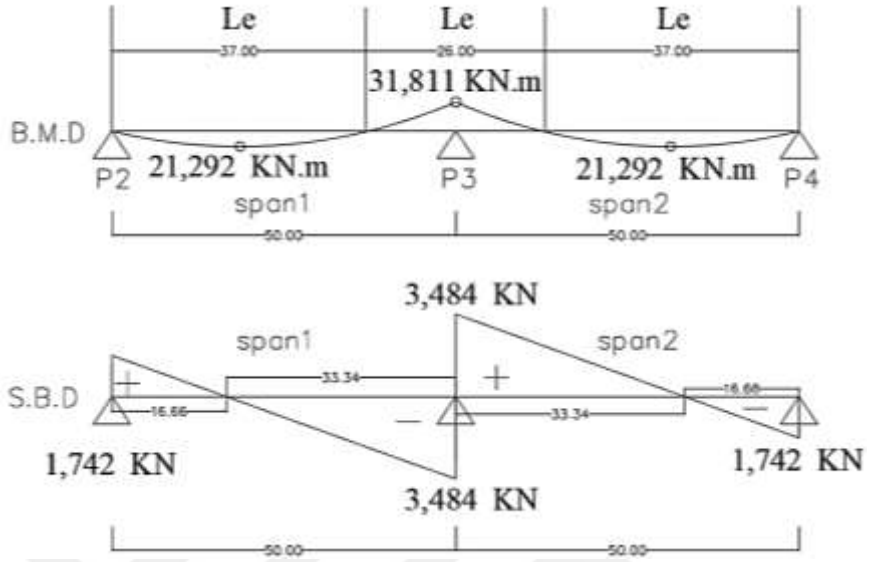

Figure A.42: Factored Maximum Bending Moment and Shear Diagram per Continuous Girder

N = (r + m) – 2j

Where:

R= reaction number

M= member number

J= joint number

N= (3+45) – 2 (24) = 0 then ok (the truss is stably)

A.2 Theoretical calculation of the experimental specimen

A.2.1 LOADING

For this experiment test the hydraulic jack capacity 3000 KN, the design applied load will be 300 KN**,** each jack will act as two points of load on the top concrete surface of specimens, each load point (hydraulic jack) well gets 150 KN, as shown in Figure A.43**,** illustrates the specimens' dimensions, the design concept It

aims to prepare a design free of safety factors for the purpose of reaching the required failure state during the site inspection according to the loading system.

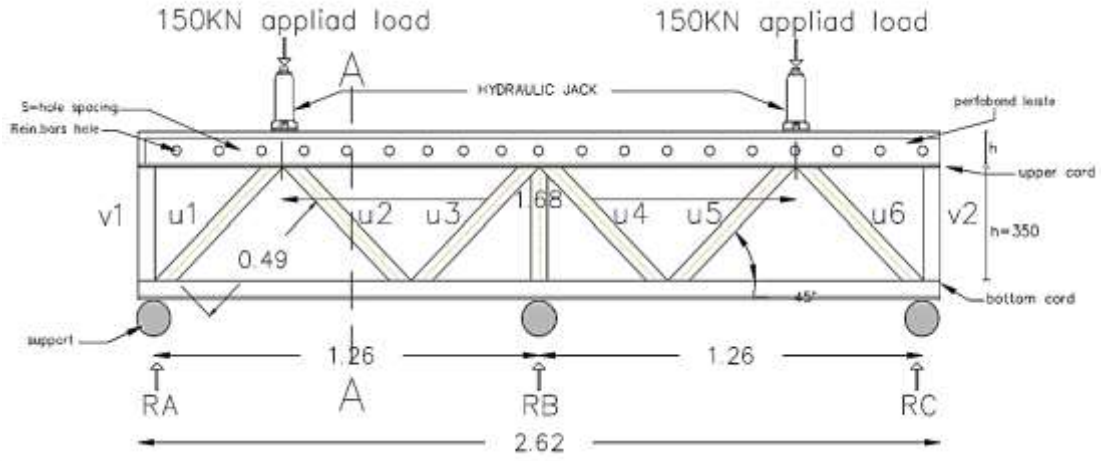

(a) The layout of the truss girder

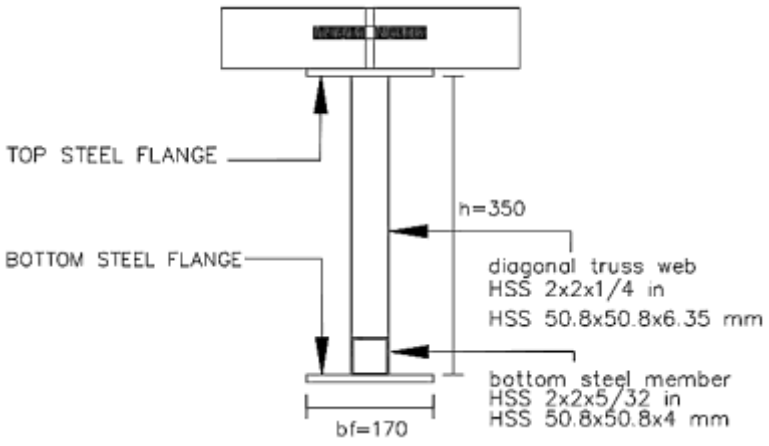

(b)

Figure A.43: Specimens' Dimensions and Loading Situation (a) the Layout of the Truss Girder (b) Section A-A

A.2.2 Analysis the internal Forces and Reactions

By using the equilibrium of the forces at ultimate stage to distribute the applied load:

The reaction A and C = 0.318(P) = 0.38(150) = 57 KN

The reaction B = 1.38(P) = 1.38 (150) = 207 KN

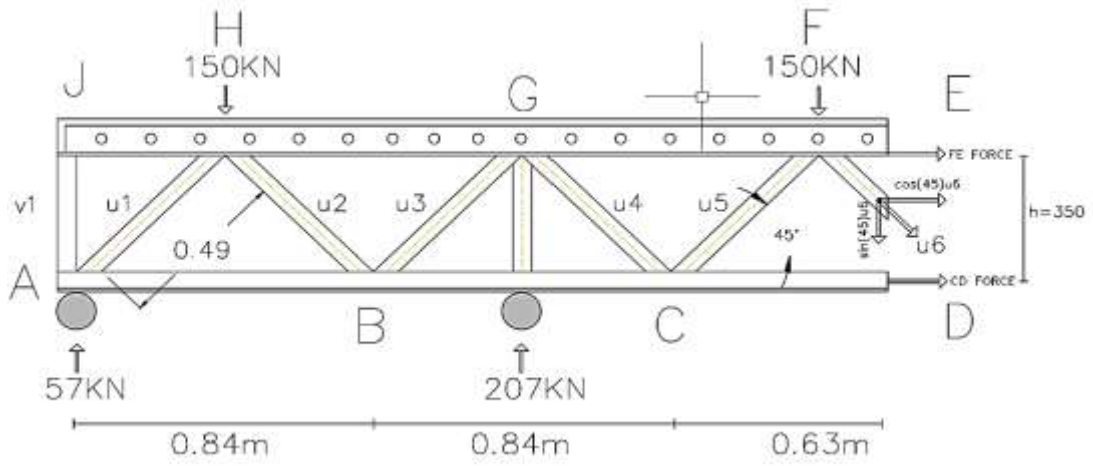

Figure A.44: First Cutting Section

Using section method to find the internal force of members:

ΣMF=0

(57KN) * (0.84+0.84+0.42) – (150KN) * (0.84+0.84) + (207KN) * (0.84) – CD (0.35) =0

CD = 118.8 KN (T)

ΣFY=0

57 KN + 207 KN – COS 45 * U6 – 150 KN – 150N KN

U6 = -51.42 KN (T) ► U6 = 51.42 KN (C)

ΣFX=0

118.8 KN - SIN (45) U6 + FE =0

FE = -82.8 KN (T) ► FE= 82.8 KN(C)

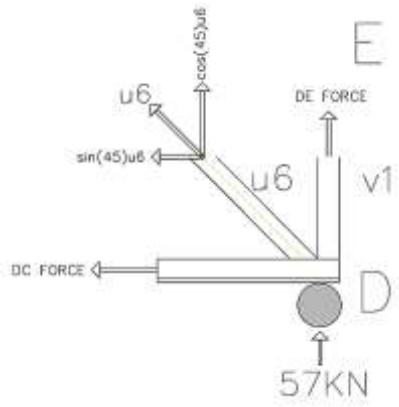

Figure A.45: Second Cutting Section

ΣFY=0

57 KN + DE + COS 45 U6 =0

DE = -92.99 KN (T) ► DE= 92.99 KN (C) ► DE= 93 KN (C)

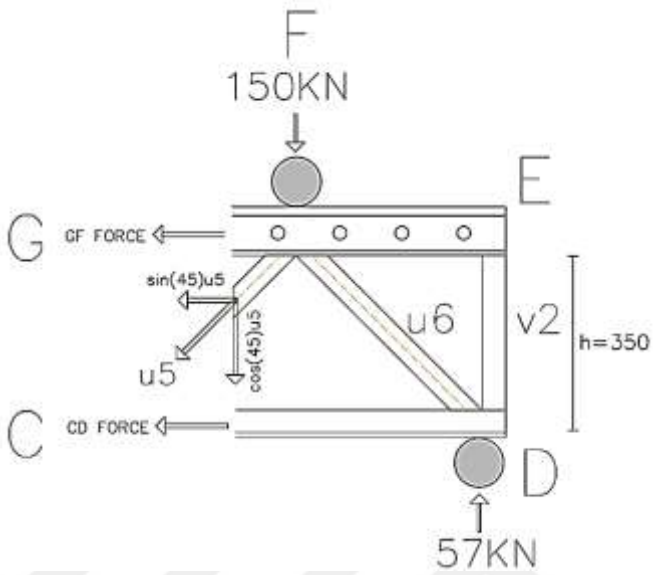

Figure A.46: Third Cutting Section

ΣMC=0

150 KN * (0.42) – 57 KN * 0.84 – GF * 0.35 = 0

GF = 43.2 KN (T)

ΣFY=0

57 KN -150 - COS 45 U5 =0

U5 = - 132 .85 KN (T) ► U5 = 132.85 KN(C)

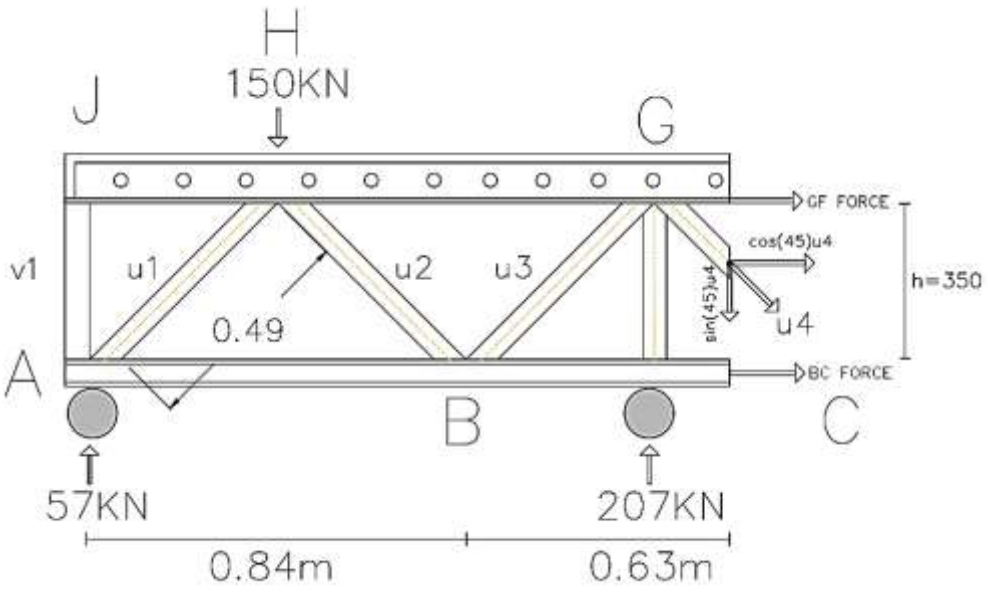

Figure A.47: Fourth Cutting Section

ΣMG=0

-150 KN * (0.84) + 57 KN * 1.26 – BC * 0.35 = 0

BC = -154.8 KN ► BC= 154.8 KN (C)

ΣFY=0

57 KN +207-150 - COS 45 U4 =0

U4 = 162.8 KN (T)

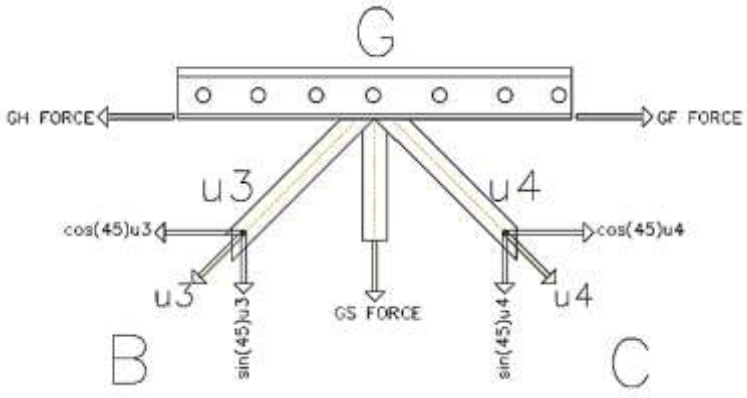

Figure A.48: Fifth Cutting Section

U3 = U4 = 162.8 KN (T)

GF = GH = 43.2 KN (T)

ΣFY=0

-GS - COS 45 U4 – COS 45 U3 =0

-GS – COS 45(162.8) – COS 45 (162.8) = 0

GS = -227.92 KN ► GS= 227.92 KN (C) = GS= 228 KN (C)

Table A.8: Internal Forces for the Truss Members

No.	Member	Forces	No.	Member	Forces
1	AB (bottom cord)	118.8 KN (T)	9	GF (upper cord)	43.2 KN (T)
2	BC (bottom cord)	154.8 KN (C)	10	FE (upper cord)	82.8 KN(C)
3	CD (bottom cord)	118.8 KN (T)	11	U1 (diagonal)	51.42 KN (C)
4	DE (vertical)	93 KN (C)	12	U2 (diagonal)	132.85 KN(C)
5	GS (vertical)	228 KN (C)	13	U3 (diagonal)	162.8 KN (T)
6	JA (vertical)	93 KN (C)	14	U4 (diagonal)	162.8 KN (T)
7	JH (upper cord)	82.8 KN(C)	15	U5 (diagonal)	132.85 KN(C)
8	HG (upper cord)	43.2 KN (T)	16	U6 (diagonal)	51.42 KN (C)

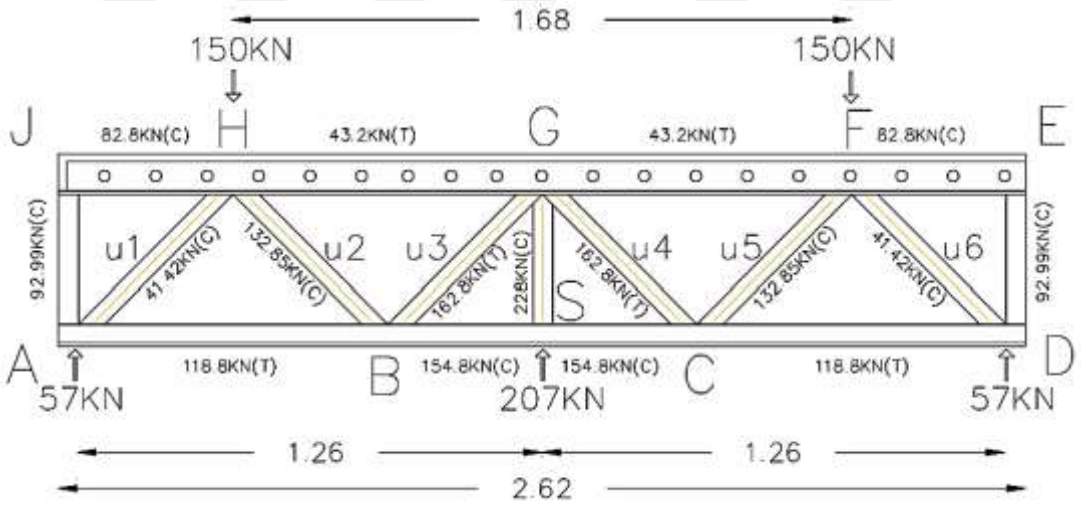

Figure A.49: Internal Forces in All Structure Members

A.2.3 Bending moment and shear force diagram

The shear force will be transferred along the diagonal members; we cut the section and determine the shear force diaphragm due to the internal force, while the bending force will be generated due to the upper and bottom internal force.

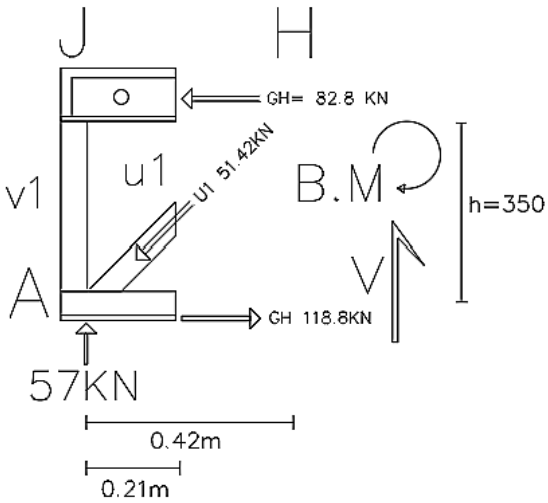

Figure A.50: Section of Member U1

The shear force at point A = 57 KN

AT section u1:

V - sin 45 (51.42) = 0 ► V= 36 KN

Upper cord moment ΣM JH =0

MJH + 57 KN (0.21) - 118.8 KN (0.35) = 0

MJH = 29.61 KN.m

bottom cord moment ΣM AB =0

MAB + 57 KN (0.21) – 82.3 (0.35) = 0 ► MAB= 16.83 KN.m

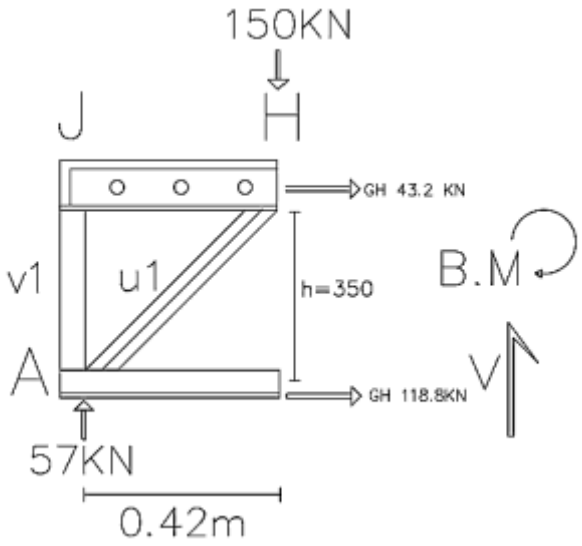

Figure A.51: Section of Member AB

AT section AB

ΣFY=0

57 -150 + v = 0 ► V = 93 KN

Upper cord moment ΣM H =0

MH + 57(0.42) -118.8(0.35) = 0 ► MH = 17.64 KN.m

bottom cord moment ΣM AB =0

MAB +57(0.42) +43.2(0.35) =0 ► MAB = - 39 KN.m

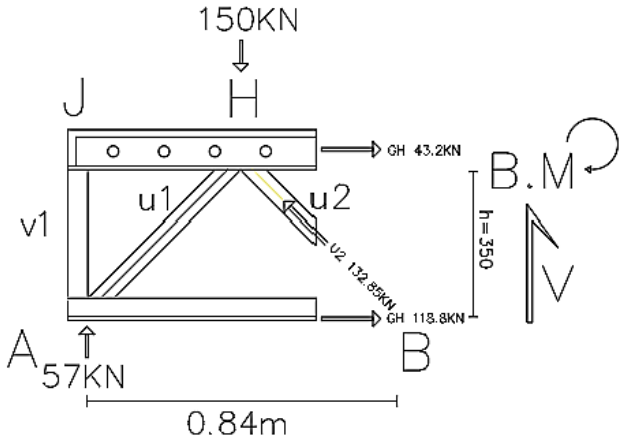

Figure A.52: Section of Member U2

At section u2:

ΣFY=0

V= sin 45 (132.85) = 93 KN

Upper cord moment ΣM HG =0

MHG + 57(0.42+0.21) -118.8(0.35) -150(0.21) = 0 ► MH = 37.17 KN.m

bottom cord moment ΣM AB =0

MAB +57(0.42+0.21) +43.2(0.35) -150(0.21) =0 ► MAB = -19.53 KN.m

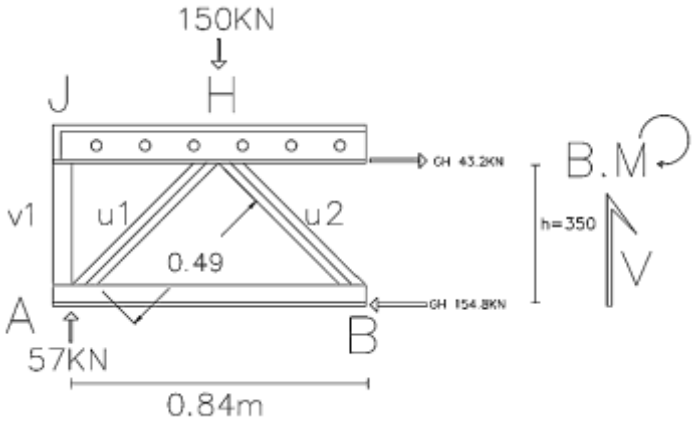

Figure A.53: Section at B

At section B:

ΣFY=0

57 -150 + v = 0 ► V = 93 KN

Upper cord moment ΣM HG =0

MHG +57(0.84) +154.8(0.35) -150(0.42) =0 ► MHG = -39.06 KN.m

bottom cord moment ΣM B =0

MB + 57(0.84) + 43.2(0.35) -150(0.42) = 0 ► MB = 1.2 KN.m

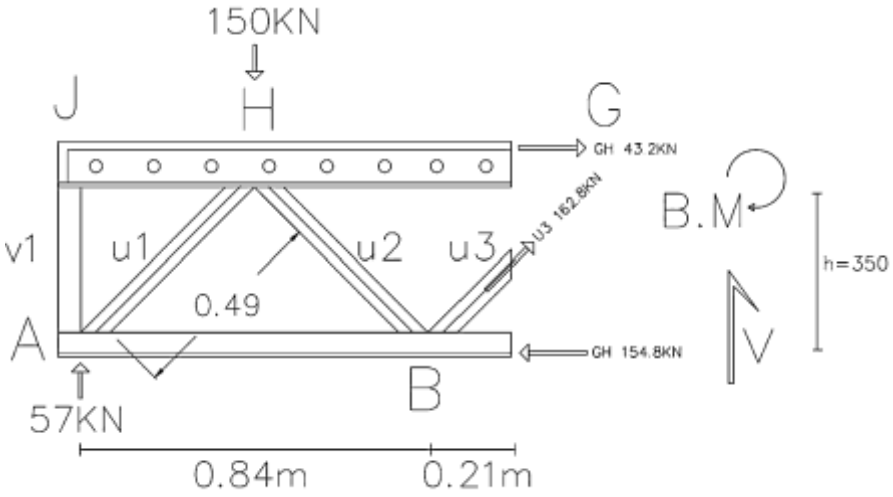

Figure A.54: Section at BC

At section BC:

ΣFY=0

V= SIN (45) 162.8 KN ► V = 138.52 KN

Upper cord moment ΣM HG =0

MHG + 57(0.84+0.21) + 154.8(0.35) -150(0.42+0.21) = 0

MHG = -19.53 KN.m

bottom cord moment ΣM BC =0

MBC +57(0.84+0.21) +43.2(0.35) -150(0.42+0.21) =0

MHG = 19.53 KN.m

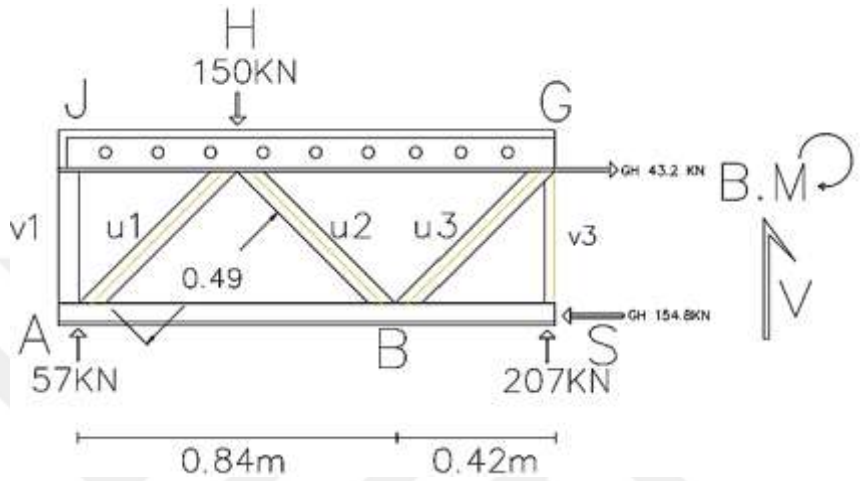

Figure A.55: Section at G

At section G:

ΣFY=0

V+ 57 KN + 207KN -150KN = 0 ► V = -114 KN

Upper cord moment ΣM HG =0

MG + 57(0.84+0.42) -150(0.84) + 154.8(0.35) = 0

MG=0 KN

bottom cord moment ΣM BC =0

MBC +57(0.84+0.42) +43.2(0.35) -150(0.84) =0

MBC = 39.06 KN.m

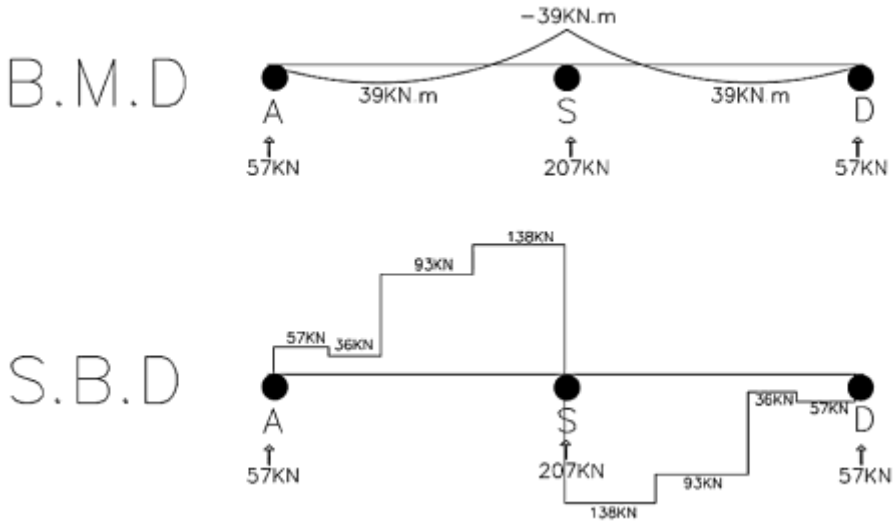

Figure A.56: The Shear Force and Bending Moment Diagram

A.2.4 Vertical and Diagonal Steel Member Design

The maximum internal comparison force = 228 KN ► 51.25 kip

The maximum internal tension force = 162.8 KN ► 36.59 kip

The steel properties: St-37 ► fy = 35 ksi and fu = 58 ksi

For the tension diagonal member design:

1. Yielding stage: -

   Pu = $\neg_t$ Pn which Pn = Ag * Fy

   36.59 kip = 0.9 * Ag * 35 ksi

   Ag = 1.16 in^2

2. Rupture stage: -

   Pu = $\neg_t$ pn which (Pn = Ae * Fu)

   36.59 kip = 0.75 * Ae * 58 ksi

   Ae = 0.841 in^2

   Because there are no bolts in the connection structure then we take (U) = 1

   Ae = u*An then An = 0.841 in^2

   So, we take the Ag = 1.16 in^2

   r min = L/300 = (0.94m/0.0254)/300 = 0.06 in

From the AISC steel construction manual table (1-12) we select the HSS Square 2*2*1/4

the selected section had the following properties:

Ag = 1.51 in^2

r = 0.704 in

For the compression diagonal member design:

Use 2*2*1/4 L = 0.49 m = 19.29 in

Pu = $\neg_c$ Fcr * Ag

$\frac{kL}{r} = \frac{1*19.29}{0.704} = 27.4$ for truss structure k= 1

$4.71\sqrt{\frac{E}{Fy}} \blacktriangleright 4.71\sqrt{\frac{29000}{35}} = 135.57 > \frac{kl}{r}$ then use the (Fcr) formula

Fe = $\frac{\pi 2 * Es}{(\frac{kl}{r})^2}$ where Es = 29000 ksi or 200 GPa

Fe = $\frac{\pi 2 * 29000}{(27.4)^2} =$ 381 ksi

Fcr = ((0.658) $\frac{Fy}{Fe}$) * Fy

Fcr = ((0.658) $\frac{35}{381}$) * 35 =

Pu = $\neg_c$ Fcr * Ag

Pu = 0.9 * Fcr * 1.51 in^2 =

The comparison load is 51.25 kip $<$ pn $=$ kip

For the upper and lower truss cords members:

The maximum tension force with 118.8 KN = 26.70 kip

1. Yielding stage:

Pu = $\neg_t$ Pn

26.70 = 0.9 * Ag * 35

Ag = 0.847 in^2

2. Rupture stage

Pu = $\neg_t$ pn which (Pn = Ae * Fu)

26.70 = 0.75 * Ag * 58

Ag = 0.613 in^2

So, we use the bigger area gross = 0.847 in^2

r min = $\frac{L}{300}$ = $\frac{0.84*0.0254}{300}$ 0.11 in

The minimum required depth of perfobond ribs = 50 mm = 1.96 in

Flange thickness = 7 mm = 0.27 in

From the AISC steel construction manual table (9-1) we use MT 2* 3f

The selected section properties:

Ag = 0.875, d = 1.90 in, tw= 0.130 in, bf= 3.80 in, tf = 0.160 in, rx, 0.493 in, ry= 0.926 in

A.2.5 Stresses due the internal forces and perfobond ribs shear connector design

For the steel materials properties that were used in the experimental test:

ST-37 the Fy = 235 MPa

Modulus of elasticity (Es) = 210 GPa (from the steel laboratory test results)

Concrete strength (f_c') = 45 MPa (from the steel laboratory test results at 28 day)

Modulus of elasticity (Ec) = 4700$\sqrt{(f_c')}$ = 29 GPa **(ACI-318-19)**

Stresses distribution of (S1-S1) and (S2-S2) from (SCTG) samples as shown in **Figure (A-57)**, the same process for (DCTG) samples, **Figure (A-60).**

A.2.5.1 Composite Action of the single composite truss girder specimen one

It's needed to calculate the Ieff:

n = $\frac{Es}{Ec} = \frac{210 * 10^3}{29 * 10^3}$ = 6.8 = 7 (the concrete 7 times less stiff than steel)

The width of the concrete slab = 400 mm / 7 = 57.14 mm

Finding the natural axis (N.A) of the section

Ac = 400 *100 = 40000 mm^2

Act = n * Ac = 7 * 40000 mm^2 = 280000 mm^2

AS2 = AS3 = (6 * 170) * 2 = 2040 mm^2 (1020 mm^2 for each flange)

AS1 = (50.8 *50.8) – (46.8 * 46.8) = 390.4 mm^2

At = 280000 + 2040 + 390.4 = 282430.4 mm^2

$y' = \frac{\Sigma A.y}{A\ total}$ =

Where the (y) is the distance from the reference axis (at bottom of the section to the centroid pf each part of the section), (Figure A.58 & Figure A.59):

$y' = \frac{(280000*412)+(1020*359)+(1020*3)+(390.4*56)}{282430.4}$ = 409 mm

Finding the moment of inertia to the section

Ic = $\frac{bh3}{12} = \frac{(400)(100)3}{12}$ = 33333333.3 mm^4

Transferred to the neutral axis

Ic (n.a) = Ic + Act * (centroid of concrete $- y')^2$

Ic (n.a) = 33,333,333 + 280,000 mm^2 * $(412 - 409)^2$ = 35,173,333 mm^4

Isf = $\frac{bh3}{12} = \frac{170 * 6^3}{12}$ = 3060 mm^4

Is (t.f) (n.a) = 3060 + 1020 $(359 - 409)^2$ = 2,553,060 mm^4

Is (b.f) (n.a) = 3060 + 1020 $(3 - 409)^2$ = 168,135,780 mm^4

Itotal = 35,173,333 + 2,553,060 + 168,135,780 = 205,862,173 mm^4 = 205 * 10^6 mm^4

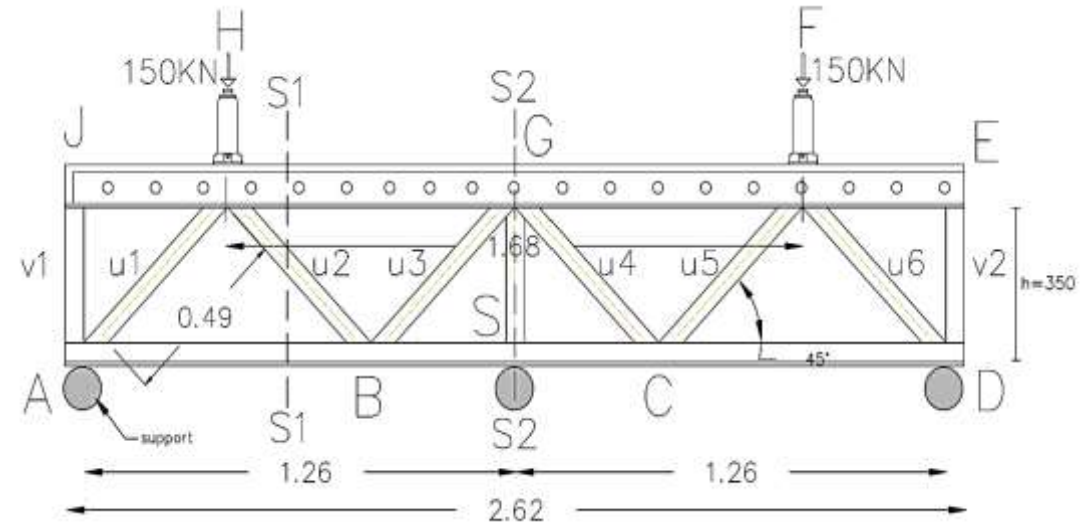

Figure A.57: Position of the Section (S1-S1) & (S2-S2) for (SCTG)

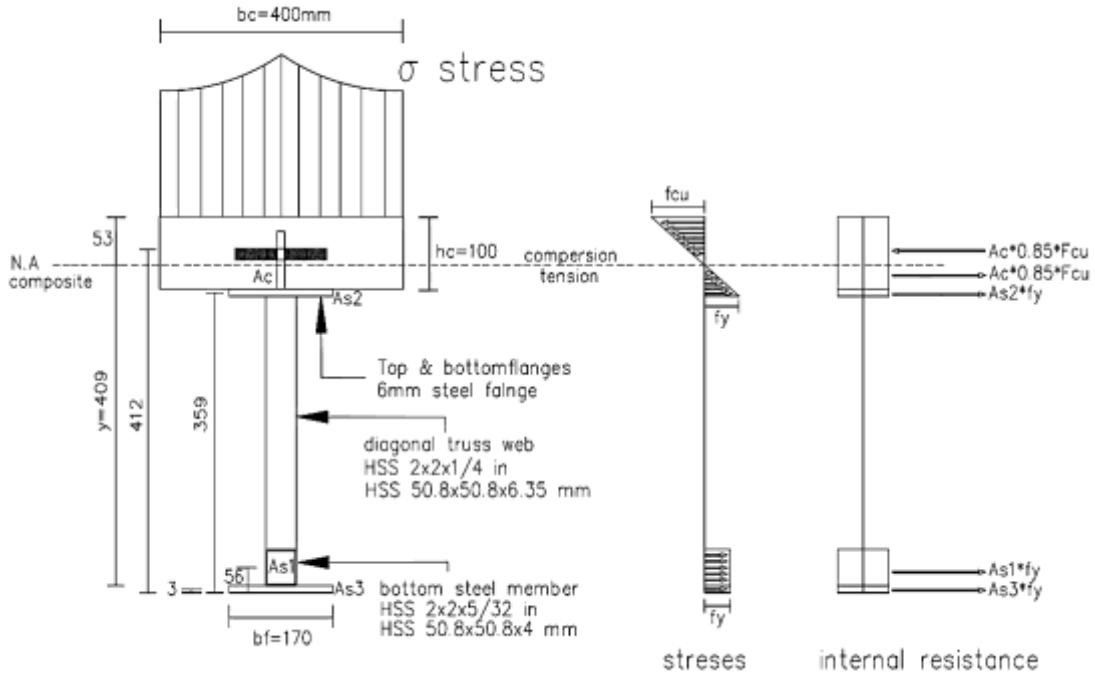

Figure A.58: Natural Axis of (S1-S1) Section for (SCTG)

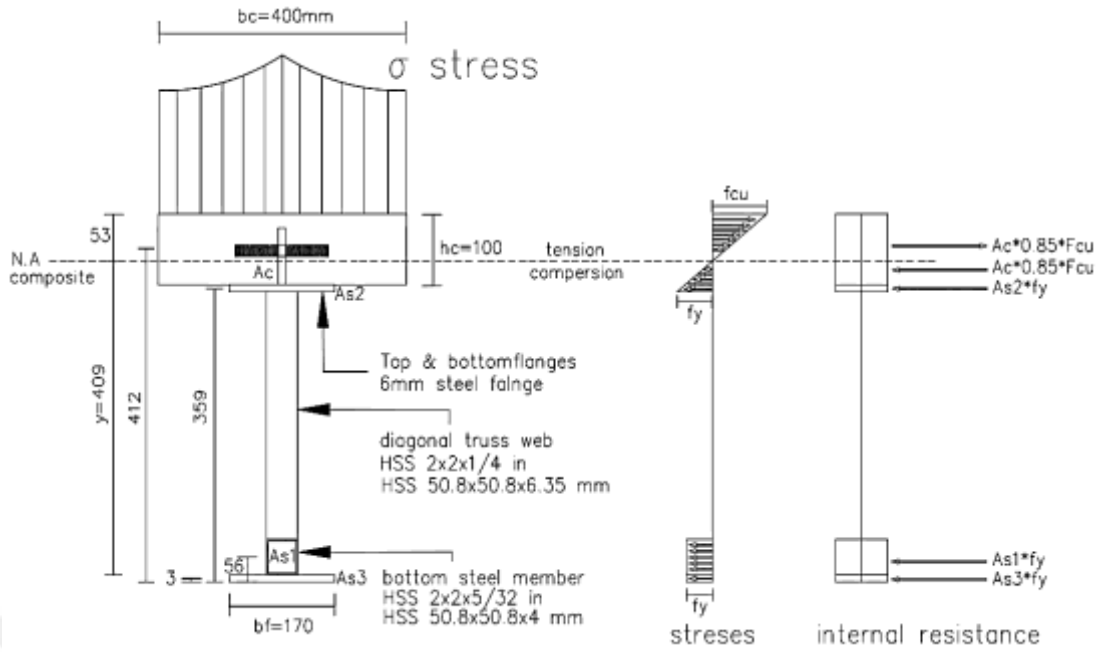

Figure A.59: Natural Axis of (S2-S2) Section for (SCTG)

A.2.5.2 Composite Action of the Double composite truss girder specimen one

It's needed to calculate the Ieff

n = $\frac{Es}{Ec} = \frac{210 * 10^3}{29 * 10^3}$ = 6.8 = 7 (the concrete 7 times less stiff than steel)

the width of the concrete slab = 400 mm / 7 = 57.14 mm

Finding the natural axis (N.A) of the section

Ac1 = 400 *100 = 40000 mm^2

Ac2 = 170 * 100 = 17000 mm^2

Ac1t = n * Ac1 = 7 * 40000 mm^2 = 280000 mm^2

Ac2t = n * Ac2 = 7 * 17000 mm^2 = 119000 mm^2

AS1 = AS2 = (6 * 170) * 2 = 2040 mm^2 (1020 mm^2 for each flange)

At = 280000 + 119000 + 2040 = 401,040 mm^2

$y' = \frac{\Sigma A.y}{A\ total} =$

Where the (y) is the distance from the reference axis (at bottom of the section to the centroid pf each part of the section), (Figure A-61 & Figure A-62):

$y' = \frac{(280000*462)+(119000*50)+(1020*409)+(1020*103)}{401{,}040}$ = 339 mm

Finding the moment of inertia to the section

Ic1 = $\frac{bh3}{12} = \frac{(400)(100)3}{12}$ = 33,333,333 mm^4

Ic2 = $\frac{bh3}{12} = \frac{(170)(100)3}{12}$ = 14,166,666 mm^4

Transferred to the neutral axis

Ic1 (n.a) = Ic1 + Ac1t * (centroid of concrete $- y')^2$

Ic1 (n.a) = 33,333,333 + 280,000 mm^2 * $(462 - 339)^2$ = 4,269,453,333 mm^4

Ic2 (n.a) = Ic2 + Ac2t * (centroid of concrete $- y')^2$

Ic2 (n.a) = 14,166,666 + 119000 mm^2 * $(50 - 339)^2$ = 9,953,165,666 mm^4

Is1 =Is2 = $\frac{bh3}{12} = \frac{170* 6^3}{12}$ = 3060 mm^4

Is1 (n.a) = Is1 + As1t * (centroid of steel section $- y')^2$

Is1 (t.f) (n.a) = 3060 + 1020 $(409 - 339)^2$ = 5,001,060 mm^4

Is2 (n.a) = Is2 + As2t * (centroid of steel section $- y')^2$

Is2 (b.f) (n.a) = 3060 + 1020 $(103 - 339)^2$ = 56,812,980 mm^4

I total = 4,269,453,333 + 9,953,165,666 + 5,001,060 +56,812,980 = 142 * 10^8 mm^4

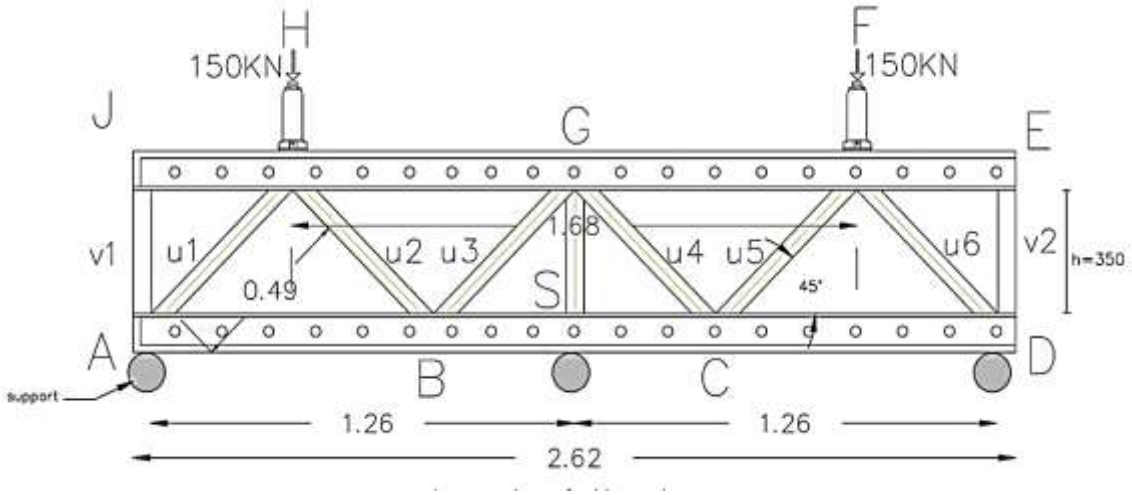

Figure A.60: position of the section

(S1-S1) & (S2-S2) for (DCTG)

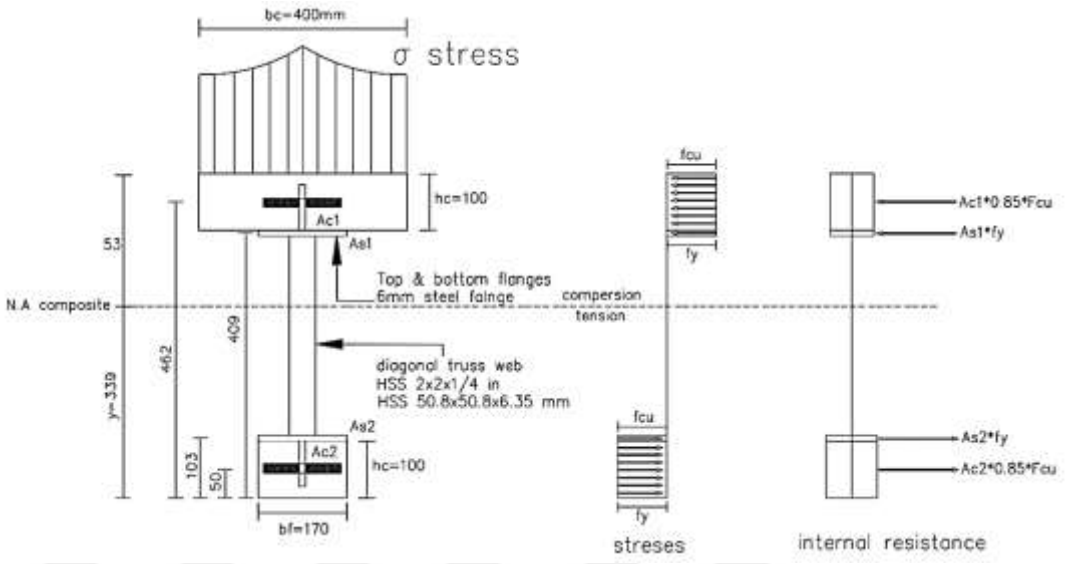

Figure A.61: Natural Axis of (S1-S1) Section for (DCTG)

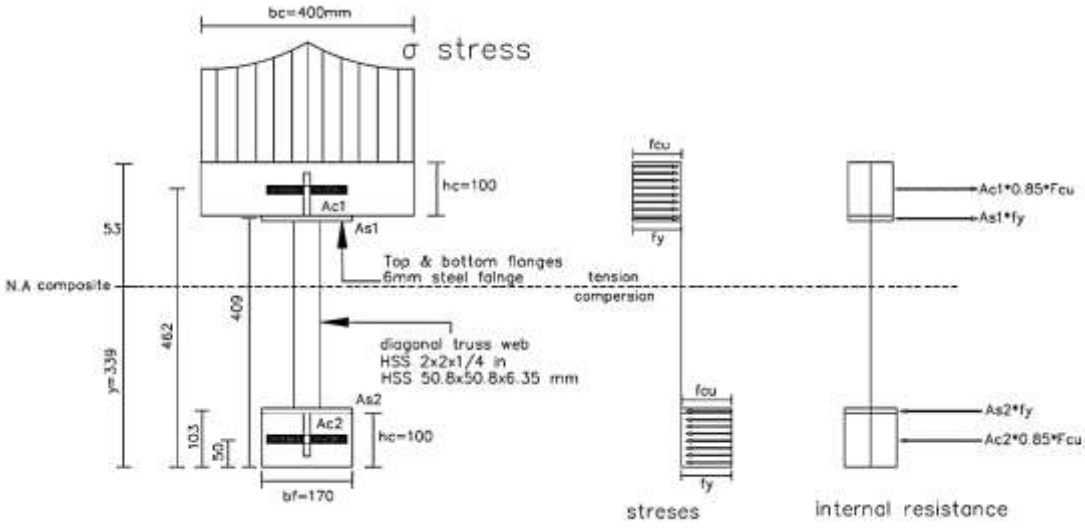

Figure A.62: Natural Axis of (S2-S2) Section for (DCTG)

A.5.2.3 Shear flow and Analysis of the shear connector capacity

The maximum shear force = 138 KN

The shear flow q = $\frac{v*Q}{I}$

Where:

V = maximum shear force KN

Q = first moment of inertia (A) area above the interaction face * (y) distance from area of center to the natural axis.

I = moment of inertia of the entire composite section

Q = 100 * 400 * (412 – 409) = 120,000 mm^3

q = $\frac{138\ kn * 120{,}000}{205{,}862{,}173}$ = 0.088 KN/mm

The shear connector ribs properties:

The length of the ribs (Lr) = 50 mm

The thickness of the ribs (Tr) = 6 mm

The concrete strength (fck) = 35 MPa

Strength of yield steel (fy) = 235MPa

Reinforcement bar diameter (dr) = 12 mm

First the contribution of concrete dowel acting the ribs holes

V dowel = K1* Ah*$\sqrt{fck}$

Where:

K1= empirical factor (0.5-0.6)

Ah = cross sectional area of the hole

Ah = $\frac{\pi(dh)^2}{4} = \frac{\pi(30)^2}{4}$ = 706 mm^2

V dowel = 0.55 * 706 mm^2 * $\sqrt{45}$ = = 2,604 N = 2.4 KN

Ribs steel bearing acting against surrounding concrete

V rib = K2 * Tr *Lr * fy

Where:

K2 = empirical factor (0.8 – 1)

Tr = thickness of the perfobond plate

Lr = effective length of the rib

Fy = yield strength

V rib = 0.9 * 6 mm * 100 * 235 = 126,900 N = 126 KN

Contribution of reinforcement bars inside the holes

V r.bars = Nr * Ar * fy

V r.bars = 1 * 113 $mm^2 * 235 =$ 26,555 N = 26 KN

V total = 2.4 KN + 126 KN + 26 KN = 154 KN (of one hole of 50 mm plate for ¬12)

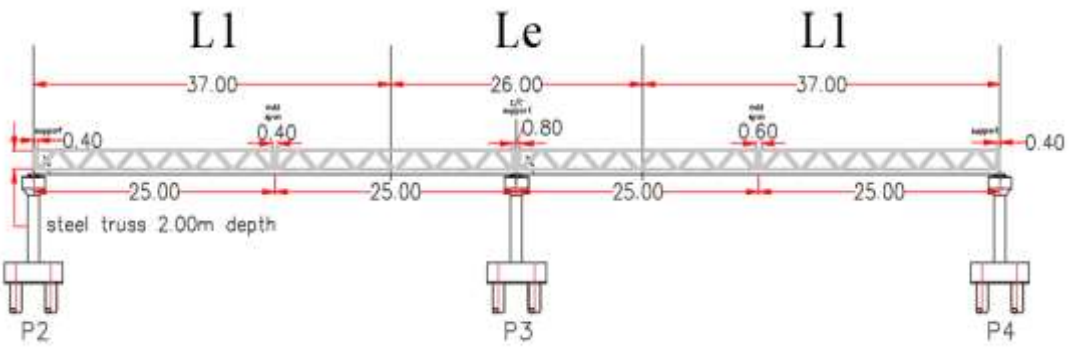

Figure A.63: Perfobond Leiste Distribution Over Bridge Spans

Appendix B.1.1: HSS members and plate steel materials test results

Zwick / Roell

10.11.24

Test report

Temp.=22.2 C
RH.= 22.2 %

Test results:

Nr	Specimen identifier	$R_{p0.2}$ MPa	R_{eH} MPa	R_m MPa	S_0 mm²	A_t %
1	7083-1	289	299	414	226.80	36.4
2	7083-2	272	-	403	227.08	38.6
3	7083-3	267	269	406	228.00	38.3
4	7084-1	508	-	523	211.12	5.9
5	7084-2	519	-	530	204.16	5.5
6	7084-3	507	-	508	190.24	6.7

Series graph:

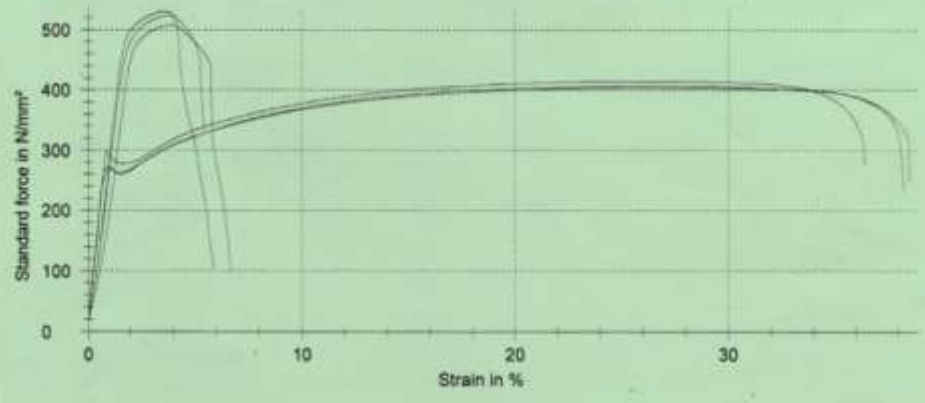

Statistics:

Series n = 6	$R_{p0.2}$ MPa	R_{eH} MPa	R_m MPa	S_0 mm²
x̄	394	284	464	214.57
s	129	21.1	62.3	15.48
v	32.80	7.42	13.42	7.22

7083-7084.zs2

Page 1/1

Appendix B.6: Conplast SP-423 Sheet

Conplast SP423

FOSROC constructive solutions

Workability retention superplasticiser

Uses

- Gives increased working life to fresh concrete.
- Increases workability without extra water, reducing placing time and costs.
- Improves* cohesion, minimising segregation and improving surface finish.
- Aids pumping by improving cohesion and reducing workability loss.
- Allows a reduction in water:cement ratio, enhancing durability by producing low permeability concrete with reduced shrinkage cracking potential.
- Chloride free, safe for use in pre-stressed and reinforced concrete.
- Can be used with concrete containing micro-silica and other cement replacements.

Standard compliance

Conplast SP423 complies with BS5075 Part 3 and ASTM C494 Type G.

Description

Conplast SP423 is a chloride free workability retention admixture based on selected organic polymers. It is supplied as a brown solution which instantly disperses in water.

Conplast SP423 disperses the fine particles in the concrete mix, enabling the water content of the concrete to perform more effectively. The increased workability, cohesion and retardation minimises loss of workability.

Technical support

Fosroc provides a technical advisory service for on-site assistance and advice on mix design, admixture selection, evaluation trials and dispensing equipment. Technical data and guidance can be provided for admixtures and other products for use with fresh and hardened concrete.

Dosage

The optimum dosage of Conplast SP423 to meet specific requirements should always be determined by trials using the materials and conditions that will be experienced in use. The normal dosage range is 0.6 to 1.5 litres per 100 kg of cementitious materials, including PFA, GGBFS and micro-silica.

Use at other dosages

Dosages outside the typical range quoted above may be used if necessary and suitable to meet particular mix requirements. Contact the Fosroc Technical Service Department for advice in these cases.

Properties

Appearance:	Brown liquid
Specific gravity:	Typically 1.17 at 20°C
Chloride content:	Nil to BS 5075
Alkali content:	Typically less than 72.0g. Na_2O equivalent per litre of admixture. A fact sheet on this subject is available.

Instructions for use

Mix design for workability retention

The mix design should be one suitable for use as a pump mix. To obtain the best results for workability retention, the initial workability should be above 150 mm slump. The retardation and improved cohesion provided by Conplast SP423 then act to enhance the workability retention characteristics. Advice on mix design for flowing concrete is available from Fosroc.

In correctly designed flowing concrete, the improved dispersion of the cement particles and the more efficient use of mixing water will improve mix cohesion. The improved cohesion obtained with Conplast SP423 will also help to minimise bleed and segregation. After initial trials, minor modifications to the mix design may be made to optimise performance.

Compatibility

Conplast SP423 is compatible with other Fosroc admixtures used in the same concrete mix. All admixtures should be added to the concrete separately and must not be mixed together prior to addition. The resultant properties of concrete containing more than one admixture should be assessed by the trial mixes.

Conplast SP423 is suitable for use with all types of ordinary Portland cements and cement replacement materials such as PFA, GGBFS and micro-silica.

Dispensing

The correct quantity of Conplast SP423 should be measured by means of a recommended dispenser. Normally, the admixture should then be added to the concrete with the mixing water to obtain the best results.

Appendix B.8: Concrete materials of (C35) parameter at Abaqus program

Table B. 1: CDP Compressive Behavior of Concrete (C35)

No	Yield Stress	Inelastic Strain	No	Yield Stress	Inelastic Strain
1	17.5	0	19	27.466761	0.002423
2	20.420381	9.00E-06	20	26.071812	0.002661
3	23.201699	2.60E-05	21	24.689812	0.002898
4	25.79471	5.30E-05	22	23.338987	0.003133
5	28.147291	9.20E-05	23	22.032631	0.003367
6	30.208536	1.47E-04	24	20.779913	0.003597
7	31.9334	0.000219	25	19.586658	0.003824
8	33.287268	0.000312	26	18.456056	0.004048
9	34.249664	0.000425	27	17.389276	0.004268
10	34.816428	0.000559	28	16.385982	0.004485
11	35	0.000713	29	15.44475	0.004699
12	34.827785	0.000886	30	14.563403	0.00491
13	34.339025	0.001076	31	13.739267	0.005117
14	33.580805	0.00128	32	12.969369	0.005322
15	32.60388	0.001495	33	12.250587	0.005524
16	31.458944	0.00172	34	11.579755	0.005723
17	30.193679	0.001951	35	10.953744	0.00592
18	28.85076	0.002186	36	10.5	0.006072

Table B.2: CDP Tensile Behavior of Concrete (C35)

No	Yield Stress	Inelastic Strain
1	4.2	0
2	2.330096	0.000321
3	1.650807	0.00058
4	1.292702	0.000821
5	1.069362	0.001055
6	0.915842	0.001286
7	0.803371	0.001514
8	0.717171	0.001741
9	0.648848	0.001967
10	0.593266	0.002192